THE DESIGN, SYNTHESIS, AND EVALUATION OF ZWITTERIONIC AND CATIONIC LIPIDS FOR *IN VIVO* RNA DELIVERY AND NON-VIRAL CRISPR/CAS GENE EDITING

APPROVED BY SUPERVISORY COMMITTEE

Daniel J. Siegwart, Ph.D.

Joseph M. Ready, Ph.D.

Jinming Gao, Ph.D.

Uttam K. Tambar Ph.D.

DEDICATION

To my family, and everyone who helped me get here.

ACKNOWLEDGEMENT

There are so many people to thank for their contributions to my development as a person and a scientist during my Ph.D. studies at UT Southwestern. I genuinely believe that this is the most important section of my dissertation, as without the contributions and support of so many people, the realization of this personal and scientific achievement simply would not be possible.

I would like to thank my advisor Dr. Daniel Siegwart for your continuous scientific and professional support and guidance, and most importantly patience with my scientific development over these last five and a half years. It has truly been an honor to grow and develop together as your first graduate student and to be able to contribute to building a research program from the ground up. Thank you for giving me this opportunity.

I also want to thank all of the members of the Siegwart Lab, past and present, particularly Drs. Yunfeng Yan, Kejin Zhou, Petra Kos and Hu Xiong who provided invaluable advice and support as postdoctoral advisors. Thank you for letting me talk your ears off with many questions over the years and for your continued willingness to help in many ways. I will cherish the relationships that we have developed.

I would also like to thank all of the members of the UT Southwestern Chemistry community (faculty, students, postdoctoral researchers, and administrators) with whom I have had the pleasure of interacting over the course of my studies. Your willingness to share your time, guidance, reagents, and equipment have been critically important and appreciated as we slowly built our research program. In particular I would like to that my dissertation committee Drs. Joseph Ready, Jinming Gao, and Uttam Tambar, as well as Dr. Mike White who provided important guidance throughout my studies that aided my developed as a scientist. I am truly grateful. I also

want to thank my friends at UT Southwestern and in Dallas who helped to keep me sane throughout the challenges of graduate school.

I would like to thank the many collaborators with whom I have had the pleasure of working over the years. These relationships have helped to provide very important perspective and to shape me as a scientist. In particular I want to thank Dr. Hao Zhu and his students Shuyuan Zhang and Dr. Liem Nguyen who really helped to bring our biological studies to a much higher level, and to quickly accelerate the translational potential of our delivery platforms. Many of our biological studies would not have been possible without your contributions and I am grateful for having had the opportunity to work with you in their development.

Finally, and most importantly, I want to thank my family for their continuous love, support, and probably most trying for them, patience throughout this process. Obviously, none of this would be possible without you guys and it means the world to share this accomplishment with you. This has certainly been an eventful five and a half years but no matter what challenges we face, I am glad that we have each other, no matter what. Mom and Dad thank you for all that you have done and continue to do to support me throughout my life. Thank you for always being there whenever I need anything. Your love and support are truly examples for which to strive and emulate as we begin our own family. Kyle and Tyler, I admire all that you have achieved and your willingness to chase your dreams inspires me every day to be better. Lauren, I love you so much and I am so proud of everything that you have accomplished! I know that without your love and support I would not have been able to complete this Ph.D. It took a bit longer than expected but finally that time has arrived! Here's to continuing our crazy life adventure together, but doing so in the same city!

THE DESIGN, SYNTHESIS, AND EVALUATION OF ZWITTERIONIC AND CATIONIC LIPIDS FOR *IN VIVO* RNA DELIVERY AND NON-VIRAL CRISPR/CAS GENE EDITING

by

JASON BRIAN MILLER

DISSERTATION

Presented to the Faculty of the Graduate School of Biomedical Sciences

The University of Texas Southwestern Medical Center at Dallas

In Partial Fulfillment of the Requirements

For the Degree of

DOCTOR OF PHILOSOPHY

The University of Texas Southwestern Medical Center at Dallas

Dallas, Texas

May 2018

THE DESIGN, SYNTHESIS, AND EVALUATION OF ZWITTERIONIC AND CATIONIC LIPIDS FOR *IN VIVO* RNA DELIVERY AND NON-VIRAL CRISPR/CAS GENE EDITING

Publication No._____

Jason Brian Miller

The University of Texas Southwestern Medical Center at Dallas, Graduation Year

Supervising Professor: Daniel John Siegwart, Ph.D.

Abstract: The delivery of nucleic acids is an emerging therapeutic modality in clinical development for the treatment of many genetic diseases. The use of RNA interference (RNAi) as a therapeutic is an exciting and rapidly developing field that offers a promising alternative to small molecule drugs for the treatment of dysregulatory diseases, including cancer. Small interfering RNA (siRNA) can be designed against any mRNA target, and upon loading into the RNA-induced silencing complex (RISC) can enable sequence-specific target recognition and degradation. Meanwhile, messenger RNA is currently being utilized for protein replacement

therapy and for the development of vaccines by expressing viral antigens on dendritic cells. However, because RNA molecules are unable to passively diffuse across plasma membranes due to a high molecular weight (~13 kDa for siRNA, >300 kDa for mRNA), hydrophilicity and strong anionic charge, while also being unstable and highly immunogenic when injected systemically, nucleic acid therapeutics require carriers for effective delivery. To date, many successful carriers have been designed using amphiphilic lipid-like compounds containing amine-rich cores, but the challenges of efficient endosomal release and delivery to organs outside of the liver remain major hurdles in the field of RNA therapeutics.

This dissertation reports the design, synthesis and characterization of two new classes of lipids with unique chemical structures and *in vivo* RNA delivery capabilities to the lung: zwitterionic amino lipids (ZALs) and cationic sulfonamide amino lipids (CSALs). ZALs contain an amine rich core, hydrophobic tails introduced via conjugate addition or epoxide opening, and a zwitterionic sulfobetaine head group. ZALs were designed with a combination of cationic and zwitterionic lipid properties, to help stabilize and effectively deliver long RNA molecules. A lead compound, ZA3-Ep10, was effective for *in vivo* messenger RNA delivery and the first reported demonstration of *in vivo* non-viral gene editing by delivering mRNA components encoding the CRISPR/Cas gene editing platform. CSALs contain a unique chemical scaffold containing an internal quaternary ammonium group and a sulfonamide linker. A rational investigation of structure-activity relationships revealed that CSALs containing an acetate sidearm, a dimethyl amino head group and higher hydrophobic content were effective in delivery siRNA to human cancer cells *in vitro*. CSALs also demonstrated lung localization upon systemic delivery *in vivo* while also demonstrating the ability to redirect liver targeting ionizable lipid nanoparticles to the

lung. These new classes of materials demonstrate the importance of structural consideration in material design for the development of nucleic acid therapeutics, while also providing structural templates for developing carriers for effective delivery to tissues outside of the liver.

TABLE OF CONTENTS

PRIOR PUBLICATIONS

1. Miller, J. B.; Zhang, S.; Kos, P.; Xiong, H.; Zhou, K.; Perelman, S. S.; Zhu, H.; Siegwart, D. J., Non-Viral CRISPR/Cas Gene Editing *In vitro* and *In vivo* Enabled by Synthetic Nanoparticle Co-Delivery of Cas9 mRNA and sgRNA. *Angewandte Chemie International Edition* **2017,** *56* (4), 1059-1063.
2. Miller, J. B.; Kos, P.; Tieu, V.; Zhou, K.; Siegwart, D. J., Development of Cationic Quaternary Ammonium Sulfonamide Amino Lipids for Nucleic Acid Delivery. *ACS Applied Materials & Interfaces* **2018,** *10* (3), 2302-2311.
3. Siegwart, D. J., Miller, J. B., "Cationic Sulfonamide Amino Lipids and Amphiphilic Zwitterionic Amino Lipids." *U.S. Patent Application* 2017/0349543 (**2017**).
4. Siegwart, D.J., Thomas, P.J., Johnson, A. E., Torres, M. J., Miller, J. B., "Compositions for the delivery of tRNA as nanoparticles and methods of use therewith." *U.S. Patent Application 2017/0354672* (**2017**).

LIST OF FIGURES

LIST OF APPENDICES

LIST OF DEFINITIONS

ANA - aribonucleic acid

ApoB - apolipoprotein B

ApoE - apolipoprotein E

ARCA - anti-reverse cap analog

ASGPr - asialoglycoprotein receptor

ASO - antisense oligonucleotide

aTTR - transthyretin mediated amyloidosis

bp - base pairs

Cas9 - CRISPR associated protein 9

Cl - chloride

CRISPR - clustered regularly interspaced palandromic repeat

CSAL - cationic sulfonamide amino lipid

Ctrl - control

DCM - dichloromethane

DHA - docosahexaenoic acid

DLS - dynamic light scattering

DMD - Duchenne muscular dystrophy

DMEM - Dulbecco's modified eagle medium

DNA - deoxyribonucleic acid

DOPC - 1,2-dioleoyl-sn-glycero-3-phosphocholine

DOPE - 1,2-dioleoyl-sn-glycero-3-phosphoethanolamine

DPC - dynamic poly conjugate

DPhPE - 1,2-diphytanoyl-sn-glycero-3-phosphoethanolamine-N-(7-nitro-2-1,3-benzoxadiazol-4-yl)

DPPC - 1,2-dipalmitoyl-sn-glycero-3-phosphocholine

DSB - double strand break

dsDNA - double-stranded DNA

DSPC - 1,2-distearoyl-sn-glycero-3-phosphocholine

dT - deoxyribothymidine

ED_{50} - effective dose, 50% activity

EPO - erythopoietin

EPR effect – enhanced permeation and retention effect

Et - ethyl

EtOAc - ethyl acetate

EtOH - ethanol

Fah - fumarylacetoacetate hydrolase

FVII - factor VII

g - gram

H&E - hematoxylin and eosin

hFIX - human factor IX

HDR - homology directed repair

I.M. - intramuscular

I.P. - intraperitoneal

I.V. - intravenous

indel - insertion or deletion

iPSCs - induced pluripotent stem cells

IVT - *in vitro* transcription

L - liter

LCMS - liquid chromatography/mass spectrometry

LDL - low density lipoprotein

LLC - lewis lung carninoma

LNA - locked nucleic acid

LNP - lipid nanoparticle

LODER - local drug eluter

LUNAR - lipid-enabled and unlocked-nucleic acid modified RNA

MALDI-TOF - matrix-assisted laser desorption ionization time of flight

MC3 - DLin-MC3-DMA

Me - methyl

MeOH - methanol

μg - microgram

mg - milligram

mg/kg - milligram/kilogram (drug dose)

miRNA - micro-RNA

μL - microliter

mL - milliliter

mol - mole

mRNA - messenger RNA

MS - mass spectrometry

ng - nanogram

NHEJ - non-homologous end joining

NMR - nuclear magnetic resonance

NP - nanoparticle

NSG - non-obese severely compromised immunodeficient mice

nt - nucleotide

OAc - acetate

OMe - methoxy

OPiv - pivalate

PAGE - polyacrylamide gel electrophoresis

PAM - protospacer adjacent motif

PBAVE – poly (butyl amino vinyl ester)

PBS - phosphate buffered saline

PCR - polymerase chain reaction

pDNA - plasmid DNA

PEG – poly(ethylene glycol)

PFA - paraformaldehyde

PS - phosphorothioate

qPCR - quantitative polymerase chain reaction

RISC - RNA-induced silencing complex

RNA - ribonucleic acid

RNAi - RNA interference

RNP - ribonucleoprotein

RT-PCR - reverse transcription-polymerase chain reaction

SDS - sodium dodecyl sulfate

sgRNA - single guide RNA

siRNA - short-interfering ribonucleic acid

siRNN - short-interfering ribonucleic neutrals

SMA - spinal muscular atrophy

SNALP - stable nucleic acid lipid particle

ssRNA - single-stranded RNA

tBu - t-butyl

tdTO - tdTomato

TEM - transmission electron microscopy

THF - tetrahydrofuran

TTR - transthyretin

UNA - unlocked nucleic acid

wt - weight

wt:wt - weight to weight ratio

ZAL - zwitterionic amino lipid

ZFN - zinc finger nuclease

ZNP - zwitterionic amino lipid nanoparticle

CHAPTER ONE

INTRODUCTION

1.1 Therapeutic potential of nucleic acids

The therapeutic application of nucleic acids offers a promising alternative to traditional small molecule drugs for a number of clinical indications, including genetic diseases and cancer. These dysregulatory diseases can be classified as those in which a functional element in the cell is upregulated (such as an oncogene), downregulated (such as the Let-7[6] or MiR-34[7] families of regulatory microRNA (miRNAs) in lung and liver cancers), deleted (such as CFTR in cystic fibrosis[8] or dystrophin in Duchenne Muscular Dystrophy[9-11]) or mutated (such as CFTR or $KRAS^{G12D}$ in many pancreatic and colorectal cancers[12]), resulting in a malignant phenotype. Furthermore, many of these therapeutic targets have been classified as difficult to treat specifically with small molecule drugs or 'undruggable.' Nucleic acid therapeutics offers a potential approach for the treatment of these diseases.

Proteins that are deleted or downregulated can be replaced using using viral or non-viral gene therapy. Non-viral gene therapy can come in the form of plasmid DNA (pDNA) or messenger RNA (mRNA), which utilizes the cellular transcriptional and translational machinery to express an exogenous protein. Meanwhile, malignancies caused by overexpression or sequence mutation of a particular gene offer a therapeutic opportunity to treat with either small or short-interfering RNA (siRNA) to specifically downregulate the expression, or by using gene-editing approached to delete the target. The exogenous nucleic acids must be delivered to the cell in order to reach therapeutic potential. A number of approaches have been developed for clinical translation of this technology including encoding the exogenous nucleic acid in a viral particle, or delivery using a

non-viral carrier, of which the most potent in class utilizes cationic, ionizable lipid nanoparticles to deliver nucleic acid payloads to hepatocytes in the liver.[13-15]

Since the initial observation of RNA interference (RNAi) by Fire and Mello[16] in *c. elegans* in 1998, and subsequent observation in mammalian cells by Tuschl,[17] there has been tremendous investment by the academic, biotechnology, and pharmaceutical industry to harness the power of this technology to treat human disease.[18-19] RNAi is a critical regulatory mechanism by which cells can control the expression of particular proteins using a ribonucleoprotein complex known as the RNA-induced silencing complex (RISC). The RISC complex is loaded with a short ssRNA (~18-27 nt) that is complementary to a target sequence in the transcriptome. When this complex recognizes its complementary target, RISC will bind and degrade the messenger RNA, thus preventing expression of the protein. While RNAi functions endogenously using miRNA, exogenous siRNA can be can be carried out using exogenous small-interfering RNA (siRNA), which can be designed to target genes in a highly sequence-specific manner. To date, much of the therapeutic delivery of RNAi molecules has been achieved to the liver using lipid nanoparticles

Currently, the technologies of messenger RNA (mRNA) and genome engineering, which includes zinc-finger nucleases (ZFNs), transcription activator-like effector nucleases (TALENs), and clustered-regularly interspaced palindromic repeat (CRISPR)-CRISPR associated protein (Cas) have come to the forefront gene therapy and nucleic acid therapeutics.[20] mRNA therapeutics are currently being explored in the clinic for vaccines, immune-oncology, and for protein replacement therapies.[21] Meanwhile, genome engineering technologies are being used to develop immune-oncology therapeutics, as well as specific targeting of genetic diseases.[22] Unlike RNAi, the protein machinery in gene editing technologies is exogenous and must be delivered, either as

a protein or encoded in a pDNA or mRNA. The large size and structure of exogenous mRNA likely requires a different set of carrier parameters in terms of chemical structure and formulation composition, which is an active area of research across academia and industry.

1.2 Barriers to the delivery of nucleic acid therapeutics

Despite the great potential of nucleic acid therapeutics for treating a variety of diseases, many barriers must be overcome for successful clinical implementation of these therapeutics. Because nucleic acids have a high molecular weight (siRNA/miRNA ~ 13 kDa, mRNA > 330 kDa) are highly hydrophilic and anionic, they are unable to passively diffuse across the highly anionic hydrophobic cell membranes. In order to stabilize and effectively deliver nucleic acid therapeutics, several classes of nanocarriers have been developed including polymers,[9, 23] cationic lipids,[24-25] and amphiphilic lipid-like compounds[1, 6, 13, 26-28] containing nucleic acid-binding amine-rich regions, and nanoparticle-stabilizing hydrophobic regions. Following systemic delivery, nucleic acids must avoid degradation by abundant serum nucleases, while the carriers must evade phagocytosis and renal clearance, extravasate across the vascular endothelial barrier, and traverse the extracellular space to reach the target cell.[15] Effective nanomaterials typically have a size between 80-120 nm in diameter, and thus are large enough to avoid clearance by the renal system (< 30 nm), but small enough to penetrate the endothelial pores in rapidly forming tumor blood vessels using the enhanced permeation and retention (EPR) effect.[14] Many challenges including organ and cell-type specificity, efficient endosomal release, and non-liver targeting remain major bottlenecks in the field of RNAi therapeutics.

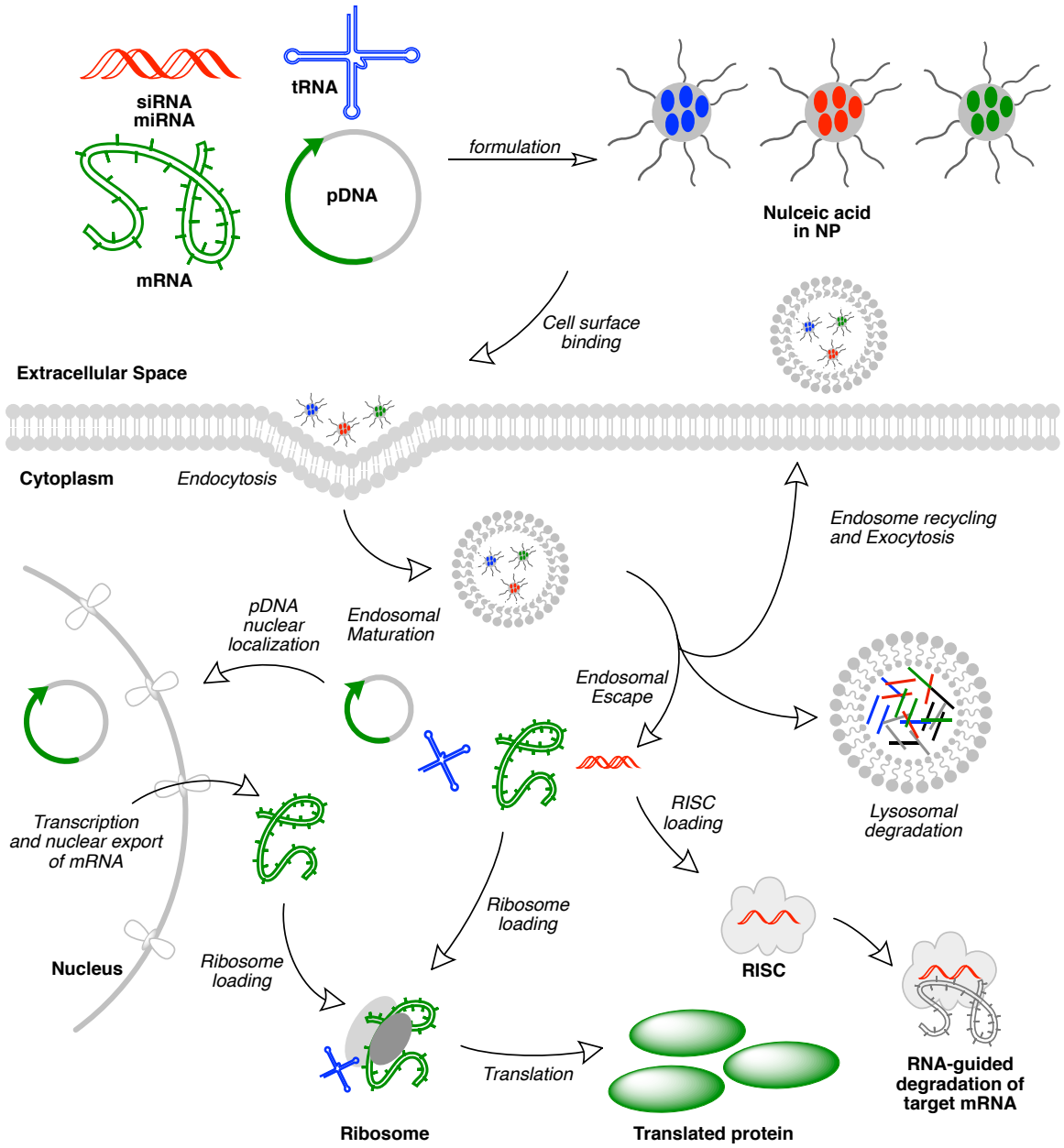

Figure 1.2.1. Intracellular barriers to the functional delivery of different nucleic acid payloads via nanoparticles. Adapted in part from Yin et al.[4]

The most potent class of nanocarriers characterized to date are lipid nanoparticles (LNPs) comprised of an ionizable cationic lipid-like species, cholesterol, a zwitterionic phospholipid and PEG-lipid, the most effective of which are able to silence target genes in mouse hepatocytes in the

liver with an ED_{50} < 0.01 mg/kg siRNA.[27, 29] Even some of the most efficacious *in vivo* carriers explored to date (C12-200 and DLin-MC3-DMA), which have shown potent silencing of endogenous target genes in the liver with RNAi, and also the effective delivery of mRNA, were estimated to allow only 2-3% of siRNA to enter the cytoplasm in cells,[30-32] while as much as 70% of the internalized siRNA is exocytosed.[31] This suggesting a need to further develop new classes of materials to gain an understanding of the underlying mechanisms of nanoparticle uptake and release.

Depending on the type of cargo being delivered, there are different intracellular barriers to functional delivery. Following uptake through a number of possible pathways including endocytosis and micropinocytosis,[33] the nucleic acid cargo must first escape into the cytosol prior to lysosome formation which would result in hydrolysis of the contents. The two prevailing mechanisms by which nanomaterials can escape the intracellular vesicle are the proton sponge effect resulting from the buffering capacity of the amine rich nanomaterials[34] or a mechanism of lipid flipping by fusogenic properties during nonlamellar phase transitions resulting in the loss of contents.[34] During endosomal maturation, as the pH in the vesicle decrease, this enables the cationic lipid component of the nanocarrier to become protonated, and interact with the anionic vesicular membrane causing instability. Hybrid mechanisms have also been proposed whereby the amino groups in the LNP are protonated leading to simultaneous nanoparticle disassembly and fusion and disruption of endosomal membrane leading to nucleic acid escape. Following escape to the cytosol, the identity of the nucleic acid will dictate the barriers to functional delivery. Plasmid DNA designed to encode a protein of interest must be translocated to the nucleus, transcribed to mRNA, which then must be exported back to the cytosol and translated into protein.

mRNA has a kinetic advantage over pDNA in that it bypasses the nucleus and can be loaded directly into the ribosome for translation of the target protein. Meanwhile, a small RNA must be loaded into RISC and then guide the complex to its target.

1.3 Lipid nanoparticles as delivery vehicles for nucleic acids

1.3.1 The formulation of lipid nanoparticles

Lipid nanoparticles utilized for siRNA delivery are typically composed of a cationic lipid, which functions to bind the anionic phosphate backbone of the nucleic acid via electrostatic interactions, and a number of helper lipids including cholesterol, a zwitterionic phospholipid, and a poly(ethylene glycol) (PEG)-lipid. There are a number of approaches to the formulation of lipid nanoparticles and liposomes. The most commonly used methods are the lipid thin-film rehydration and extrusion method and the ethanol dilution method,[35-36] while the most clinically translatable approach to lipid nanoparticles for nucleic acid delivery is the utilization of the ethanol dilution method using a microfluidic mixing platform.[35, 37-39] In the ethanol dilution method, the nucleic acid is dissolved in acidic buffer below the pKa of the cationic lipid, while the lipid mixture is dissolved in ethanol. These two solutions are rapidly mixed where the interaction between the siRNA and cationic lipid is driven by electrostatic interactions, while subsequent raising of the pH to physiological levels causes hydrophobic packing to become the dominant force. Cholesterol a key component of plasma membranes, residing between lipid tails in bilayers, helps to stabilize the hydrophobic interactions within the nanoparticle.[40] The zwitterionic phospholipid plays a critical role of stabilizing the interface of the hydrophobic and hydrophilic domains inside the nanoparticle, while the highly hydrophilic PEG chain of the PEG-lipid decorates the shell of the

nanoparticle, and plays a critical role in preventing nanoparticle aggregation and conferring stealth properties. This PEG coating results in reduced phagocytosis and activation of the immune system and increased circulation time, enabling tissue accumulation by the EPR effect.

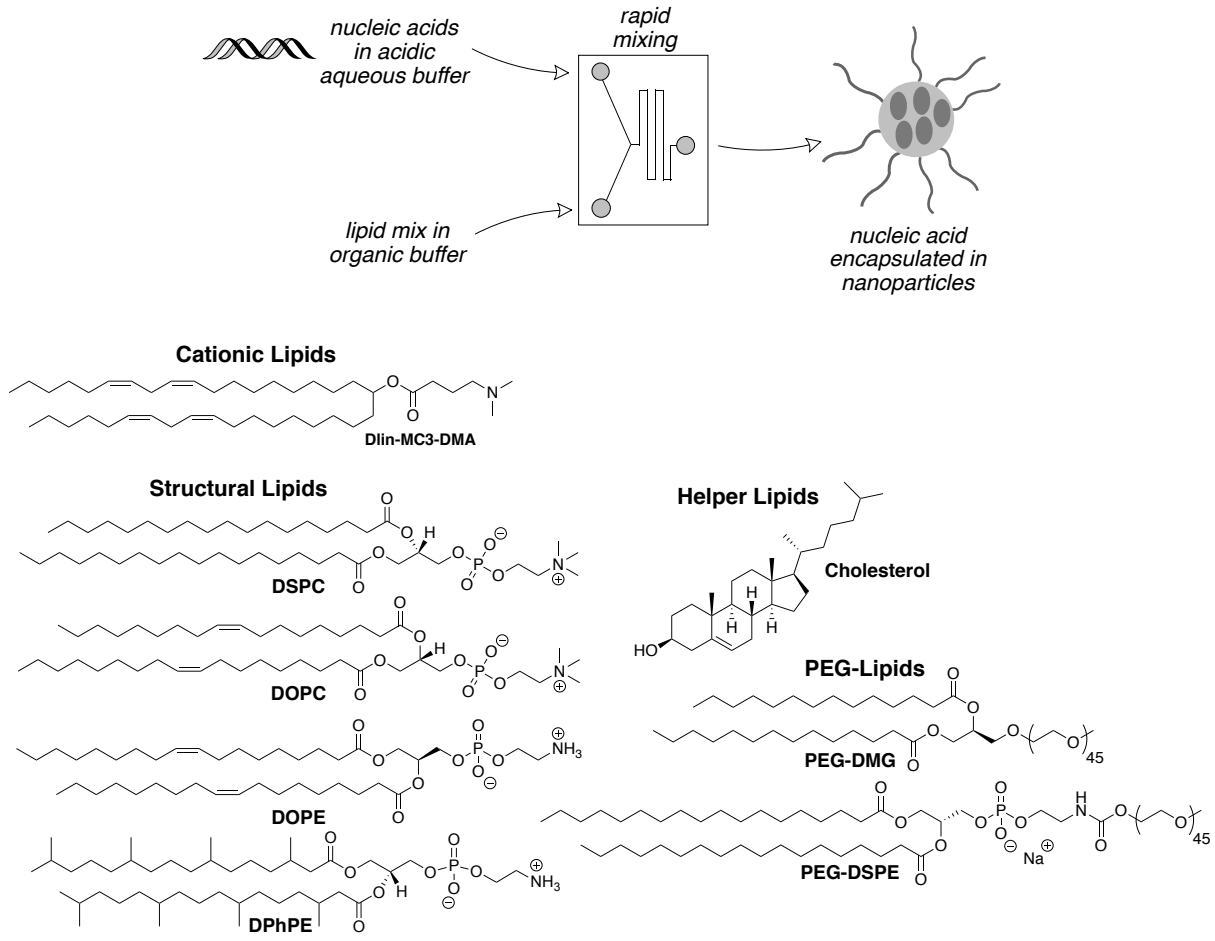

Figure 1.3.1. Lipid nanoparticles are formulated by rapid mixing with the aid of a cationic lipid, a structural zwitterionic lipid, a helper lipid, and a PEG-lipid.

Recent work by Leung, et al.[38] coupled electron microscopy with computational modeling to understand the key molecular interactions in nanoparticle formation. Using DLin-KC2-DMA SNALPs containing cholesterol, DSPC, and PEG-DMG, they observed that the siRNA resided in aqueous pockets which were bordered by the polar moieties of the phospholipid and the cationic

lipid, highlighting the critical role that both the cationic and zwitterionic groups have in forming stable nanoparticles. The PEG-lipid which forms a hydrophilic shell on the outside of the nanoparticle reduces protein adsorption *in vivo* plays a critical role in stabilizing nanoparticles in circulation.

1.3.2 Development of cationic ionizable lipids for in vivo delivery to the liver

Cationic ionizable lipids when formulated in nanoparticles represent the most efficacious class of materials for small RNA delivery *in vivo*, particularly to the liver. Discovery of these potent carriers has largely been aided by a library-based screening approach for favorable properties aiding effective RNA delivery. However, the lead compounds in an *in vitro* screen are often inefficacious in animal experiments, which is a major hurdle in the discovery of new materials for therapeutic RNA delivery. Alabi, et al.[41] developed a set of biophysical chemical properties as a predictive measure for effective materials *in vivo*, as simply relying on *in vitro* silencing efficacy does not fully encompass the barriers to delivery of an injected nanomedicine. A typical chemical approach to building a library of cationic lipid-like materials to identify new involves a large panel of amines with a specific subset of hydrophobic electrophiles, a variety of using a library of amines coupled to hydrophobic lipid tails using robust combinatorial chemistry approaches, followed by *in vitro* delivery screening, and *in vivo* hit validation.

Using a broad library, with well-defined, fine structural changes in the amine core and hydrophobic tails can lead to elucidation and understanding of coupled structure-activity relationships (SAR) for further carrier development. A non-exhaustive panel of some of the most potent carriers discovered to date is shown in Figure 1.3.2. These cationic lipid-like species are formulated with helper lipids cholesterol, DSPC, and PEG-lipid to help stabilize the nanoparticle

and enable potent delivery of siRNA to hepatocytes, which is the typical target for *in vivo* screening of lead materials.[1, 6, 13, 27, 42] Mechanistic studies of ionizable lipids revealed that apolipoprotein E (ApoE)[27, 43] serves as an endogenous targeting ligand by binding the LNPs and transporting them to the hepatocytes and internalizes using the low density lipoprotein (LDL) receptor. Interestingly, this mechanism was not observed in the stronger cationic lipid-like compound 98N12 when compared to the SNALP DLin-KC2-DMA.[43]

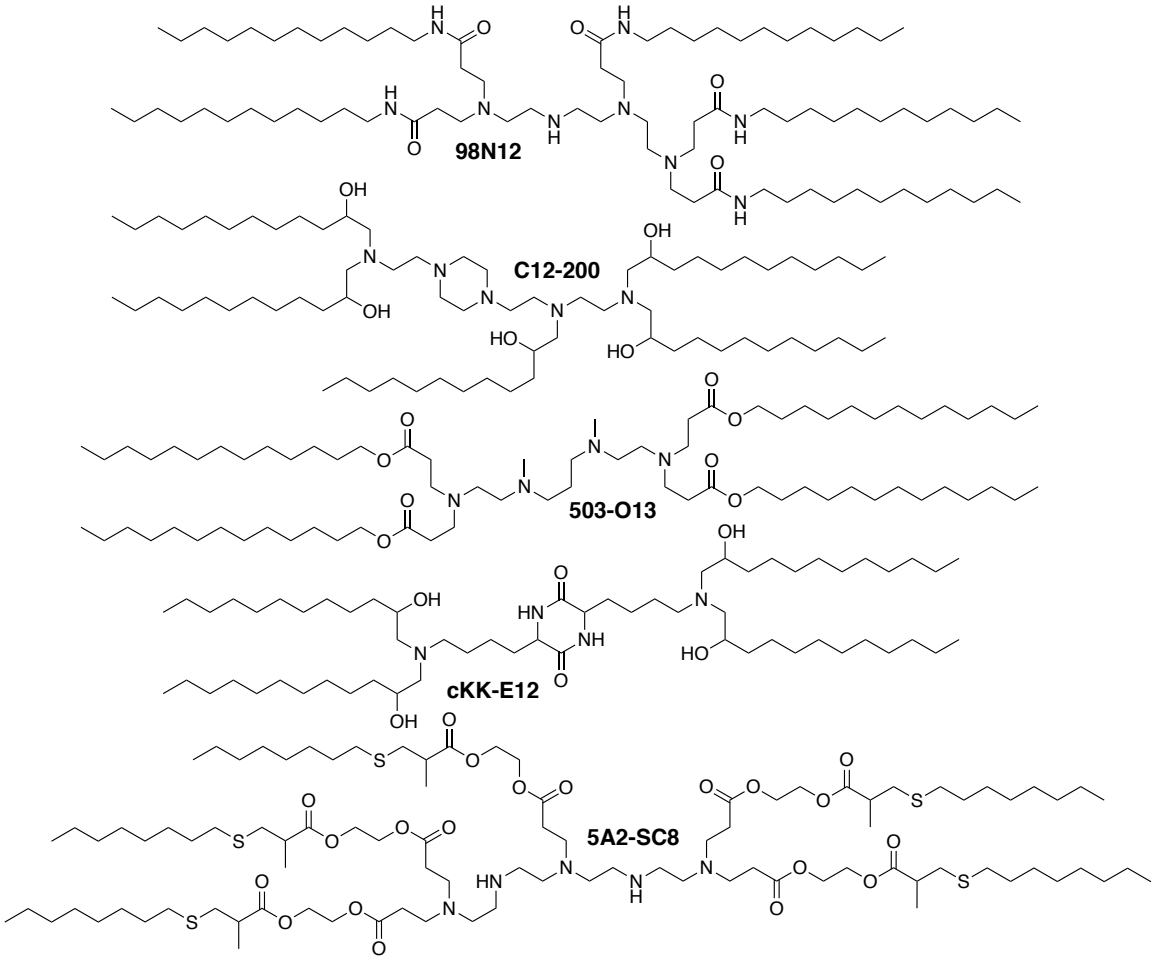

Figure 1.3.2. Cationic lipid-like materials for small RNA delivery identified through combinatorial chemistry library screens.

1.3.3 The evolution of Stable Nucleic Acid Lipid Particles (SNALPs) for siRNA delivery

SNALPs have been the most effective clinically translated lipid nanoparticle system for small RNA delivery to date. The clinical driver of this platform has been Alnylam's development of RNAi therapies in the liver, where SNALPs have shown potent target silencing in hepatocytes. Patisiran (ALN-TTR02), a Dlin-MC3-DMA SNALP delivering siRNA to the liver recently successfully completed a Phase III clinical trial (APOLLO, NCT01960348)[44] in patients with a rare hereditary disease, transthyretin (TTR)-mediated amyloidosis. Regulatory filings are expected for Patisiran in 2018, aiming to become the first FDA-approved LNP-mediated RNAi therapeutic.

Heyes et al.[45] demonstrated the importance of unsaturated bonds in the hydrophobic tails of cationic lipids. Comparing an analogous set of two-tailed lipids linked via ether bond to an ionizable *N,N*-dimethylamino glycerol head group, the role of the alkyl tail structure on LNP uptake and delivery was evaluated *in vitro*. Stearyl tails with fully saturated alkyl tails showed strong uptake, but no siRNA mediated gene silencing was observed. Meanwhile introduction of one (DODMA) or two (DLinDMA) unsaturated bonds greatly improved silencing efficacy likely owing to the ability of these tails to adapt the inverse hexagonal phase more readily. Building from DLin-DMA, Semple et al.[26] modified the spacing between the dimethylamine head group and linolenyl tails, while introducing a ketal ring linker. Introduction of the ketal ring on DLin-DMA showed ~2-fold increase in FVII silencing, while extension of the linker length in the head group by a single methylene to form DLin-KC2-DMA (KC2) resulted in 10-fold improvement. Interestingly, the silencing efficacy decreased upon further linker length extension, likely due to

the pKa becoming slightly more basic. This silencing potency was also translated to non-human primates.

Using KC2 as a template, further improvement of SNALP design was demonstrated by Jayaraman, et al.[28] where using two-tailed linolenyl lipids, a large panel of cationic head groups was correlated between LNP pKa and *in vivo* silencing of FVII, and identified DLin-MC3-DMA (MC3), which contains a single ester linkage between the head and tails, had a pKa of 6.44, and silenced FVII with an ED_{50} of 0.03 mg/kg siRNA. This study demonstrated that the optimal pKa of LNP for *in vivo* efficacy in hepatocytes should be between 6.2 and 6.5, while this is merely one of several factors in designing potent nanocarriers.[41] Maier et al.[29] replaced one of the linolenic olefins with a biodegradable ester linkage, resulting in the identification of L319 with an ED_{50} of <0.01 mg/kg, and pKa of 6.38. Furthermore, pharmacokinetic studies demonstrated that L319 is rapidly cleared from tissue and excreted, a major consideration in RNAi therapeutics where the transient nature of silencing requires repeat dosing for therapeutic benefit.

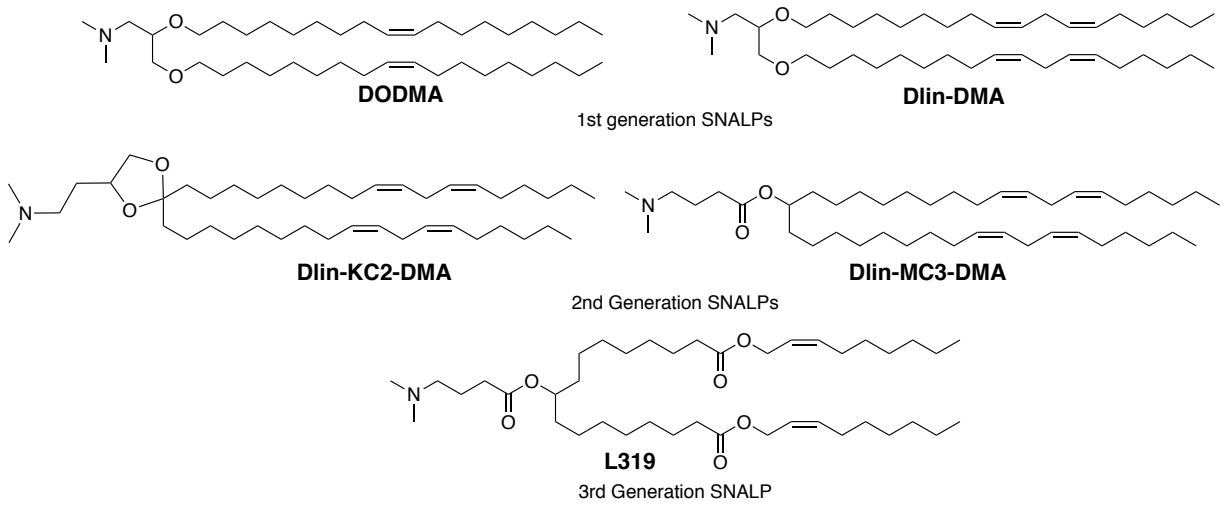

Figure 1.3.3. The structural evolution of SNALPs for small RNA delivery.

1.3.4 Utility of cationic lipids with permanent positive charges

Cationic lipids bearing a permanent positive charge have also been well-explored for nucleic acid delivery as components of liposomes and lipoplexes. Silence Therapeutics has utilized their Atu-PLEX platform, which contains a guanidine head group and two primary amine side arms to effectively deliver siRNA to the vascular endothelium in the liver, heart, and lung.[46] Interestingly, this liposomal formulation uses a diphytanoyl zwitterionic phospholipid in the formulation. Marina Biotech has also reported a guanadinium-based amphoteric liposome[47] which when formulated with cholesterylhemisuccinate (CHEMS), cholesterol and PEG-DMPE silencing in the liver was observed with $ED_{50} < 0.1$ mg/kg for FVII. Marina has also attempted to advance its Smarticles platform, which contains a cationic lipid DOTAP into the clinic with Mirna Therapeutics for the delivery of a Mir34 mimic for advanced cancer.[48]

Nitto Denko[49] has developed a vitamin-A coupled liposome with the cationic lipid DC-6-14, which demonstrated effective treatment of cirrhosis in a rat model by targeting hepatic stellate cells. Due to their ability to easily encapsulate nucleic acids, and well-characterized formation of liposomal particles, cationic lipids containing permanent positive charge remain of interest in the developing carriers for RNA delivery.

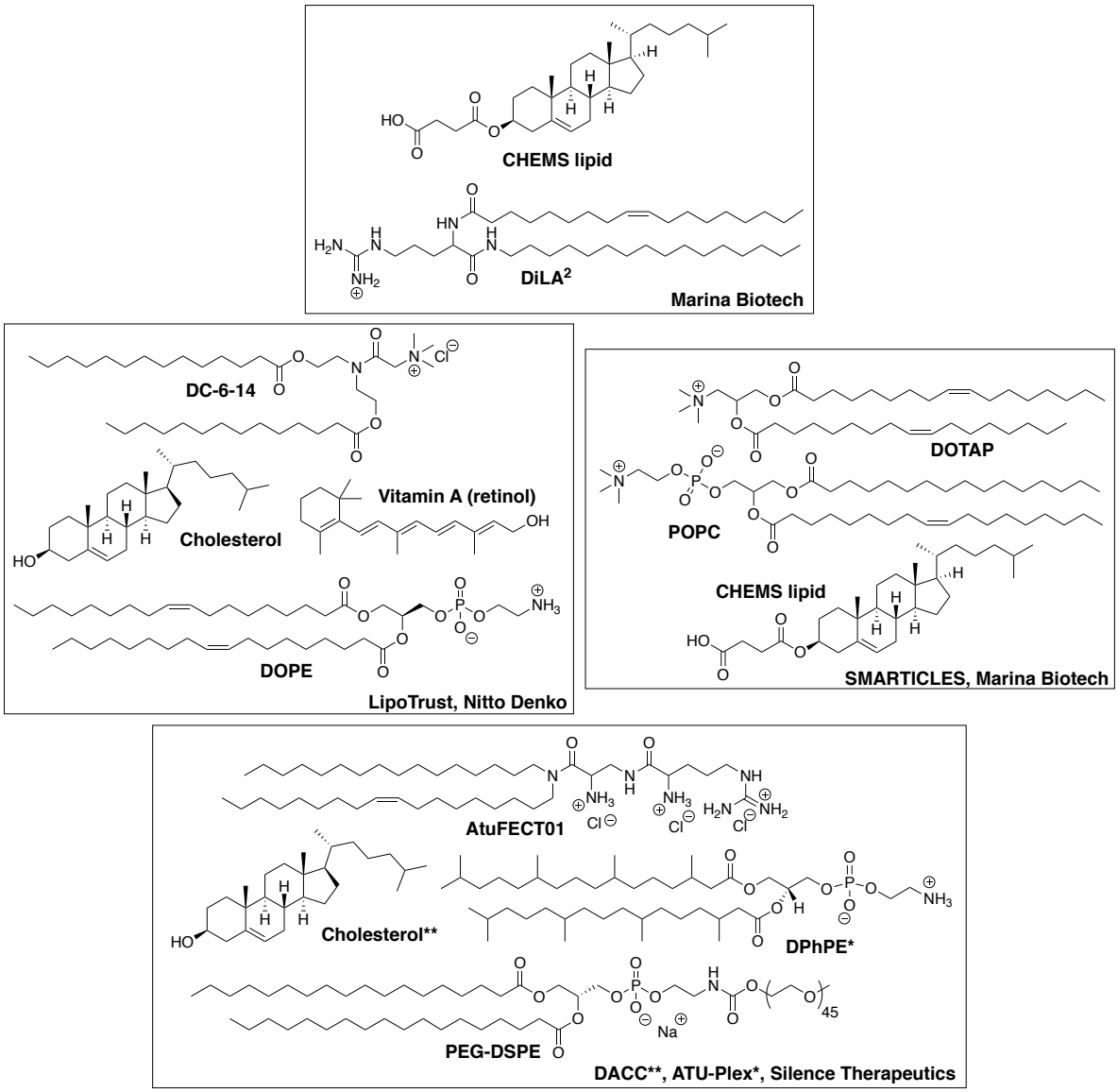

Figure 1.3.4. Cationic lipids with permanent positive charges have been used in liposomal formulations for *in vivo* siRNA delivery.

1.3.5 Synthetic zwitterionic materials and their applications

Synthetic lipids can be generally divided into four classes: cationic, anionic, neutral, and zwitterionic.[50-53] Among carriers for nucleic acids, cationic lipids represent the most investigated

class due to ability of cationic charges to electrostatically bind anionic nucleic acids. Yet, zwitterionic lipids (such as phosphatidyl cholines) are found throughout nature and are key components of cellular membranes, organelles, and are involved in cellular transport pathways.[40, 54] Furthermore, phospholipids including DSPC and DOPE are critical components of many lipid nanoparticle formulations. Despite these observations, synthetic zwitterionic lipids have not often been reported, especially in the context of nucleic acid delivery.

Significant work has been done to demonstrate the non-fouling properties of zwitterionic materials on surface coatings and in implants.[55] Kim et al.[56] when studying the behavior of cationic, anionic, zwitterionic, and neutral gold nanoparticles observed increased circulation times for neutral and zwitterionic surfaces. Similar to nonionic non-fouling materials, such as PEG, zwitterionic groups are highly hydrated, preventing nonspecific interactions.[55] The Szoka group[57-59] has presented several studies of fundamental zwitterion and lipid properties, but these systems have not been fully evaluated in drug delivery applications.

1.3.7 In vivo RNA delivery beyond the liver: targeting the lung

Most lipid nanoparticles (LNPs) reported to date demonstrate efficacious *in vivo* delivery in small and large animal models only in liver hepatocytes,[60] while some materials have been seen to be effective in other tissues. Designing materials with predictable accumulation and activity in tissues other than the liver, particularly the lung is of great interest. Dahlman et al.[61] reported 7C1, a low-molecular weight linear PEI functionalized with a hydrophobic epoxide, that effectively delivered siRNA to endothelial cells following I.V. administration and were effective in lowering the tumor burden in a primary lewis lung carcinoma (LLC) model when targeting VEGFR-1 and DII4. Additionally, Fehring et al.[24] using Silence Therapeutics DACC liposomal formulation

containing Atu-FECT, cholesterol and PEG-lipid greatly improved survival in an LLC model. Due to direct access to the lungs through the airway, this is the preferred route of administration for lung targeted delivery, though the mucosal barrier provides a challenge. Choi et al.[62] examined the effects of nanoparticle charge and size on the ability to be retained in the lung tissue following aerosol administration. This study showed that particles <34 nm and neutral in charge are rapidly cleared to the lymph nodes.

1.4 Modified nucleic acids and conjugates

1.4.1 Chemical and structural modifications of RNAi molecules and ASOs

Systemic administration of unprotected RNA molecules results in rapid degradation by serum nucleases and immune stimulation.[63-64] To improve the therapeutic potential of naked siRNA molecules, a common approach has been the chemical modification of ribose backbone to impart chemical stability, nuclease resistance, and charge neutralizing properties on the nucleic acid. These modifications are designed to increase nuclease resistance, reduce activation of the innate immune system, and improve pharmacokinetics to make the nucleic acid more drug-like.[65] Strategic implementation of these chemical modification has proved critical in advancing naked RNAi molecules and antisense oligonucleotides (ASOs) to the clinic.

Common modifications of the nucleic acid backbone are shown in Figure 1.4.1. Modifications of RNA at the 2'-hydroxyl position prevents hydrolysis and improves nuclease resistance, while also improving binding affinity[66] and sequence specificity to the target sequence. Particularly the 2'-OMe and 2'-F modifications are most often utilized in RNAi as these modifications are acceptable substrates for RISC, clinically translated nucleic acid therapeutics.

Several other modifications have also been employed in ASOs, which do not require loading into RISC to effectively change biology in the cell. In one example, conversion of the ribose backbone to the arabinonucleic acid (ANA), Kalota, et al. demonstrated that by inversion of the 2'-position has been shown to have increased cytosolic stability and silencing efficacy compared to unmodified DNA ASOs.[67]

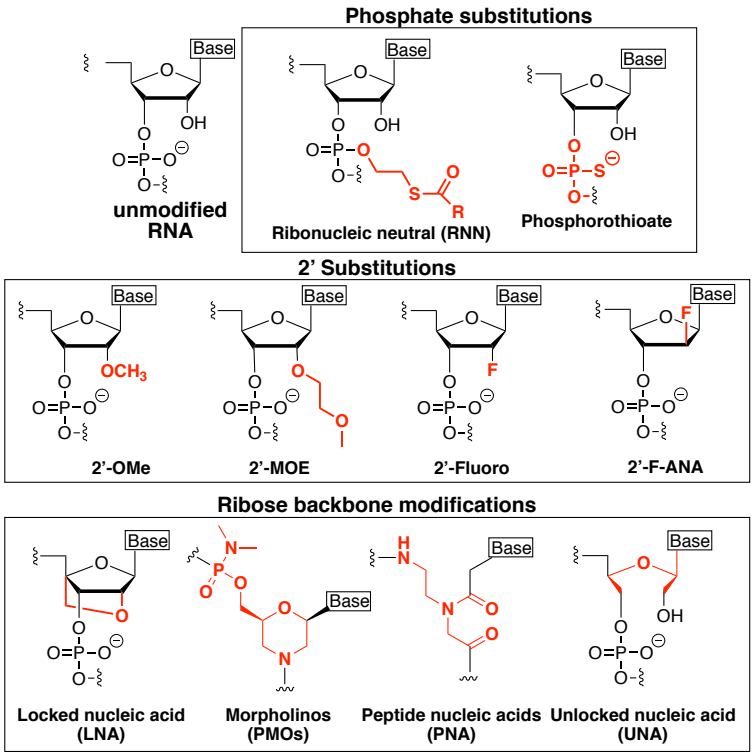

Figure 1.4.1 Some common nucleic acid modifications that protect RNAi and ASO molecules from nuclease degradation and impart more drug-like properties on the molecules.

The phosphodiester backbone is often manipulated in RNAi and ASO molecules to increase stability. Conversion of this moiety to a phosphorothioate (PS) is a common approach to increase nuclease resistance, often at the 3' and 5' termini. These modifications are commonly employed in ASOs and RNAi molecules, especially at the terminal nucleotide positions to prevent exonuclease degradation. Braasch, et al.[68] demonstrated that PO/PS heteroduplexes were more

stable than PO/PO duplexes in the presence of 50% mouse serum *in vitro* without changing the pharmacokinetic properties. Nusinersen (Spinraza, IONIS pharmaceuticals) is an FDA approved single-stranded ASO that employs a combination of 2'-MOE and PS linkages for the treatment of spinal muscular atrophy (SMA) via intrathecal injection.[69] Another modification of the PO linkage was reported by Meade, et al.[70] where the PO linkages of 2'-OMe and 2'-F modified dsRNAs were converted to a charge-neutral phosphotriester bearing a thioester, termed short interfering ribonucleic neutrals (siRNNs) with improved albumin binding, and *in vivo* hepatocellular silencing of apolipoprotein B (ApoB) mRNA when appended with a liver targeting ligand. This technology is being developed by Solstice Biologics for clinical translation.

Another strategy for RNA stabilization via chemical modification is transformation of the ribose backbone. Peptide nucleic acids, in which the ribonucleic backbone is converted to a dipeptide, which is achiral, chemically stable, able to function in antisense applications by steric inhibitition of translation.[71-72] In a locked nucleic acid (LNA), which increases the structural rigidity the 2'- and 5'- and raises the binding affinity. LNA analogs of RNA are currently being explored by Regulus Therapeutics, who are utilizing this technology to target miRNAs that are upregulated in the kidney diseases Alport syndrome (miR-21) and autosomal dominant polycystic kidney disease (miR-17).[73-75] Conversion of the ribose backbone to a phosphorodiamidate morpholino oligomer (PMO) which are not natural substrates for nucleases[76] and has been implemented in the clinic as eteplirsen (Sarepta Therapeutics) for the treatment of Duchenne muscular dystrophy (DMD) using exon-skipping.[77-79] Lu-Nguyen et al.[79] demonstrated that systemic administration (10 mg/kg for 10 weeks) of a combination of PMOs conjugated to cell-penetrating arginine-rich B peptide (BPMOs) that targeted both dystrophin for exon-skipping and

myostatin pre-mRNA resulted in a rescue of dystrophin expression across all tissues and dramatic therapeutic effects in an *mdx* mouse model.

Unlocked nucleic acids (UNAs), originally developed by Marina Biotech,[80] are formed when the 2'-3' bond of the ribose backbone is cleaved resulting in an acyclic structure. These nucleic acids exhibit both potent on-target silencing reduced off-target silencing. UNA substitution was well-tolerated in the 3'-overhangs of both the passenger and guide strand of siRNA, while UNA substitution at the 5'-terminus of the passenger strand promotes strand specific silencing. UNAs are currently being clinically developed by Arcturus Therapeutics in a number of partnerships in its lipid-enabled and UNA modified RNA (LUNAR) delivery platform for both RNAi and messenger RNA delivery. The cationic lipid component of the LUNAR platform comprises a two-tailed species linked to a dialkyl tertiary amine via an S-thiocarbamate bridge.[81] Yanagi et al.[82] demonstrated reduced tumor size in a xenograft model of colorectal cancer following systemic LUNAR delivery of PCTAIRE1 siRNA, while systemic administration of miR-124 to a murine model of glioblastoma produced a pronounced survival benefit by stimulation of antitumor immune response.[83]

1.4.2 RNA duplex conformations for RNAi therapeutics

In addition to chemical structure modifications that have been frequently explored, a number of approaches for modification of the structure of the RNA duplex have been investigated. These changes in combination with chemical modifications and protective formulations have enabled a variety of small nucleic acid modalities to be translated to the clinic. Traditional exogenous RNAi molecules, famously covered by the Tuschl I and Tuschl II patents[18-19] contain a two-nucleotide 3' overhang on both the sense (passenger) and antisense (guide) strand. These

overhangs are often converted to deoxyribothymidine (dT) to prevent exonuclease degradation, while maintaining RISC loading and potent silencing. The vast majority of RNAi-related research utilizes these structures, but a few other flavors of duplex structures have also been explored. AtuRNAi, a technology implemented by Silence Therapeutics[84-86] in clinical translation uses blunt-ended RNA to limit exonuclease degradation. The lead clinical candidate Atu027[86] was a liposomal formulation using the AtuFect01 cationic lipid, which with an AtuRNAi targeting kinase N3, in the vascular endothelium, which was evaluated for advanced solid tumors. This platform advanced to Phase I/II in Europe for pancreatic cancer, but no longer appears as part of Silence's research program. Dicerna has developed an asymmetric RNAi molecule termed Dicer substrate RNA (DsiRNA),[87] which is has the advantage of preferentially loading the antisense RNA strand to improve silencing outcomes. This technology was delivered by an undisclosed LNP by Dudek, et al.[87] to silence of β-cateninin and reduced liver tumor burden in a mouse model. As outlined above, ASOs and ssRNAs have already been clinically developed.

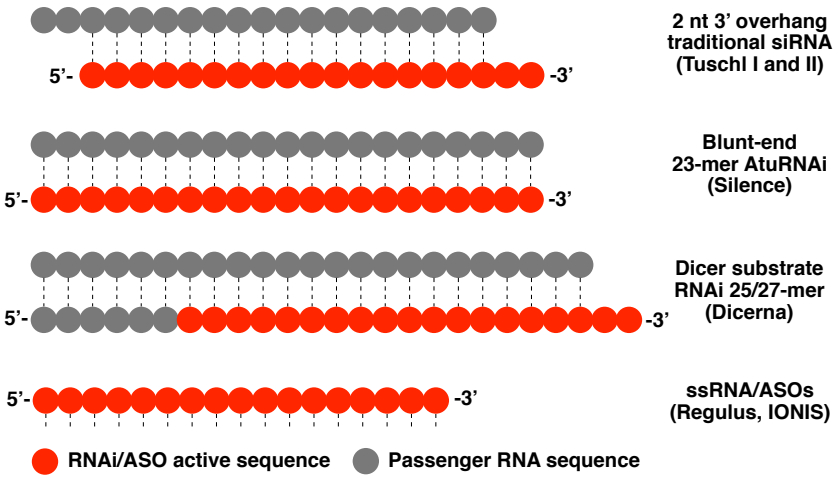

Figure 1.4.2. RNAi molecules can adopt a variety of conformations. Traditional siRNAs or miRNAs contain 2 nt 3' overhangs following processing by Dicer, while blunt-end and asymmetric molecules have also been explored.

1.4.3 Conjugates for siRNA delivery

siRNA conjugates are another extensively explored method in clinical development of nucleic acids.[88] These conjugates can function by promoting target specific organ accumulation or cell-type specific uptake, or endosomolytic siRNA release as in the case of the previously discussed dynamic poly conjugate platform. The conjugated siRNA can employ RISC-acceptable chemical modifications to maintain RNA integrity and silencing efficacy following systemic administration. Folic acid interactions with the folic acid receptor[89-90] and cRGD peptides which bind αvβ3 integrin, a marker for angiogenesis,[91-92] have been effectively exploited to target nanomedicines and siRNA conjugates various cancers. Hydrophobic conjugates have also been implemented to improve retention of siRNA in the brain.[93-94] Nikan et al.[94] reported increased retention of docosahexaenoic acid (DHA) conjugates following intrastriatal injection and increased silencing of Huntingtin mRNA compared to cholesterol conjugated analogs.

Meanwhile, the most widely utilized targeting ligand in nucleic acid delivery is the *N*-acetylgalactosamine,[95] which targets the ASGPr receptor in hepatocytes. Alnylam[95] reported a triantennary GalNAc ligand that greatly improved silencing efficacy in the liver (ED_{50} < 1 mg/kg). This targeting ligand platform has been clinically developed by Alnylam for a variety of indications in the liver including its since halted the development Revusiran for aTTR. Related approaches to appending the GalNAc ligand to siRNA and nanoparticles continue to be commercially developed by a number of other companies due to its potent liver-targeting capabilities.

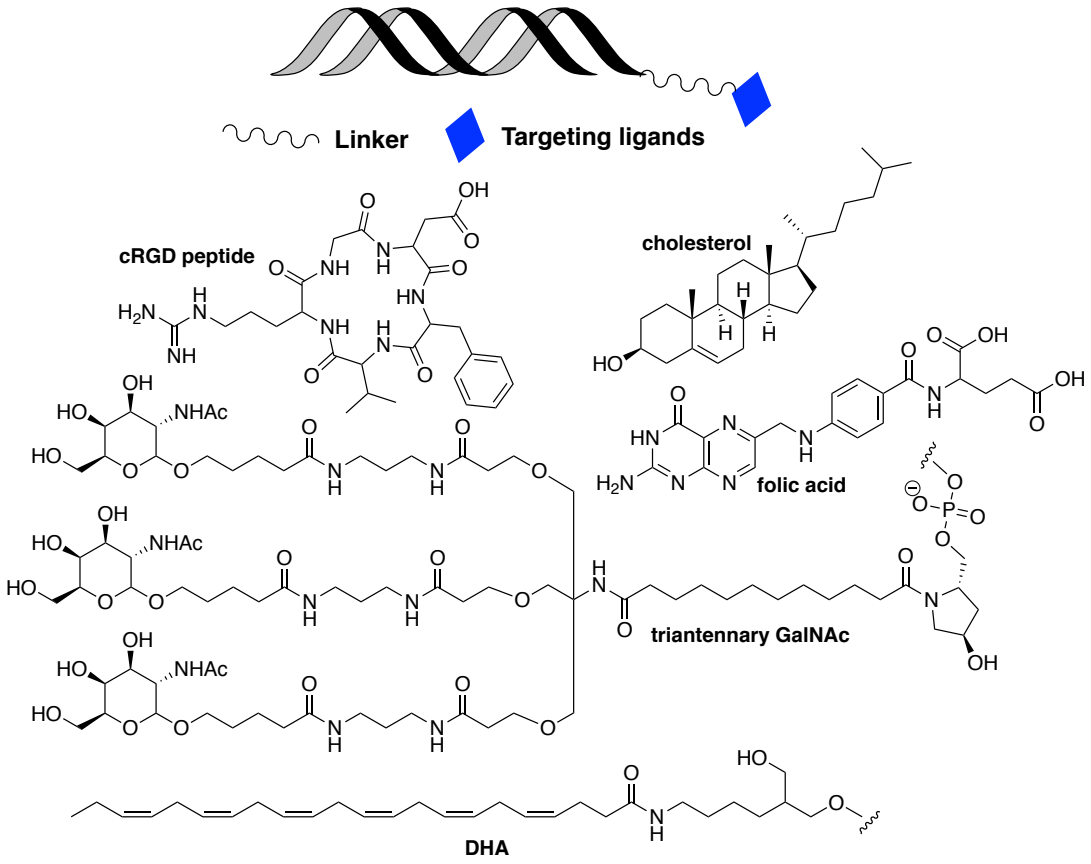

Figure 1.4.3 siRNA conjugates that have shown utility *in vivo*

1.4.4. Polymeric materials and conjugates for siRNA in the clinic

Although lipid nanoparticles are generally regarded as more potent for siRNA delivery, particularly to the liver, several polymeric systems for the delivery of therapeutic siRNA have been translated to the clinic for a variety of indications. CALAA-01 (Calando Pharmaceuticals) consists of a cationic cyclodextrin polymeric nanoparticle (~70 nm), which is stabilized by adamantly-PEG and utilizes transferrin to target malignant cells as the transferrin receptor is upregulated in many malignant cells.[96-97] This is the first example of a polymeric system for RNAi administered to

humans, which targeted silencing RRM2 in solid tumors, but the system did not clear Phase I clinical trials following administration to 24 patients.

Arrowhead has been developing its Dynamic PolyConjugate (DPC) systems,[98-99] which consists of a co-polymer of butyl and amino vinyl ether (PBAVE) backbone conjugated to an siRNA molecule through a cleavable disulfide linker, and a combination of PEG and galactose derivatives throughout the polymer. The galactose is capable of targeting the asialoglycoprotein receptor (ASGPr) in hepatocytes, and avoiding uptake by Kupffer cells, the macrophages that reside in the liver.[98] DPCs demonstrate good silencing of ApoB in mouse livers, albeit at 2.5 mg/kg siRNA dose, orders of magnitude behind some of the most efficient LNP systems. The DPC system is nevertheless appealing in its flexibility to append many different ligands to an endosomolytic backbone. Arrowhead was advancing its ARC-520 DPC siRNA treatment targeting HBV antigens in the liver, but a recent report by Woodell, et al.[100] described the mechanisms by which HBV burden can remain high in patients and non-human primates treated with nucleot(s)ide viral replication inhibitors (NUCs). Arrowhead has built an extensive research program around its DPC platform and is continuing its clinical development. Merck has also developed highly similar conjugate platform.[101]

Another type of polymeric platform for siRNA delivery in cancer is the local drug eluter (LODER), poly(lactic-co-glycolic)-acid siRNA depot being developed by Silenseed[102] for the selective silencing of mutant G12D KRAS, which is prevalent in pancreatic cancer. The LODER capsule can be injected into an inoperable tumor, and degradation of the PLGA scaffold results in the sustained release of therapeutic siRNA. This system led to prolonged survival in an aggressive

orthotopic pancreatic tumor model. Silenseed is currently recruiting for a Phase 2 clinical trial (NCT01676259) in combination with chemotherapeutics in unresectable pancreatic cancer.

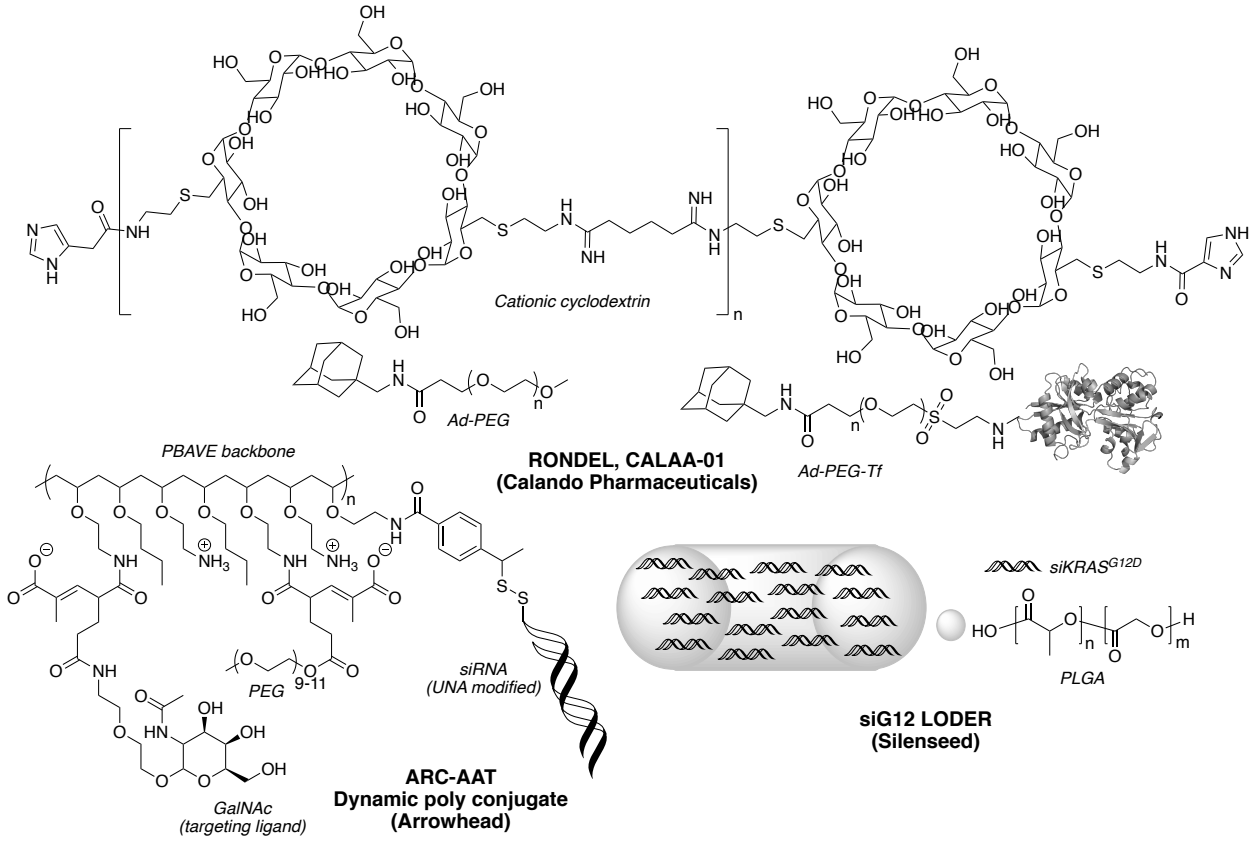

Figure 1.4.4. Polymeric materials for siRNA delivery that have been translated to the clinic.

1.5 Therapeutic Delivery of Messenger RNA (mRNA)

1.5.1 Materials for messenger RNA delivery

Messenger RNA represents a major emerging therapeutic modality which is currently being investigated in the clinic for a variety of indications including the development of vaccines against infectious diseases, immuno-oncology by the expression of tumor antigens on dendritic cells, and for protein replacement therapy in a variety of genetic diseases.[103-104] For functional

mRNA delivery to produce a protein, the single-stranded mRNA requires protection to prevent rapid degradation following systemic administration. mRNA has the distinct advantage over plasmid DNA and viral vector delivery in that following endosomal escape, the mRNA does not need to localize to the nucleus, thus rapidly producing protein upon endosomal escape. This phenomenon was capitalized on by Zangi, et al.[105] who injected human VEG-F mRNA with the commercial transfection reagent RNAiMax intramyocardially to direct differentiation of heart progenitor cells in a mouse model of myocardial infarction. This study demonstrated pulse-like expression of the following chemically modified mRNA delivery, and reduced infarct size compared to a pDNA encoding the same protein. Furthermore, there is no opportunity for mRNA to integrate into the genome, which eliminates a safety concern for pDNA and viral vectors for protein replacement, and the protein expression is more short-lived, which is advantageous, such as in the case of an exogenous nuclease (i.e. Cas9) to reduce potential off-target effects of gene-editing.

A variety of synthetic materials have been investigated for the non-viral delivery of mRNA *in vivo* (Figure 1.5.1). Due to the high cost of quality commercial mRNA (~$1500 per mg), large library screening approaches, which is the typical approach to identify small-RNA delivery vehicles, can be cost-prohibitive. Thus, two main strategies for identifying robust materials for mRNA delivery have emerged: 1) the reformulation of potent cationic lipids to make the nanoparticle more amenable to stabilizing the long sequence of mRNA, and 2) using existing scaffolds as inspiration for SAR to make changes that facilitate delivery.

1.5.2 Materials for mRNA delivery by reformulating potent small RNA carriers

Using a reformulation strategy, Kauffman, et. al[106] optimized the lipid composition of C12-200 LNPs, which are potent in delivering siRNA to hepatocytes in non-human primates,[1] for mRNA delivery. The optimal formulation for siRNA was 5:1 weight ratio C12-200:siRNA, 50:38.5:10:1.5 molar ratio of the lipid mix containing C12-200: cholesterol: DSPC: PEG-lipid. Following multiple rounds of fraction factorial design, the optimal formulation for *in vivo* mRNA delivery for was identified as 10:1 wt ratio, 35:46.5:16:2.5 molar ratio C12-200: cholesterol: DOPE: PEG-lipid emerged. The increased content of zwitterionic lipid suggests that this moiety may be important for stabilizing the long mRNA sequences, which be discussed below. Further development of C12-200 LNPs by Yin et al.[107] for the *in vivo* delivery of Cas9 mRNA, which is considerably larger than erythropoietin (EPO) or luciferase, involved further increasing the weight ratio and also the introduction of arachidonic acid as an excipient, although no further explanation was provided. The formulation parameters developed by Kauffman were applied to cKK-E12 for the co-delivery of Cas9 mRNA and modified sgRNA by Yin,[108] which resulted in potent *in vivo* gene editing.

A number of publications have reported the use of the SNALP MC3 for the delivery of mRNA for therapeutic purpose. Unlike other platforms, MC3 has been efficacious using an LNP formulation that was optimized for siRNA, although specific details are limited. Thess et al.[109] reported successful administration of EPO mRNA in pigs and delivery with meaningful physiological response of an increase in reticulocyte count to non-human primates. Ramaswamy et al.[81] reported the therapeutic delivery of human factor 9 mRNA (hFIX) to a mouse model of FIX deficient hemophilia B using the Arcturus LUNAR platform with its ATX lipid in head-to-head

comparison with DLin-MC3-DMA. The formulation conditions were 50:40:7:3 cationic lipid: cholesterol: DSPC: PEG-DMG, which interestingly contains considerably lower zwitterionic lipid content compared to those implemented in the optimization of the lipidoid formulations for mRNA delivery. In this assay, ATX outperformed MC3 two-fold in the delivery of FIX protein. Interestingly, the structure of the ATX lipid is almost identical to the third generation SNALP L319 (Figure 1.5.1), with the substitution of the ester group of L319 with a carbamothioate group, and shortening the spacer from three to two carbons.

1.5.3 Development of New Materials for mRNA delivery by structural modification of effective materials for small RNA delivery

A number of compounds for mRNA delivery have been developed by using potent siRNA carriers as chemical scaffolds for structure optimization. Fenton et al.[110] modified the cKK-E12 scaffold, which showed effective mRNA delivery, and highly potent siRNA delivery to the liver, to introduce two unsaturated bonds in the lipid tails, similar to the evolution of SNALPs, which led to the identification of OF-02. OF-02 LNPs showed a spherical multilamellar nanostrucuture, and improved expression in the liver compared to cKK-E12. Further structural expansion resulted in OF-Deg-Lin,[111] which introduced an ester bond which shifted the *in vivo* expression profile from exclusively in the liver to the spleen, highlighting the drastic impact that structural modifications on synthetic materials can have.

Li et al.[112] reported a class of materials with a phenyl ring core, which is not prevalent in the small RNA delivery among efficacious materials. The library explored the spacing between the tertiary amino groups and the benzamide moieties, where TT3-LLN emerged as a lead compound. Interestingly, when formulated with various phopsholipids for *in vitro* delivery, DOPE

was the most phospholipid compared to DOPE and POPE. Meanwhile, TT3-LLN was effective in protein replacement in FIX knockout mice and for non-viral gene editing *in vivo*.[113] Li et al.[114] explored the effects of local spacing around a core trazinane trione (TNT) ring. TNT-a_{10} was previously reported to effectively deliver siRNA and pDNA,[115] while swapping the positions of the tertiary amine and secondary alcohol relative to the TNT ring to form TNT-b_{10} resulted in improved mRNA delivery, and efficient expression in the spleen in mice.

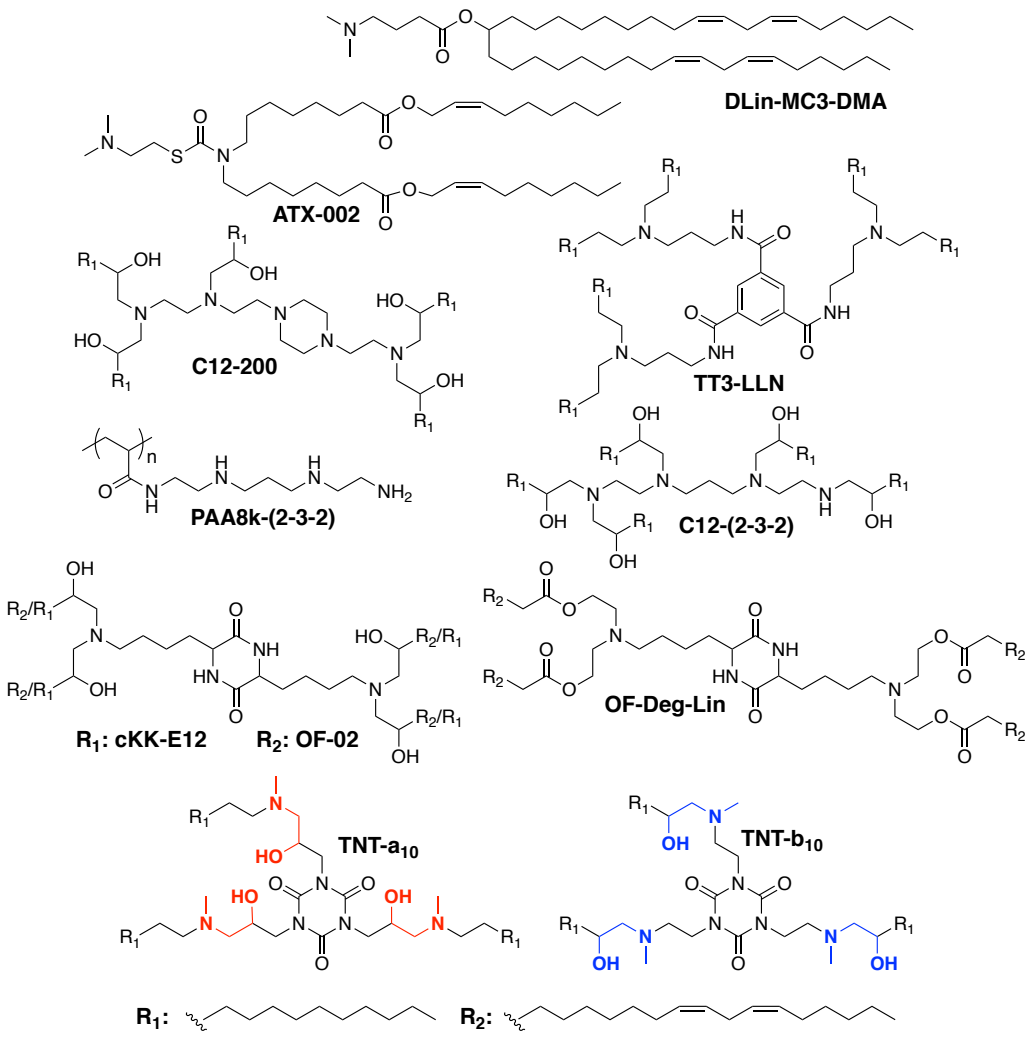

Figure 1.5.1 Materials that have shown *in vivo* efficacy for messenger RNA delivery via improvement of the formulation or the modification of the chemical structures.

Jarzebinska et al.[116] reported a small library of polymers and lipids based on linear oligoalkylamines which have been effective cores for small RNA delivery, including work done in the our lab (5A2-SC8).[6] Modifying a poly(acrylic acid) backbone with a small library of oligoalkylamines with discrete carbon spacing between amine groups resulted in the identification of PAA8k-(2-3-2) which was significantly more effective that other structural analogues (2-2-2) and (3-3-3) for mRNA delivery. This system was also utilized for mRNA delivery to porcine lungs following aerosol delivery. Meanwhile, synthesis of a cationic lipid using this (2-3-2) amine as a core to react with epoxydodencane resulted in an effective lipid-like material for *in vivo* delivery to the liver.

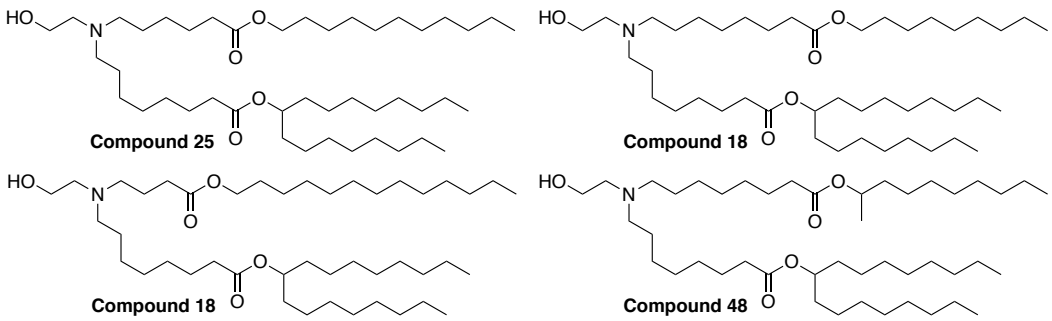

Table 1.5.1

Compound	Dh.nm	PDI	Binding (%)	pKa	Luc Fold-MC3*	EPO Fold-MC3*	EPO Fold-MC3**	% Lipid remaining in liver^
18	86.2	0.042	97.5	6.56	3.22	8.6	0.81	0.018
25	85.8	0.10	95.8	6.68	1.89	7.1	2.13	1.32
26	91.9	0.16	97.43	6.64	4.24	-	4.95	20
48	82.3	0.092	96.55	6.68	10	-	3.84	7.22
MC3	79.7	0.11	97.3	n.d.	1	1	1	87
*I.V. administration mouse, 0.5 mg/kg mRNA 6h; **2 mg/kg rat; ^I.V. administration rat, 2 mg/kg mRNA, 48h								

Figure 1.5.2. Degradable synthetic lipids developed by Moderna show improved mRNA expression *in vivo* in rodent models, compared to MC3 lipid, considered the best-in class, while much faster liver clearance. **Table 1.5.1** shows particle and expression data extracted from Bennenato et al. [3] Moderna Therapeutics patent.

Moderna Therapeutics[3] also recently released a systematic comprehensive study in a patent which reported a large library structurally related lipids for mRNA delivery which are formulated using a classic LNP formulation (50:38.5:10:1.5 ionizable lipid: cholesterol: DSPC or DOPE: PEG-lipid molar ratio). The lead four compounds from that study are shown in Figure 1.5.2 and expression data in a variety of animal models in comparison to MC3, the current clinical benchmark, was also shown. The lead materials showed increased expression compared to MC3, but of note, following 48h, Moderna reports an 87% retention of MC3 lipid in the liver. Meanwhile these new compounds are rapidly degraded within hours. The lead compound from this study compound 25, was utilized by An et al.[117] for the therapeutic delivery of hMUT mRNA to the liver for the treatment of methylmalonic academia, and showed a pronounced survival benefit.

1.5.4 Chemical modifications on mRNA and their effects on expression and stability

The therapeutic delivery of mRNA requires the preparation of high quality material in a controlled manner. Unlike small RNA, due to the large size of messenger RNA (> 1000 nt) these molecules have been prepared enzymatically by *in vitro* transcription. Several design considerations including chemical structure and sequence have been explored.

The 5'-cap 7-methylguanosine (m7G) cap, which incorporates a 5'-5' triphosphate linkage is a critical structural motif as this site is recognized to initiate translation, in addition to preventing degradation by 5'-exonucleases.[118] mRNA prepared by *in vitro* transcription is capped typically with Cap 0 post transcriptionally or co-transcriptionally using anti-reverse cap analog (ARCA). Subsequent methylation of Cap 0 to Cap 1 primers mRNA for translation following administration to the cell. Novel cap analogs have been developed by BioNTech which have shown favorable *in*

vitro functional properties. Notably, introduction of a phosphorothioate group at the β position increased affinity to the translation initiating protein eIF4E, showed resistance to decapping enzyme Dcp2, doubled mRNA half-life in cells, and improved translational efficiency five-fold following electroporation.[119-120] Conversion of the β phosphate of a traditional cap analog (m^7GpppG) to a boranophosphate resulted in two-fold increase in total protein expression of electroporated luciferase mRNA.[104]

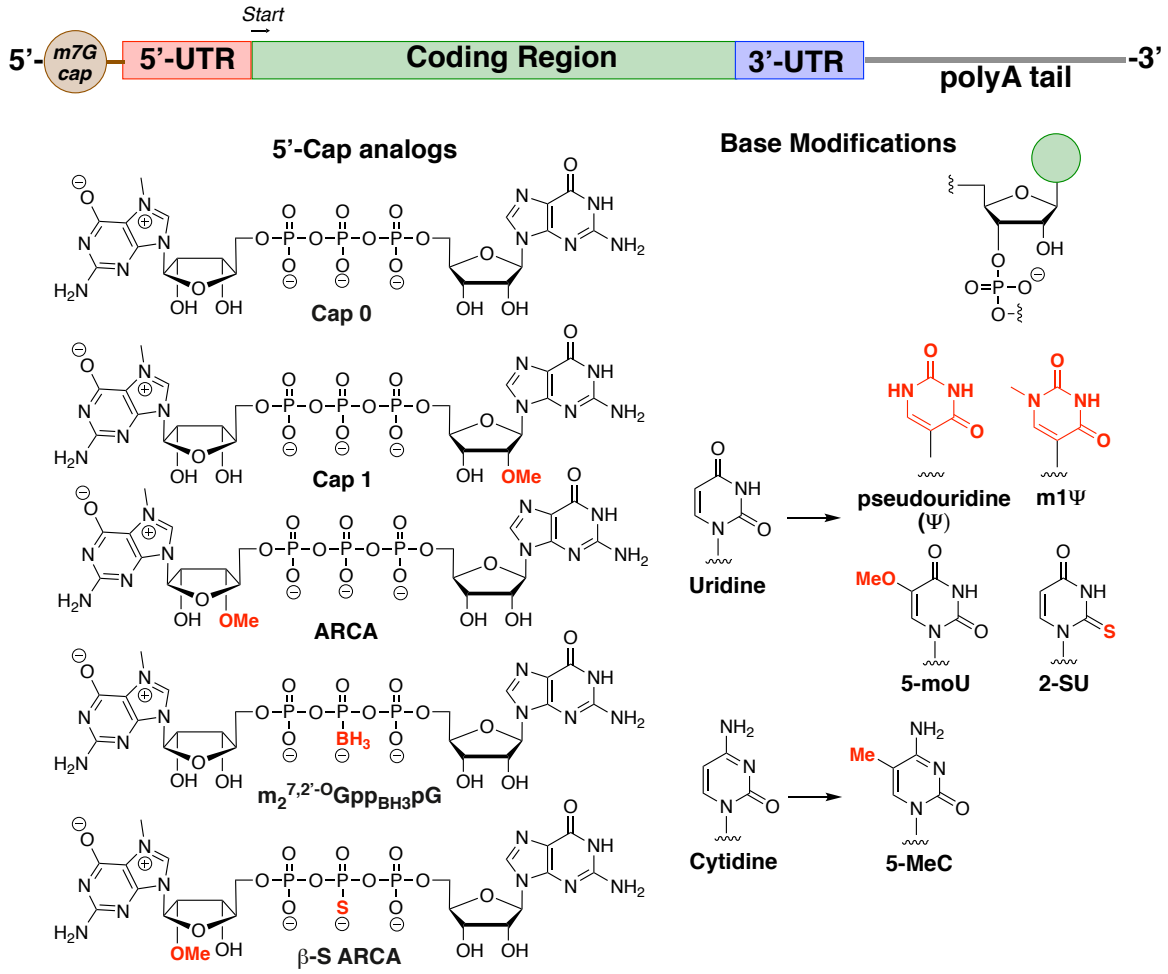

Figure 1.5.3. Cap analogs and nucleobase modifications that have shown improvements over wild-type mRNA expression and immune stimulation.

Similar to RNAi molecules, chemical modifications of nucleobases in mRNA are also suitable and may confer decreased immunogenicity, improved stability, and translational efficiency following delivery. The most common nucleobase modifications are replacement of uridine with pseudouridine (Ψ)[121-124] and cytidine with 5-methyl cytidine, which has been claimed to reduce innate immune response that is known to be activated by RNA molcules. Li, et al.[125] using LF2000 transfection of mRNAs observed that Ψ, 5-methoxyuridine (5-moU), and and N^1-methylpseudouridine (m1Ψ) demonstrated increased expression of eGFP and FLuc mRNA, but the results were highly cell-type and sequence dependent. Additionally, 5-meC did not show improved expression in this system, while 5-moU showed improved intracellular mRNA stability as evaluated by RT-PCR compared to other modifications. Svitkin, et al.[126] also reported improved translation of m1Ψ modified mRNA in cell free *in vitro* translation assays by reducing the immune stimulatory phosphorylation of eIF2α which inhibits translation, and by increasing the ribosome density on the transcript. Kauffman, et al.[123] used mRNA-optimized C12-200 LNPs for hepatocellular of uridine and pseudouridine modified mRNAs to assess the effect of this modification on pharmacokinetic properties and the immune response. This paper was an effort to reconcile contradictory reports in the literature on the effect of pseudouridine modification. While the nanoparticle properties were unaffected by this structural change, *in vivo* expression and cytokine and chemokine activation profiles were similar for both mRNA species, suggesting that this modification may not be necessary for clinical translation. However, fine differences in underlying biology in terms of expression profiles indifferent cell and tissue types, in addition to effects in the mRNA sequences will likely have a cooperative effect on mRNA expression.

Another common strategy for improving the efficacy of exogenous mRNA is codon optimization, in which has been widely used in the pharmaceutical industry in development of mRNA therapeutics.[109, 117, 127-128] This strategy is based on the concept of reducing rare codons in favor of common codons, as ribosomal translation of the message through these sites will be more efficient, while codon substitution will have no effect on the translational outcome.[127] In a collaboration between CureVac and Acuitas, Thess et al.[109] compared sequence optimization versus chemical modification for the intraperitoneal delivery of erythropoietin (EPO) mRNA *in vivo* using TransIT, a lipopolymeric commercial carrier from Mirus Bio. This study demonstrated that sequence-engineered, unmodified EPO mRNA showed increase expression in mice compared to Ψ-modified analogs, and these codon-optimized sequences were successfully delivered to pig and non-human primate models using SNALPs with strong sustained multi-day expression of EPO detected in serum. Both chemically modified and codon optimized approaches are being explored for clinical translation for the non-viral delivery of therapeutic messenger RNA.

1.6 CRISPR/Cas gene editing

1.6.1 A brief overview of CRISPR biology

CRISPR/Cas technology is an incredibly powerful gene-editing tool that can introduce permanent changes to the genome and can be readily modified for any target in the genome, provided there is a nearby 3-base sequence (NGG) known as a protospacer adjacent motif (PAM).[129-133] Cas9 is an RNA-guided nuclease that uses a 100 nt ssRNA called a single-guide RNA (sgRNA) to scan the genome in a sequence specific way and created a double strand break (DSB) in the genomic DNA in the locus to which the 20-nt RNA sequence is complimentary to the

genome. Following this occurrence, error-prone DSB-repair pathway non-homologous end-joining (NHEJ)[134] can insert or delete bases from the site of repair (indels), resulting a frameshift of the target gene. With the addition of a DNA template that has homology to the genomic region flanking the DSB site, homology-directed repair (HDR)[135] can occur to enable precision genome editing. Unlike RNAi, where the functional protein machinery is endogenous to the mammalian cell, Cas9 is a bacterial protein, and must be introduced to the cell. Strategies for doing so effectively include encoding Cas9 in a plasmid, in a viral particle, or the delivery of a ribonucleoprotein complex directly.[136]

Another favorable approach of great interest is the delivery of the Cas9 protein encoded as a messenger RNA, as this provides an improved safety profile compared to pDNA and viral delivery, which can result in integration into the genome and sustained expression of a powerful nuclease in the cell. Additionally, mRNA delivery may provide less of a challenge than RNP delivery due to the large size of the Cas9 protein (~160 kDa). Compared to other approaches to genome engineering, CRISPR/Cas has the distinct advantage of simplicity by being able to change the target by simply changing the sgRNA sequence. In the advent of the era of mRNA medicines, the non-viral delivery of CRISPR/Cas components offers an appealing target for the rapid development of a variety of treatments and potentially cures for a diverse range of clinical targets.[137] Co-delivery of Cas9 mRNA and sgRNA via a nanoparticle faces similar extracellular barriers compared to other nucleic acid carriers, but there are other inherent challenges to this system. If the sgRNA and Cas9 mRNA are delivered in a single particle, both RNAs will escape the endosome, while the sgRNA must remain stable in the cyotsol until the Cas9 has been translated. Following loading of the sgRNA into the Cas9 to form the RNP, the complex must

translocate to the nucleus to scan the genomic DNA. As a result, sequential delivery of Cas9 mRNA in advance of guide RNA has been investigated.[113]

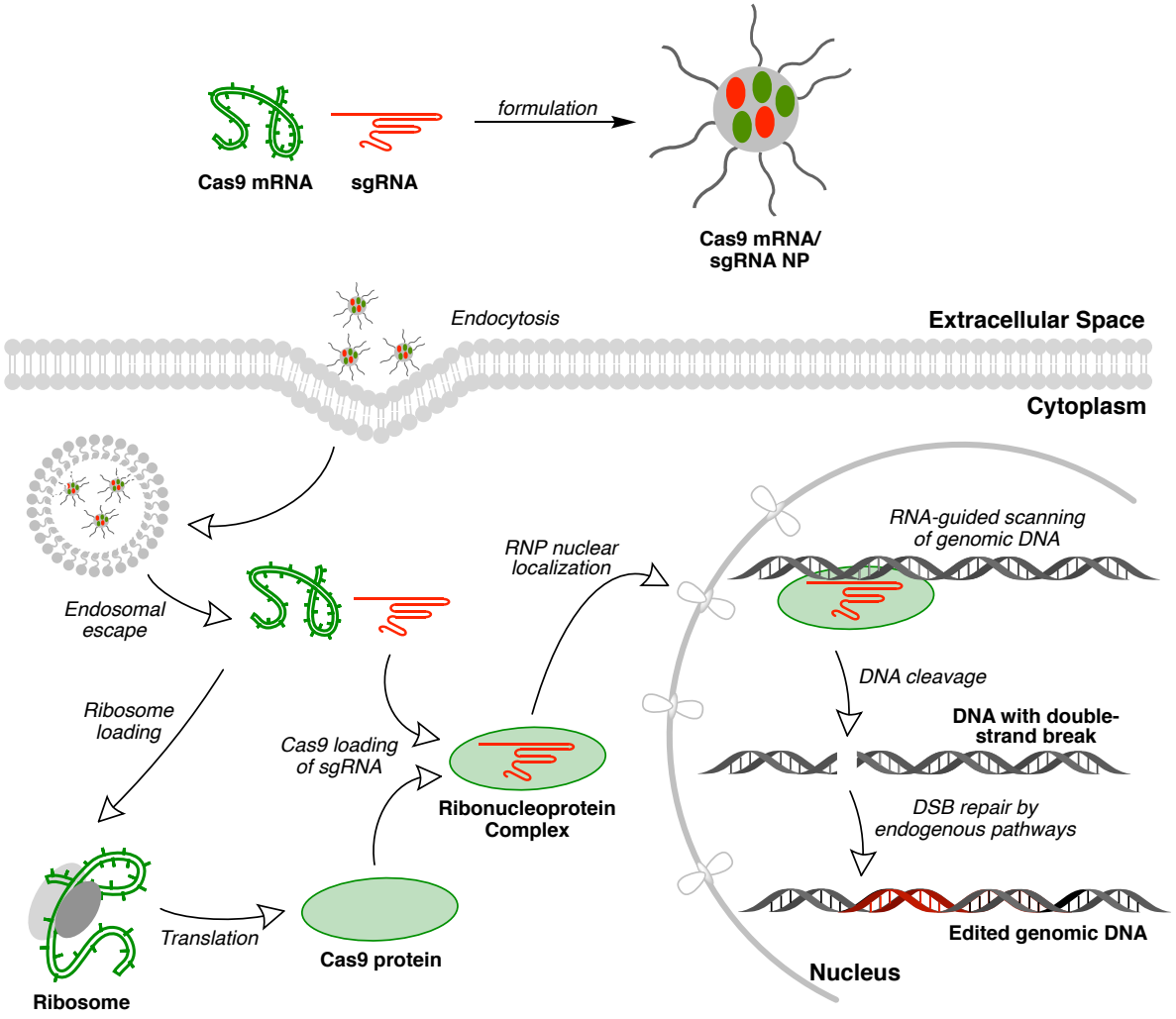

Figure 1.6.1. The intracellular challenges of non-viral gene-editing using co-delivery of mRNA and sgRNA.

1.6.2 Materials for non-viral gene-editing by mRNA delivery

Despite the challenges associated with co-delivery of Cas9 mRNA and sgRNA, a number of approaches have been developed for the non-viral gene-editing using mRNA, in addition to work that we have published, which was the first report of non-viral gene editing *in vivo* by co-

delivery of Cas9 mRNA and sgRNA in a single nanoparticle.[138] Yin et al.[107] used a combination of C12-200 LNPs to deliver Cas9 mRNA and AAV encoding sgRNA and an HDR repair template to rescue the expression of fumarylacetoacetate hydrolase (Fah) in knockout ($Fah^{-/-}$) in mice. A 6% correction was sufficient for a pronounced survival benefit in this model. Jiang et al.[113] utilized the TT3-LLN system to deliver Cas9 mRNA and sgRNA against PCSK9 and HBC, two important therapeutic liver targets. Editing was performed by sequential injection of LLNs encapsulating Cas9 mRNA, following by LLNs encapsulating sgRNA 6h later at the peak of *in vivo* Cas9 protein expression using this system, and was observed to be ~30% after 48h treatment.

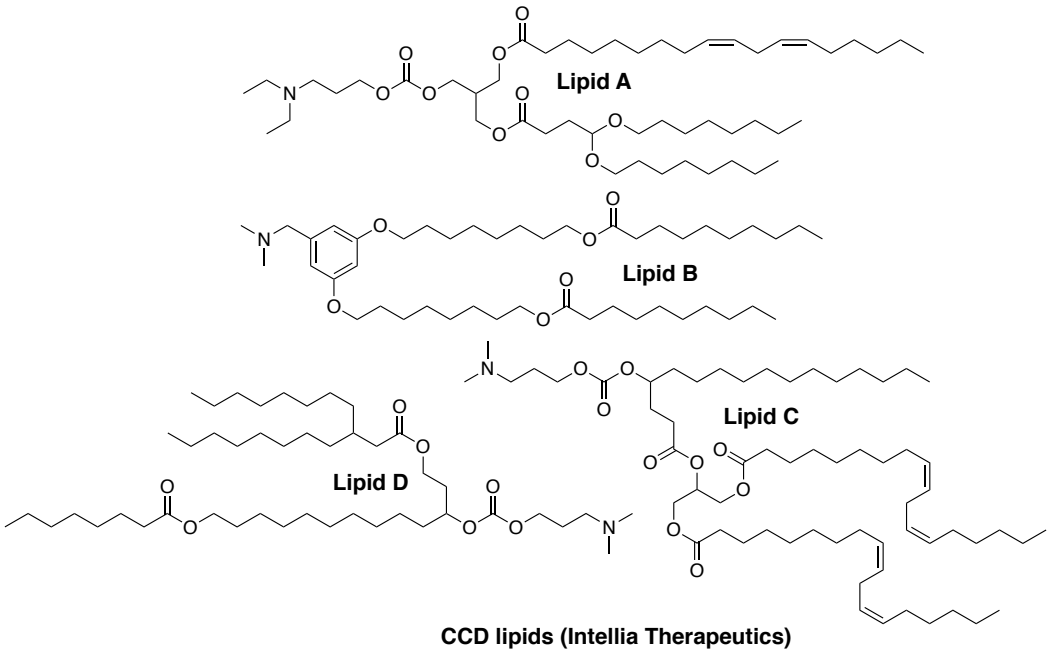

Figure 1.6.2. Intellia Therapeutics CCD lipids have shown utility for Cas9 mRNA and sgRNA co-delivery.

Recently, Yin et al.[108] reported the optimized chemical modification of sgRNAs for improved activity *in vitro* and *in vivo*. Using *in vitro* experiments and guided by key interactions within the Cas9/sgRNA crystal structure, the authors identified introduced sites for 2'-OMe, 2'-F and PS linkage chemical modifications along the sgRNA sequence. The optimal scaffold, termed

e-sgRNA, led to significant increases in editing efficiency both *in vitro* and *in vivo*. Using cKK-E12 LNPs encapsulating e-sgRNA and Cas9 mRNA (though it is unclear if the RNAs are mixed and formulated together, or if they are formulated separately and injected together), the authors observed 50-60% indels in the liver when targeting PCSK9, Fah, or the ROSA26 locus, which was much higher activity compared to unmodified sgRNA targeting the same sequence. This key advance may play a major role in directing future approaches to non-viral gene editing with CRISPR.

Intellia Therapeutics has also reported a new class of lipids termed CCD lipids[139] which are effective at co-delivering Cas9 mRNA and sgRNA together. Of note, there are striking similarities between the CCD lipids and the mRNA delivering materials described by Moderna[3] for mRNA delivery, regarding the asymmetry of three hydrophobic tails. The CCD lipids are reported to be effective in editing genes in the liver up to 60% using certain formulations, while also rapidly cleared.

1.7. Outlook

There is a need to develop new nanocarriers for the effective delivery of nucleic acids to organs other than the liver. This survey of the literature has provided insight into the materials designs currently in exploration for the delivery of small RNA, long RNA and gene-editing components, while there is an obvious need in the field of nanomedicine to exhibit control over organ localization. The design and synthesis of new materials with utility in nucleic acid delivery one approach to address this concern, to allow researchers to harness the terrific powers of controlling biology using nucleic acids.

CHAPTER TWO
ZWITTERIONIC AMINO LIPIDS, A NEW CLASS OF MATERIALS FOR *IN VIVO* mRNA DELIVERY AND NON-VIRAL GENE EDITING

2.1 INTRODUCTION

The CRISPR/Cas (clustered regularly interspaced short palindromic repeat / CRISPR-associated protein (Cas)) technology can edit the genome in a precise, sequence dependent manner, resulting in a permanent change.[130, 133, 140-142] Because of the ability to target disease causing mutations, it holds incredible promise for one-time cures of genetic diseases. To date, successful editing has been mediated mainly by viral vectors, which require laborious customization for every target and present challenges for clinical translation due to immunogenicity, generation of antibodies that prevent repeat administration, and concerns about rare but dangerous integration events. There remains a clear need to accomplish CRISPR/Cas editing via synthetic nanoparticles (NPs) to expand the safe and effective applications of gene editing.

CRISPR/Cas enables sequence-specific DNA editing by the RNA-guided CRISPR-associated protein 9 (Cas9) nuclease that forms double-strand breaks (DSBs) in genomic DNA. Cas9 is guided by programmable RNA called single guide RNA (sgRNA).[130] The Cas9/sgRNA complex recognizes the complementary genomic sequence with a 3' protospacer adjacent motif (PAM) sequence. Following DNA cleavage, DSB repair pathways enable directed mutagenesis, or insertions / deletions (indels) that delete the targeted gene.[12, 143-146] For therapeutic utility, transient Cas9 expression is preferred to limit off-target genomic alteration. Because both Cas9 protein and sgRNAs must be present in the same cells, co-delivery of Cas9 mRNA and sequence targeted sgRNA in one NP is an attractive method, particularly for *in vivo* use where tissue

penetration and cellular uptake is more challenging. CRISPR/Cas editing using viruses,[9-12, 144] membrane deformation,[147] ribonucleoprotein complex delivery,[148-150] and hydrodynamic injection[145] are functional, but have limitations that could hinder *in vivo* therapeutic use in the clinic, including persistent expression of Cas9 and off target editing.

Although great advances have been made in the delivery of short RNAs (siRNA, miRNA) (~22 base pairs (bp) in length) by lipid nanoparticles (LNPs),[14] the ideal chemical and formulation composition is largely unknown for longer RNA cargo (mRNA, sgRNA). Highly effective LNPs are composed of a cationic lipid, zwitterionic phospholipid, cholesterol, and lipid poly(ethylene glycol) (PEG). Cationic lipids bind RNAs at low pH during mixing, and promote intracellular release as the pH decreases during endosomal maturation.[30, 32] Computational modeling has shown that phospholipids function by solubilizing small RNAs inside of aqueous pockets within multi-component LNPs.[38] High cationic lipid density may thus minimize phospholipid stabilizing interactions with longer RNAs in LNPs. Cationic lipids also take up space within LNPs and could minimize interactions with longer RNAs at pH 7.4. Recent reports on mRNA delivery using alternative helper phospholipids (e.g. DOPE) further suggests that associated solubilizing forces may improve NP construction.[111, 116, 151-152] We therefore hypothesized combining the chemical and structural roles of zwitterionic lipids[53, 58-59, 153] and cationic lipids[13, 27-28, 111] into a single lipid compound might improve delivery of longer RNAs by increasing molecular interactions within the LNP.

In this chapter, we report the development of a new class of lipid-like materials termed zwitterionic amino lipids (ZALs) that are uniquely suitable for delivery of long nucleic acids, ~4,500 nucleotide (nt) Cas9 mRNA and ~100 nt sgRNAs, including co-delivery from the same

NP. ZAL nanoparticles (ZNPs) are able to effectively induce permanent DNA editing in cells. This approach simplifies CRISPR/Cas engineering because different sgRNAs can be easily designed, synthesized and packaged into these versatile synthetic carriers. Our publication on this topic was the first example of a successful non-viral system for *in vitro* and *in vivo* co-delivery of Cas9 mRNA and sgRNA to enable gene-editing.[138]

2.2 RESULTS AND DISCUSSION

2.2.1 Design and chemical synthesis of a library of Zwitterionic Amino lipids

Zwitterionic amino lipids (ZALs) were rationally synthesized to contain a zwitterionic sulfobetaine head group, an amine rich linker region, and assorted hydrophobic tails (Scheme 2.2.1). A zwitterionic electrophilic precursor (SBAm) was prepared by the ring-opening reaction of 2-(dimethylamino)ethyl acrylamide with 1,3-propanesultone, which was easily isolated by in situ precipitation in acetone. Conjugate addition of six symmetrical polyamines to SBAm afforded a series of zwitterionic amines with some structural diversity. The library design used key chemical motifs that are prevalent in many effective materials for small RNA delivery, namely N-methyl amines (ZA1, ZA4, ZA5) and piperazine rings (ZA6). Additionally, direct comparison of ZA1 and ZA2 allowed for evaluation of the steric bulk on the amine, while comparison of ZA4 and ZA5 allowed for evaluation of spacing of cationic charges in the zwitterionic materials. The number of available reactive amine sites for hydrophobic tail addition ranged from two to five, which enabled evaluation of the balance of hydrophobic and cationic content which is a critical balance for effective delivery materials. The zwitterionic amines were reacted with hydrophobic epoxides and acrylates to append 6 to 18 carbon alkyl tails and alcohol / ester groups to enhance

ZAL-RNA interactions. ZAL structures were confirmed by MALDI-TOF ms and ^{1}H NMR for select species (See 2.3 Materials and methods).

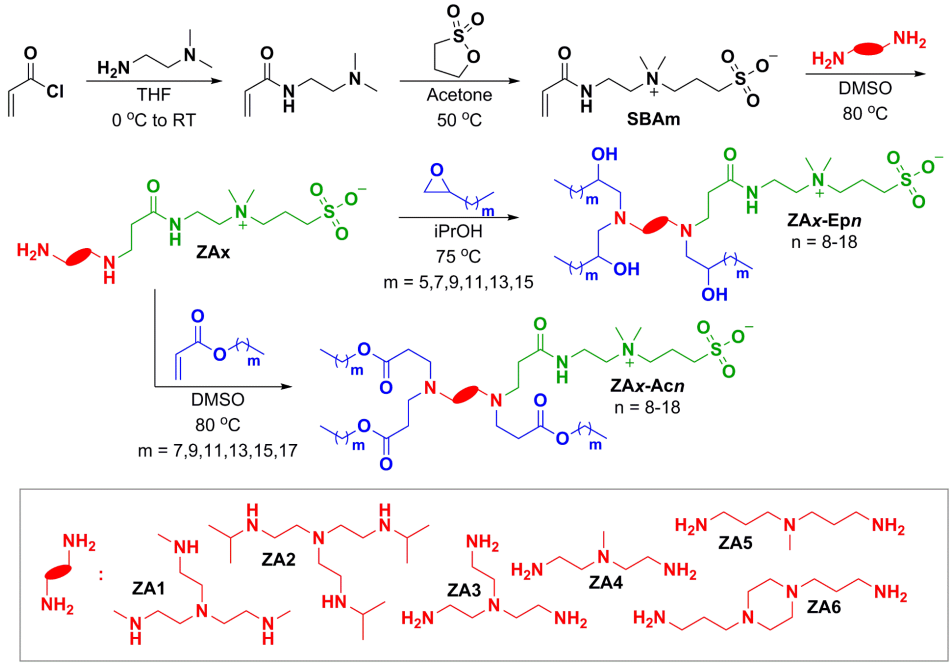

Scheme 2.2.1 ZALs were designed to increase molecular interactions with longer RNAs by combining the chemical and structural roles of zwitterionic lipids and cationic lipids into a single lipid compound. High efficiency reactions provided access to a library of unique charge unbalanced lipids. Reprinted with permission from Reference 138. Copyright 2016 John Wiley and Sons.

2.2.2 Evaluation of the ZAL library for siRNA delivery

To verify that ZNPs could generally bind and deliver RNA, the 72-member library was first screened for siRNA delivery to HeLa cells that stably expressed firefly luciferase (HeLa-Luc) (Figure 2.2.1). ZALs were formulated with cholesterol as a helper lipid to deliver siRNA against luciferase. This allowed structural identification of key amine cores, including ZA1, ZA3, and ZA6, and demonstrated a hit rate (>50% luciferase silencing) of 18%. ZA5 was also active, but showed higher toxicity than other amine cores. Regardless of tail structure, two-tailed species (ZA1 and ZA2) showed significantly lower delivery efficacy than amine cores with higher

numbers of tails, highlighting the importance of hydrophobicity in stabilizing nanoparticle interactions. Interestingly, epoxide-based ZALs (ZAx-Epn), were significantly more active than acrylate-based ZALs (ZAx-Acn), which can be easily observed when plotting the activity as a heat map (Figure 2.2.2). With lead compounds identified for siRNA delivery, focus was shifted to the delivery of sgRNAs and mRNA with a goal of enabling non-viral gene editing.

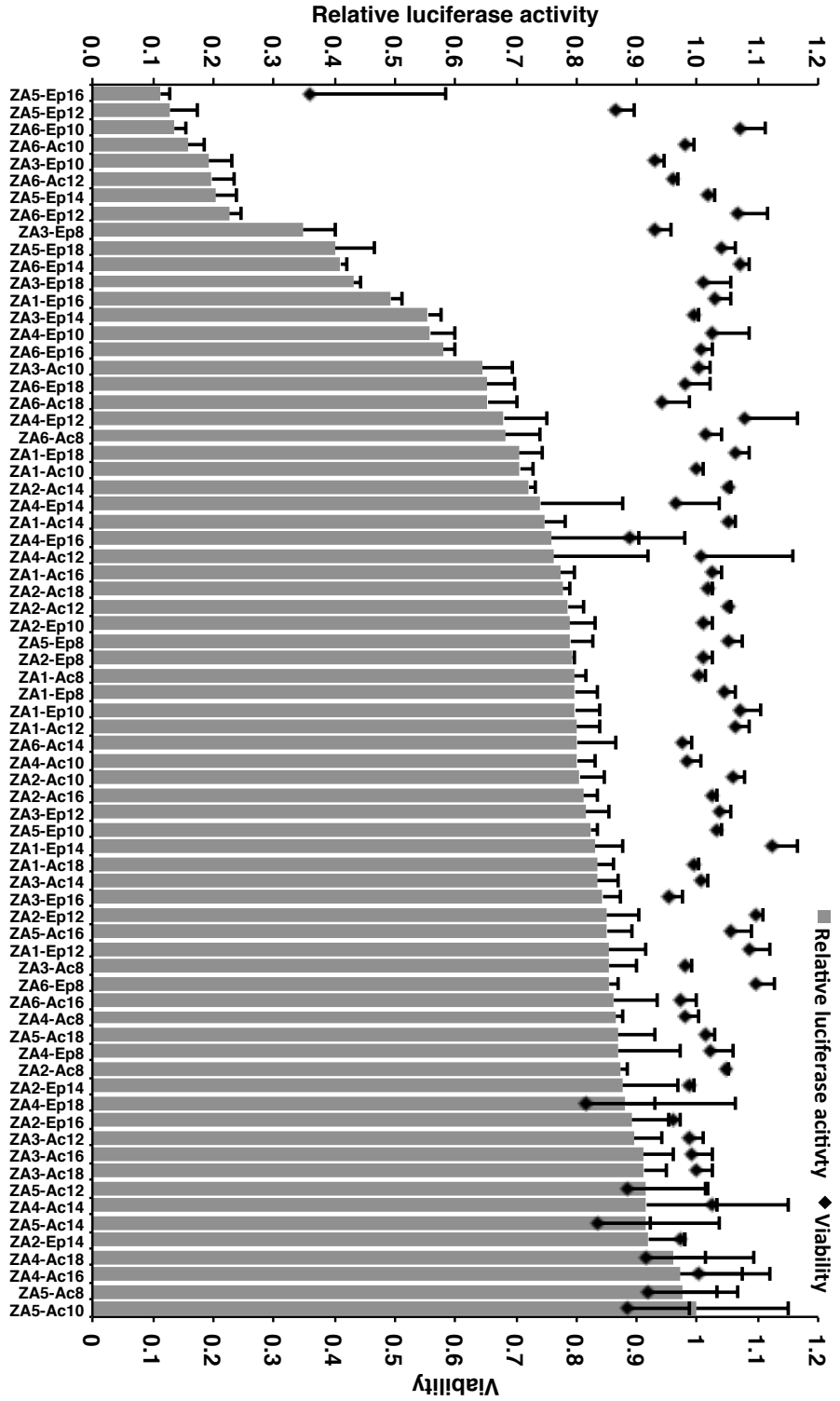

Figure 2.2.1. siRNA delivery to HeLa-Luc cells by the 72-member ZAL library. Cells were treated with 34 nM siRNA for 24 h and cell viability (dots) and relative luciferase activity (bars) were determined by normalizing to untreated cells.

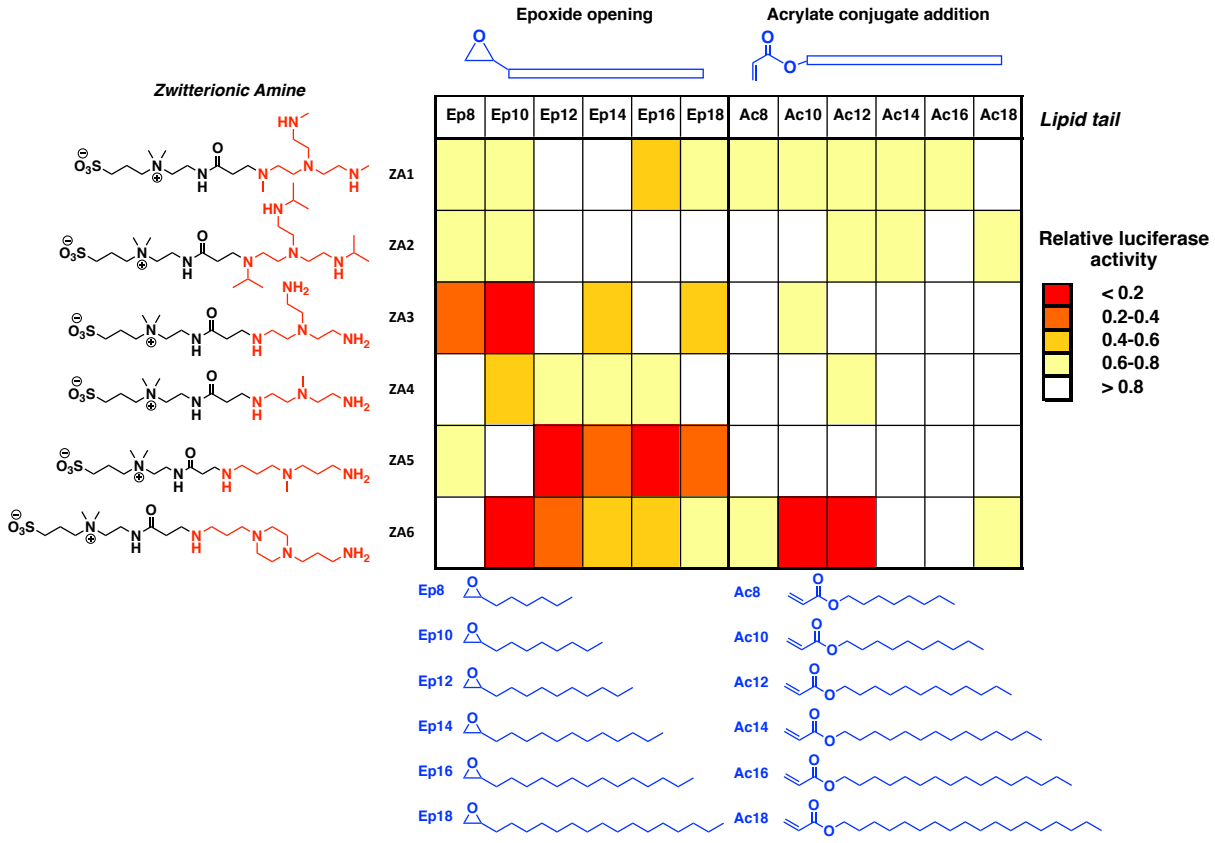

Figure 2.2.2. The heat map of siRNA delivery of the ZNPs to HeLa-Luc cells reveals structure-activity relationships within the library. Epoxide derived ZALs were generally much more potent than acrylate derived ZALs, while key core amines ZA3, ZA5, and ZA6 showed potent delivery.

2.2.3 Generation of reagents and assays for the study of non-viral gene editing

ZALs were evaluated for their ability to deliver CRISPR/Cas9 components using a stable cell line expressing both Cas9 and luciferase (HeLa-Luc-Cas9). With the assistance of Sofya Perelman from the Neal Alto Lab at UTSW, a cell line stably expressing Cas9 was generated by lentiviral transduction of HeLa-Luc cells, followed by single cell sorting to identify a clone with both high Cas9 and luciferase expression (Figure 2.2.3). sgRNAs against luciferase were designed

and generated according to previously reported methods targeting the first third of the gene (Table 2.4.1)[131] and evaluated by pDNA transfection using commerical reagents (Figure 2.2.4). The most active sgRNA against luciferase (sgLuc5, henceforth sgLuc) as well as control sgRNAs were synthesized by *in vitro* transcription.

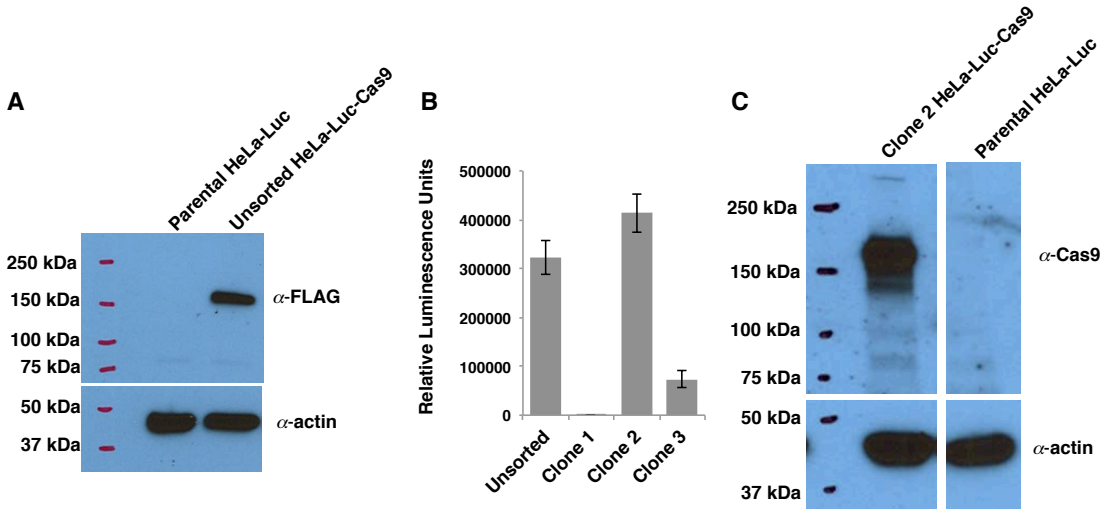

Figure 2.2.3. Cas9 expression was validated in HeLa-Luc-Cas9 cells by western blot. **(A)** Blotting with α-FLAG antibody in the pool of cells after Blasticidin S selection. **(B)** Luciferase expression of single cell clones as evaluated by the One-Glo assay (5,000 cells, 48h growth). **(C)** Cas9 expression of single cell clone 2 of HeLa-Luc-Cas9 blotted with α-Cas9.

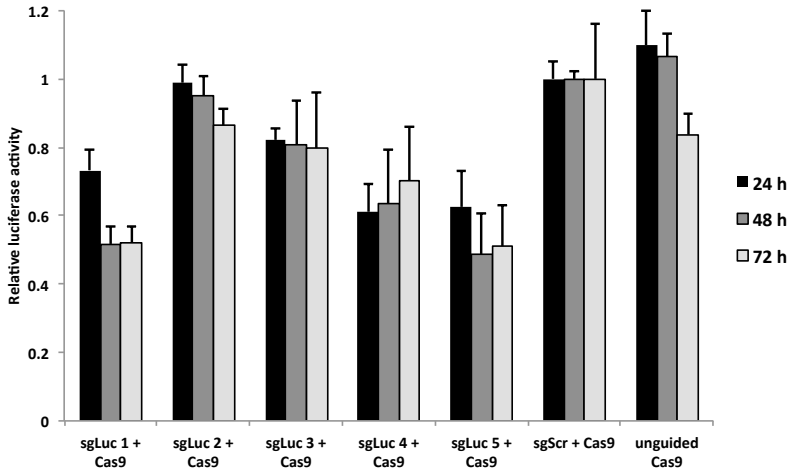

Figure 2.2.4. The evaluation of panel of single guide RNAs against luciferase using commercial reagent (LF3000) transfection of plasmid DNA encoding sgRNA and Cas9 protein reveals sgLuc5 as the most potent sgRNA sequence for silencing luciferase in unsorted HeLa-Luc cells. Values are normalized to non-targeting sgRNA control and plotted as mean +/- standard deviation (N = 4).

2.2.4 Evaluation of ZNPs for the in vitro gene editing by sgRNA delivery

Due to the zwitterionic moiety of the ZAL structure, we aimed to evaluate the ability of ZALs to formulate and deliver longer RNA in the absence of zwitterionic phospholipids. ZNPs formulated with cholesterol and PEG-lipid were loaded with sgLuc and evaluated for delivery to HeLa-Luc-Cas9 cells. Luciferase and viability were measured after 48 hours (h) relative to untreated cells. As anticipated from the chemical design combining cationic and zwitterionic functionalities, ZNPs do not require inclusion of helper phospholipids for nanoparticle formulation (Figure 2.2.10C). Among the lead ZALs, ZA3-Ep10 was found to be the most efficacious for delivery of sgLuc (Figure 2.2.5). Additionally, the ZNP-sgRNA formulations of ZA3-Ep10 maintained strong activity independent of weight ratio of ZAL:sgRNA and PEG-density (0-2%) (Figure 2.2.6).

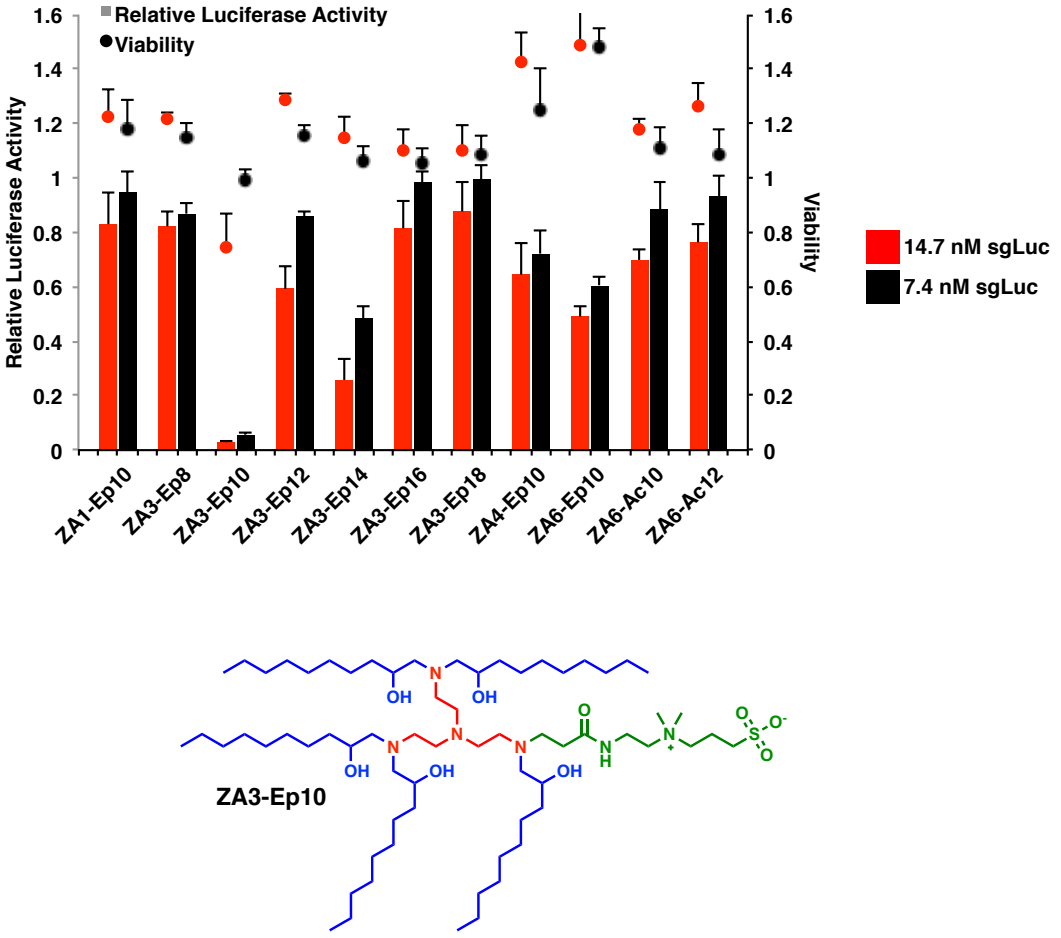

Figure 2.2.5. Lead ZALs identified from the siRNA screen were evaluated for sgRNA delivery to HeLa-Luc-Cas9 cells. ZNPs were formulated at 50:38.5:1 (ZAL:cholesterol:PEG-lipid molar ratios) in the lipid mix and 20:1 ZAL:sgRNA weight ratio. sgRNA was administered at both 14.7 nM and 7.4 nM for 48 h. ZA3-Ep10 emerged as the most highly potent (>95% luciferase silencing). Viability (dots) and relative luciferase activity (bars) were determined relative to untreated cells (N = 4 +/- standard deviation).

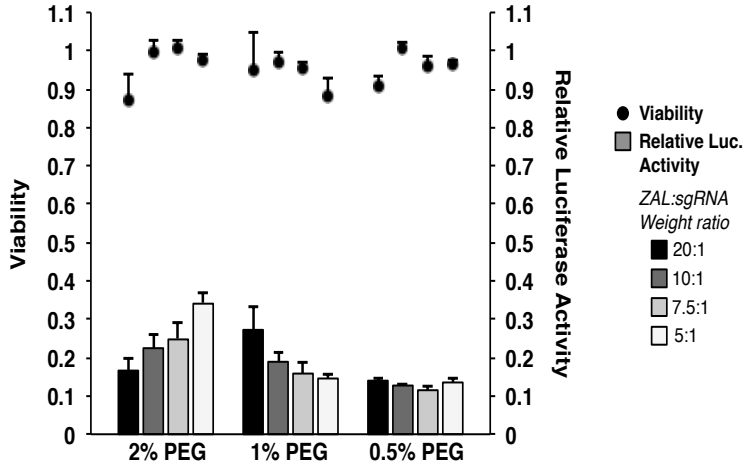

Figure 2.2.6. The optimization of ZA3-Ep10 ZNPs for sgRNA delivery was explored by tuning the PEG content of the formulation (2%, 1%, and 0.5%) and the ZAL:sgRNA weight ratio (20:1, 10:1, 7.5:1 5:1). All formulations were potent for sgLuc delivery at 7.4 nM, 48 h incubation, while 7.5:1 weight ratio and 0.5% PEG showed the best luciferase editing.

ZNP-mediated editing of luciferase DNA resulted in a dose-dependent, sequence-specific decrease in luciferase expression (Figure 2.2.7B), and this dose-responsiveness was independent of weight ratio in the formulation (Figure 2.2.8). Furthermore, ZNP gene-editing verified CRISPR/Cas editing using the Surveyor nuclease assay,[154] which can detect the indels formed during the double-strand break repair (Figure 2.2.7A).

Given that sgRNAs require loading into Cas9 nucleases in cells and trafficking to the nucleus to perform sequence-guided editing, we wanted to understand the kinetics of this process, particularly in comparison to RNAi-mediated gene silencing. siLuc-mediated mRNA degradation is a fast process, where expression decreased by 40% within the first 4h, ~80% at 10h, and was silenced by 92% by 20h, remaining low for about 3 days. Thereafter, the protein expression steadily increased and reached baseline level 6 days after transfection (Figure 2.2.9). In contrast, sgLuc-mediated DNA editing was kinetically slower, possibly due to the requirements to load into

Cas9 and survey the DNA for PAMs, and due to turnover of the existing luciferase mRNA transcripts. It took 20h for luciferase expression to decrease by 40%, ultimately going down by 95% after 2 days, but as gene-editing is permanent, this loss of signal persisted indefinitely. The low luciferase expression (5%) persisted throughout the duration of the assay (9 days) due the permanent genomic change, even after multiple rounds of cellular division, suggesting that edited cells grew at the same rate of non-edited cells (Figure 2.2.10).

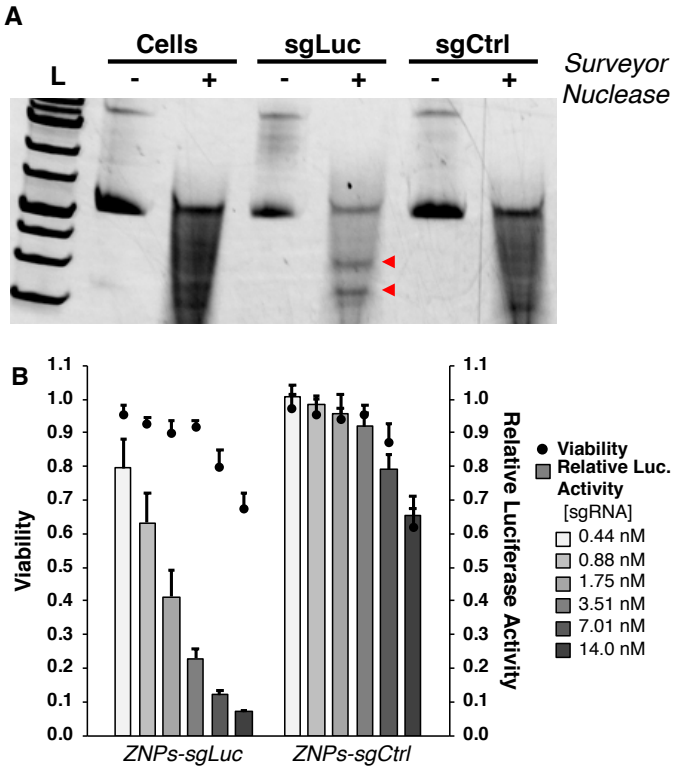

Figure 2.2.7 Sequence specific editing by ZNP delivery of sgRNA to HeLa-Luc-Cas9 cells comparing ZNPs targeting luciferase against an off-target control sequence. A) The Surveyor assay confirmed sequence specific editing as indicated by the red arrows. B) Luciferase-editing resulted in dose-responsive silencing in HeLa-Luc-Cas9 cells (N = 4 +/- standard deviation). Reprinted with permission from Reference 138. Copyright 2016 John Wiley and Sons.

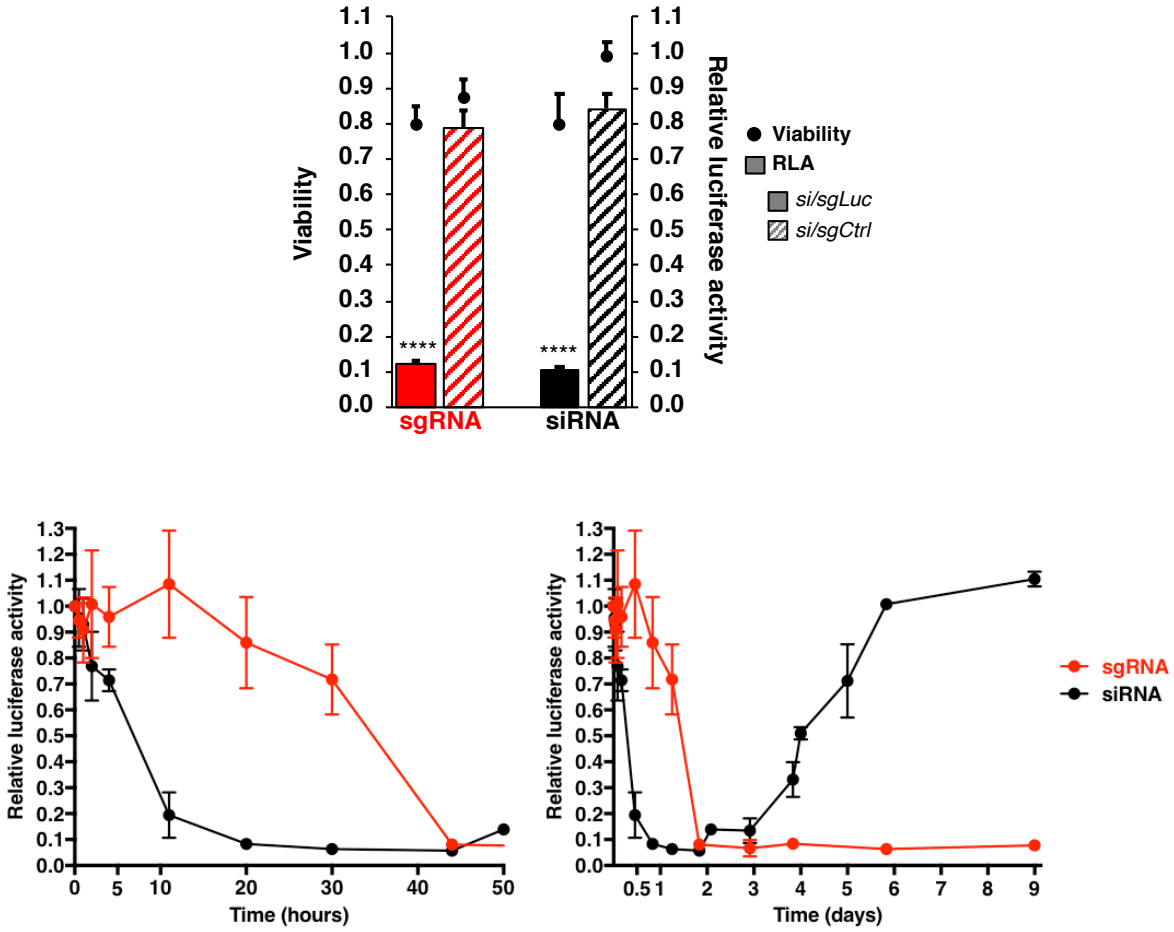

Figure 2.2.8. ZNPs enable permanent CRISPR/Cas-mediated DNA editing. (A) Sequence specific silencing of luciferase by siRNA (9 nM) and editing by sgRNA (7 nM) in HeLa-Luc-Cas9 cells. N = 4 ± stdev, **** $p < 0.0001$ **(B)** Kinetically, silencing with siRNA is transient while sgRNA delivery results in permanent loss of luciferase signal after 2 days. Magnification of the early time points of the kinetic curve of luciferase silencing comparing sgRNA versus siRNA by ZA3-Ep10 ZNPs shows that siRNA silencing is much faster than sgRNA editing. Reprinted with permission from Reference 138. Copyright 2016 John Wiley and Sons.

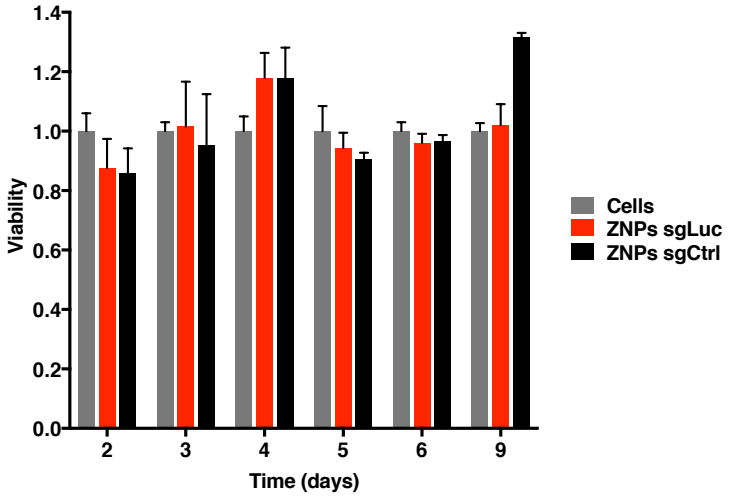

Figure 2.2.9. The relative viability of ZNP edited HeLa-Luc-Cas9 cells (sgLuc) versus unedited cells (sgCtrl) shows similar growth rates by the Cell-Titre Glo assay when normalized to untreated cells (N = 5 +/- S.E.M.)

2.2.5 Evaluation of ZNPs for in vitro and in vivo mRNA delivery

Having demonstrated that ZA3-Ep10 ZNPs could effectively deliver sgRNAs (~100 nt), we next examined their ability to deliver even longer mRNA (1,000 to 4,500 nt). We delivered mRNA encoding mCherry mRNA (~1,000 nt) or luciferase mRNA (~2,000 nt) to IGROV1 human ovarian cancer cells (Figure 2.2.10). Bright mCherry expression was visible, and luciferase expression was observed to be dose-dependent. Notably, high expression required low mRNA doses (<600 pM). In contrast to sgRNA, which did not show a dependence on PEG lipid mole ratio in the formulation (Figure 2.2.6), delivery efficacy of mRNA decreased with higher PEG lipid ratios (Figure 2.2.11), while there was only a modest change in ZNP size (Figure 2.2.11). Optimization of PEGylation, particularly in view of *in vitro* to *in vivo* translation, is an ongoing challenge to be explored for each target disease, organ, and cell type.[155]

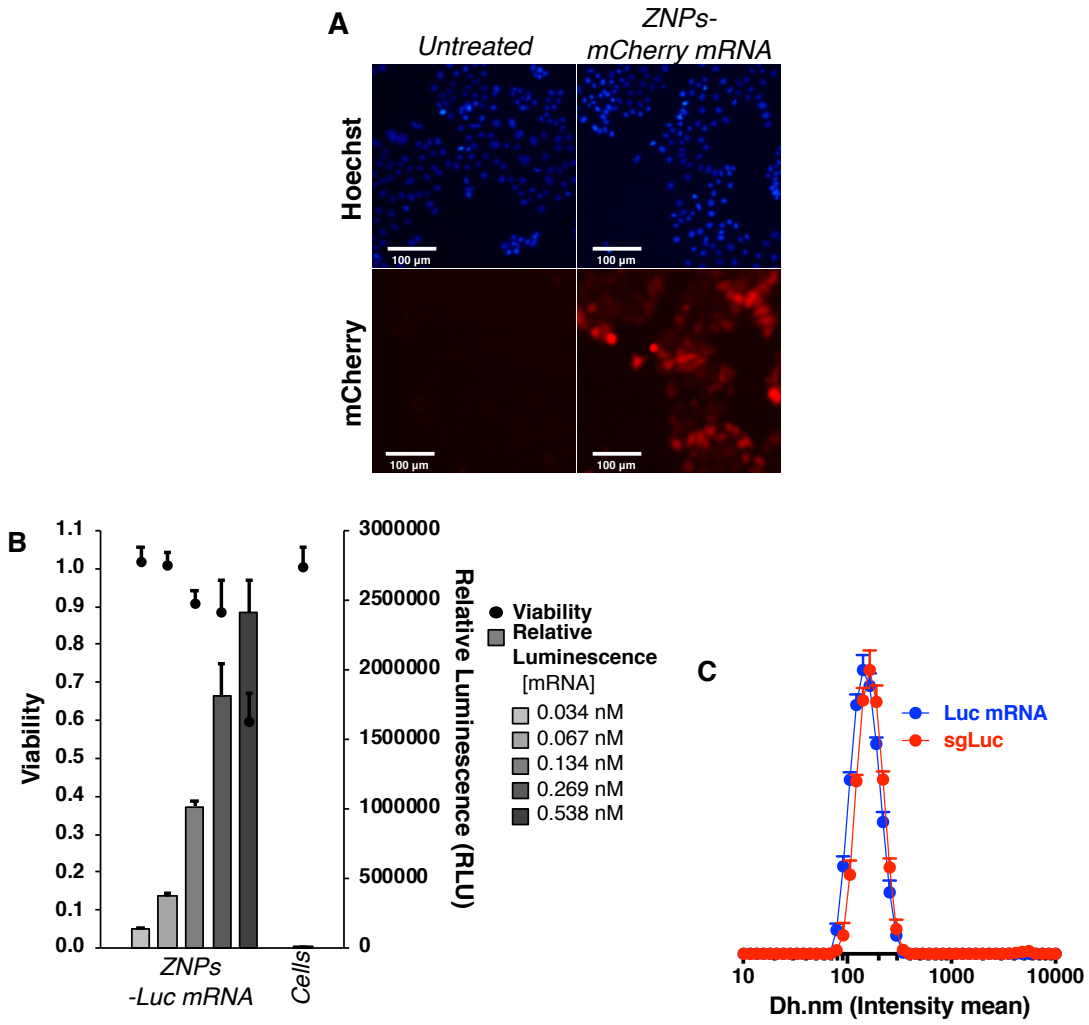

Fig. 2.2.10 ZNPs enable *in vitro* delivery mRNAs *in vitro*. ZA3-Ep10 ZNPs can deliver **(A)** mCherry mRNA (18h) and **(B)** luciferase mRNA (24h) to IGROV1 cells in a dose responsive manner. C) The size of the RNA cargo does not effect ZNP size as measured by DLS. Reprinted with permission from Reference 138. Copyright 2016 John Wiley and Sons.

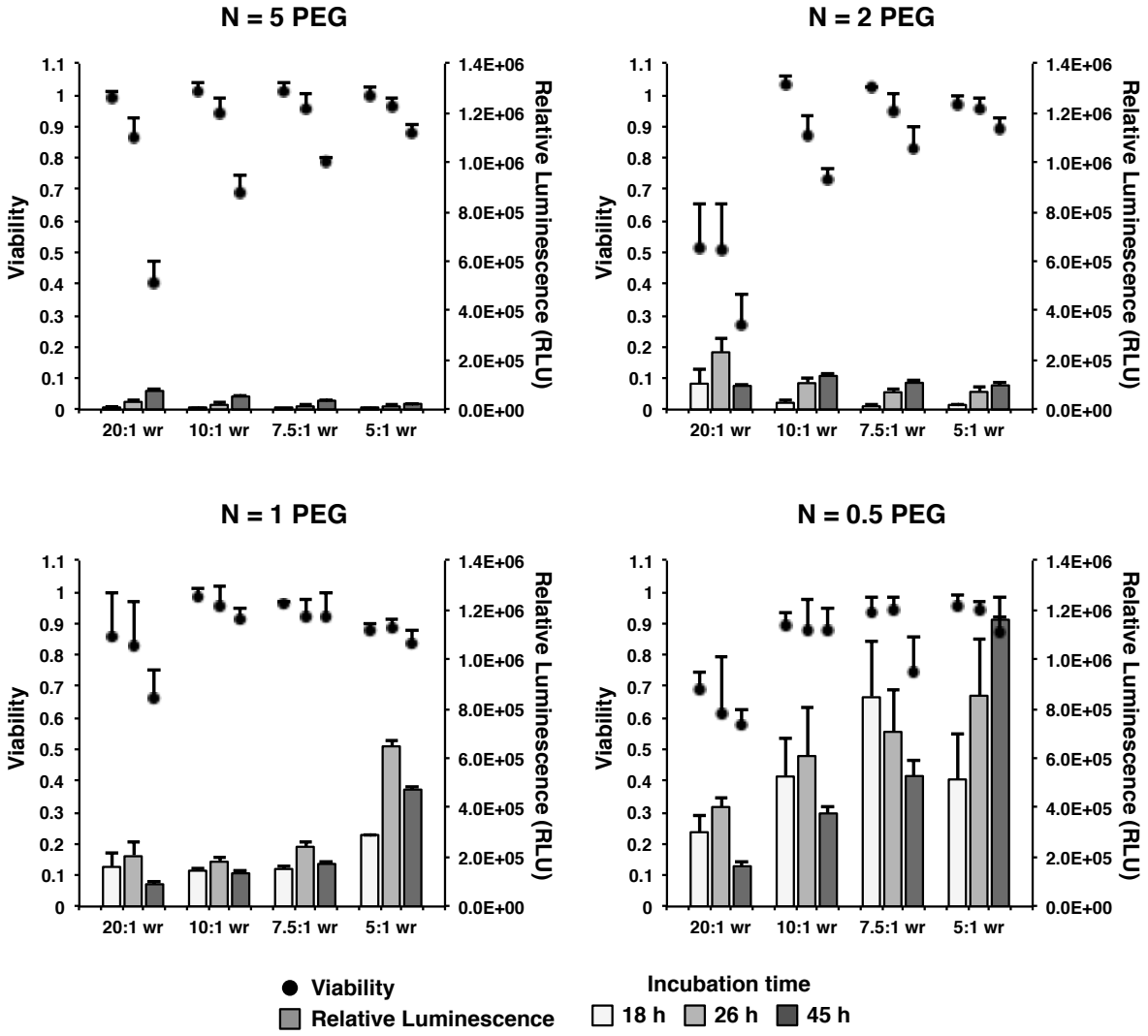

Figure 2.2.11. The optimization of the ZA3-Ep10 ZNPs for mRNA delivery was performed in IGROV1 cells. The weight ratio of the ZAL:mRNA was set at 20:1, 10:1, 7.5:1 and 5:1. The lipid mix was prepared with a relative molar ratio of 50:38.5:n, ZAL:cholesterol:PEG-lipid, where n = 5, 2, 1 or 0.5. Cells were treated in 96-well plates with 100 ng mRNA and incubated for the indicted time (18 h light gray, 26 h gray, 45 h dark gray) prior to evaluation of cell viability (dots) and luciferase expression (bars) using the One-Glo + Tox assay. Cell viability was determined compared to untreated cells and luminescence was normalized to viability to determine relative luminescence. Values are plotted as a mean +/- standard deviation, N = 4.

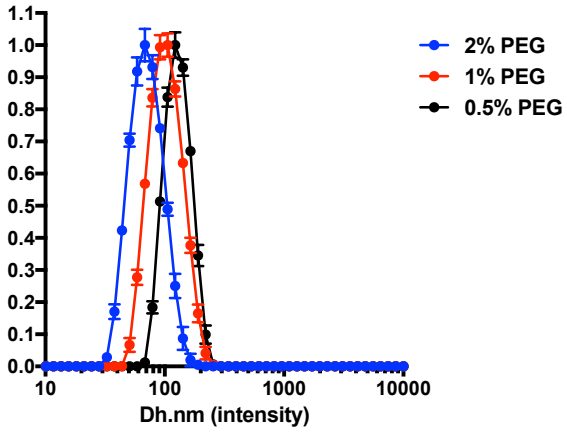

Figure 2.2.12. The effect of PEG lipid composition of ZA3-Ep10 Luc mRNA NPs formulated for *in vivo* assays. The ZAL:cholesterol ratio was fixed at 50:38.5 molar ratio while PEG-lipid was included at the indicated percentage. As expected increased PEG leads to smaller particle size, but poorer expression of mRNA.

Our report attempts to address some of those concerns by examining different formulations in multiple cell types and mouse strains. In order to validate the hypothesis of the critical role of the zwitterionic group in stabilizing long RNAs for effective delivery, formulations of a cationic 5-tailed analogue of ZA3-Ep10, A3-C14 (C14-110 in the literature),[1] which has previously been reported as effective for *in vivo* siRNA deliver to hepatocytes using cholesterol, DSPC, and PEG-lipid was titrated with various zwitterionic phospholipids DSPC, DOPE, and DOPC (Figure 2.2.13). Increasing molar proportions of DOPE in the formulations showed an improvement in binding, particle size, and function delivery of sgRNA and mRNA, while siRNA did not require additional zwitterionic content (Figure 2.2.14). The introduction of DSPC did not improve mRNA delivery, while supplementing with DOPC improved delivery greatly. Meanwhile, efficacy of ZA3-Ep10 ZNPs was consistent across all RNA cargos, and outperformed the cationic analogue supplemented with phospholipid.

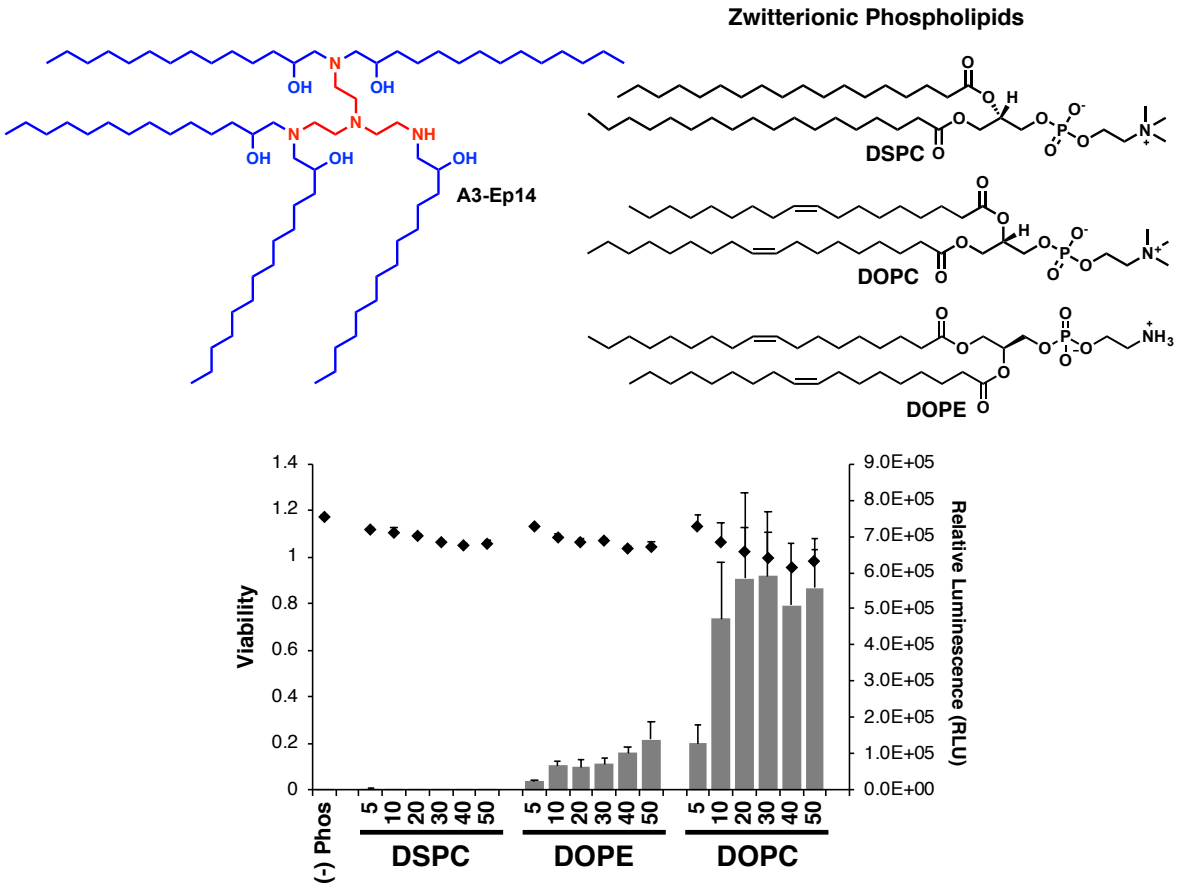

Figure 2.2.13. Comparing the effect of zwitterionic phospholipid identity and concentration on mRNA delivery of A3-Ep14, a cationic structural analogue of ZA3-Ep10, which is known to effectively deliver siRNA. LNPs were formulated at 50:38.5:0.5:n cationic lipid: cholesterol: PEG-lipid: phospholipid, and n was tuned from 5 to 50. Luciferase expression was evaluated 24h after administration to IGROV1 cells.

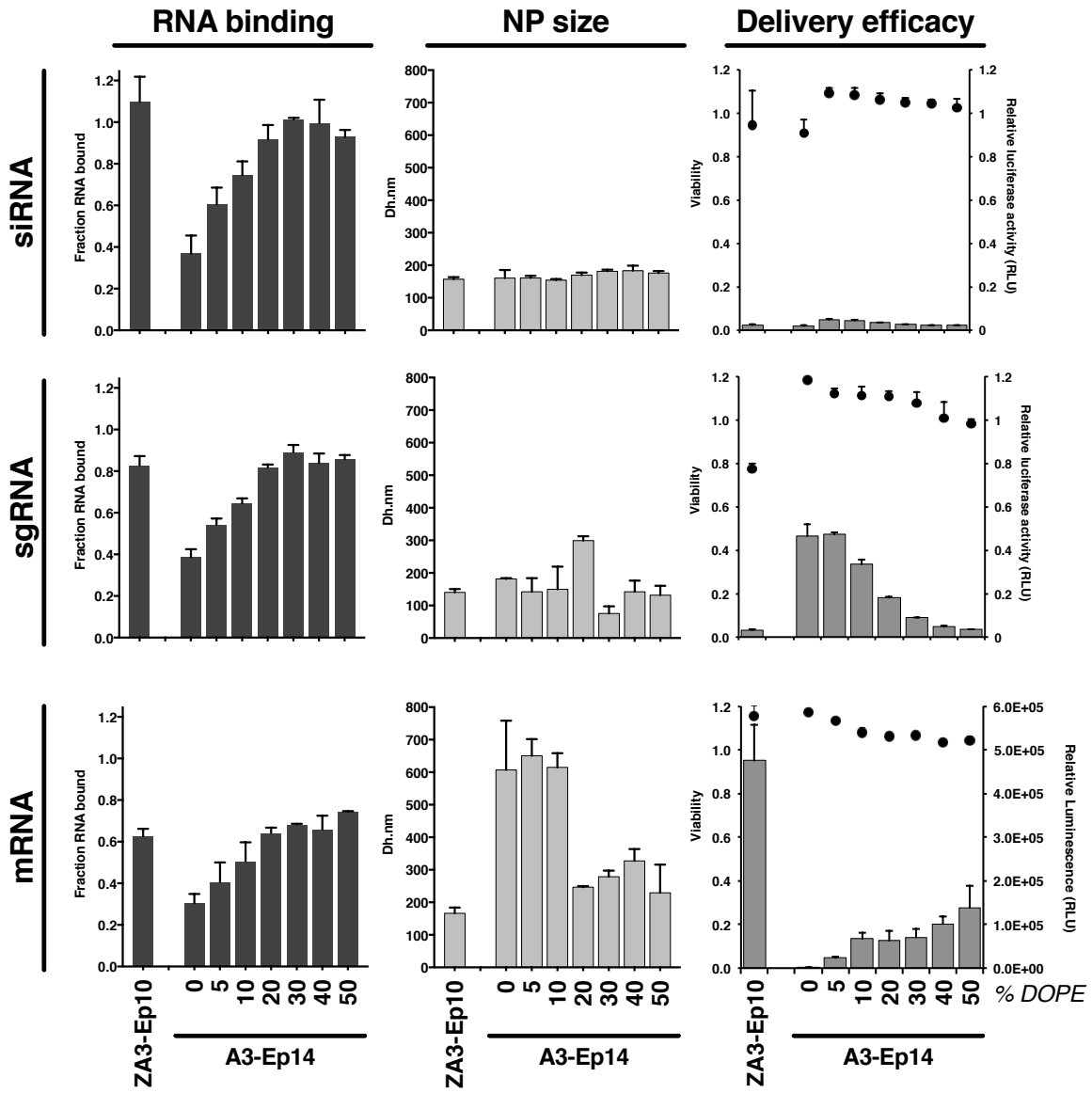

Figure 2.2.14. Comparing the RNA encapsulation, nanoparticle size and delivery efficacy of ZA3-Ep10 and a cationic structural analogue (A3-Ep14, also referred to as C14-110 in the literature), which is known to deliver small RNA. The ZNP or LNP formulation was fixed at 7.5:1 weight ratio ZAL or Cationic analogue to RNA. The lipid mixture for the NPs was 50:38.5:0.5 ZAL or cationic analogue: cholesterol: PEG-lipid, while for the A3-Ep14 NPs the zwitterionic phospholipid was titrated from 0 to 50% in the lipid mix. The nanoparticles were formulated by manual mixing using the *in vitro* formulation protocol. RNA binding was determined by the Ribogreen assay (N = 3 +/- standard deviation), while nanoparticle size was determined by dynamic light scattering (N = 3 +/- standard deviation). Luciferase silencing or editing of siLuc and sgLuc NPs was assayed in HeLa-Luc-Cas9 cells (7.35 nM sgRNA, 17.9 nM siRNA), while luciferase expression by Luc mRNA NPs was evaluated in IGROV1 cells (0.77 nM mRNA). Cells were assays after 40 h incubation time by the One-Glo + Tox assay and plotted with viability (dots) and luciferase expression (bars) as mean +/- standard deviation (N = 4).

The optimal formulation was next evaluated *in vivo* through intravenous (I.V.) administration of ZA3-Ep10 mRNA ZNPs to multiple strains of mice. Bioluminescence imaging following Luc mRNA delivery in athymic nude mice (Figure 2.2.15, 1 mg/kg), C57BL/6 mice (2.2.15, 4 mg/kg), and NOD scid gamma (NSG) mice (Figure 2.2.16, 1 mg/kg) resulted in expression of luciferase in liver, lung, and spleen tissue 24h after injection which was quantified by ROI analysis (Figure 2.2.17). Based on the high lung signal, we were motivated to explore co-delivery (one pot) CRISPR/Cas editing in lung cells.

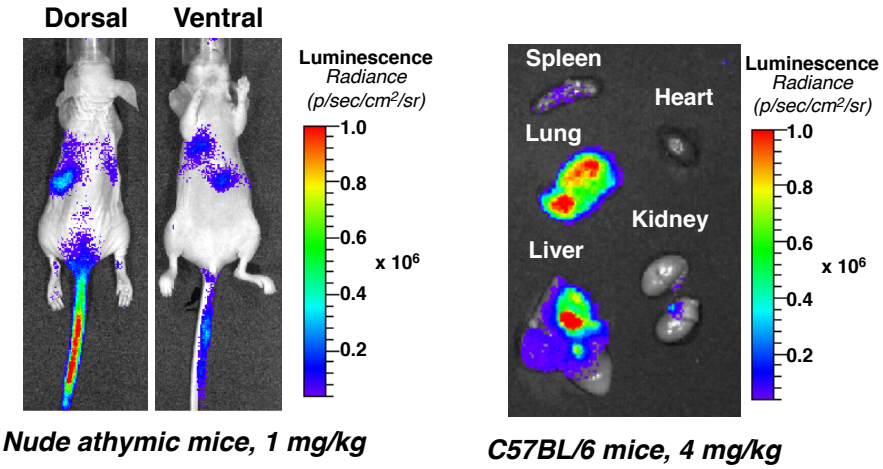

Figure 2.2.15 *In vivo* luciferase expression was achieved by systemic I.V. administration of ZA3-Ep10 Luc mRNA ZNPs (24h). Bioluminescence imaging both *in vivo* (**Left**, athymic nude mice, 1 mg/kg) and *ex vivo* (**Right**, C57BL/6 mice, 4 mg/kg) revealed expression of luciferase in liver, lung and spleen tissue. Reprinted with permission from Reference 138. Copyright 2016 John Wiley and Sons.

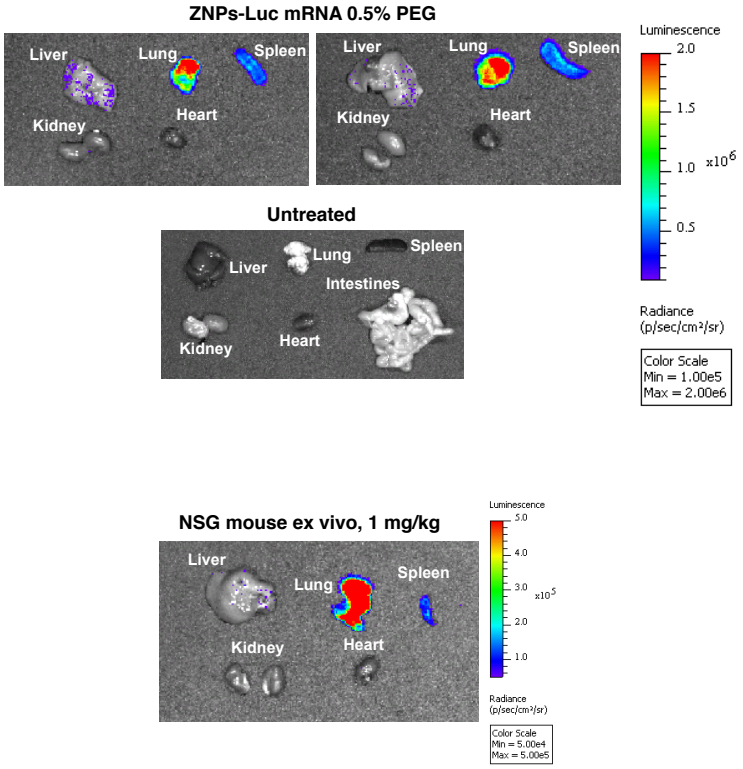

Figure 2.2.16. Bioluminescence imaging shows that *in vivo* expression of luciferase after Luc-mRNA administration by I.V. injection correlates with *in vitro* activity. Mice were injected with 1 mg/kg Luc mRNA and imaged 24 h after treatment. An untreated mouse was used as a negative control. The top right panel shows the *ex vivo* expression of the animal shown in Figure 3E.

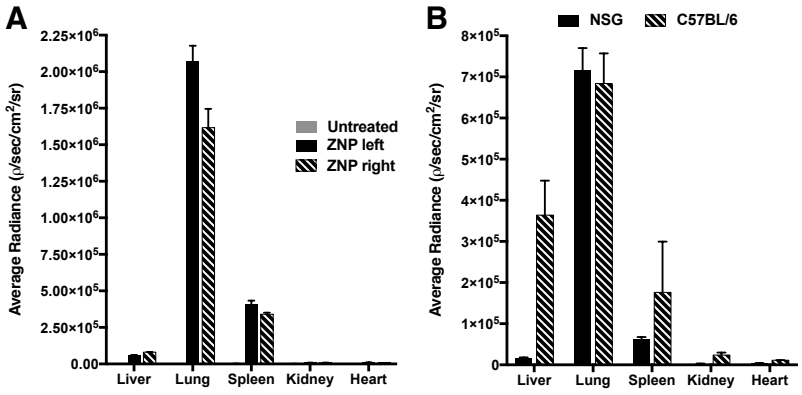

Figure 2.2.17. Quantitation of the *ex vivo* images by ROI analysis. **(A)** Quantitation of the athymic nude mice images shown in Figure 2.2.16 (top) and **(B)** quantitation images of the images in Figure 2.2.16 (bottom, NSG) and Figure 2.2.15 (C57BL/6). A minimum of 5 ROIs per organ was measured and plotted as mean +/- S.E.M.

2.2.6 Evaluation of ZNPs for delivery of Cas9 as mRNA, and non-viral gene editing

Due the very long length of Cas9 mRNA (~4,500 nt), delivery using synthetic carriers is particularly challenging. Remarkably, we found the level of Cas9 mRNA in A549 lung cancer cells was very high after only 4h incubation with ZA3-Ep10 Cas9 mRNA ZNPs (Figure 2.2.18A). Synthetically introduced mRNA decreased from > 4 fold actin to 0.7 fold actin over the next 45h. Because translation of mRNA takes time, protein expression was low at 4h, increased considerably by 12h, and was the highest by 36h (Figure 2.2.18A/B) and was also dose dependent (Figure 2.2.18C and Figure 2.2.19). For ultimate *in vivo* utility, the use of synthetic NP carriers alleviates concerns of viral delivery. Moreover, delivery of Cas9 mRNA allows for transient expression of Cas9, minimizing persistence that can lead to off-target genomic alteration. This can reduce the significant therapeutic danger of incorporating an exogenous nuclease into the genome.

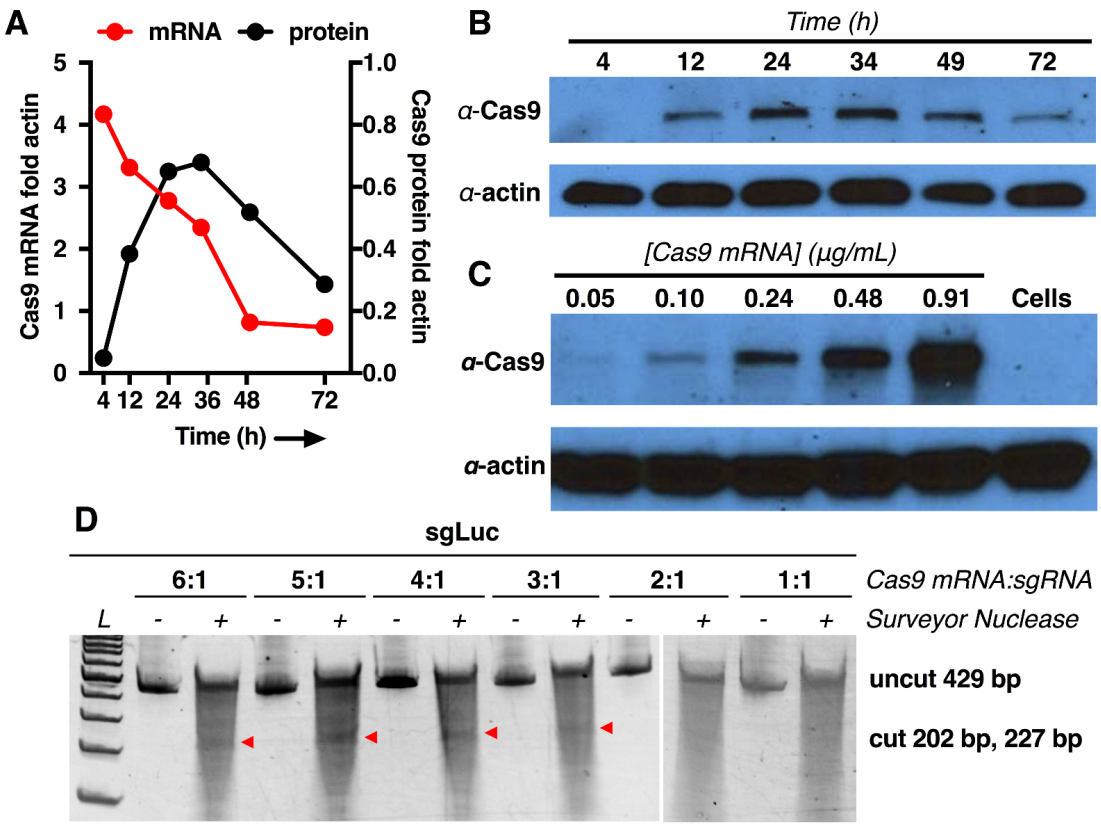

Figure 2.2.18. ZNPs enable co-delivery of Cas9 mRNA and sgRNA for CRISPR/Cas editing. (A) The kinetics of mRNA and protein expression after ZNP delivery of Cas9 mRNA (0.48 ng/mL mRNA) to A549-Luc cells. Cas9 mRNA levels (**A** red curve) and protein expression (**A** black curve**, B**) were measured over time. **(C)** ZNPs enable dose responsive expression of Cas9, detectable as low as 0.05 μg/mL delivered mRNA. (**D**) Surveyor confirmed editing of the luciferase target at mRNA:sgRNA ratios of 3:1 or higher (wt). Co-delivery of Cas9 mRNA and sgCtrl showed no editing (**Figure 2.2.22**). Reprinted with permission from Reference 138. Copyright 2016 John Wiley and Sons.

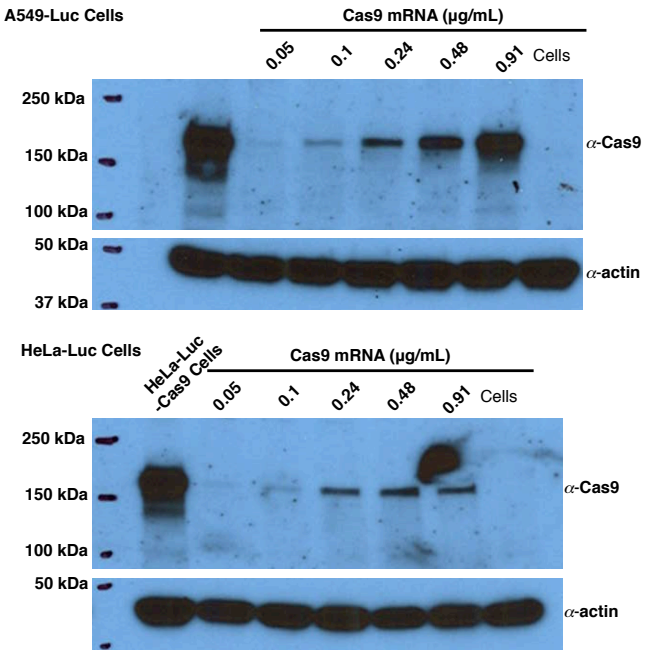

Figure 2.2.19. ZA3-EP10 Cas9 mRNA ZNPs enable dose responsive expression of Cas9 in both A549-Luc cells and HeLa-Luc cells with detectable Cas9 protein at 0.05 μg/mL mRNA concentration. Stable HeLa-Luc-Cas9 cells were used as a positive control while untreated cells did not show any bands.

As illustrated above, optimal delivery of mRNA and sgRNA is kinetically different. Indeed, we found that staged delivery in separate ZNPs was an effective treatment method. ZNP delivery of mRNA for 24h, to enable Cas9 protein expression, followed by sgRNA delivery in separate ZNPs enabled efficacious *in vitro* editing in both HeLa-Luc and A549-Luc cells (Figures 2.2.20, 2.2.21). However, when considering *in vivo* utility, Cas9 mRNA and sgRNA must be present in the same cell. We therefore reasoned that co-delivery of mRNA and sgRNA from a single NP would provide a greater editing efficiency since this method would guarantee delivery to the same individual cells. We explored a variety of conditions and found that effective editing of the target gene by ZNPs encapsulating both Cas9 mRNA and sgRNA required a ratio of mRNA:sgRNA greater than or equal to 3:1 (wt) as confirmed by the Surveyor assay (Figure 2.2.18D), while control ZNPs did not show any editing (Figure 2.2.21). Interestingly, the

encapsulation efficiency of sgRNA and Cas9 mRNA in ZNPs increased with a decreased sgRNA: mRNA weight ratio, suggesting that the smaller RNA is easier to encapsulate efficiently, despite similar particle properties (Figure 2.2.22).

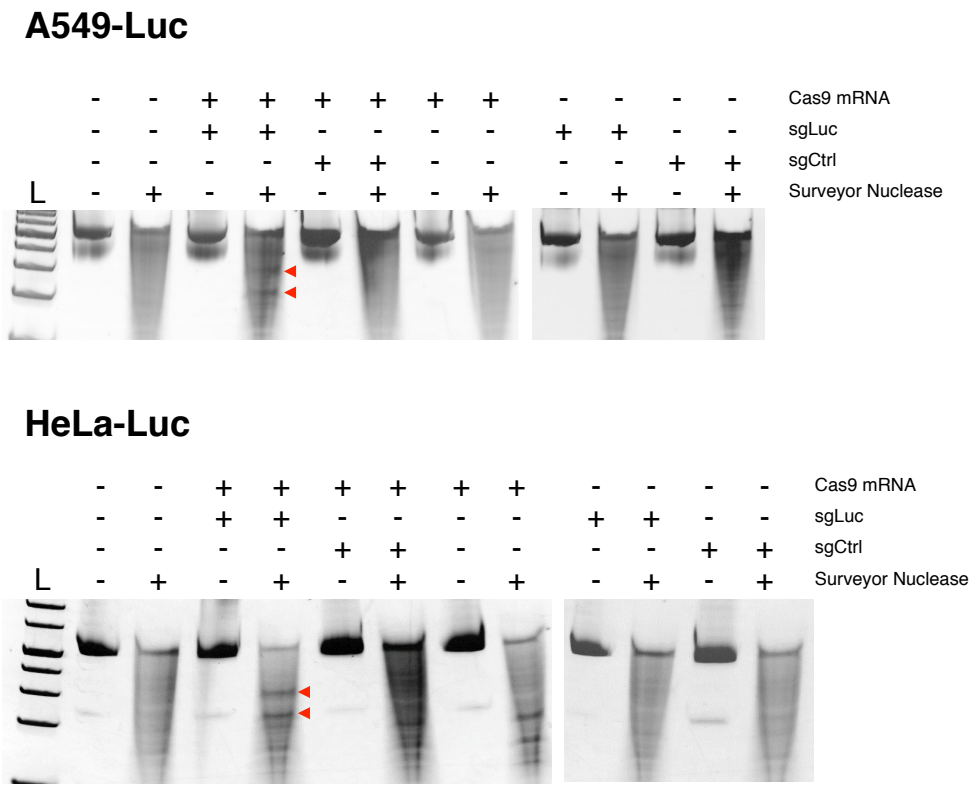

Figure 2.2.20. Co-delivery of Cas9 mRNA and sgLuc leads to editing in staged delivery at 2 μg per well Cas9 mRNA and 1 μg sgLuc in a 6-well plate in both A549-Luc and HeLa-Luc. Meanwhile, unguided Cas9, Cas9-sgCtrl, or sgLuc alone do not show edited bands. The expected genomic DNA amplicon was 510 bp while the expected cut bands indicating editing are 233 bp and 277 bp (red arrows).

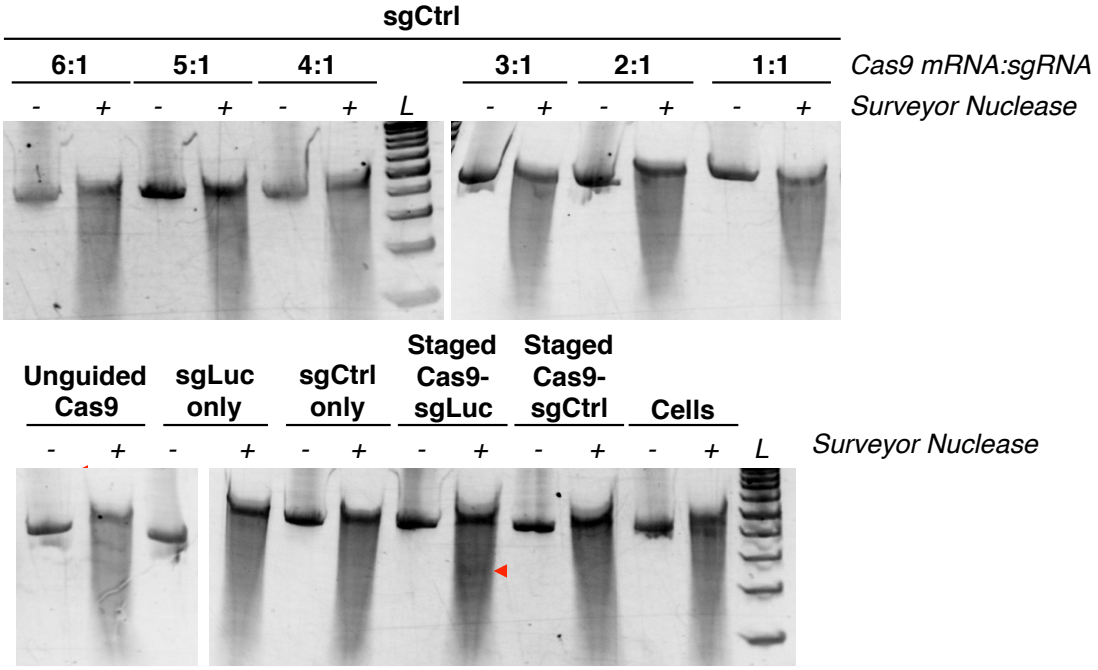

Figure 2.2.21. Control ZNPs (Cas9+sgCtrl, unguided Cas9, sgLuc only and sgCtrl only) did not show editing of luciferase target in A549-Luc cells. Staged co-delivery shows editing with sgLuc under similar conditons with 2:1 Cas9 mRNA:sgLuc wr.

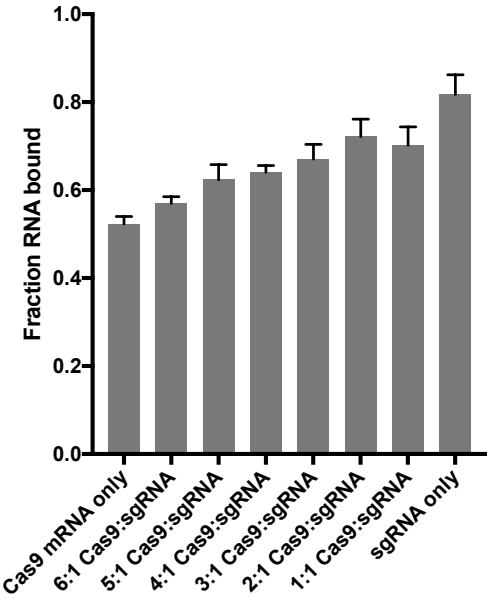

Figure 2.2.22. The encapsulation of Cas9 mRNA and sgRNA in co-delivery ZNPs. ZAL: total RNA was fixed at 7.5:1, with a lipid mixture of 50:38.5:0.5 ZA3-Ep10: cholesterol: PEG-lipid. Data are plotted as mean +/- standard deviation (N = 4).

To examine co-delivery *in vivo*, we utilized genetically engineered mice containing a homozygous Rosa26 promoter Lox-Stop-Lox tdTomato (tdTO) cassette present in all cells.[9] Co-delivery of Cas9-mRNA and sgRNA against LoxP[156] enabled deletion of the Stop cassette and induction of tdTO expression (Figure 2.2.23A, Table 2.4.1). The positive control for this model was a liver-specific Cre-recombinase AAV, which showed strong tdTO expression in liver tissue and slide sections (Figure 2.2.24). This is a challenging model for a synthetic carrier due to the need for two cuts on the same allele to be made for the tdTO to be expressed. Furthermore, the PAM sequences within the LoxP sites of the LSL cassette are NAG, which is a weaker PAM compared to the typical NGG sequence. However, this approach allowed for a single sgRNA sequence to be co-delivered with Cas9 mRNA, albeit at the expense of activity. ZNPs encapsulating Cas9 mRNA and sgLoxp at a 4:1 mRNA:sgRNA (Figure 2.2.25) weight ratio were

administered intravenously at a 5 mg/kg RNA dose. One week after administration, fluorescence signal from tdTO was detected in the liver and kidneys upon whole organ *ex vivo* imaging. (Figure 2.2.23B). Detailed examination of sectioned organs using confocal fluorescence microscopy showed tdTO-positive cells in liver, lung, and kidney tissues (Figure 2.2.23C). Importantly tdTO positive cells were not observed when animals were treated with sgCtrl ZNPs (Figure 2.2.26) and no significant change in body weight of treated animals was observed (Figure 2.2.27). To quantify editing, primary hepatocytes were isolated from perfused livers and tdTO cells were counted by flow cytometry, which showed 1-3% editing (Figure 2.2.28). To further confirm editing, tissue harvested ~2 months after ZNP LoxP treatment showed strong fluorescent signal in the liver and kidney (Figure 2.2.29). This proof-of-principle data indicates that intravenous co-delivery of Cas9 mRNA and targeted sgRNA from a single ZNP can enable CRISPR/Cas editing *in vivo*.

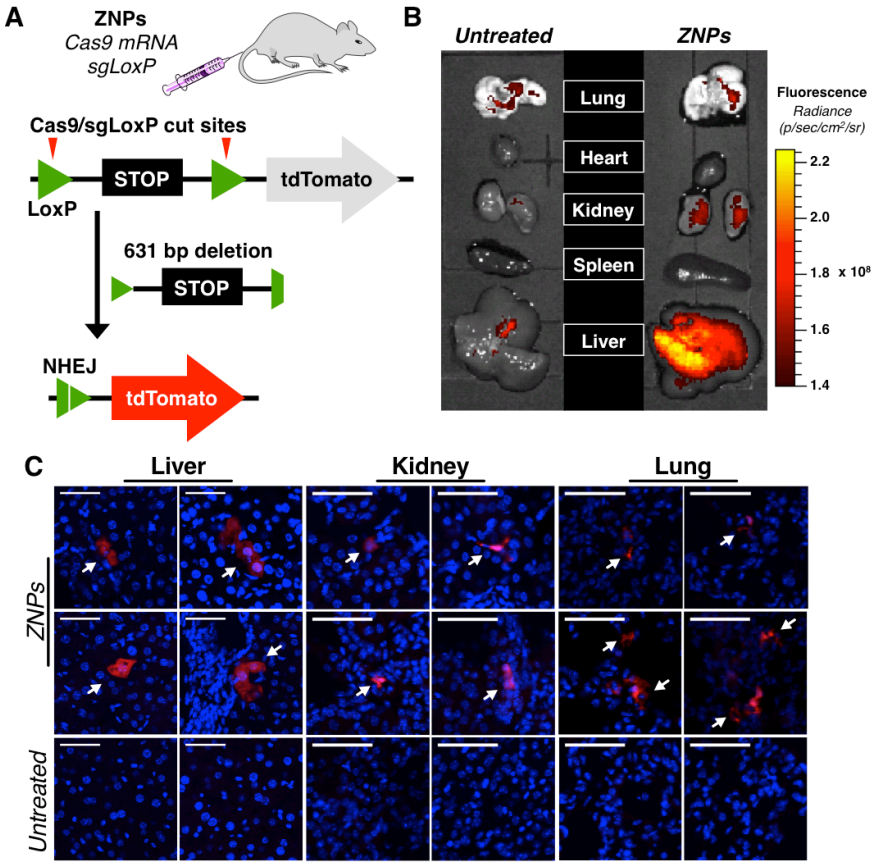

Figure 2.2.23 ZNPs enabled non-viral CRISPR/Cas editing *in vivo*. (A) Schematic representation shows that co-delivery of Cas9 mRNA and sgLoxP deletes the stop cassette and activates downstream tdTomato protein. **(B)** After administration of ZNPs encapsulating Cas9 mRNA:sgRNA (4:1, wt) at 5 mg/kg total RNA, tdTomato fluorescence was detected in the liver and kidney upon whole organ *ex vivo* imaging. **(C)** Confocal fluorescence microscopy of tissue sections showed tdTomato positive cells in liver, lung, and kidneys. Scale bars = 50 mm). Reprinted with permission from Reference 138. Copyright 2016 John Wiley and Sons.

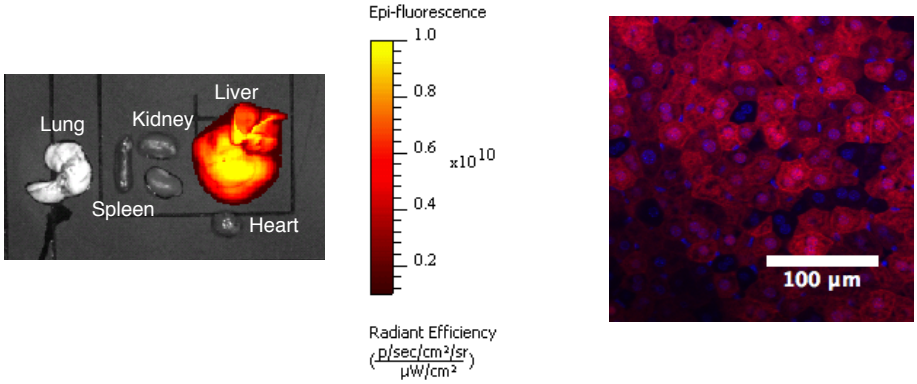

Figure 2.2.24. The Cre recombinase AAV positive control demonstrates expression of tdTomato in liver *ex vivo* at the whole organ level and in cells from tissue sections.

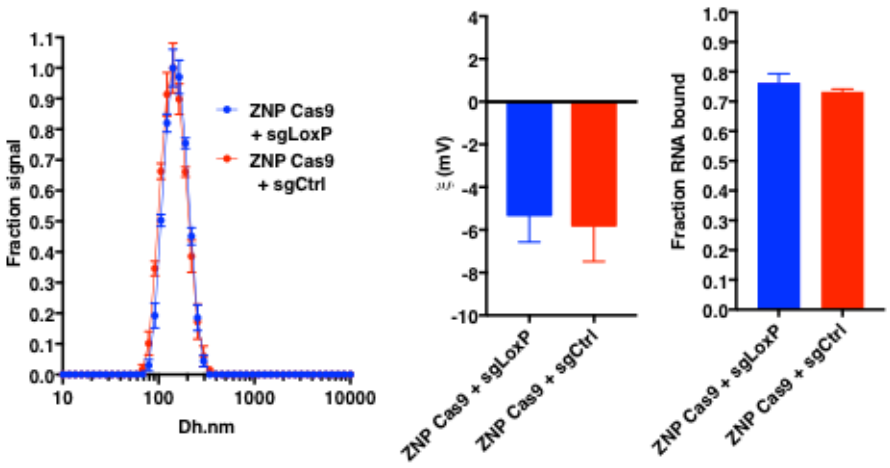

Figure 2.2.25. Particle properties of *in vivo* administered ZNPs encapsulating Cas9 mRNA and sgRNA. For size and zeta potential measurements, N = 5 for RNA encapsulation N = 4. Data are plotted as mean +/- standard deviation.

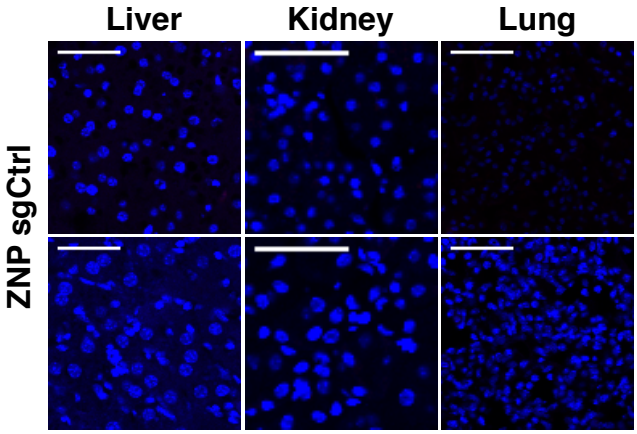

Figure 2.2.26. Delivery of ZNPs encapsulating Cas9 and sgCtrl does not show tdTomato positive cells in sectioned tissue slides.

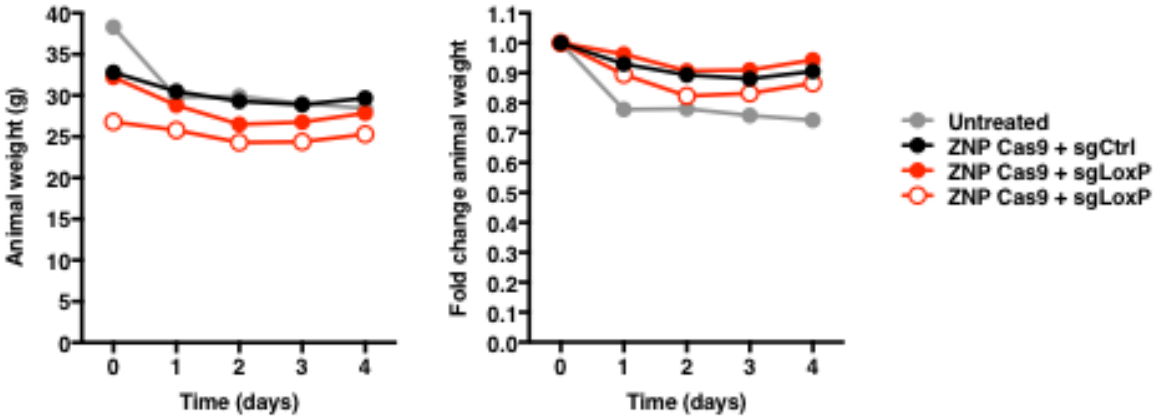

Figure 2.2.27. Measurement of animal body weight after systemic administration of ZNPs encapsulating Cas9 mRNA and sgRNA at 5 mg/kg total RNA dose. Each curve represents a single animal.

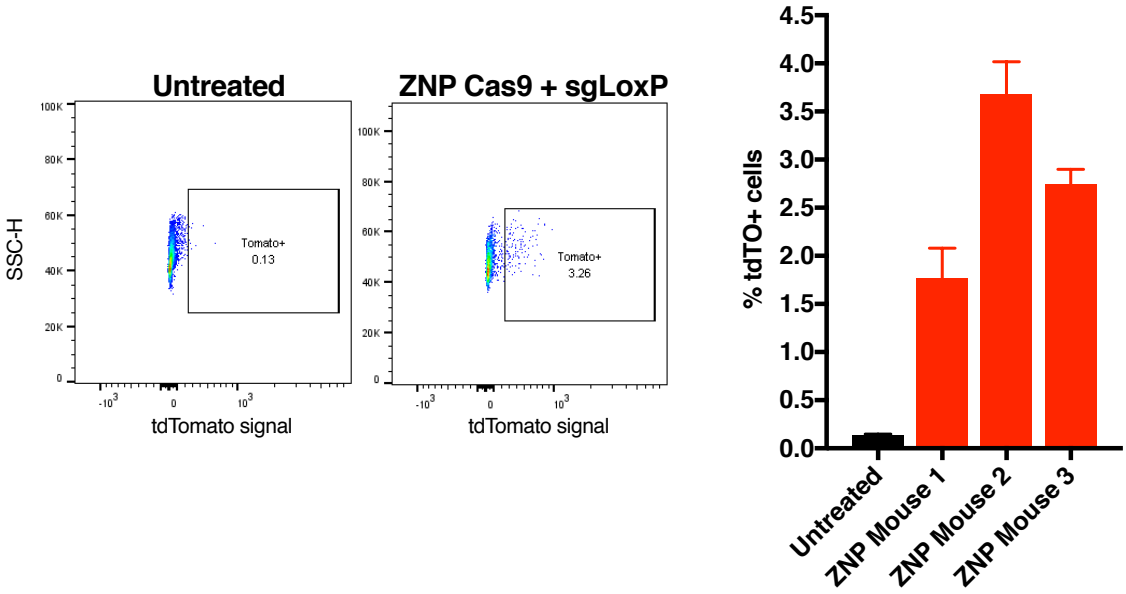

Figure 2.2.28. Quantification of tdTomato positive hepatocytes in animals treated with ZNPs as determined by flow cytometry of isolated primary hepatocytes. The left panel shows representative plots of samples from an untreated LSL-tdTO mouse and a ZNP-Cas9 mRNA-sgLoxP treated mouse. Mouse 1 and mouse 2 were treated at 2 mg/kg total RNA 2 times on consecutive days, while mouse 3 received a single dose at 5 mg/kg total RNA and all animals were harvested ~ 1 week after ZNP administration. Each sample was run four times and values are plotted as mean +/- standard deviation.

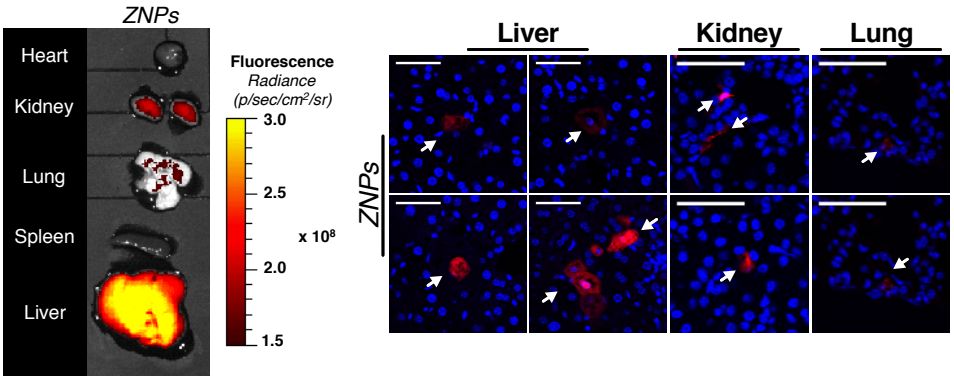

Figure 2.2.29. A ZNP treated tomato mouse shows significant fluorescent signal in the liver and kidneys ~2 months after editing by ZNPs encapsulating Cas9 mRNA and sgLoxP (5 mg/kg).

2.2.7 Chemical modifications of ZA3-Ep10 to establish SAR

Having identified a lead ZAL that was able to demonstrate effective delivery of mRNA and non-viral gene-editing *in vivo*, our aim was to better understand the relative roles of each motif played in effective mRNA delivery. Opportunities for modifications on the ZA3-Ep10 scaffold include modification of the secondary alcohol handles, changing the linker region connecting the sulfobetaine head group to the acrylamide in the zwitterionic acrylamide, and changing the identity of the zwitterion itself. Additionally, the introduction of degradable bonds into the ZA3-Ep10 scaffold would greatly improve the translatable potential of these materials, due to the high likelihood of repeat dosing in mRNA therapeutics. Active work is underway in exploring these structural changes, but preliminary studies have been performed with a subset of materials by modification of the secondary alcohol moieties, introduction of degradable bonds in the tails, and the introduction of unsaturated bonds into the tails, which may increased fusogenicity.

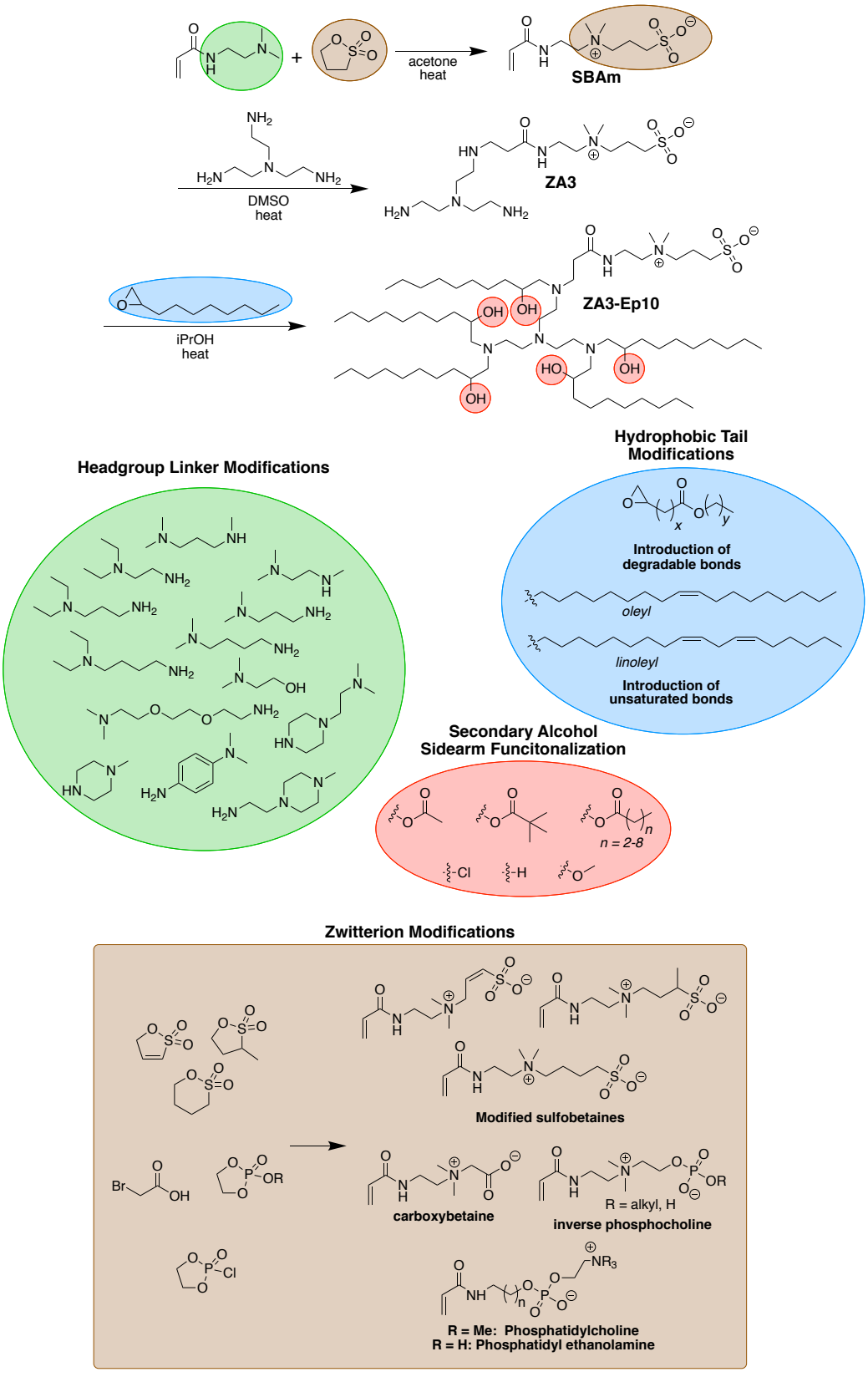

Figure 2.2.30. Opportunites for structure-activity relationship establiship by modification of the linker amine, zwitterionic head group, hydrophobic tail and secondary alcohol of ZA3-Ep10.

The secondary alcohols were readily esterified by reaction in simple anhydrides acetic anhydride and pivalic anhydride (Scheme 2.2.2). NMR and mass spectrometry analysis of ZA3-Ep10-OAc indicated that the degree of acetylation was between 80 and 100% (N = 4 or 5). Previous work in the Siegwart lab using a class of cationic lipids termed CSALs (See Chapter 3), showed that modification of a secondary alcohol with an acetate or pivalate modification improved siRNA delivery *in vitro*.[157] The effects of these modifications on ZNP activity is of great interest, as potential hydrogen bonding interactions may be critical in stabilizing ZAL-RNA interactions. As acrylate derived ZALs were not effective in delivery, it was hypothesized that the secondary alcohol moiety may allow key interactions for effective delivery of mRNA. Masking this group with an ester allowed us to probe for those potential roles.

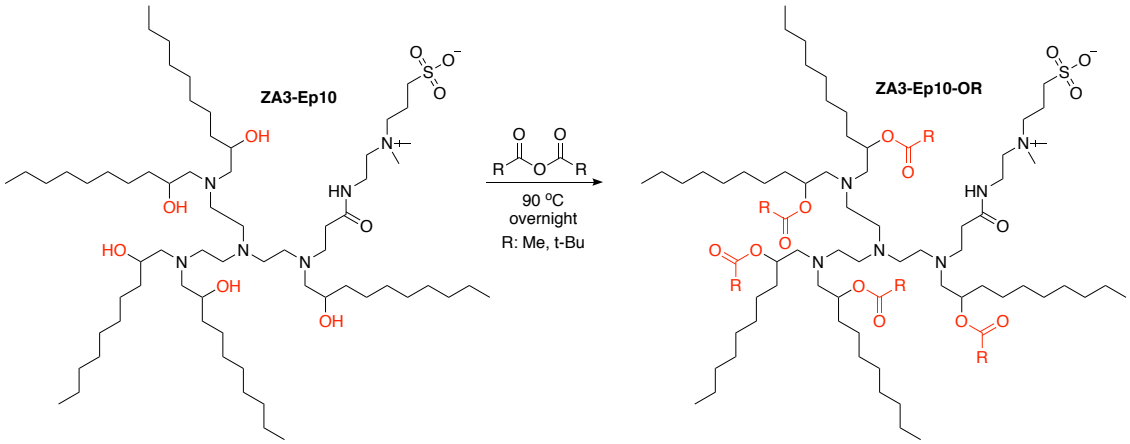

Scheme 2.2.2. The synthesis of ZA3-Ep10-OR by esterification of the secondary alcohols.

Degradable bonds were introduced into the ZA3-Ep10 scaffold by utilizing a hydrophobic glycidic ester (GEn) as the tail. Reaction with the zwitterionic amines (i.e. ZA3) results in the formation of an α-hydroxy ester, thus maintaining the presence and relative spacing of the secondary alcohol moieties around the amine core, while introducing a degradable ester bond in each tail. The synthesis of glycidic esters was optimally performed using sodium hypochlorite in

the presence of an ammonium salt phase-transfer catalyst Table 2.2.1.[158] Subsequent reaction of ZA3 with the glycidic ester hydrophobes resulted in the synthesis of ZA3-GE8, ZA3-GE12 and ZA3-GEOle.

Table 2.2.1 Optimization of conditions for hydrophobic glycidic ester synthesis.

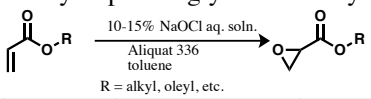

Entry	R	Time	Temp	Solvent	Oxidant	Additive	Result
1	Octyl	0.5 h	RT	MeOH	H_2O_2 (3.5 equiv)	NaOH (0.6 equiv)	hydrolysis
2	Dodecyl	4 d	reflux	DCM	*m*-CPBA (1.5 equiv)	-	20% conversion (NMR)
3	Dodecyl	5.5 h	0 °C to RT	MeOH	H_2O_2 (3.5 equiv)	-	S.M. only (TLC)
3*	Dodecyl	o/n	RT	MeOH	H_2O_2 (3.5 equiv)	NaOH (0.1 equiv)	Hydrolysis
4	Dodecyl	5 d	reflux	DCM	*m*-CPBA (3 equiv)	Na_2CO_3 (1.2 equiv)	S.M. only (TLC)
5	Dodecyl	2 h	60 °C	AcOH	H_2O_2 (? equiv)	NaOH (? Equiv)	Trace (NMR)
6	Dodecyl	3 d	RT	MeOH	H_2O_2 (6 equiv)	$NaHCO_3$ (sat. aq.)	S.M. only (NMR)
7	Dodecyl	24 h	60 °C	MeOH	NaOCl (bleach, 1.2 equiv)	Aliquat 336 (0.3 equiv)	Product observed (TLC) hydrolysis on workup
8	Dodecyl	1 h	40 °C	-	NaOCl (bleach, 1.2 equiv)	Aliquat 336 (0.3 equiv) $NaHCO_3$ (Sat. aq.,	39% conversion NMR), 6.3% yield (pure), 9.7% yield (90% purity, 10% S.M.)
9	Dodecyl	1h	40 °C	-	NaOCl (bleach, 1.2 equiv)	Aliquat 336 (0.3 equiv) $NaHCO_3$ (2 equiv)	31.5% conversion (NMR)
10	Dodecyl	1h	40 °C	-	NaOCl (bleach, 2.4 equiv)	Aliquat 336 (0.3 equiv) $NaHCO_3$ (4 equiv)	60% conversion (NMR)
11	Dodecyl	1h	40 °C	-	NaOCl (10-15% soln, 2.3 equiv)	Aliquat 336 (0.3 equiv) $NaHCO_3$ (4 equiv)	75% conversion (NMR)
12	Dodecyl	2.5 h	RT	toluene	NaOCl (10-15% soln, 2.3 equiv)	Aliquat 336 (0.3 equiv)	≥ 95% conversion, 69% Yield
13	Oleyl	2.5 h	RT	toluene	NaOCl (10-15% soln, 2.3 equiv)	Aliquat 336 (0.3 equiv)	≥ 95% conversion (NMR), 56% Yield

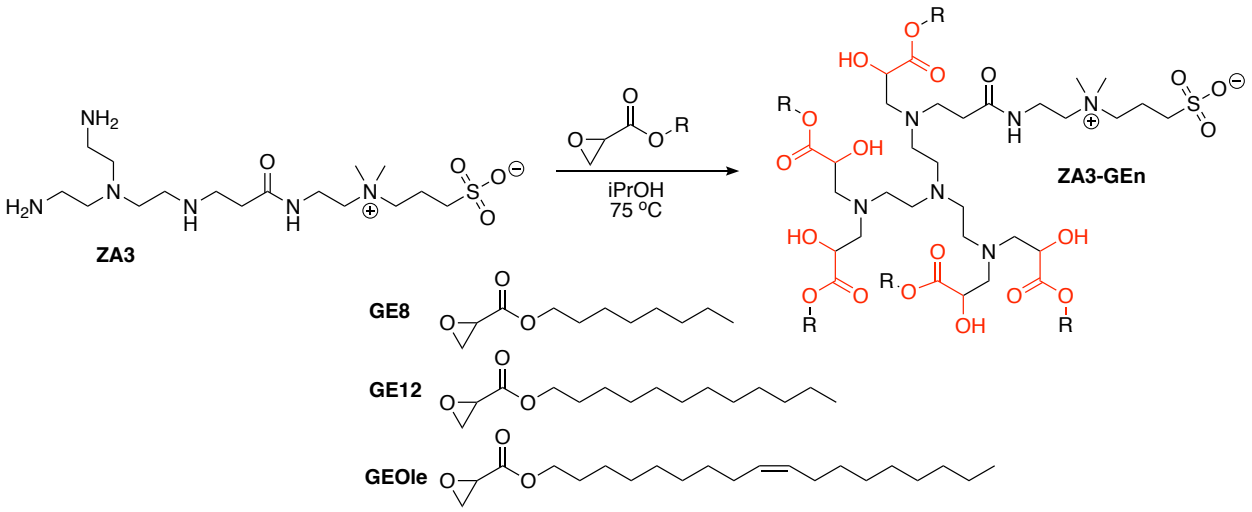

Scheme 2.2.3 Synthesis of hydrophobic glycidic ester functionalized ZALs.

ZA3 was also reacted with oleyl acrylate to form ZA3-AcOle to determine if the introduction of an unsaturated bond in the lipid tails would improve delivery, while also enabling favorable degradation properties.

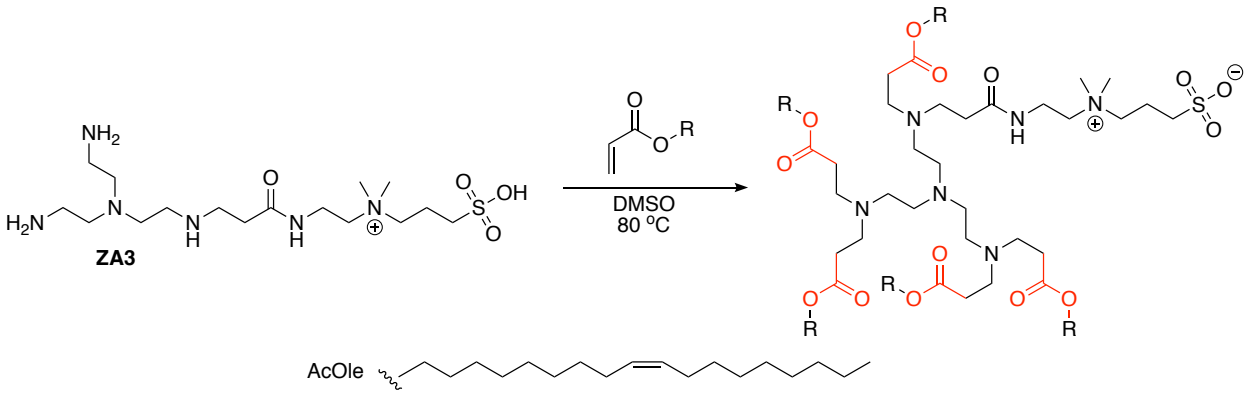

Scheme 2.2.4 Synthesis of ZA3-AcOle.

2.2.8 Characterization of mRNA and sgRNA delivery of structurally modified ZALs

Newly synthesized ZALs ZA3-Ep10-OAc, ZA3-GE8, ZA3-GE12, and ZA3-AcOle were formulated with sgLuc and Luc mRNA to determine the effects on delivery efficacy.

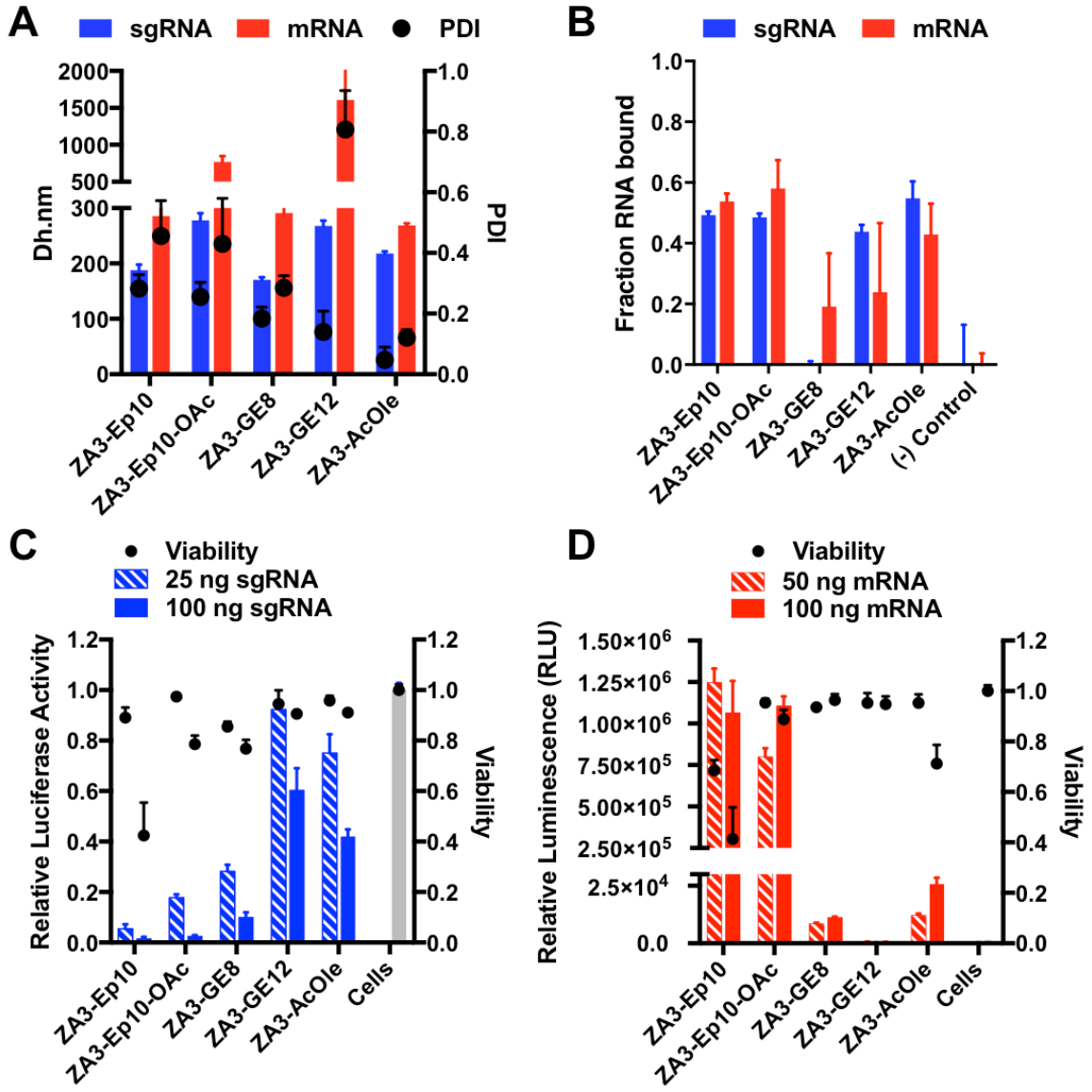

Figure 2.2.31 *In vitro* delivery of newly designed ZALs to determine SAR. Nanoparticles were formulated by manual mixing at 50:38.5:0.5 ZAL: cholesterol: PEG-lipid at N:P 8.16:1. Particles were characterized for size (A) RNA encapsulation (B) and *in vitro* delivery of sgRNA to HeLa-Luc-Cas9 cells (C) or Luc mRNA to IGROV1 cells (D). Data are plotted as a mean +/- standard deviation (B N = 3, A,C,D N = 4).

ZA3-Ep10 was used as a benchmark positive control. Formulations were characterized for nanoparticle size by DLS, RNA binding, and delivery efficacy at two doses. For sgRNA, all species showed reasonable particle size (100-300 nm) while binding was moderate. Meanwhile

for mRNA, ZA3-Ep10-OAc and ZA3-GE12 showed a larger particle size as measured by dynamic light scattering (DLS). ZA3-Ep10-OAc and ZA3-GE8 showed good luciferase silencing when delivering sgLuc to HeLa-Luc-Cas9 cells, while the acetate functionalized ZAL produced strong luciferase signal upon mRNA delivery. Interestingly, ZA3-Ep10-OAc was also considerably less toxic when compared to the parental ZAL.

Having identified ZA3-Ep10-OAc as a potent mRNA delivery carrier with low toxicity, *in vivo* evaluation was performed in parallel to ZA3-Ep10. Systemic I.V. administration of ZA3-Ep10-OAc ZNPs resulted in exclusive luciferase expression in the spleen, while ZA3-Ep10 as expected showed strongest signal in the lung, while also demonstrating some liver and spleen signal. Interestingly intramuscular injection (I.M.) of ZNPs at 0.5 mg/kg mRNA resulted in strong local expression of both carriers. ZA3-Ep10 delivering mCherry was used as a negative control.

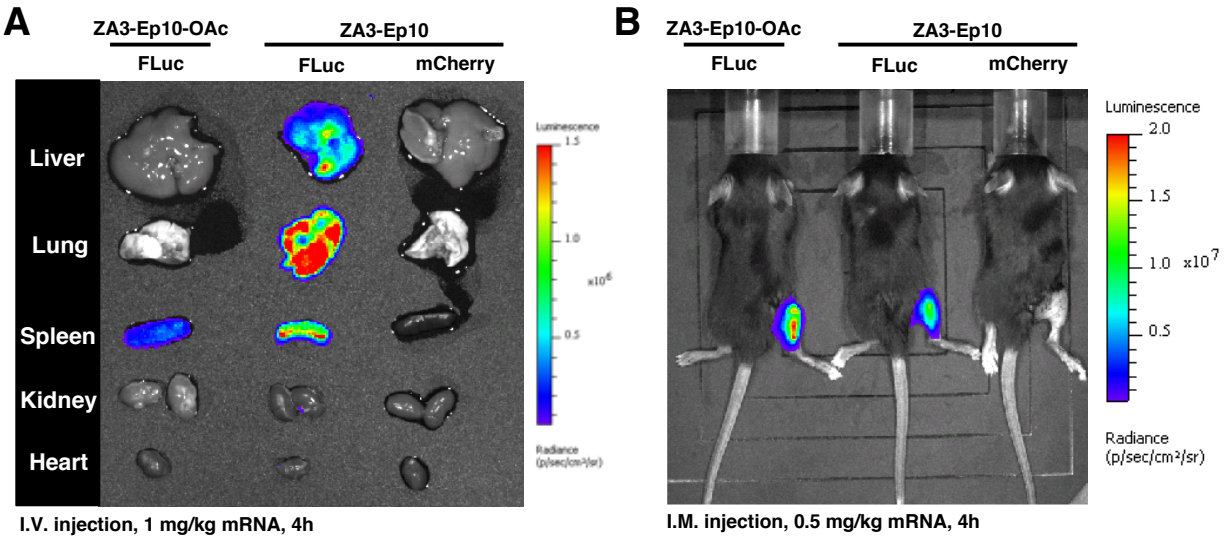

Figure 2.2.32 *In vivo* evaluation of ZA3-Ep10-OAc ZNPs for *in vivo* mRNA deliver by A) I.V. injection 1 mg/kg and B) I.M. injection at 0.5 mg/kg. IVIS imaging was performed at 4 h post injections.

The kinetics of expression following intramuscular delivery was studied (Figure 2.2.33) and showed that after a single dose at 0.5 mg/kg, the luciferase expression from ZA3-Ep10 peaked around 4 hours, and was largely gone by 24h. For ZA3-Ep10-OAc, significantly higher signal was observed, with a maximum between 8 and 16h, while the signal significantly lower by 24h. In both cases, luciferase expression was detectable at 3 d post injection.

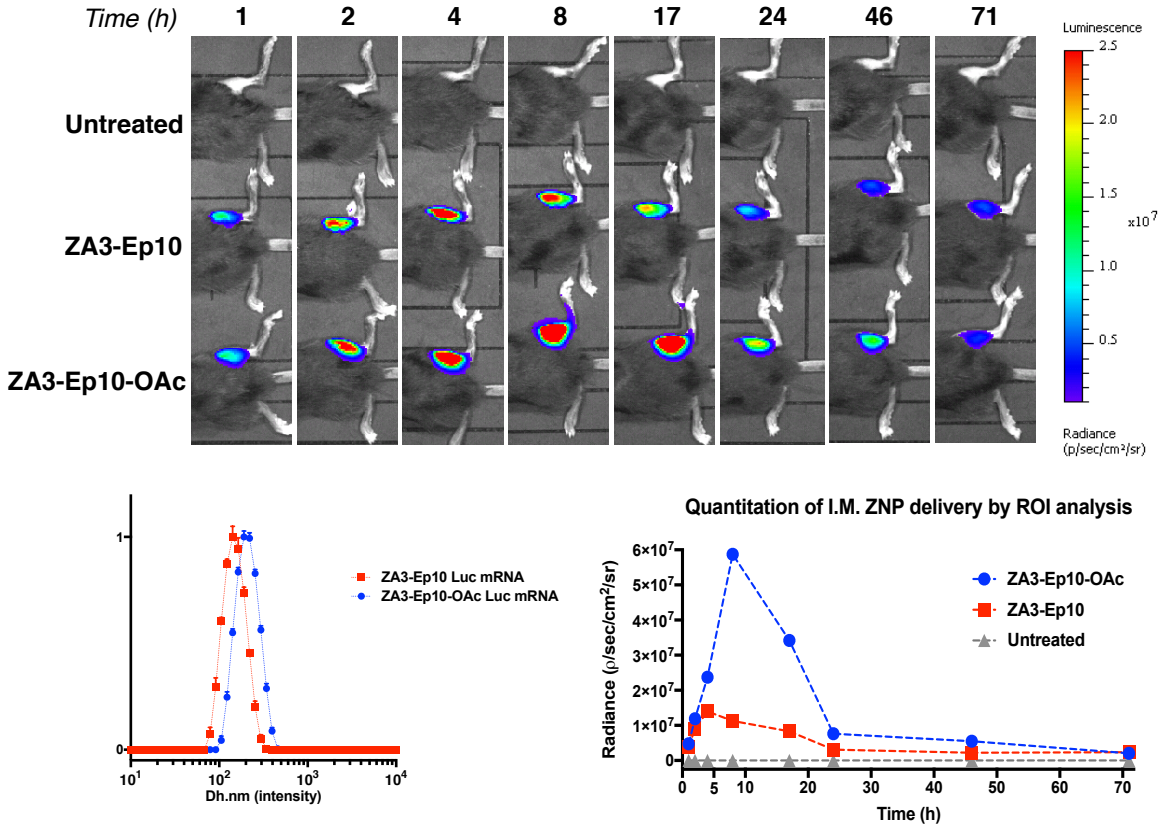

Figure 2.2.33. The kinetics of luciferase expression following I.M. injection of ZA3-Ep10 or ZA3-Ep10-OAc ZNPs (0.5 mg/kg mRNA).

2.2.9 Utility of ZNPs for mRNA delivery to iPSCs and correction of dystrophin using exon skipping CRISPR/Cas

In collaboration with the Yi-Li Min of the Eric Olson lab, ZNPs have been evaluated in pilot studies for the delivery of mRNA using ZNPs to induced pluripotent stem cells (iPSCs) and cardiomyocytes derived from iPSCs. The experiments in this section were designed by me and Yi-Li while the biological assays and corresponding figures were prepared by Yi-Li. These studies confirmed that ZA3-Ep10-C2Me was considerably less toxic than ZA3-Ep10, while both were effective in delivering mCherry mRNA to iPSCs. (Data not shown). The Olson lab is interested in using gene editing to develop a cure for Duchenne Muscular Dystrophy (DMD), a devastating disease affecting. Using a dual AAV system encoding Cas9 and guide RNAs, Long et al.[11] demonstrated rescue of dystrophin protein in skeletal muscle and rescue of forelimb grip strength. Co-delivery of sgRNA and Cas9 mRNA is a viable alternative to AAV treatment for this treatment. Administration of ZA3-Ep10 and ZA3-Ep10-OAc CRISPR ZNPs was evaluated for the rescue of dystrophin. Editing in patient-derived iPSCs bearing a deletion of exon 44 in dystrophin (Δ44) was confirmed by ZA3-Ep10 (Figure 2.2.34 left) while ZA3-Ep10 also produced strong dystrophin expression by western blot (Figure 2.2.34 right). Administration of these ZNPs to Δ44 dystrophin knockout mice via I.M. injection (3 x 0.5 mg/kg total RNA) resulted in minor rescue of dystrophin expression using ZA3-Ep10 ZNPs but not ZA3-Ep10-OAc (Figure 2.2.35). This may indicate that ZA3-Ep10-OAc requires formulation optimization to be suitable for Cas9 mRNA delivery, but the therapeutic potential of this approach is currently under investigation.

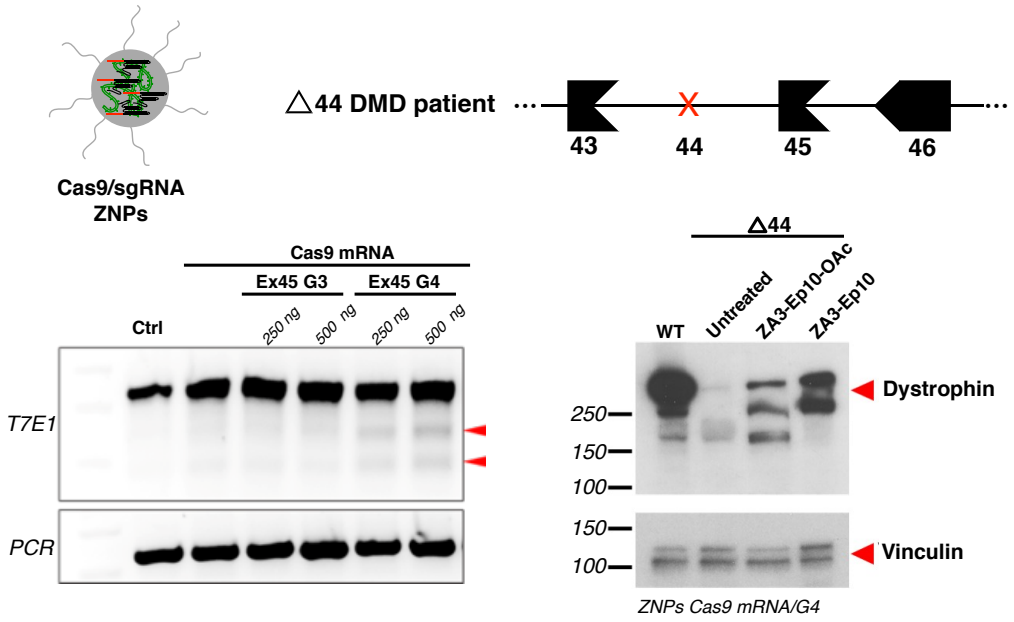

Figure 2.2.35 Editing of dystrophin in Δ44 dystrophin knockout iPSCs is confirmed by the T7E1 assay, while the rescue of dystrophin protein (right) is observed by ZA3-Ep10 ZNPs by western blot. Minor dystrophin rescue is also observed using ZA3-OAc-C2Me. Nanoparticles were prepared by Jason Miller, biological assays were performed by Yi-Li Min.

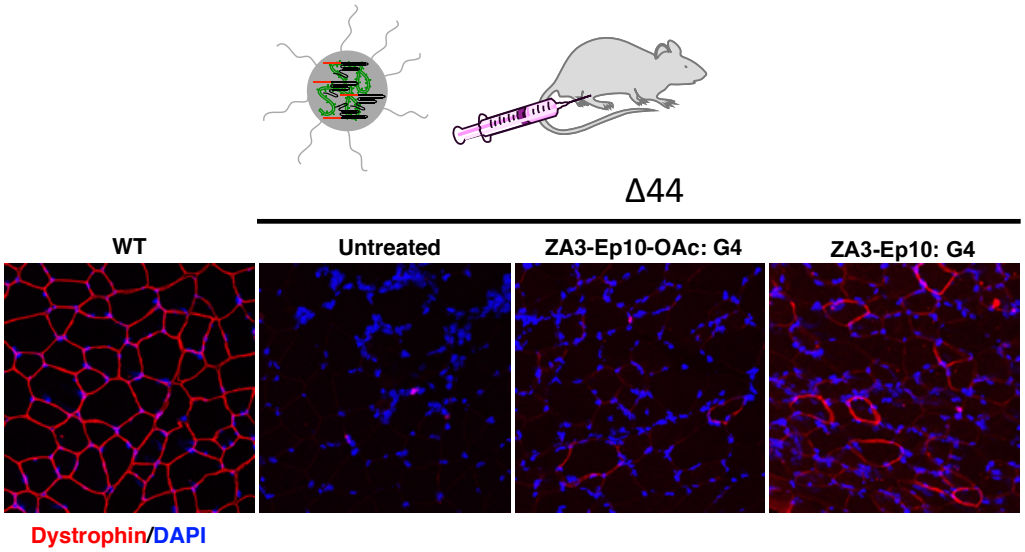

Figure 2.2.36 The rescue of dystrophin expression in knockout mice by non-viral gene-editing using ZNPs. ZNPs were administered at 0.5 mg/kg on 3 consecutive days and tissue was harvested one week after treatment. The animal model was created by, and biological experiments were processed by Yi-Li Min from the Olson lab. Dystrophin is stained red, DAPI is stained blue.

2.3 CONCLUSION

Zwitterionic amino lipids are a novel class of lipid materials that are effective for the *in vivo* delivery of messenger RNA and for gene editing using CRISPR/Cas nanoparticles *in vitro* and *in vivo*. This study was the first report of non-viral delivery system for *in vitro* and *in vivo* co-delivery of Cas9 mRNA and targeted sgRNA. Given that multiple long RNAs can be packaged together, it is likely that ZNPs will be able to deliver DNA repair templates to mediate HDR gene correction, which will be the focus of future studies. Additionally, future work will focus on the further therapeutic development of ZNPs for the treatment of DMD, while the clinical utility will be expanded using chemistry approaches to install pharmacodyamically favorable features. The use of scalable and translatable technologies, such as ZNPs, will provide powerful tools for *in vivo* gene editing to understand biology, create animal models, and treat diseases.

2.4 MATERIALS and METHODS

2.4.1 Materials

a) Chemicals and reagents for synthesis. All chemicals were purchased from Sigma-Aldrich unless otherwise indicated. 1,2-epoxydecane was purchased from TCI America. 1,2-epoxyoctadecane was purchased from Alfa Aesar. Hydrophobic acrylates octyl acrylate (Ac8), decyl acrylate (Ac10), tetradecyl acrylate (Ac14), and hexadecyl acrylate (Ac16) were synthesized as described below. Organic solvents were purchased from Fisher Scientific and purified with a solvent purification system (Innovative Technology). Lipid PEG2000 was chemically synthesized, as previously described.[6] $CDCl_3$, methanol-*d4*, and DMSO-*d6* were purchased from Cambridge Isotope Laboratories.

b) Nucleic acids and other reagents for biological assays. All siRNAs were purchased from Sigma-Aldrich. DNA oligonucleotides were purchased from Integrated DNA Technologies. Luciferase, mCherry, and Cas9 messenger RNA (mRNA) were purchased from Tri-Link Biotechnologies. Lipofectamine 3000 and OptiMEM were purchased from Invitrogen. Single guide RNA was prepared by *in vitro* transcription (IVT) using the MEGAshortscript T7 transcription kit (Life Technologies) followed by purification using the MEGAclear Transcription Clean-Up Kit (Life Technologies) according to the manufacturer's protocols. The Ribogreen reagent was purchased from Life Technologies. ONE-Glo + Tox and Cell Titer Glow were purchased from Promega. RIPA buffer and TRIzol reagent were purchased from Thermo Scientific. QuickExtract DNA Extraction Solution was purchased from Epicentre. Real-time qPCR

was performed using iTaq Universal SYBR Green 2X Supermix (Bio-Rad). All antibodies were purchased from Cell Signaling.

c) Cell culture. Dulbecco's Modified Eagle Medium (DMEM) was purchased from Hyclone containing high glucose, L-glutamine, and without pyruvate or phenol red. RPMI-1640 was purchased from Sigma Aldrich. Dulbecco's modified phosphate buffered saline (PBS), Trypsin-EDTA (0.25%) and fetal bovine serum (FBS) were purchased from Sigma-Aldrich. HeLa-Luc and A549-Luc cells were cultured in DMEM supplemented with 5% FBS. IGROV1 cells were cultured in RPMI-1640 supplemented with 5% FBS.

d) Animal studies. All experiments were approved by the Institutional Animal Care & Use Committee (IACUC) of The University of Texas Southwestern Medical Center and were consistent with local, state and federal regulations as applicable. C57BL/6 and athymic nude Foxn1nu mice were purchased from Envigo. NOD scid gamma (NSG) mice were purchased from the UT Southwestern animal breeding core. Rosa-CAG-LSL-tdTomato mice were purchased from The Jackson Laboratory (Stock number: 007909).

2.4.2 Instrumentation

a) Nuclear magnetic resonance (NMR) spectroscopy. ^{1}H and ^{12}C NMR were performed on a Varian 400 MHz spectrometer or a Varian 500 MHz spectrometer.

b) Mass spectroscopy (MS). MS was performed on a Voyager DE-Pro MALDI-TOF. LCMS was performed on an Agilent LCMS system equipped with UV-vis and evaporative light scattering detectors (ELSD).

*c) Flash chromatography***.** Flash chromatography was performed on a Teledyne Isco CombiFlash Rf- 200i chromatography system equipped with UV-vis and evaporative light scattering detectors (ELSD).

d) Nanoparticle size and zeta potential analysis. Particle sizes and zeta potentials were measured by Dynamic Light Scattering (DLS) using a Malvern Zetasizer Nano ZS (He-Ne laser, $\lambda = 632$ nm).

e) Nanoparticle formulation for in vivo studies. Zwitterionic amino lipid (ZAL) nanoparticles (ZNPs) for *in vivo* studies were prepared using a two-channel microfluidic mixer with herringbone rapid mixing features (Precision Nanosystems NanoAssemblr). Ethanol solutions of lipid mixes (ZALs, cholesterol, and PEG-lipid) were rapidly combined with acidic aqueous solutions of nucleic acid at an aqueous: EtOH volumetric ratio of 3:1 and a flow rate of 12 mL/minute.

f) Real-time qPCR. RT qPCR was run on a Bio-Rad C1000 Touch Thermal Cycler (CFX384 Real-time System). Each reaction was made with iTaq Universal SYBR Green 2X Supermix (Bio-Rad).

g) Confocal laser scanning microscopy. Tissue sections were imaged using confocal laser scanning microscopy with a Zeiss LSM-700 and images were processed using ImageJ (NIH).

h) Flow cytometry. Flow cytometry was performed with BD FACSAria Fusion machine (BD Biosciences).

2.4.3 Chemical synthesis

2.4.3.1 Synthesis of 3-((2-acrylamidoethyl)dimethylammonio)propane-1-sulfonate (SBAm): A flame-dried 500 mL round-bottom flask equipped with a stir bar, and an addition funnel under a nitrogen atmosphere was charged with *N,N*-dimethyl ethenediamine (20 g, 226.9 mmol) and

triethylamine (1 equiv, 227 mmol, 31.6 mL) in 250 mL dry THF, and cooled to 0 °C. Acryloyl chloride (0.9 equiv, 204.2 mmol, 16.6 mL) was dissolved separately in 50 mL dry THF and added dropwise via an addition funnel to the stirring amine solution. The reaction was allowed to warm to room temperature overnight which resulted in a yellow solution with white precipitate. The precipitate was filtered off and the filtrate was concentrated in vacuo. The crude product was purified by a silica gel column (20% MeOH in DCM). The product was dried with anhydrous sodium sulfate and concentrated under reduced pressure to yield the dimethylamino acrylamide intermediate as an orange liquid (9.36 g, 32.2% yield for step 1).

In a 250 mL round-bottom flask equipped with a stir bar, the dimethylamino acrylamide intermediate (9.36 g, 65.8 mmol) was dissolved in 100 mL acetone. In one portion, 1,3-propanesultone (1.1 equiv, 72.4 mmol, 8.85 g) was added. A rubber stopper with a needle vent was installed and the reaction mixture was heated to 50 °C overnight, yielding the formation of an off white solid precipitate. The precipitate was collected by vacuum filtration, washed with copious amounts of acetone, and dried under vacuum overnight yielding the SBAm product as a light yellow solid (14.77 g, 84.9% yield for step 2). Mass calculated *m*/z 264.11, observed M^{+1} (LCMS direct injection) *m/z* 265.1. ^{1}H NMR (400 MHz, D_2O) δ 6.33 – 6.17 (m, 2H), 5.80 (dd, J = 8.8, 2.7 Hz, 1H), 3.77 (t, J = 6.8 Hz, 2H), 3.52 (dd, J = 12.0, 5.5 Hz, 4H), 3.17 (s, 6H), 2.97 (t, J = 7.2 Hz, 2H), 2.30 – 2.17 (m, 2H).

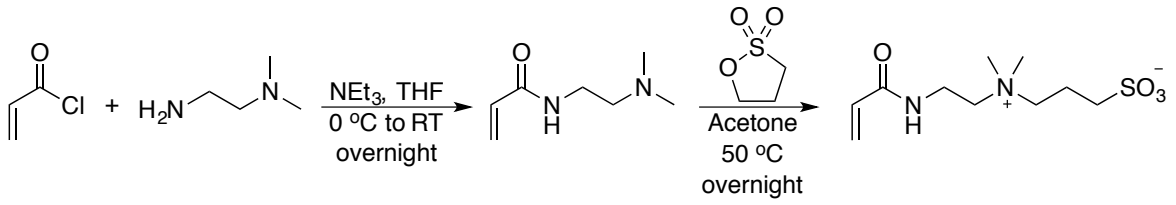

2.4.3.2 General synthesis of propanesulfonate amide-bearing zwitterionic amines (ZAx). In a 20 mL vial equipped with a stir bar, 3-((2-acrylamidoethyl)dimethylammonio)propane-1-sulfonate (SBAm, 1.5 g, 5.67 mmol, 1 equiv) was dissolved in 5.67 mL deionized water to a concentration of 1M. The corresponding amine (28.35 mmol, 5 equiv) was added via pipette in one portion, the vial covered and stirred at room temperature overnight. After overnight reaction, the amino SBAm reaction mixture was transferred to several 50 mL polypropylene conical tubes was precipitated in >10 volumes acetone to remove the residual amine starting material, collected by centrifugation (4000 x g, 10 minutes). The supernatant was decanted, the pellet washed with acetone, and dried under vacuum to yield the amino SBAms, which were used without further purification.

ZA1: Light yellow sticky solid (2.40 g, 93.6% yield). Mass calculated *m*/z 452.31, observed M^{+1} (LCMS direct injection) *m/z* 453.3. ^{1}H NMR (400 MHz, D_2O) δ 3.65 (t, J = 6.8 Hz, 2H), 3.48 (ddd, J = 13.7, 9.5, 5.7 Hz, 4H), 3.14 (s, 6H), 2.95 (t, J = 7.2 Hz, 2H), 2.68 (s, 2H), 2.65 – 2.54 (m, 14H), 2.54 – 2.48 (m, 2H), 2.29 (d, J = 1.0 Hz, 9H), 2.22 – 2.16 (m, 4H).

ZA2: Reaction done on a 0.776 g SBAm scale. Viscous yellow oil (0.36 g, 24.8% yield). Mass calculated *m*/z 536.41, observed M^{+1} (LCMS direct injection) *m/z* 537.4. ^{1}H NMR (500 MHz, Deuterium Oxide) δ 3.50 (t, J = 7.0 Hz, 2H), 3.33 (ddd, J = 22.0, 11.2, 5.7 Hz, 4H), 2.98 (s, 6H), 2.83 – 2.62 (m, 4H), 2.57 (dt, J = 21.3, 7.3 Hz, 4H), 2.44 (p, J = 7.1 Hz, 6H), 2.30 – 2.23 (m, 1H), 2.11 – 2.01 (m, 2H), 0.92 – 0.86 (m, 9H), 0.84 (d, J = 6.5 Hz, 4H).

ZA3: Brown sticky solid (2.61 g, quantitative yield). Mass calculated *m*/z 410.58, observed M^{+1} (LCMS direct injection) *m/z* 411.3. ^{1}H NMR (500 MHz, D_2O) δ 3.62 (t, J = 6.7 Hz, 2H), 3.50 – 3.40 (m, 4H), 3.11 (d, J = 1.4 Hz, 6H), 2.92 (td, J = 7.2, 1.3 Hz, 2H), 2.82 – 2.68 (m, 5H), 2.66 – 2.49 (m, 8H), 2.41 (ddd, J = 8.2, 5.9, 1.3 Hz, 2H), 2.23 – 2.14 (m, 2H).

ZA4: Light yellow sticky solid (2.01 g, 92.9% yield) Mass calculated *m*/z 381.24, observed M^{+1} (LCMS direct injection) *m/z* 382.2. ^{1}H NMR (400 MHz, D_2O) δ 3.66 (t, J = 6.8 Hz, 2H), 3.49 (ddd, J = 13.7, 8.7, 5.8 Hz, 4H), 3.14 (s, 6H), 2.96 (t, J = 7.2 Hz, 2H), 2.86 – 2.64 (m, 6H), 2.57 – 2.40 (m, 5H), 2.28 – 2.14 (m, 6H).

ZA5: Sticky yellow solid (2.32 g, 84.1% yield). Mass calculated *m*/z 409.27, observed M^{+1} (LCMS direct injection) *m/z* 410.2. ^{1}H NMR (400 MHz, D_2O) δ 3.52 (t, J = 6.8 Hz, 3H), 3.35 (ddd, J = 13.8, 9.0, 5.6 Hz, 5H), 3.00 (s, 7H), 2.82 (t, J = 7.2 Hz, 3H), 2.65 (t, J = 7.1 Hz, 3H), 2.49 (q, J = 6.4, 5.5 Hz, 1H), 2.39 (t, J = 7.4 Hz, 2H), 2.26 (dq, J = 15.4, 5.4, 3.7 Hz, 7H), 2.14 – 1.99 (m, 7H), 1.55 – 1.41 (m, 4H).

ZA6: Sticky yellow solid (2.71 g, quantitative yield). Mass calculated *m*/z 464.31, observed M^{+1} (LCMS direct injection) *m/z* 465.3. ^{1}H NMR (500 MHz, D_2O) δ 3.64 (t, J = 6.9 Hz, 2H), 3.52 – 3.42 (m, 4H), 3.12 (s, 7H), 2.94 (t, J = 7.2 Hz, 3H), 2.82 – 2.68 (m, 5H), 2.53 (t, J = 7.4 Hz, 2H), 2.45 – 2.30 (m, 7H), 2.26 – 2.15 (m, 4H), 1.64 (tdd, J = 15.5, 12.1, 7.6 Hz, 4H).

2.4.3.3 Hydrophobic acrylate (Acn) synthesis. Hydrophobic acrylates were synthesized by the reaction of hydrophobic primary alcohols with acryloyl chloride at large scale. In a dry 250-mL round bottom flask under argon, the appropriate hydrophobic alcohol (10 or 15 g, 1 equiv) and triethylamine (1 equiv) were dissolved in 85 mL dry tetrahydrofuran and cooled to 0 °C on ice. Acryloyl chloride (0.9 equiv) was dissolved separately in 15 mL dry THF and added dropwise to the solution of alcohol and triethylamine, resulting in the formation of a white precipitate. The reaction was stirred and allowed to warm to room temperature. The precipitate was removed by fitration, the solvent removed under reduced pressure and the desired acrylate pruified on a column of silica gel with 5-10% ethyl acetate in hexanes to yield the products as pale yellow oils.

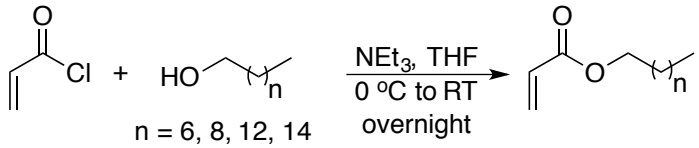

Ac8: 10 g alcohol scale, pale yellow oil, 9.75 g, 76.6% yield.

^{1}H NMR (400 MHz, $CDCl_3$) δ 6.37 (d, J = 17.3 Hz, 1H), 6.10 (dd, J = 17.3, 10.4 Hz, 1H), 5.79 (d, J = 10.5 Hz, 1H), 4.13 (t, J = 7.0 Hz, 2H), 1.65 (q, J = 6.9 Hz, 2H), 1.42 – 1.16 (m, 10H), 0.86 (t, J = 6.7 Hz, 3H).

Ac10: 10 g alcohol scale, pale yellow oil, 10.98 g, 90.9% yield.

^{1}H NMR (400 MHz, $CDCl_3$) δ 6.38 (d, J = 17.3 Hz, 1H), 6.10 (dd, J = 17.3, 10.4 Hz, 1H), 5.79 (d, J = 10.5 Hz, 1H), 4.13 (t, J = 6.8 Hz, 2H), 1.66 (q, J = 7.0 Hz, 2H), 1.41 – 1.18 (m, 14H), 0.86 (t, J = 6.6 Hz, 3H).

Ac14: 15 g alcohol scale, pale yellow oil, 15.28 g, 90.5% yield.

^{1}H NMR (400 MHz, $CDCl_3$) δ 6.37 (dd, J = 17.3, 1.5 Hz, 1H), 6.09 (dd, J = 17.3, 10.4 Hz, 1H), 5.77 (dd, J = 10.4, 1.5 Hz, 1H), 4.12 (t, J = 6.8 Hz, 2H), 1.69 – 1.59 (m, 2H), 1.39 – 1.15 (m, 21H), 0.85 (d, J = 7.1 Hz, 3H).

Ac16: 15 g alcohol scale, pale yellow oil, 11.27 g, 68.3% yield.

^{1}H NMR (400 MHz, $CDCl_3$) δ 6.39 (dd, J = 17.4, 1.5 Hz, 1H), 6.11 (dd, J = 17.3, 10.4 Hz, 1H), 5.80 (dd, J = 10.4, 1.5 Hz, 1H), 4.14 (t, J = 6.7 Hz, 2H), 1.72 – 1.61 (m, 2H), 1.25 (s, 26H), 0.87 (t, J = 6.8 Hz, 3H).

2.4.3.4 Synthesis of Amino SBAm epoxide and acrylate libraries of zwitterionic amino lipids (ZALs): A zwitterionic amino lipid (ZAL) library of all previously described amino SBAms was prepared by introduction of hydrophobic tails through reaction with 1,2-epoxy alkanes and

hydrophobic acrylates. The epoxides (1,2-epoxyoctane, 1,2-epoxydecane, 1,2-epoxydodecane, 1,2-epoxytetradecane, 1,2-epoxyhexadecane, and 1,2-epoxyoctadecane) were purchased commercially and encoded to include the total number of carbon atoms in the molecule (Ep*n*, 8-18). The hydrophobic acrylates were either purchased commercially (Ac12, Ac18) or synthesized by the reaction of the appropriate primary alcohol with acryloyl chloride (Ac8, Ac10, Ac14, Ac16), and encoded to include the number of carbon atoms in the hydrophobic tail, but not including the acrylate moiety (Ac*n*, 8-18). To prepare the library, in a 4 mL vial equipped with a stir bar, the zwitterionic amines (0.1 mmol or 0.05 mmol) were weighed out by balance, and dissolved to a concentration of 1 M in *i*PrOH for epoxide ZALs or in DMSO for acrylate ZALs. The appropriate hydrophobic electrophile was added with N equivalents, where N is the number of amine reactive sites that would yield complete conversion of primary and secondary amines to tertiary amines. The vials were sealed and the reactions stirred for several days at 75 °C for epoxides and 80 °C for acrylates. After reaction, the reactions were precipitated in acetone to yield the zwitterionic aminolipids. The crude products were used to screen the library for siRNA delivery efficacy without further purification.

2.4.3.5 Alternative Synthesis of amino SBAm ZA3: A 20 mL vial equipped with a stir bar was charged with 3-((2-acrylamidoethyl)dimethylammonio)propane-1-sulfonate (SBAm, 0.8111 g, 3.068 mmol) and dissolved in 3 mL DMSO. Via syringe, tris(2-aminoethyl) amine (5 equiv, 15.32 mmol, 2.24 g) was added yielding a cloudy yellow/brown suspension. The reaction mixture was sealed and stirred at 80 °C overnight, yielding an orange cloudy suspension. The reaction mixture was further diluted in DMSO, transferred to several 50 mL conical tubes and precipitated in 10 volumes ethyl acetate. The precipitate collected by centrifugation (4,000 x g, 10 minutes), and the

supernatant decanted to yield a sticky yellow/brown. The product was re-precipitated in DMSO/EtOAc several times to remove any residual tris(2-aminoethyl) amine, and finally dissolved in MeOH transferred to round-bottom flask and concentrated under reduced pressure. The product was dried overnight under vacuum to remove residual solvent, re-dissolved in methanol and precipitated in ethyl acetate, and dried under vacuum to yield 110SBAm as an orange/brown oil (1.4058 g, >100% but ^{1}H NMR shows residual DMSO) and used in subsequent reactions without further purification.

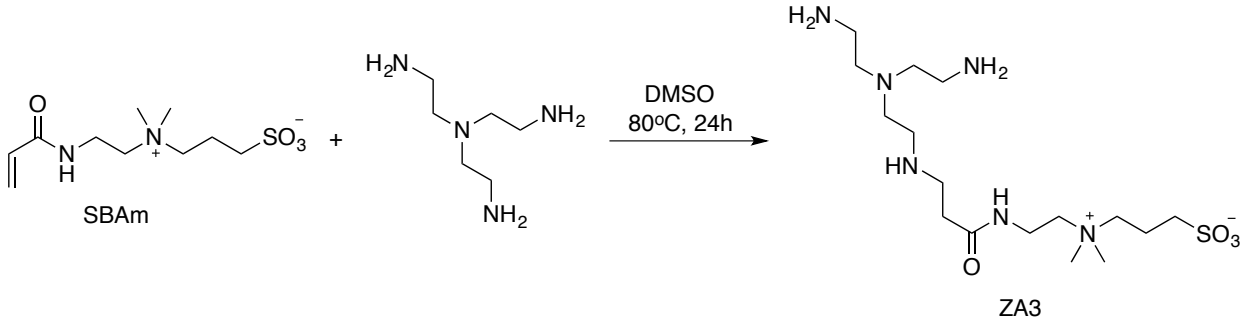

2.4.3.6 Synthesis of ZA3-Ep10: A 20 mL vial equipped with a stir bar was charged with 110SBAm (300 mg, 0.7307 mmol) and iPrOH (730 µL, 1M SBAm) and stirred briefly at RT to yield a yellow/brown suspension. 1,2-epoxydecane (4.384 mmol, 685 mg, 6 equiv) was added, the vial was sealed and stirred overnight at 75 °C for approximately 24h resulting in a clear yellow/brown solution. The iPrOH was removed under reduced pressure to yield a yellow/brown oil. The crude product was dissolved in minimal 5% MeOH in DCM and purification was carried out on a silica gel column (24g) using the Combiflash system (Teledyne Isco). The product was eluted and fractionated with a solvent gradient of 5% MeOH in DCM to 20% MeOH, 2% saturated ammonium hydroxide in DCM and the product elution tracked by ELSD. The product containing fractions were concentrated under reduced pressure, and dried under vacuum overnight to yield

the product as a sticky yellow solid (192.5 mg, 22.1% yield). Mass calculated *m*/z 1191.0246, observed M^{+1} (LCMS direct injection) *m/z* 1192.8. ^{1}H NMR (400 MHz, $CDCl_3$) δ 8.72 (d, J = 5.8 Hz, 1H), 4.56 – 3.92 (m, 2H), 3.76 – 3.54 (m, 12H), 3.20 (d, J = 3.3 Hz, 6H), 2.88 (dq, J = 36.8, 13.1 Hz, 10H), 2.69 – 2.60 (m, 4H), 2.54 (d, J = 14.2 Hz, 3H), 2.49 – 2.30 (m, 9H), 2.22 (dd, J = 11.0, 5.5 Hz, 2H), 1.44 – 1.23 (m, 66H), 0.87 (t, J = 6.7 Hz, 15H).

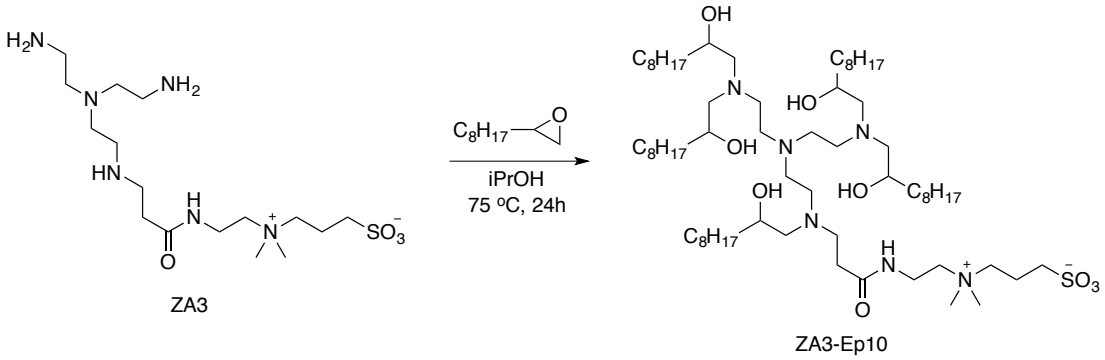

ZA3

ZA3-Ep10

2.4.4 Nucleic Acid Sequences

Small interfering RNAs (siRNAs)

dT are DNA bases. All others are RNA bases. siRNAs were chemically synthesized as oligonucleotides and annealed into dsRNA by Sigma Aldrich.

siLuc (siRNA against Luciferase).

sense: 5'-GAUUAUGUCCGGUUAUGUA[dT][dT]-3'

antisense: 5'-UACAUAACCGGACAUAAUC[dT][dT]-3'

siCtrl (non-targeting siRNA)

sense: 5'-GCGCGAUAGCGCGAAUAUA[dT][dT]-3'

antisense: 5'- UAUAUUCGCGCUAUCGCGC[dT][dT]-3'

Single guide RNAs (sgRNAs). Guide RNAs were designed using the CRISPR.mit.edu platform and cloned into pSpCas9(BB)-2A-GFP (PX458) as previously reported.[131]

Table 2.4.1. sgRNA sequences

Guide name	Target	Guide sequence (5' to 3')	PAM	Strand
sgLuc1	Luciferase	CTTCGAAATGTCCGTTCGGT	TGG	Positive
sgLuc2	Luciferase	CCCGGCGCCATTCTATCCGC	TGG	Positive
sgLuc3	Luciferase	TCCAGCGGATAGAATGGCGC	CGG	Negative
sgLuc4	Luciferase	GGATTCTAAAACGGATTACC	AGG	Positive
sgLuc5	Luciferase	ATAAATAACGCGCCCAACAC	CGG	Negative
sgLoxP	LoxP	CGTATAGCATACATTATACG	AAG	Negative
sgCtrl	Mouse F7	GCTTCGATAATATCCGCTAC	TGG	Positive

Table 2.4.2. BbsI sgRNA cloning oligos

Probe	Sequence (5' to 3')*
sgLuc1_Top	CACCG**CTTCGAAATGTCCGTTCGGT**
sgLuc1_Bottom	AAACACCGAACGGACATTTCGAAGC
sgLuc2_Top	CACCG**CCCGGCGCCATTCTATCCGC**
sgLuc2_Bottom	AAACGCGGATAGAATGGCGCCGGGC
sgLuc3_Top	CACCG**TCCAGCGGATAGAATGGCGC**
sgLuc3_Bottom	AAACGCGCCATTCTATCCGCTGGAC
sgLuc4_Top	CACCG**GGATTCTAAAACGGATTACC**
sgLuc4_Bottom	AAACGGTAATCCGTTTTAGAATCCC
sgLuc5_Top	CACCG**ATAAATAACGCGCCCAACAC**
sgLuc5_Bottom	AAACGTGTTGGGCGCGTTATTTATC
sgLoxP_Top	CACCG**CGTATAGCATACATTATACG**
sgLoxP_Bottom	AAACCGTATAATGTATGCTATACGC
sgCtrl_Top	CACCG**GCTTCGATAATATCCGCTAC**
sgCtrl_Bottom	AAACGTAGCGGATATTATCGAAGCC

*Guide sequence shown in **bold.**

Table 2.4.3 T7 template PCR primers

Primer	Sequence (5' to 3')
IVT sgLuc-fwd	TAATACGACTCACTATAGGGATAAATAACGCGCCCAACAC
IVT sgLoxP-fwd	TAATACGACTCACTATAGGGCGTATAGCATACATTATACG
IVT sgCtrl-fwd	TAATACGACTCACTATAGGGGCTTCGATAATATCCGCTAC
IVT-rev (common)	AAAAGCACCGACTCGGTGCC

Table 2.4.4. Surveyor assay PCR primers

Primer	Sequence (5' to 3')	Amplicon	Expected cut bands
Luc 1_Forward	ggaaccgctggagagcaact	510 bp	233 bp, 277 bp
Luc 1_Reverse	gtccctatcgaaggactctggca		
Luc 2_Forward	GCTGGAGAGCAACTGCATAA	429 bp	202 bp, 227 bp
Luc 2_Reverse	CATCGACTGAAATCCCTGGTAATC		

Table 2.4.5. Real time qPCR primers

Primer	Sequence (5' to 3')
Cas9 forward	ggaaccgctggagagcaact
Cas9 reverse	gtccctatcgaaggactctggca
hActinB forward	AGAAGGATTCCTATGTGGGCG
hActinB reverse	CATGTCGTCCCAGTTGGTGAC

2.4.5 Biological assays

*2.4.5.1 sgRNA preparation***.** Single guide RNAs were designed using the CRISPR.mit.edu platform and cloned into PX458 plasmid with standard BbsI cloning. T7 transcription templates were amplified by PCR and gel purified. sgRNAs were synthesized by *in vitro* transcription using the MEGAshortscript T7 transcription kit (Life Technologies) followed by purification using the MEGAclear Transcription Clean-Up Kit (Life Technologies) according to the manufacturer's protocols.

*2.4.5.1 Screening of sgRNA using pDNA***.** sgRNA-cloned PX458 plasmids were used to evaluated efficacy of the sgRNAs against luciferase by transfection of the plasmid encoding both sgRNA and Cas9. Lipofectamine 3000 (LF3000, Invitrogen) was used to transfect the sgRNA-Cas9 plasmids according to manufacturer's protocols. HeLa-Luc cells were seed in a 96-well white-opaque tissue culture plate at a density of 10,000 cells per well. LF3000 pDNA particles were added to the cells at a dose of 100 ng pDNA per well. After 6 hours, the medium was removed and exchanged for 200 μL fresh growth medium. After 24, 48 and 72h, the relative expression of luciferase was determined using the One-Glo + Tox assay (Promega) and normalized to control. Non-targeting sgRNA (sgScr) and unguided Cas9 plasmids were used as a control. (N = 4 +/- standard deviation).

2.4.5.3 HeLa-Luc-Cas9 cell line preparation. HeLa-Luc-Cas9 stable cells were prepared by lentiviral transduction. Parental HeLa-Luc cells[6, 159] were seeded at a density of 70,000 cells per well in a 24-well plate in complete growth medium and allowed to attach in the incubator overnight. The medium was replaced with 1 mL pre-warmed pseudoparticle medium (DMEM, 3% FBS, 20 mM HEPES, 4 μg/mL polybrene). Cas9-Blast lentivirus supernatant was thawed on ice and 50-100 μL was added to the desired well. The cells were spinoculated at room temperature for 1 hour at 1,000 x g, and returned to the incubator overnight, after which the pseudoparticle medium was exchanged for complete growth medium. After 48h total time post spinoculation, selective pressure was applied (5 and 10 μg/mL Blasticidin S) and cells were maintained and expanded. Single cell clones were isolated by single cell sorting by flow cytometry. Cas9 protein expression was confirmed by western blot compared to parental HeLa-Luc cells by blotting for FLAG tag before single cell sorting and for Cas9 after single cell sorting.

2.4.5.4 In vitro ZAL nanoparticle (ZNP) formulations. ZNPs were prepared by the ethanol dilution method. The RNA (whether an siRNA, sgRNA, or mRNA) was diluted in acidic aqueous buffer (unless otherwise indicated, 10 mM citric acid/sodium citrate buffer pH 3). The lipid mix was prepared in ethanol, with the appropriate molar ratios of ZAL, cholesterol and PEG-lipid from ethanol stock solutions of each component. Via pipette, the lipid dilution was added to the RNA dilution at a final volumetric ratio of 1:3, rapidly mixed by pipette, and incubated for 15-20 minutes. After this incubation period, the particles were either diluted 3-fold in, or dialyzed against 1X Dulbecco's Modified PBS without calcium and magnesium (Sigma-Aldrich). Dialyses were performed in Pur-A-Lyzer Midi dialysis chambers (Sigma-Aldrich) for 1 hour per 200 μL sample per chamber.

2.4.5.6 ZAL siRNA delivery library screen. The library of ZALs functionalized with epoxide and acrylate hydrophobic tails was screened for siRNA delivery efficacy in HeLa-Luc cells. In a white opaque 96-well plate tissue culture plate, HeLa cells were seeded at a density of 10 x 10^3 cells per well in 100 μL growth medium (DMEM without phenol red, 5% FBS), and allowed to attach overnight. The medium was exchanged for 200 μL fresh growth medium the day of the assay. Crude ZALs products were prepared using a formulation lipid mixture of 50:38.5 (ZAL: cholesterol), and a ZAL:siRNA ratio such that the number of hydrophobic tails in the ZAL times the ZAL:siRNA mole ratio in the formulation was ~1000, which resulted in a weight ratio range across the library of 16:1 to 45:1 ZAL:siRNA, with an average of 29.5 +/- 6.3 weight ratio across the library. ZAL NP formulations were performed in a 96-well plate by rapid mixing of ZAL lipid mix (20 μL) and siLuc dilution (60 μL, 13.33 ng/μL in 10 mM citric acid-sodium citrate buffer, pH 5) at 3:1 aqueous:EtOH *v:v* ratio with a multichannel pipette. After a 15-20 minute incubation

period, the formulations were diluted in 12 volumes (240 μL) PBS. The nanoparticles (40 μL) were added to the HeLa-Luc cells at a dose of 100 ng siRNA per well. The nanoparticles were incubated with the cells for 24 h after which time the cell viability and luciferase expression were evaluated with the ONE-Glo + Tox Assay cell viability and luciferase assay (Promega).

*2.4.5.7 sgRNA delivery to HeLa-Luc-Cas9 cells***.** Select ZALs were evaluated in the delivery of single guide RNA (sgRNA) to HeLa-Luc-Cas9 cells. In a white opaque 96-well plate tissue culture plate, HeLa-Luc-Cas9 cells were seeded at a density of 5 x 10^3 cells per well in 100 μL growth medium (DMEM without phenol red, 5% FBS), and allowed to attach overnight and then supplemented with an additional 100 μL DMEM. ZNPs encapsulating sgRNA were formulated using the *in vitro* nanoparticle formulation protocol at the indicated lipid composition and weight ratio (maintaining 50:38.5 (ZAL:cholesterol mole ratio), tuning PEG-lipid additive from 5% to 0.5%, and tuning weight ratio from 20:1 ZAL:sgRNA to 5:1 ZAL:sgRNA). Non-targeting control sgRNA (sgCtrl) was used as a negative control. The nanoparticles were added to the cells at the appropriate dose of sgRNA and incubated with the cells for 48 h. The cell viability and luciferase expression were evaluated with the ONE-Glo + Tox Assay (Promega), normalized to untreated cells (N = 4 +/- standard deviation).

2.4.5.8 Kinetic assay of sgRNA and siRNA delivery. The kinetics of luciferase expression after silencing/editing by siRNA and sgRNA were determined in HeLa-Luc-Cas9 cells. For time points < 48h, ZNPs encapsulating sgRNA or siRNA were delivered to HeLa-Luc-Cas9 cells in 96-well plates at a density of 5K cells per well. After 0.5, 1, 2, 4, 11, 20, 30 and 44 h time point, the cell viability and luciferase expression were determined by the One-Glow + Tox assay. For longer time points, cells were treated in 6-well plates. Beginning at the 2 day time point, cells were aspirated,

washed with 1X PBS, trypsinized in 200 μL trypsin and re-suspended in 1800 μL medium. 1 mL of each cell suspension was added to a fresh 6-well plate containing 1 mL DMEM (2 mL total) and returned to the incubator. Of the remaining cell suspension, 50 μL was transferred to a 96-well white-opaque plate (10 wells per sample). Cell viability was determined using the Cell-Titer Glo assay normalized to untreated cells, while relative luciferase expression was determined using the One-Glo assay and normalized against control (siCtrl or sgCtrl). Data was plotted as an average of 5 measurements +/- standard deviation.

*2.4.5.9 Luciferase mRNA delivery in vitro assay***.** ZNPs with mRNA (Tri-Link Biotechnologies) were prepared using the *in vitro* nanoparticle formulation method outlined above. IGROV1 cells were seeded in white opaque 96-well tissue culture plates at a seeding density of 5 x 10^3 cells per well in 100 μL RPMI 1640 medium supplemented with 5% FBS, and allowed to attach overnight. After overnight incubation, an additional 100 μL medium was added to the wells. The ZAL:mRNA nanoparticles were prepared at ZAL:mRNA weight ratios of 20:1, 10:1, 7.5:1 and 5:1, and lipid mixture molar compositions of 50:38.5:n ZAL:cholesterol:PEG-lipid, where n = 5, 2, 1, and 0.5 at each weight ratio. The ZAL-mRNA nanoparticles were added to the cells at the appropriate mRNA dose and incubated for the indicated time (ranging from 6 h to 48 h), after which time cell viability and luciferase expression were evaluated with the ONE-Glo + Tox Assay (Promega) and normalized to untreated cells (N = 4 +/- standard deviation).

*2.4.5.10 In vitro co-delivery of Cas9 mRNA and sgRNA***.** ZNPs were evaluated in the co-delivery of Cas9 mRNA (Tri-Link biotechnologies) and single guide RNA (sgRNA) to luciferase expressing cancer cells. Cells were seeded at a density of 250,000 per well in 6-well plates and 2-mL DMEM. ZNPs were formulated using the *in vitro* formulation protocol. For co-delivery in a

single particle, Cas9 mRNA and sgRNA were combined in acidic buffer together at pH 3 prior to the addition of ZAL lipid mix at the appropriate ZAL:total RNA weight ratio. Cells were incubated with ZNPs for 72 h prior to evaluation of editing by the surveyor assay. As a negative control, ZNPs with Cas9 only (unguided Cas9), sgLuc only, and Cas9 plus sgCtrl were added. sgRNA dose was fixed at 0.5 μg per well, while Cas9 mRNA dose was tuned from 0.5 μg (1:1) to 3 μg (6:1) per well. ZAL:total RNA ratio was fixed at 7.5:1. Staged co-delivery was carried out by the addition of Cas9 mRNA ZNPs followed by the addition of sgRNA ZNPs 24h later at a total ratio of 2:1 Cas9 mRNA to sgRNA. Following an additional 48h incubation time, cells were evaluated by gene editing by the surveyor assay.

2.4.5.11 Nucleic acid binding experiments. Nucleic acid binding was evaluated using the Ribogreen assay (Molecular Probes). In short, nanoparticles were prepared using the *in vitro* or *in vivo* formulation protocols. The nanoparticle formulations (5 μL) were added to a black 96-well opaque microplate (Corning). A standard curve of the appropriate nucleic acid was prepared in the same medium as the nanoparticles. Ribogreen reagent was diluted 1:1000 in 1 X PBS and 50 μL was added to each well via multichannel pipette. The mixture was stirred on an orbital mixer for 5 minutes, and the fluorescence of each well was read using a plate reader (λ_{Ex} 485 nm, λ_{Em} 535 nm). The amount of free nucleic acid was determined by fitting the signal from each nanoparticle sample to the nucleic acid standard curve, and the fraction bound determined by the following formula: Fraction nucleic acid bound = (total nucleic acid input-free nucleic acid)/ total nucleic acid input) (N = 3 or 4 +/- standard deviation).

*2.4.5.12 In vivo nanoparticle formulations***:** *In vivo* nanoparticle formulations were performed using the NanoAssemblr microfluidic mixing system (Precision Nanosystems). Lipids were

dissolved in ethanol and nucleic acids were diluted in 10 mM citric acid-sodium citrate buffer pH 3. The lipid mixture and nucleic acid dilution were combined at a volumetric ratio of 3:1 nucleic acid:lipid mix at a total flow rate of 12 mL per minute, and a waste collection of 0.1 mL at the start and end of each formulation. The nanoparticles were dialyzed against 1 X PBS in Pur-A-Lyzer midi dialysis chambers (Sigma-Aldrich) for 1 hour per 200 μL volume in each chamber, and diluted in 1 X PBS to the appropriate nucleic acid concentration.

*2.4.5.13 In vivo luciferase mRNA delivery***:** All experiments were approved by the Institutional Animal Care & Use Committee (IACUC) of The University of Texas Southwestern Medical Center and were consistent with local, state and federal regulations as applicable. ZA3-Ep10 was formulated with *in vivo* formulation at 50 ZAL:38.5 cholesterol: 0.5, 1, or 2 PEG-lipid mole ratio in the lipid mix, and 7.5:1 ZAL:mRNA weight ratio. Mice were injected with ZAL-mRNA NPs at a dose of 1 mg/kg via tail vein injection or intraperitoneal injection. After 24 h and 48 h the luciferase expression was evaluated by live animal bioluminescence imaging Animals were anesthetized under isofluorane, and D-luciferin monosodium hydrate (GoldBio) substrate was injected subcutaneously in the neck scruff. After 10-12 minute incubation under anesthesia, the luciferase activity was imaged on an IVIS Lumina system (Perkin Elmer), and the images processed using Living Image analysis software (Perkin Elmer). *Ex vivo* imaging was performed on systemic organs after resection, and the tissue frozen on dry ice for *ex vivo* luciferase expression analysis.

*2.4.5.14 Nanoparticle property characterization***:** Physical properties were measured using a Zetasizer Nano ZS (Malvern) with an He-Ne laser (λ = 632 nm). Particle sizes were measured by dynamic light scattering (DLS) (5 measurements, 3 runs x 10 seconds, automatic attenuator

setting) by 173° back scattering. Zeta potential was measured in a folded capillary cell (Malvern) with samples diluted in PBS for ZAL NPs or citrate phosphate buffer pH 7.4 for CSAL NPs.

*2.4.5.15 Surveyor Assay***:** (Procedure performed by Shuyuan Zhang, Hao Zhu Lab) Genomic DNA from transfected cells was isolated using QuickExtract DNA Extraction Solution (Thermo Fisher Scientific) according to the manufacturer's protocol. Then the target region was amplified by PCR, and the PCR products were gel purified on an agarose gel (QIAquick Gel Extraction Kit, QIAgen). Surveyor assay was performed using Surveyor Mutation Detection Kit (IDT): the PCR products were first hybridized, then half of the products were cut with Nuclease S; both the uncut and cut DNA were then run on the 4-20% polyacrylamide gel (Biorad). The gels were stained with SYBR Gold Nucleic Acid Gel Stain buffer (diluted 1:10000 in TBE buffer, Thermo Fisher Scientific) and imaged by UV light.

2.4.5.16 Western blot: (Procedure performed by Shuyuan Zhang, Hao Zhu Lab) The cells were lysed in cold RIPA buffer (Thermo Scientific), the lysate cleared by centrifugation and total protein in the supernatant quantified by the BCA assay (Pierce). 50 μg total protein was loaded on 4–20% precast polyacrylamide gel and transferred to a nitrocellulose membrane (BioRad). The membrane was blocked in 5% nonfat milk for 1 hour at RT, and then incubated with primary antibody at 4°C overnight (Cas9 antibody, 1:1000, Cell Signaling, 14697S; beta-actin antibody, 1:2000, Cell Signaling, 4970). Secondary antibodies were applied at RT for 1 hour (anti-rabbit IgG, HRP-linked antibody, Cell Signaling, 7074, anti-mouse IgG, HRP-linked antibody, Cell Signaling, 7076), and then the membrane was developed and detected on X-ray film.

2.4.5.17 Real-time RT-qPCR. (Procedure performed by Shuyuan Zhang, Hao Zhu Lab) Cells were transfected with Cas9 mRNA for the indicated time point in a 6-well plate and 0.5 μg/mL mRNA

for the indicated time point. Total RNA was extracted using the TRIzol reagent according to the manufacturer's protocol. The RNA was reverse transcribed using the iScript Reverse Transcription kit (BioRad) and the real-time qPCR was run on a Bio-Rad C1000 Touch Thermal Cycler (CFX384 Real-time System). Each reaction was made with iTaq Universal SYBR Green 2X Supermix (Bio-Rad). The qPCR program is as follows:

1) 95 °C for 3min
2) 95 °C 10s and 55 °C 30s for 40 cycles
3) 95 °C 10s
4) 65 °C 5s
5) 95 °C 5s

Human β-actin was used as a control and mRNA levels were normalized to fold actin and plotted as an average of two independent experiments.

2.4.5.18 In vivo delivery of Cas9 mRNA and sgLoxP. ZA3-Ep10 ZNPs encapsulating Cas9 mRNA and sgLoxp were prepared according to the *in vivo* nanoparticle formulation protocol using the Nanoassemblr microfluidic mixing device. The lipid mix contained 50 ZA3-Ep10: 38.5 cholesterol: 0.5 PEG-lipid molar ratios, and the particles were formulated at a 7.5:1 ZAL:total RNA weight ratio. The Cas9 mRNA: sgLoxP weight ratio was maintained at 4:1. Rosa 26-LSL-tdTomato mice were injected at 5 mg/kg total RNA (4 mg/kg mRNA, 1 mg/kg sgRNA) via tail vein injection and monitored for 1 week. After which they were sacrificed and the major organs imaged using the IVIS Lumina system for fluorescence expression (dsRed filter set) compared to an uninjected Rosa 26-LSL-tdTomato mouse. A liver specific Cre recombinase adeno-associated virus (Cre-AAV8) injected intravenously via tail vein injection (4 days) was used as a positive control.

2.4.5.19 Tissue sectioning. (Procedure performed by Shuyuan Zhang, Hao Zhu Lab) Tissue were fixed in 4% paraformaldehyde (PFA) at RT for 2 hours, then changed in 30% sucrose (in PBS) at 4 °C overnight. Then the tissues were embedded in Cryo-gel (Leica Biosystems), and frozen in dry ice. The blocks were sectioned using Cryostat machine (Leica Biosystems) at 8 μm thickness. The sections were air-dried and incubated in 0.25% Triton X-100 (Biorad) 5% FBS in PBS for 1h at RT. Then the slides were mounted with DAPI (Vector Laboratories) and covered.

2.4.5.20 Primary hepatocytes isolation. (Procedure performed by Shuyuan Zhang, Hao Zhu Lab) Primary hepatocytes were isolated by two-step collagenase perfusion. Liver perfusion medium (Thermo Fisher Scientific, 17701038), liver digest medium (Thermo Fisher Scientific, 17703034) and Hepatocytes wash medium (Thermo Fisher Scientific, 17704024) were used.

2.4.5.21 Flow Cytometry. (Procedure performed by Shuyuan Zhang, Hao Zhu Lab) For detection of Tomato positive populations, primary hepatocytes (2x106/mL) were isolated and stained with DAPI (Roche, 2ug/mL) for dead cell exclusion. Cells were analyzed with BD FACSAria Fusion machine (BD Biosciences). Tomato positive cells were counted in DAPI negative (live cell) populations.

2.4.5.22 Statistical analysis. Statistical analysis was performed using a Student's t-test in GraphPad Prism.

CHAPTER THREE

CATIONIC SULFONAMIDE AMINOLIPIDS FOR NUCLEIC ACID DELIVERY

3.1 INTRODUCTION

The therapeutic application of RNA interference (RNAi) offers a promising alternative to small molecule drugs for the treatment of diseases of dysregulation, including cancer.[14-15, 160] Small interfering RNAs (siRNA) can be designed against any mRNA target, and enable the sequence-specific recognition and degradation of the target oncogene upon loading into the RNA-induced silencing complex (RISC). Because siRNAs have a relatively high molecular weight (~13 kDa) and are highly hydrophilic and anionic, they are unable to passively diffuse across cell membranes and into cells.[15] To date, many successful carriers have been designed using amphiphilic lipid-like compounds containing amine-rich cores, but challenges including efficient endosomal release and non-liver targeting remain major bottlenecks in the field of RNAi therapeutics. Even the best carriers are estimated to allow only 2-3% of siRNA to enter the cytoplasm,[30-32] and most lipid nanoparticles (LNPs) reported to date are efficacious only in liver hepatocytes,[60] suggesting a need to further develop new classes of lipids with endosomolytic properties and with capability of targeting tissues outside of the liver to further understand structure-function relationships.

Synthetic lipids can be generally divided into four classes: cationic, anionic, neutral, and zwitterionic.[50-53] Among carriers for nucleic acids, cationic lipids represent the most investigated class due to ability of cationic charges to electrostatically bind anionic nucleic acids. We recently

reported a novel class of synthetic lipids, zwitterionic amino lipids (ZALs), which were efficacious for *in vivo* mRNA delivery and CRISPR/Cas gene editing via co-delivery of Cas9 mRNA and sgRNA.[138] Our work demonstrated that zwitterionic phospholipids enhance RNA loading into LNPs. Given the biological importance of natural zwitterionic lipids and the utility of cationic lipids, we aimed to expand the chemistry of this novel scaffold by chemically synthesizing lipids that possess a unique permanent cationic charge coupled to sulfonamide-based head groups in a modular approach. We envisioned that expanding the synthetic scope of lipid chemistry would elucidate new chemical and biological properties that could be harnessed with utility in nucleic acid delivery.

In this chapter, the chemical development and biological evaluation of Cationic Sulfonamide Amino lipids (CSALs) is shown. CSALs are a novel class of modular synthetic lipids that have chemical and structural properties which make them promising candidates for RNAi-based anticancer therapies. Sulfonamide functionalities, though prevalent in many pharmaceutical drugs,[161-163] are underexplored functional groups in carriers for nucleic acid delivery. pH-Responsive aryl sulfonamide polymers and lipid analogues have been utilized to promote tumor-specific cellular uptake of nanoparticles for plasmid DNA and siRNA delivery, further suggesting potential utility in drug carriers.[164-166] Due to a positively charged quaternary ammonium, CSALs are excellent candidates for enhanced siRNA binding and endosomal membrane interaction and disruption upon cellular uptake to enable siRNA release.

The CSAL scaffold elicits key structural features found in lipids, lipidoids, which are cationic ionizable amino-lipids such as C12-200, 98N12 and cKK-E12 (Figure 1.3.2), and polymers with demonstrated potent siRNA delivery efficacy.[1, 6, 13, 27-28, 42, 159, 167-168] CSALs were

chemically synthesized from commercially available reagents via zwitterionic aminolipid intermediates bearing a sulfobetaine head group, amine-rich cores, and branching secondary alcohols. The lipid side chain functionality was introduced by reaction at the alcohol positions, while sulfonamidation to append the tertiary amine head group was achieved by S-N coupling through a sulfonyl chloride intermediate. A systematic, modular design enabled the evaluation of the relative contributions of structural modifications on the biophysical properties of CSAL nanoparticles in terms of size, surface charge, siRNA encapsulation, and *in vitro* siRNA delivery efficacy to human cancer cells. Further *in vivo* evaluation of lead compounds showed that A3-OAc-C2Me LNPs could deliver siRNA to mouse lungs, and both subcutaneous and orthotopic lung xenograft tumors. Furthermore, CSALs also showed utility as excipients in LNPs composed of liver targeting materials (C12-200), which resulted in altered liver-lung biodistribution following systemic administration. CSALs represent a unique structural bridge between zwitterionic[138] and cationic designs.[1, 6, 13, 27] These results demonstrate the importance of the functional lipid in LNPs and provide further design guidelines for nucleic acid carriers.

3.2 RESULTS AND DISCUSSION

3.2.1 Chemical design of CSALs for charge manipulation

To expand the variety of synthetic nucleic acid delivery materials, we developed a chemical route to manipulate the charges within lipids. CSALs possess a unique structure, consisting of an internal quaternary ammonium and tertiary amine head group connected via a sulfonamide linker. Each domain of the lipid (hydrophobic alkyl tail, linker amine, head group amine, and functional side chain) is amenable to chemical and structural modification, enabling systematic exploration

of the relative contributions of different structural elements. We envisioned that retention of the quaternary ammonium would enhance siRNA encapsulation and membrane disruption potential to enable endosomal escape. Meanwhile, the modular synthetic approach enabled systematic changes to the linker amine region (red), the head group amine (blue) and a lipid tail side chain (green) to explore their role in affecting biophysical properties and delivery efficacy (**Figure 3.2.1**). Steric interactions around the quaternary amine, the number of lipid tails, and lipid side chain functionality were evaluated. The initial design featured tertiary amine building blocks and hydrophobic alkyl chains implicated in previously successful designs.[1, 13-14, 28, 167-169]

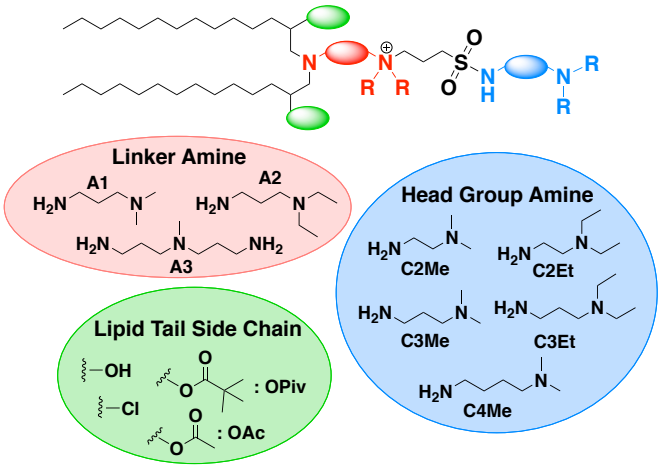

Figure 3.2.1. Cationic sulfonamide amino lipids (CSALs) were designed as a new class of lipids with defined chemical groups and physical properties to enable siRNA delivery. The modular synthetic design of CSALs enabled the establishment of structure-activity relationships by modification of the linker amine (red), lipid tail side chain (green) and the tertiary amine head group (blue).[5] Reprinted with permission from Reference 5. Copyright 2018 American Chemical Society.

With an aim to establish synthetic conditions for CSALs and understand the effects of head group spacing and lipid side chain modification, CSALs with the A1 linker amine and dimethyl amino head groups were initially evaluated. These CSALs have structural similarity to potent

LNPs used in clinical trials and in many efficacious lipidoid, dendrimer, and polymer designs.[1, 6, 9, 13-14, 23, 26-28, 42, 159, 167] Their potency is likely due to the importance of apparent pKa in LNPs for endosomal release.[28] Particularly, the combination of the two-tailed lipid bearing a dimethylamino head group has featured prominently in other potent lipids for siRNA delivery.[26, 28, 159]

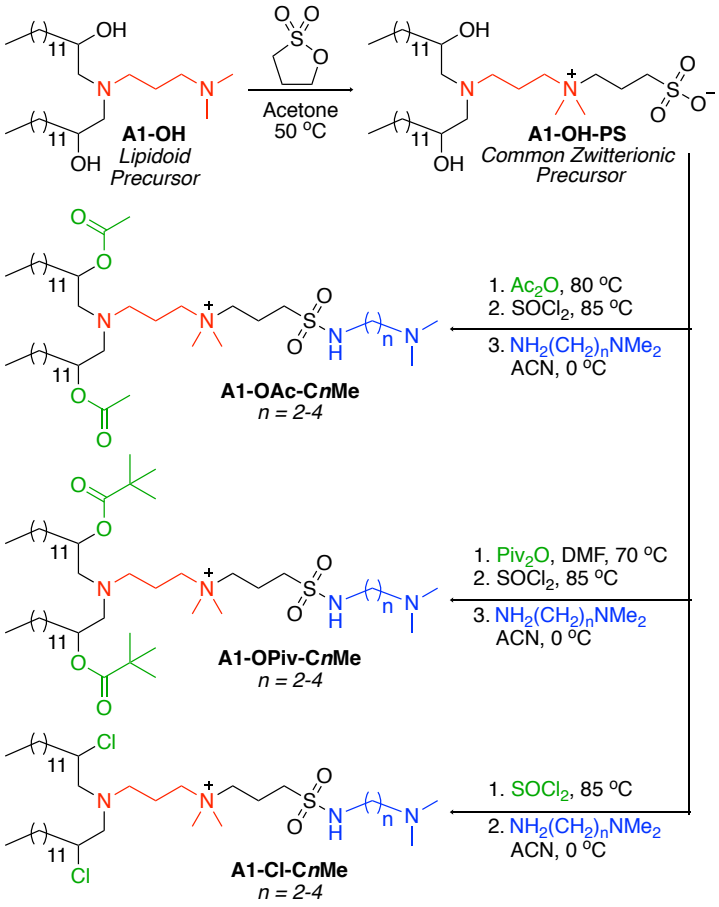

Scheme 3.2.1. CSALs based on *N*,*N*-dimethyl-1,3-propanediamine (A1) were synthesized from a common zwitterionic precursor, bearing acetate, pivalate, or chloride side chains and C2, C3, or C4 dimethylamino head groups. Reprinted with permission from Reference 5. Copyright 2018 American Chemical Society.

A1-based CSALs were synthesized using a modular design using readily available starting materials and robust reactions. The A1-OH lipidoid precursor was formed by reaction of *N*,*N*-dimethyl-1,3-propanediamine (A1) with 1,2-epoxytetradecane (**Scheme 3.4.1**) via epoxide

opening, which yielded a structure bearing two lipid tails and the secondary alcohol handles primed for further functionalization. Subsequently, the key quaternary ammonium was introduced via a sultone opening reaction with 1,3-propanesultone with the dimethyl amino head group to form the common zwitterionic precursor A1-OH-PS (**Scheme 3.2.1, 3.4.2**). This key intermediate was readily isolated from unreacted starting material by *in situ* precipitation upon sulfobetaine zwitterion formation, a strategy which has proven successful in our previous syntheses of charge-unbalanced lipids.[138] Additionally the sulfobetaine moiety has been thoroughly explored as a key component of non-fouling zwitterionic materials,[55, 170] so we hypothesized that integration of this motif into the CSAL backbone would confer biocompatible properties to CSAL nanoparticles.

Divergent synthesis from this zwitterionic precursor enabled rapid exploration of structural space to assess the relative contributions of the lipid tail side chain and head group spacing. Partial acetylation of polyethylenimine carriers has been shown to improve gene delivery efficacy,[171-172] so we hypothesized that the acetyl group may confer some important weak hydrogen-bonding interactions to stabilize siRNA, but enable release from endosomal compartments. Pivalate lipid side chains were evaluated for the potential steric effects around the acyl group, which may affect the stabilizing interactions. Chloride was evaluated as a compact electron withdrawing group, which would disrupt any stabilizing hydrogen bonding interactions in the acyl sidearms. The carbon linker length in the *N,N*-dialkyl diamines (C2, C3, C4) was also investigated, as a single methylene change in linker length has been shown to have drastic effects on delivery efficacy.[28] The secondary alcohol moieties of A1-OH-PS were esterified by reaction with acetic anhydride (**Scheme 3.4.3**) or pivalic anhydride (**Scheme 3.4.4**) to form A1-OAc-PS and A1-OPiv-PS respectively. The sulfonamide bond and tertiary amine head group were introduced via conversion

of the sulfonate to a sulfonyl chloride by heating in thionyl chloride following subsequent sulfonamidation with *N,N*-dimethyldiamine head group amines C2Me, C3Me, and C4Me (**Scheme 3.2.1**) to form CSALs A1-OAc-CnMe (**Scheme 3.4.5**) and A1-OPiv-C*n*Me (**Scheme 3.4.6**). Synthesis of the chloride lipid side chain was achieved by reaction with thionyl chloride in a single reaction during sulfonyl chloride formation, followed by similar sulfonamidation to yield A1-Cl-C*n*Me (**Scheme 3.4.7**). CSAL structures were confirmed by ^{1}H NMR and MALDI-TOF mass spectrometry (**Appendix B**). With CSALs A1-OAc-CnMe, A1-OPiv-CnMe, and A1-Cl-CnMe in hand, these compounds were evaluated for the ability to form nanoparticles capable of encapsulating and delivering siRNA to cancer cells *in vitro*.

3.2.2 Formulation CSAL and correlation of NP properties to chemical structure

Efficacious lipids for siRNA delivery are typically formulated by rapid mixing of multiple components into LNPs. To date, formulation of LNPs composed of a cationic or ionizable lipid, 1,2-distearoyl-sn-glycero-3-phosphocholine (DSPC), cholesterol, and lipid poly(ethylene glycol) (PEG)[1, 13, 28] have provided an effective method to eliminate aggregation and enhance stability at physiological conditions. Such LNPs have been utilized in human clinical trials to deliver siRNAs.[173]

We prepared formulated LNPs of CSALs, cholesterol, DSPC, and lipid PEG2000 at a ratio of 50/38.5/10/1.5 (mol/mol) and a N:P ratio of 12.5, 25, and 50 to 1 using the ethanol dilution method. In brief, siRNA diluted in citrate buffer pH 3 was rapidly mixed with lipids

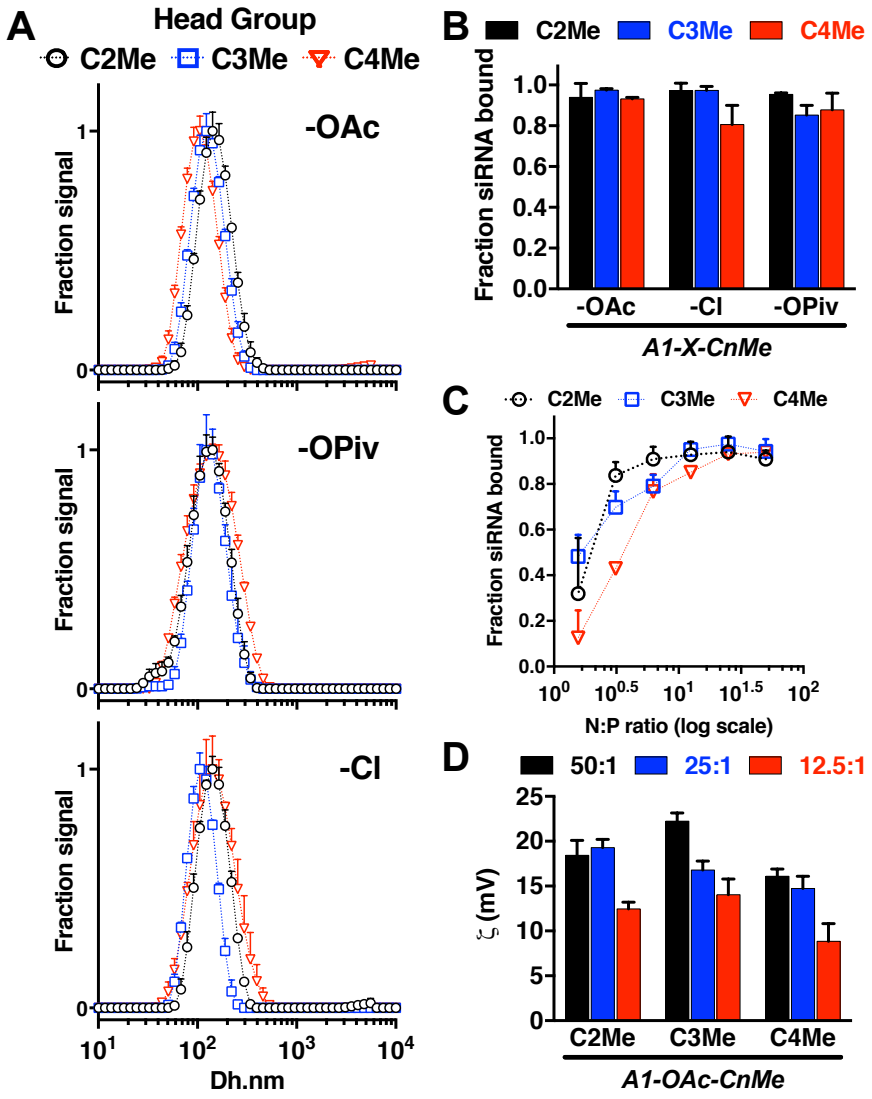

Figure 3.2.2. Biophysical characterization of an A1-based series of CSAL LNPs. (A) All LNPs possessed structurally independent size of ~100 nm. (B) siRNA encapsulation studies of CSAL LNPs showed sidearm and head group independence. (C) At lower N:P siRNA encapsulation is dependent on head group structure for A1-OAc-CnMe LNPs (D) CSAL head group structure and N:P ratio affects particle surface charge. Data plotted as mean +/- standard deviation; A: n = 5, B-D: n = 3. Reprinted with permission from Reference 5. Copyright 2018 American Chemical Society.

in ethanol at 3:1 aqueous: acidic volumetric ratio, followed by dilution in PBS. Formulated CSAL LNPs had uniform, structurally independent size (**Figure 3.2.2A**) and high siRNA encapsulation **(Figure 3.2.2B)** at N:P 25:1. LNP diameter was neither affected by the carbon linker nor the

sidearm functionality. Interestingly, when N:P ratio of A1-OAc-C*n*Me was titered from high to low to assess the roles of head group spacing on siRNA encapsulation, all CSALs showed strong binding (>80%) above N:P 6:1, while increased alkyl length correlated with decreased binding at lower CSAL:siRNA ratios. Additionally, the surface charge of the A1-OAc-CnMe LNPs was net positive and dependent on head group linker length and N:P ratio, with C4Me head group showing lower zeta potential (**Figure 3.2.3**).

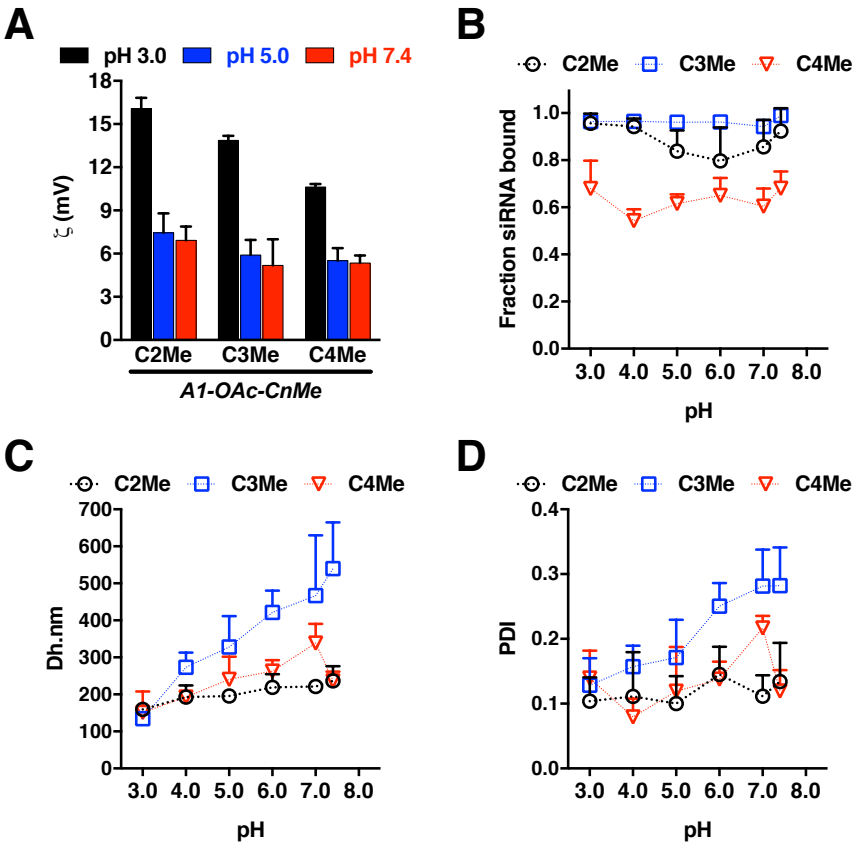

Figure 3.2.3. The effect of pH on the nanoparticle properties of A1-OAc-*CnMe* CSAL LNPs. A) The effect of mixing pH on zeta potential shows a decrease in surface charge from pH 3 to pH 5, while the positive charge is maintained at physiological pH. CSAL LNP particle properties evaluated from pH 3 to pH 7.4 (B-D). B) siRNA encapsulation is largely pH independent. Particle size (C) and PDI (D) increase at higher pH in a structurally dependent manner, where C2Me shows the best stability. Data plotted as mean +/- standard deviation, N = 5.

The effects of pH on CSAL LNPs were also studied to determine the effects of the permanent positive charge from the quaternary ammonium. Higher surface charge at pH 3 suggests changes in protonation states of surface CSALs. (**Figure 3.2.3A**) Interestingly, siRNA encapsulation in A1-OAc-CnMe CSALs was not significantly affected by formulation pH (**Figure 3.2.3B**), likely due to the permanently positively charged ammonium. In contrast to CSALs, traditional ionizable lipids require a low pH of mixing (below the pKa of the cationic lipid) to allow high siRNA loading via electrostatic interactions with negative siRNA molecules.[1, 13, 26, 28] CSAL nanoparticle size increases at higher pH, suggesting that the ionizable amine groups in CSALs also play a role in effectively compacting siRNA into LNPs (**Figure 3.2.3C**). Having established the optimal LNP formulations for uniform particle size, charge, and siRNA encapsulation to CSAL LNPs were next evaluated for the ability to deliver siRNA *in vitro*.

3.2.3 Evaluation of A1-based CSALs for in vitro delivery efficacy

A1-based CSAL LNPs with favorable nanoparticle properties for *in vitro* delivery were evaluated for delivery of siRNA against a luciferase reporter in HeLa-Luc cells (**Figure 3.2.3**). Luciferase activity and cytotoxicity were measured after 24 hours relative to untreated cells. Evaluation of the structural effects of lipid side chains and head group spacing (**Figure 3.2.3A**) revealed significantly more potent activity of acetate and pivalate lipid side chains as compared to chloride. Furthermore, lengthening of the carbon linker in the head group amine correlated with a significant decrease in delivery efficacy from C2 to C3 to C4, likely due the differences in pKa at the head group amine. In general, a higher N:P ratio improved delivery (**Figure 3.2.3B**) suggesting that CSAL is playing a key role in enabling endosomal release and delivery efficacy. This implies

the importance of hydrogen bonding within LNPs.[138] Changing the zwitterionic helper phospholipid from DSPC to DOPE, which introduces an unsaturated bond into the lipid tail to improve fluidity of the hydrophobic domains of the LNP, and a strategy that has been utilized to improve delivery of previous formulations, did not significantly affect CSAL LNP siRNA delivery to HeLa cells (**Figure 3.2.5**). Further characterization of CSAL LNP uptake using fluorescently labeled Cy5.5-labeled siRNA correlated with functional delivery efficacy (**Figure 3.2.6**) and showed that A1-OAc-C2Me and A1-OPiv-C2Me had drastically higher uptake as compared to A1-Cl-C2Me. Taken together, *in vitro* results indicated that the C2Me head group and acetate lipid side chain were the most favorable structural elements for CSAL siRNA delivery.

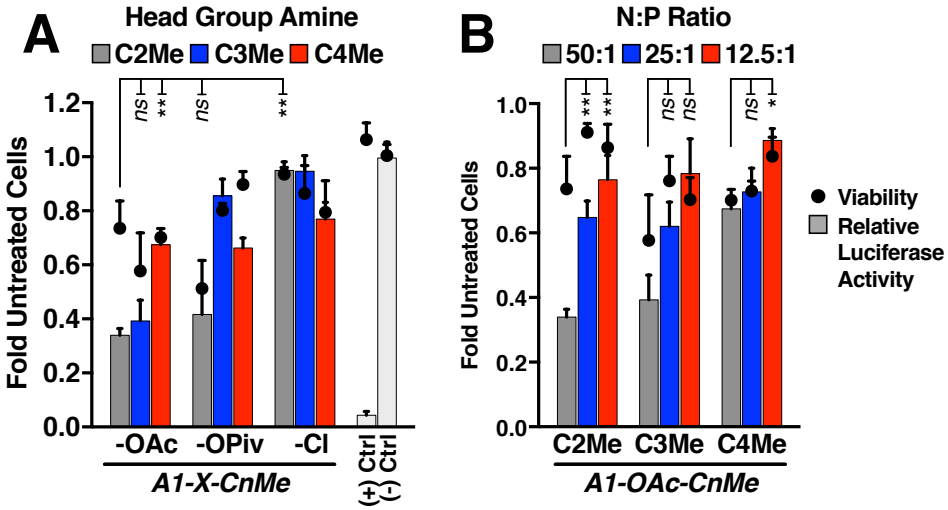

Figure 3.2.4. LNPs formulated with the A1-CSAL library (50:38.5:10:1.5) were screened for siRNA delivery to HeLa-Luc cells. **(A)** The effect of head group amine and lipid side chain at N:P ratio of 50:1. **(B)** The effect of N:P on A1-OAc CSALs 50:1, 25:1, and 12.5:1. Nanoparticle treatment was performed at 34 nM siRNA for 24 hours. The negative control was free siRNA (no lipids) and the positive control was the lipidoid C12-113 LNPs.[1-2] Data were normalized to untreated cells, with viability shown as dots and relative luciferase activity shown as bars. n = 3 +/- standard deviation. Statistical analyses were performed with a two-tailed Student's t-test (n.s. $P > 0.05$; *$P < 0.05$; **$P < 0.01$). Reprinted with permission from Reference 5. Copyright 2018 American Chemical Society.

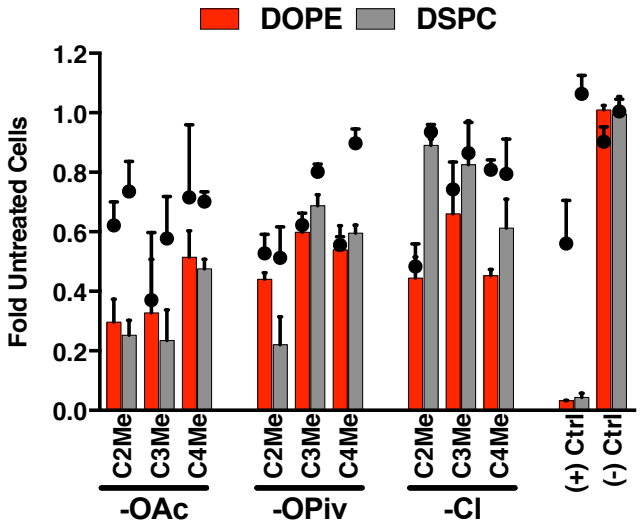

Figure 3.2.5. Delivery of CSAL LNPs to HeLa-Luc comparing DSPC and DOPE as a phospholipid showed comparable delivery efficacy with acetate CSALs and pivaloate CSALs, while chloride CSALs showed improved efficacy with DOPE. siRNA was administered at 34 nM and incubated for 24h. C12-113 was the positive control, while free siRNA was the negative control. Cell viability and relative luciferase activity were normalized to untreated cells and plotted +/- standard deviation (N = 3).

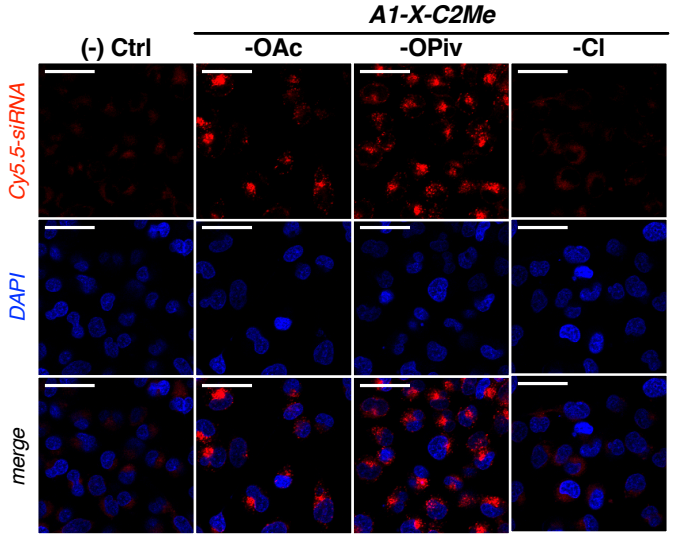

Figure 3.2.6. Cellular uptake of LNPs of A1-based CSALs with C2Me head group reflects delivery efficacy and is affected by the lipid side chain structure. Ester analogues OAc and OPiv show significantly higher uptake than chloride. LNPs were formulated at N:P 25:1 and administered at 34 nM siRNA. Cells were imaged 24h post transfection. The negative control was free siRNA. Cell nuclei were counterstained with DAPI. Scale bar = 40 μm. Reprinted with permission from Reference 5. Copyright 2018 American Chemical Society.

3.2.4 Identification of improved carriers through rational structure optimization

Combined biophysical and structure-activity analysis of the A1 series of CSAL LNPs indicated that the acetate lipid side chain and two-carbon linker were favorable for siRNA encapsulation and delivery. To further explore SAR, we synthesized a second set of CSALs to study the steric effects of the amino core and head group with a fixed acetate lipid side chain. Acetate A2- and A3-based CSALs and A1 with a diethylamine head group were chemically synthesized (**Figure 3.2.7**, **Scheme 3.4.8**) from their lipidoid precursors using the same synthetic sequence from **Scheme 3.2.1**. Additionally, the acetate lipid side chains of A1-OAc-C2Me were converted to the hydroxyl groups of A1-OH-C2Me by reaction with potassium carbonate (**Scheme 3.4.9**) to further explore the role of hydrogen bonding in CSAL LNP delivery.

LNPs were prepared using second generation CSALs to determine the steric effects of the linker and head group amines on nanoparticle properties and delivery efficacy. Increasing the steric bulk from dimethyl to diethyl on the quaternary ammonium (A2-OAc-C2Me**)** did not affect particle size while increasing the number of hydrophobic tails (A3-OAc-C2Me**)** resulted in a slight increase in size (**Figure 3.2.8A**). Meanwhile, changing the substitution of the head group amine (**Figure 3.2.8B**) or the lipid side chain to hydroxyl (**Figure 3.2.8C**) did not affect LNP size. Compared to A1, siRNA binding was decreased by conversion of the linker amine to A2 or A3, while conversion of the head group substitution to diethyl (A1-OAc-C2/3Et) resulted in a slight decrease in siRNA binding. Furthermore, conversion of the acetate lipid side chain to hydroxyl (A1-OH-C2Me), also decreased encapsulation suggesting a key role of the acetate lipid side chain in stabilizing the siRNA-CSAL interaction within the nanoparticle. Meanwhile, characterization

of CSAL LNPs formed with A3-OAc-C2Me show a traditional spherical LNP nanostructure with an electron dense core and electron diffuse shell (**Figure 3.2.8E**).

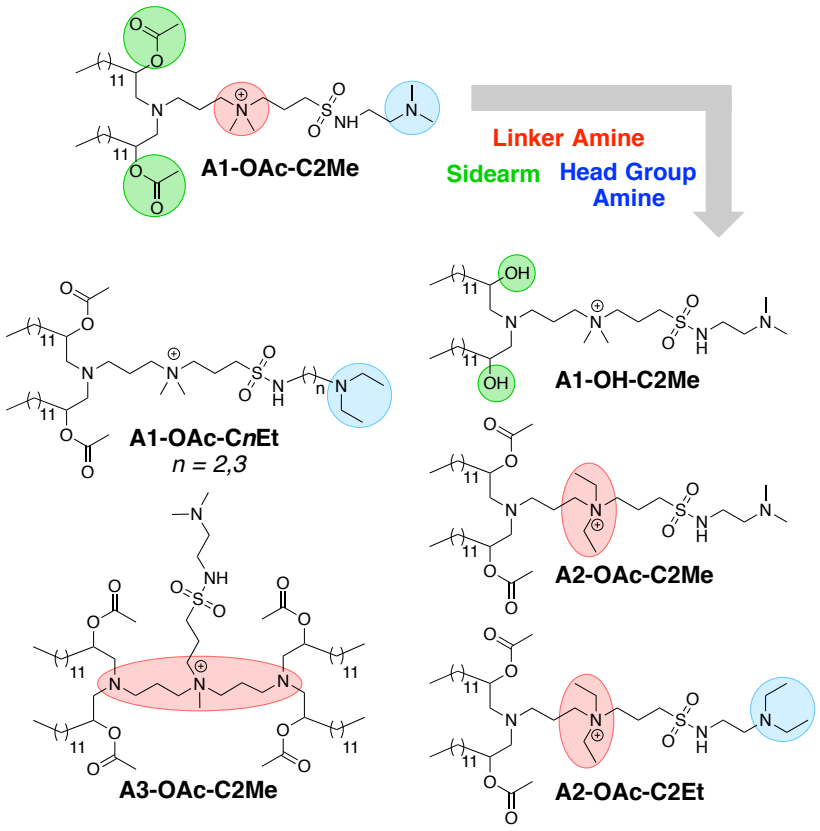

Figure 3.2.7. Second generation CSALs were designed and synthesized to probe the steric effects of the linker amine and head group amine on biophysical and delivery properties. Reprinted with permission from Reference 5. Copyright 2018 American Chemical Society.

Functional siRNA delivery was also affected by fine changes in CSAL structure (**Figure 3.2.9**). Similar to the A1-based CSALs, increased N:P ratio in second generation CSALs correlated with improved delivery efficacy, suggesting a general trend. Conversion of the head group substitution from dimethyl to diethyl significantly decreased delivery efficacy to HeLa-Luc cells for both the two- and three-carbon head group linker length. This change in

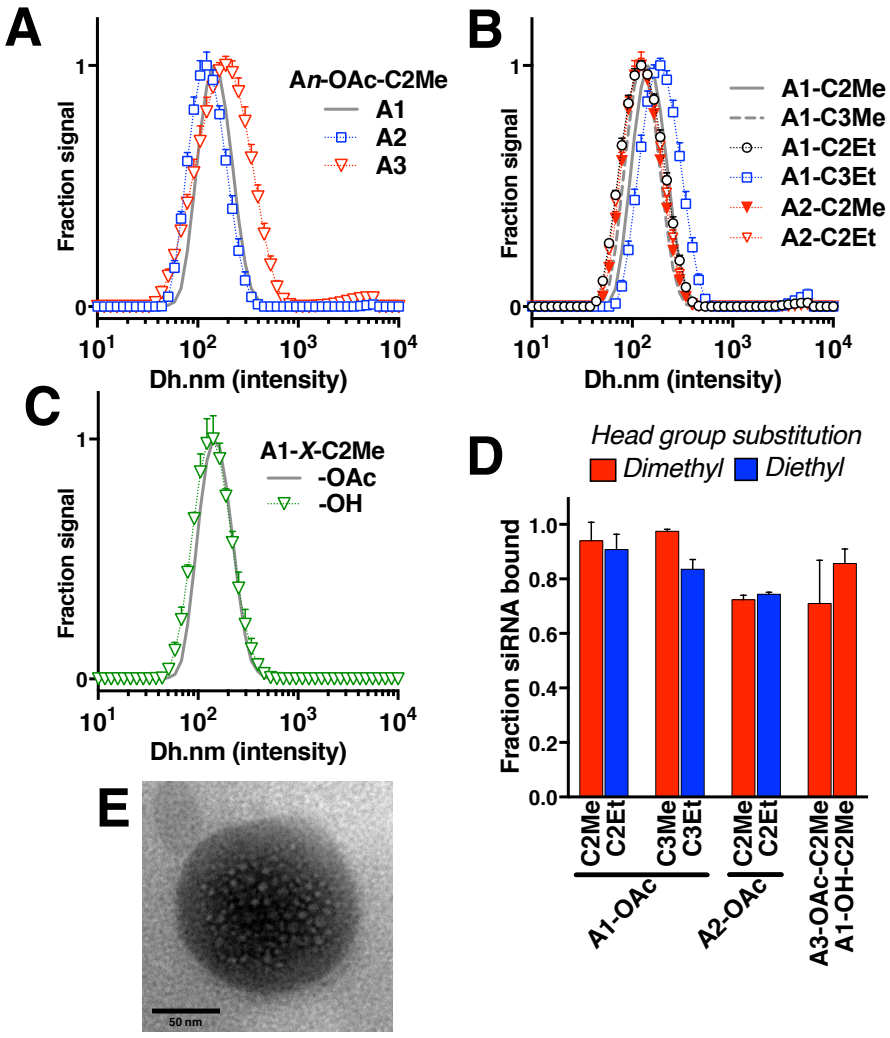

Figure 3.2.8. A second generation collection of CSAL LNPs was evaluated for the effects of CSAL structure on nanoparticle size (A-C) and siRNA encapsulation (D). Transmission electron microscopy shows a core-shell nanostructure of A3-OAc-C2Me LNPs (E). Values plotted as mean +/- standard error, A-C: n = 5; D: n = 3. Reprinted with permission from Reference 5. Copyright 2018 American Chemical Society.

activity further suggests that the microspecies pKas of amines can be significantly affected by the substitution length, which can alter global apparent LNP pKas that are known to control delivery efficacy.[6, 26, 28, 30-32]Additionally, the acetate lipid side chain proved more efficacious than the hydroxyl group. Changing the linker amine to A2 (A2-OAc-C2Me/Et) decreased delivery efficacy

compared to the A1-based analogue, while changing the linker amine to A3 (A3-OAc-C2Me) drastically improved delivery efficacy. The enhanced activity of A3-OAc-C2Me highlights the important balance of stabilizing hydrophobic and hydrophilic interactions in CSAL LNPs, which has been demonstrated in many potent carriers in library studies.[1, 6, 13, 42] Furthermore, the effect of CSAL structure on nanoparticle cellular uptake correlated with changes in delivery efficacy (**Figure 3.2.10**). A3-OAc-C2Me showed strong uptake as compared to A1-OAc-C2Me, while A1-OAc-C2Et and A1-OH-C2Me demonstrated much lower intracellular siRNA.

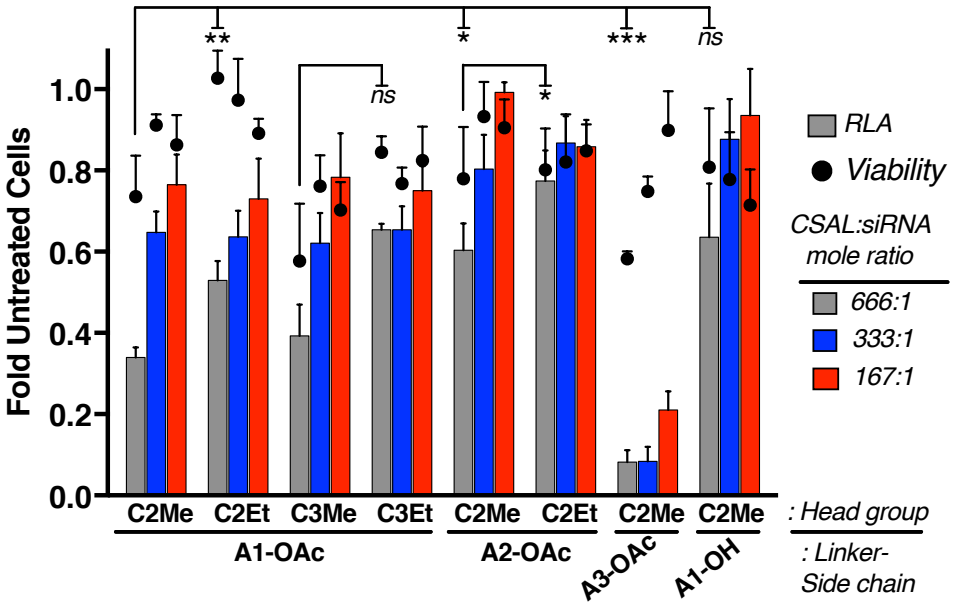

Figure 3.2.9. siRNA delivery to HeLa-Luc cells at mol:mol ratios of 666:1, 333:1, and 167:1 (CSAL:siRNA) (For A1 and A2, N:P = 50:1, 25:1, 12.5:1 respectively; for A3 N:P = 66:1, 33:1, 16:1 respectively) using formulated CSAL LNPs (50:38.5:10:1.5 CSAL: cholesterol: DSPC: PEG-Lipid) and administered at 34 nM siRNA for 24h. For clarity, the A1-OAc-C2Me and A1-OAc-C3Me data are reproduced from Figure 3.2.2 and 3. n = 3 +/- standard deviation. Statistical analyses were performed with a two-tailed Student's t-test (n.s. $P > 0.05$; *$P < 0.05$; **$P < 0.01$, ***$P < 0.001$). Reprinted with permission from Reference 5. Copyright 2018 American Chemical Society.

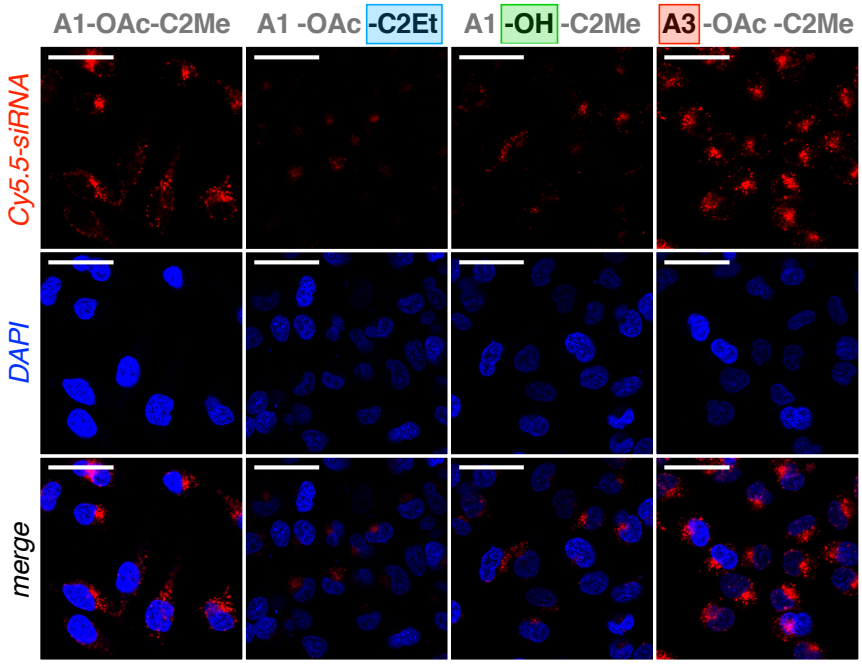

Figure 3.2.10. The effect of second generation CSAL structure on LNP uptake in HeLa-Luc cells. LNPs were formulated with Cy5.5-labeled siRNA (red) at 333:1 CSAL:siRNA *mol:mol* ratio and administered at 34 nM siRNA. Cells were fixed, counterstainined with DAPI (blue) and imaged 24h time points post transfection. Scale bar = 40 μm. Reprinted with permission from Reference 5. Copyright 2018 American Chemical Society.

To further understand the origin of these trends, we performed computational microspecies pKa modeling. This was useful because each CSAL contains multiple amines, which makes global/apparent pKa analysis more complicated than for classic cationic lipids with one amine head group.[26, 28] Modeling of the pKa of the ionizable amines using CSAL analogues showed that the C2Me head group possesses a pKa in the relevant range for endosomal escape.[6, 26, 28, 30-32] pKa modeling also indicated that the ester lipid side chains lowered the pKa compared to the alcohol analogue (**Figure 3.2.11**). Both extension of the carbon linker on the head group and increasing head group steric hindrance from dimethyl to diethyl increased the pKa, potentially contributing to the observed decrease in activity. Despite these changes in pKa, RNA encapsulation was not largely affected suggesting a key role in this function of the quaternary ammonium core. Overall,

this second group of CSALs was rationally designed to explore linker and head group properties for delivery efficacy. A3-OAc-C2Me showed the strongest delivery ability, which highlights the importance of pKa and additional hydrophobic tails.

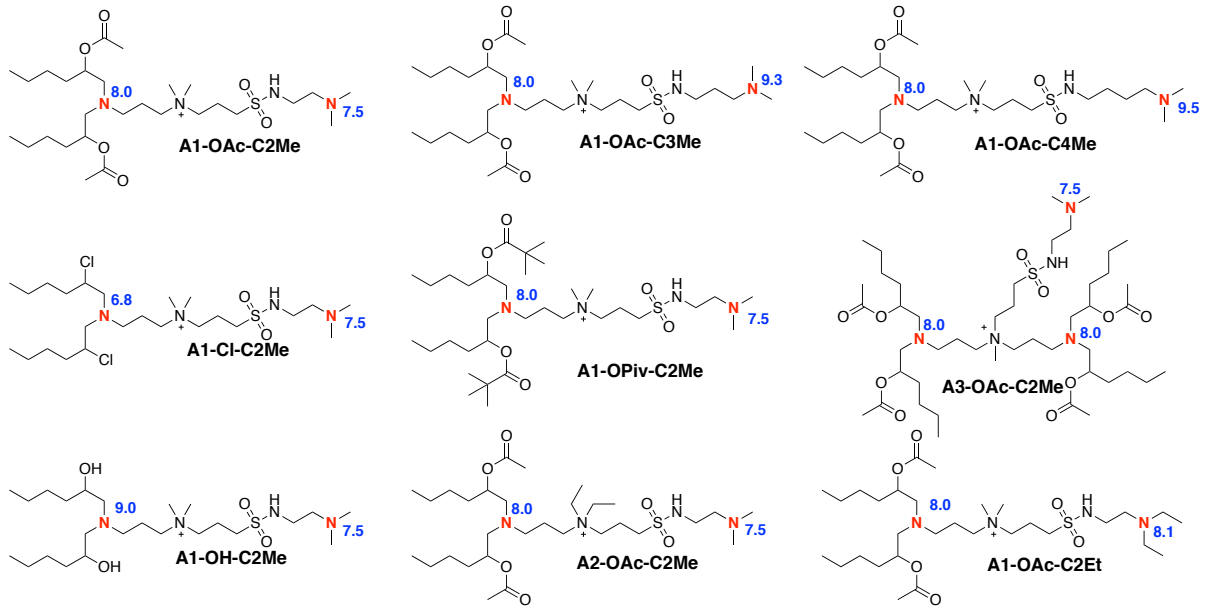

Figure 3.2.11. Microspecies pKa modeling of CSALs indicates the potential roles of various structural moieties in siRNA encapsulation and release. Longer alkyl chain in the head group amine leads to higher pKa of the head group amine. Furthermore, increasing steric bulk on the head group leads to higher pKa.

3.2.5 Examination of the effect of CSAL structure on LNP in vivo biodistribution

Given the unique sulfonamide containing chemical structure of CSALs, coupled to the *in vitro* uptake and delivery results that correlated to small changes in structure, we were motivated to examine *in vivo* biodistribution of CSAL LNPs using fluorescently labeled siRNA. *In vitro* SAR evaluation revealed that C2Me head group and acetate lipid side chain were the most favorable attributes for delivery overall, and that the A3 amine could improve delivery over A1. We thus decided to compare the organ biodistribution patterns of A1-OAc-C2Me and A3-OAc-C2Me LNPs.

Uniform LNPs were prepared at different N:P ratios with Cy5.5-labeled siRNA (**Figure 3.2.12A**). Initially the biodistribution of A3-OAc-C2Me LNPs was evaluated following systemic administration via intravenous (IV) injection at different total lipid:siRNA weight ratios. All formulations demonstrated striking lung accumulation (**Figure 3.2.12B**). Decreased kidney signal at higher weight ratios suggests that the CSAL plays a critical role in the *in vivo* stability of LNPs, as free siRNA undergoes renal clearance and kidney localization. Delivery of A1-OAc-C2Me (wt ratio 30:1) by IV injection shows strong lung accumulation but much higher kidney accumulation indicating instability (**Figure 3..2.12.C**). Furthermore, different routes of administration were compared using A3-OAc-C2Me to better understand the lung accumulation. CSAL LNPs administered via intraperitoneal injection (IP) showed much lower overall fluorescent signal and did not lead to accumulation in the lungs (**Figure 3.2.12.D**). Quantification of Cy5.5 signal was also performed by ROI analysis which confirmed the favorable lung targeting of CSAL LNPs (**Figure 3.2.12E-G)**

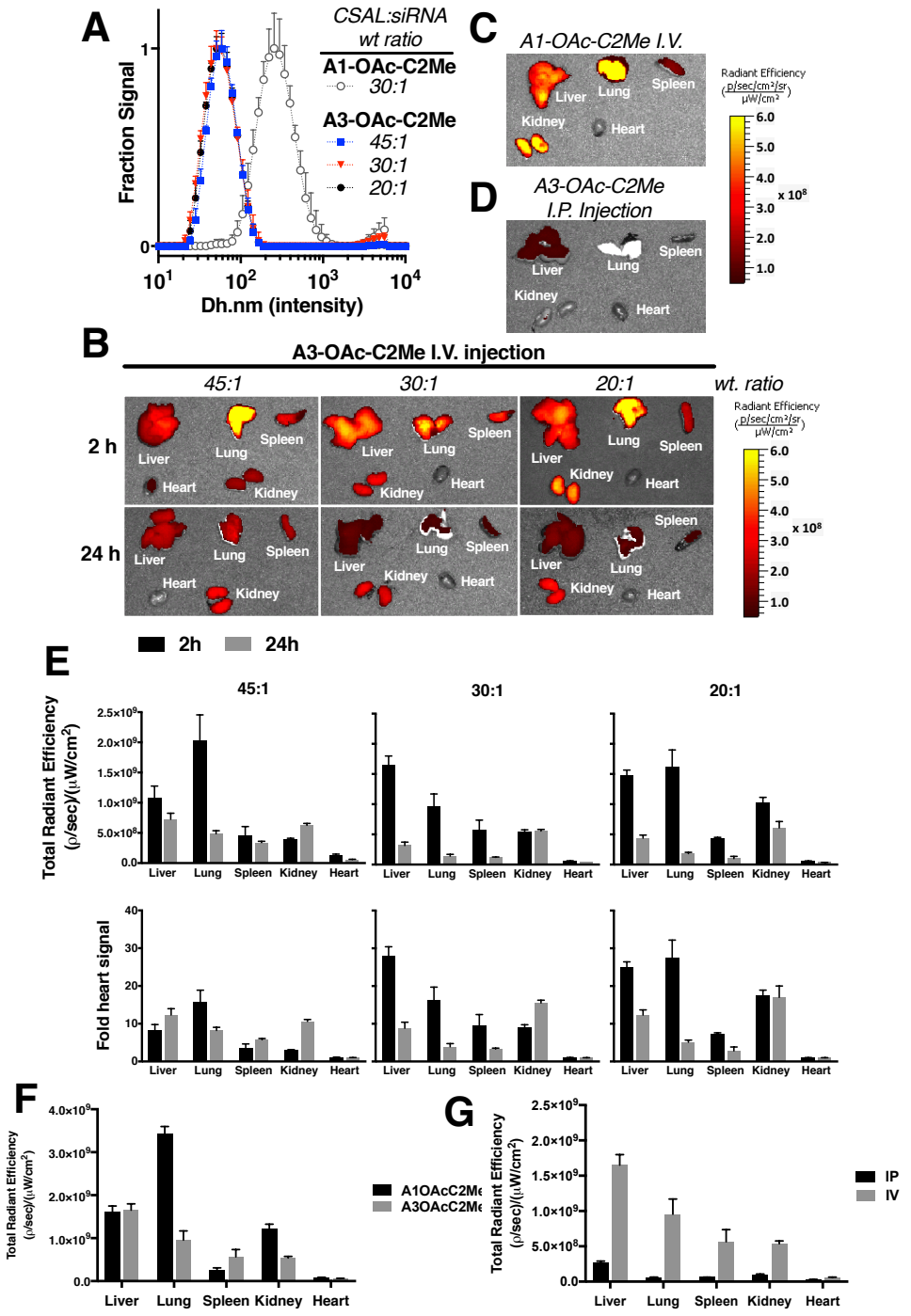

Figure 3.2.12. A1-OAc-C2Me and A3-OAc-C2Me LNPs were evaluated for biodistribution in C57BL/6J mice. LNPs were formulated using microfluidic mixing and administered at 1 mg/kg siRNA. Nanoparticle size was measured by DLS (A). IV injection of A3-OAc-C2Me NPs was evaluated at different total lipid: siRNA weight ratios (B), and compared to IP injection at 30:1 wt. ratio (D). A1-OAcC2Me LNPs were evaluated at 30:1 wt. ratio and IV administration (C). Biodistribution was quantified by ROI analysis (E-F). Reprinted with permission from Reference 5. Copyright 2018 American Chemical Society.

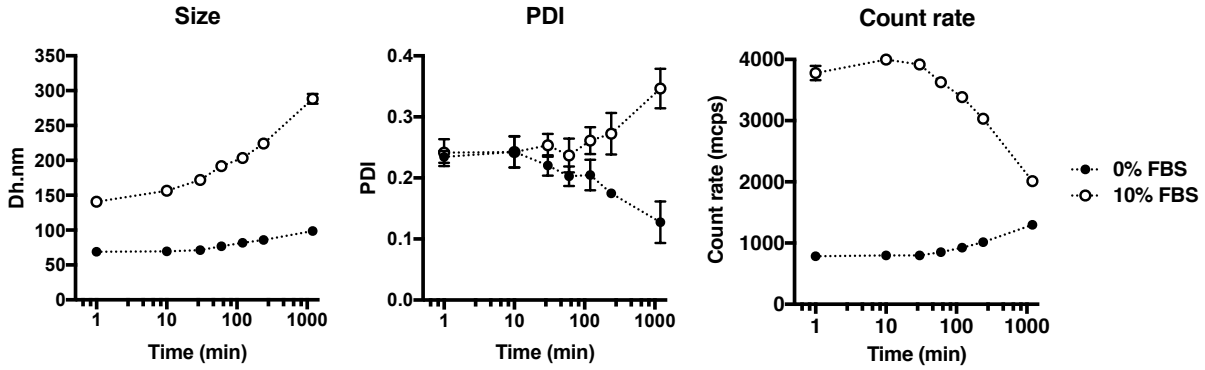

Figure 3.2.13. The stability of A3-OAc-C2Me NPs in the presence of serum. Nanoparticles were formulated by microfluidic mixing and dialyzed against 1X PBS, then diluted in PBS or PBS containing 10% FBS. Particles were incubated at ambient temperature and size was measured at 1 min, 10 min, 30 min, 1h, 2h, 4h, and 20h. Data plotted as mean +/- standard deviation, N = 5.

Given that lung vasculature is known to have smaller blood vessels than other organs, this physiological difference, coupled to the lungs being the first organ to receive blood following the heart, suggested the possibility that CSAL LNPs might accumulate in the lungs being the first sieving constraint.[174] In order to exclude the possibility that the propensity of CSAL LNPs to accumulate in the lungs following IV administration could be due to aggregation of nanoparticles, we monitored the stability of A3-OAc-C2Me LNPs in serum (**Figure 3.2.13**). The addition of 10% FBS resulted in a slight increase in the nanoparticle diameter over time, but A3-OAc-C2Me LNPs remained small in the presence of serum and did not aggregate. These results suggest that CSAL LNPs are stable in the blood and that the CSAL chemical structure itself may facilitate delivery to lungs. Similar accumulation has been observed for other carriers, such as 7C1 LNPs, which favor endothelial cell uptake, providing preferential siRNA delivery to the lungs over the liver.[61, 175]

Having identified the lungs as the favored target organ for CSAL accumulation and A3-OAc-C2Me as a potent CSAL carrier for *in vitro* target gene silencing, siRNA delivery to A549-Luc lung cancer cells *in vitro* and *in vivo* in xenograft tumors was performed. A3-OAc-C2Me

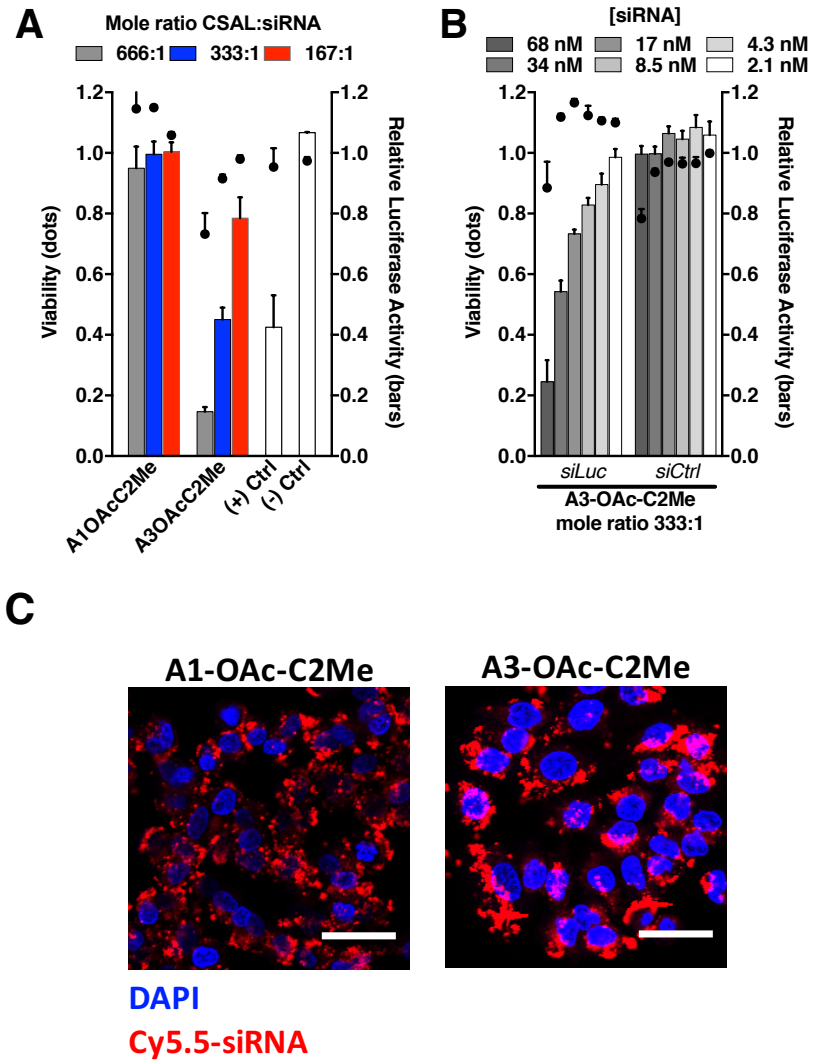

Figure 3.2.14. Delivery of CSAL LNPs to A549-Luc cancer cells for lung localized LNPs A1-OAc-C2Me and A3-OAc-C2Me (A) at 34 nM siRNA for 24h. A3-OAc-C2Me CSAL LNPs showed dose dependent, sequence-specific silencing of luciferase target in A549 cells (B). Cell viability and luciferase activity were normalized to untreated cells and plotted as mean +/- standard deviation (N = 4).The uptake of CSAL LNPs A1-OAc-C2Me and A3-OAc-C3Me in A549-Luc cells as evaluated by confocal laser scanning microscopy. CSAL LNPs loaded with Cy5.5-siRNA were formulated at 333:1 CSAL:siRNA mol:mol ratios and incubated with cells for 24h. Cells were formaldehyde fixed and counterstained with DAPI.

LNPs were able to deliver siLuc to silence luciferase expression in A549-Luc cells *in vitro* in a dose responsive manner (**Figure 3.2.14A-B**), while A1-OAc-C2Me was ineffective, despite strong intracellular nanoparticle uptake for both carriers (**Figure 3.2.14C**). Additionally, A3-OAc-C2Me

LNPs were compared to well-characterized quaternary ammonium-containing cationic lipids 1,2-dioleoyl-3-trimethylammonium-propane (DOTAP) and dimethyldioctadecylammonium bromide (DDAB) as siRNA carriers.[176] While all lipids showed similar particle size, positive surface charge, and strong siRNA encapsulation, A3-OAc-C2Me proved more efficacious in silencing the luciferase target in the lung cancer cells (**Figure 3.2.15**). Building on this result, we formed subcutaneous A549-Luc xenograft tumors in mice. Sequence-specific siRNA-mediated luciferase silencing was observed after intratumoral injection (1 mg/kg dose) of siLuc or siCtrl inside of A3-OAc-C2Me LNPs (**Figure 3.2.16)**. This *in vivo* proof of principle data consisting of lung accumulation and tumor silencing indicated potential for CSALs to be used for in lung delivery applications.

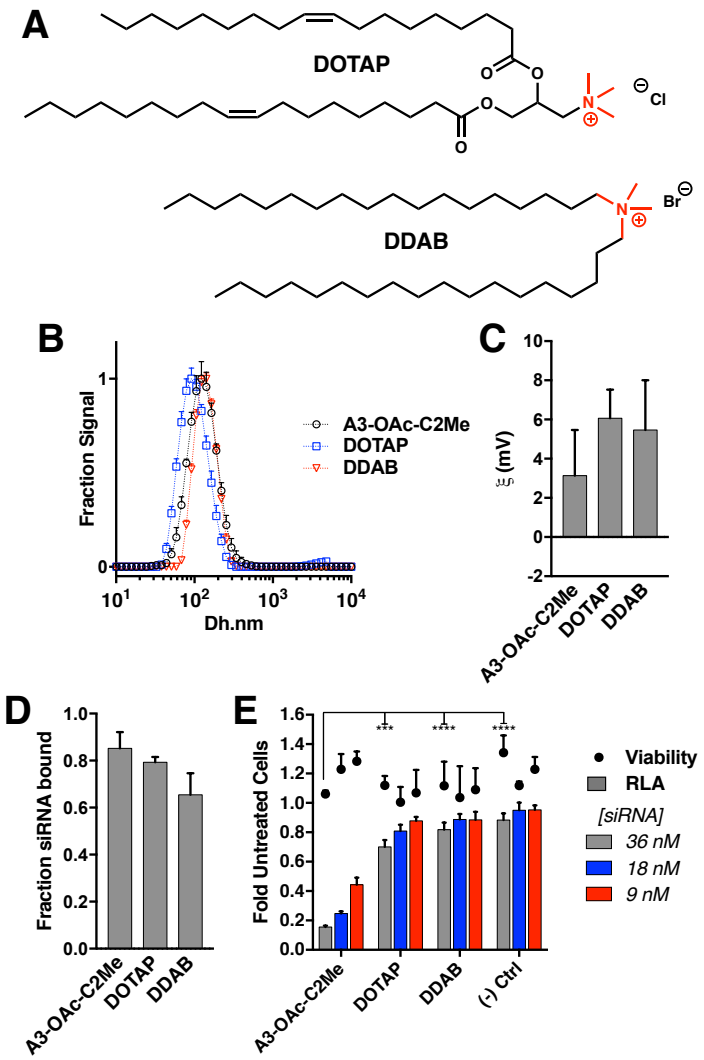

Figure 3.2.15. The lead CSAL A3-OAc-C2Me was compared to other well-characterized cationic lipids containing quaternary ammonium moieties DOTAP and DDAB. (A) The chemical structures of DOTAP and DDAB. LNPs were formulated at a lipid molar ratio of 50: 38.5: 10: 1.5 Cationic lipid/ Cholesterol/ DSPC/ PEG-lipid. A 333:1 cationic lipid:siRNA mol ratio was maintained for all formulations. The effect of the cationic lipid structure on nanoparticle size (B), zeta potential (C), and siRNA encapsulation (D) was determined. (D) LNPs were administered to A549-Luc human lung cancer cells by reverse transfection for 20h. A3-OAc-C2Me showed significant improvement of silencing compared to DOTAP and DDAB. The negative control was siRNA formulated in the absence of lipids. Values are plotted as mean +/- standard deviation (B-C n = 5; D-E n = 4). Statistical analysis was performed with a two-tailed student's T-test *** $P < 0.001$, **** $P < 0.0001$.

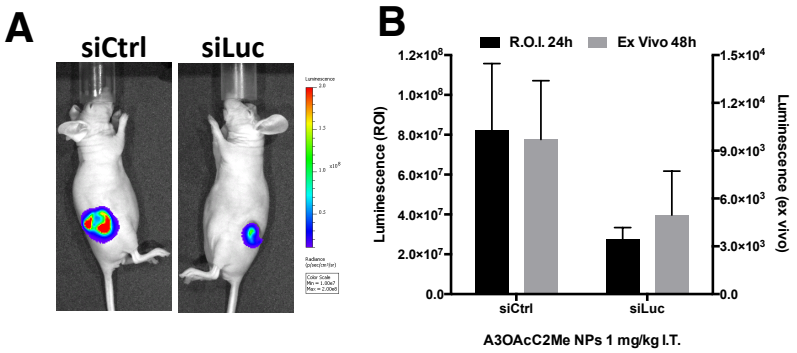

Figure 3.2.16. Delivery of A3-OAc-C2Me LNPs to A549-Luc subcutaneous tumors. CSAL LNPs were administered by intratumoral injection at a dose of 1 mg/kg. (A) A representative *in vivo* bioluminescent image of siCtrl and siLuc treated animals. (B) Luciferase expression was determined by ROI analysis of bioluminescence imaging 24h post-injection and by *ex vivo* luminescence assay normalized to total tissue mass. (N = 4 +/- S.E.M.

3.2.6 CSALs as excipients in established LNP formulations for lung delivery

In order to further utilize the unique chemical structure of CSALs to enable siRNA delivery to the lung, CSALs were evaluated as excipients in known potent siRNA delivery formulations. We prepared LNPs based on the well-characterized C12-200 lipidoid (50: 38.5: 10: 1.5 C12-200: Cholesterol: DSPC: PEG-lipid *mol:mol,* 13.5:1 C12-200: siRNA *wt:wt*), which is an effective formulation for delivery to liver hepatocytes.[1, 31, 106-107, 177] CSALs A3-OAc-C2Me and A1-OAc-C2Me were incorporated as excipients into C12-200 LNPs (50: 38.5: 10: 1.5: *Y* C12-200: Cholesterol: DSPC: PEG-lipid: CSAL *mol:mol*, 13.5:1 C12-200: siRNA *wt:wt*) to evaluate their ability to favor lung accumulation. CSAL excipients in C12-200 LNPs did not have a large effect on nanoparticle size, producing uniform LNPs ~100 nm in dimeter (**Figure 3.2.18A**). *In vitro* experiments demonstrated that inclusion of A3-OAc-C2Me (10 or 30%) improved siRNA encapsulation, while dramatically improving delivery efficacy to A549-Luc lung cancer cells (**Figure 3.2.17).** The effect on biodistribution was evaluated following tail vein injection (**Figure**

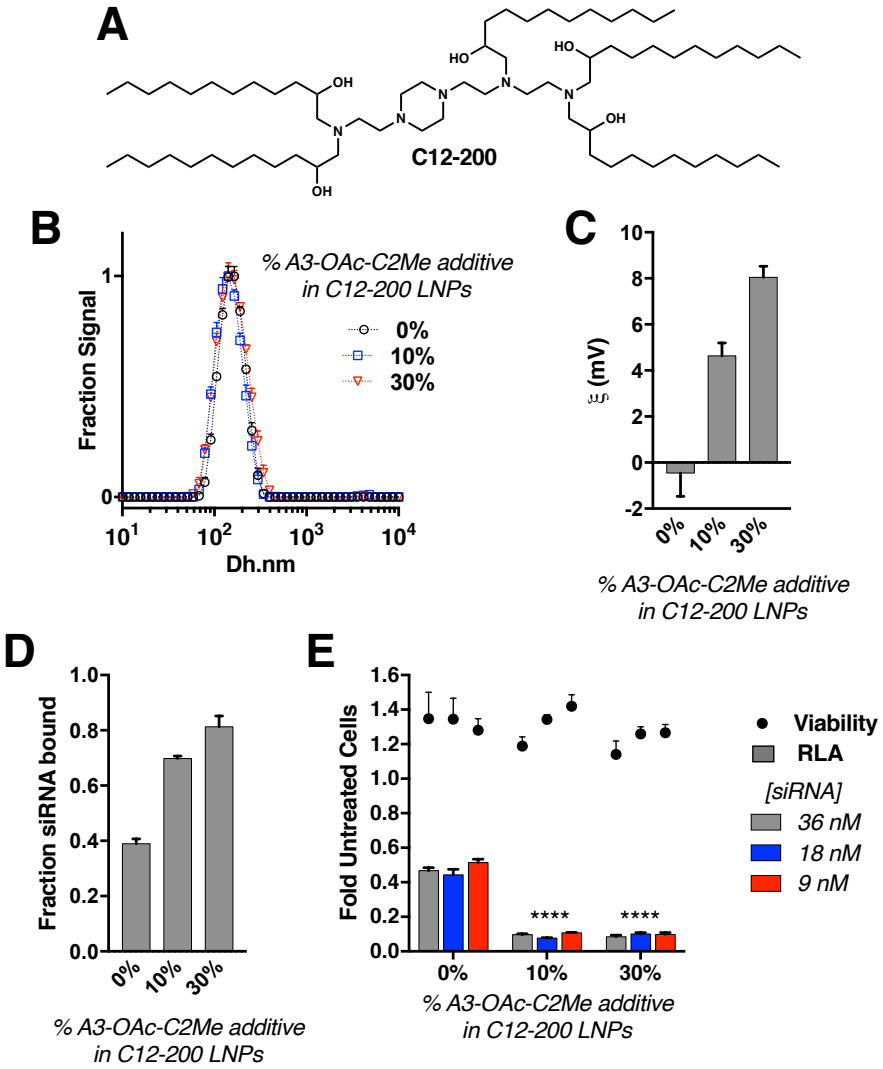

Figure 3.2.17. C12-200 LNPs were supplemented with CSAL A3-OAc-C2Me to determine nanoparticle properties and the effects on delivery efficacy to A549-Luc lung cancer cells. (A) The chemical structure of C12-200. C12-200/CSAL LNPs were formulated at a lipid molar ratio of 50: 38.5: 10: 1.5: *Y* C12-200/ Cholesterol/ DSPC/ PEG-lipid/ CSAL where *Y* was 0, 10, or 30. C12-200: siRNA weight ratio was maintained at 13.5:1 for all formulations. The effect of CSAL additives on nanoparticle size (B), zeta potential (C), and siRNA encapsulation (D) was determined. (D) C12-200/CSAL LNPs were administered to A549-Luc human lung cancer cells by reverse transfection for 20h. A3-OAc-C2Me as an additive showed significantly improved silencing of luciferase compared to C12-200 LNPs without CSAL supplementation. Values are plotted as mean +/- standard deviation (B-C n = 5; D-E n = 4). Statistical analysis was performed with a two-tailed student's T-test **** $P < 0.0001$.

mice (lung: liver ratio ~0.15:1) (**Figure 10**). Inclusion A3-OAc-C2Me (Y=10) into the C12-200 LNPs surprisingly led to 2-fold increased liver accumulation (liver:lung 0.08:1). Meanwhile, inclusion of a larger mole fraction of A3-OAc-C2Me (Y=30) led to a changed biodistribution profile with a striking 9-fold increase of lung accumulation (lung:liver 1.35:1). Inclusion of A1-OAc-C2Me (Y=30) also resulted in a promising 3-fold increase in lung accumulation (lung:liver ~0.47:1), but also showed almost 3-fold increase in kidney accumulation, which is indicative of decreased *in vivo* LNP stability. Incorporation of CSALs as excipients into liver-targeting LNPs

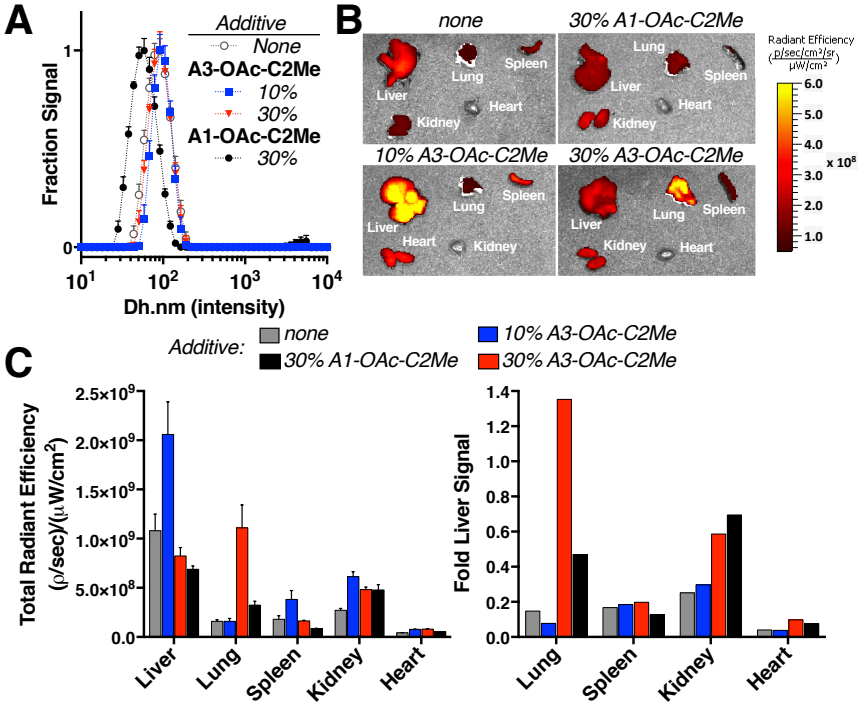

Figure 3.2.18. Incorporation of the A3-OAc-C2Me CSAL into C12-200 LNPs[1] increased lung delivery. C12-200/CSAL LNPs were formulated at a lipid molar ratio of 50: 38.5: 10: 1.5: *Y* C12-200/ Cholesterol/ DSPC/ PEG-lipid/ CSAL where *Y* was 10 or 30. C12-200: siRNA weight ratio was maintained at 13.5:1 for all formulations. (A) The effect of CSAL additives on nanoparticle size was determined by DLS. (B-C) The effect of CSAL excipients on biodistribution of C12-200 LNPs. A3-OAc-C2Me at 30 mol % incorporation led to improved lung accumulation of C12-200 LNPs. Reprinted with permission from Reference 5. Copyright 2018 American Chemical Society.

is an effective strategy for altering the biodistribution to the lungs. The data indicates that higher ratios of A3-OAc-C2Me mediate lung delivery.

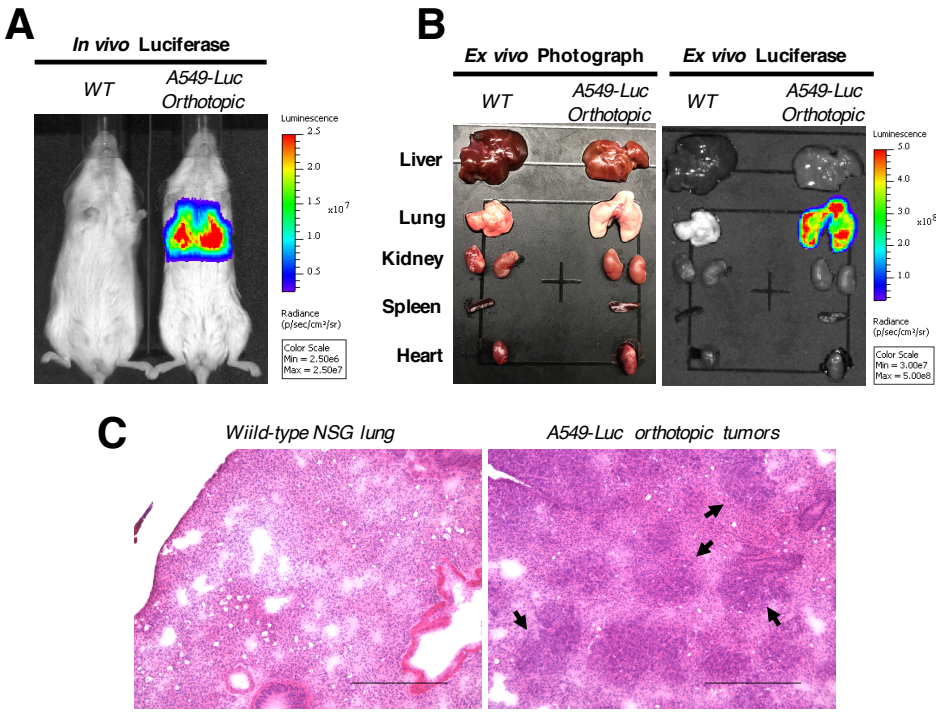

Figure 3.2.19. Orthotopic xenograft lung tumors were formed by intravenous injection of A549-Luc cells into NSG mice. Tumor formation was confirmed by bioluminescence imaging *in vivo* (A) and *ex vivo* (B). Fresh frozen tissue section stained with H&E (C) confirmed formation of tumor nodules (black arrows) compared to wild-type NSG mice. Scale bars = 400 μm.

To further explore the utility of CSAL LNPs for siRNA delivery to the lungs, orthotopic tumors were formed in NOD scid gamma (NSG) mice by tail vein injection of A549-Luc lung cancer cells (**Figure 3.2.19**). This treatment formed tumors exclusively in the lungs, which could be measured by bioluminescence imaging (BLI). The presence of tumors was also confirmed by H&E staining of lung tissue sections (**Figure 3.2.19C**) in all animals, which showed defined tumor nodules, indicated by strong nuclear staining, throughout the lung tissue. Administration of A3-

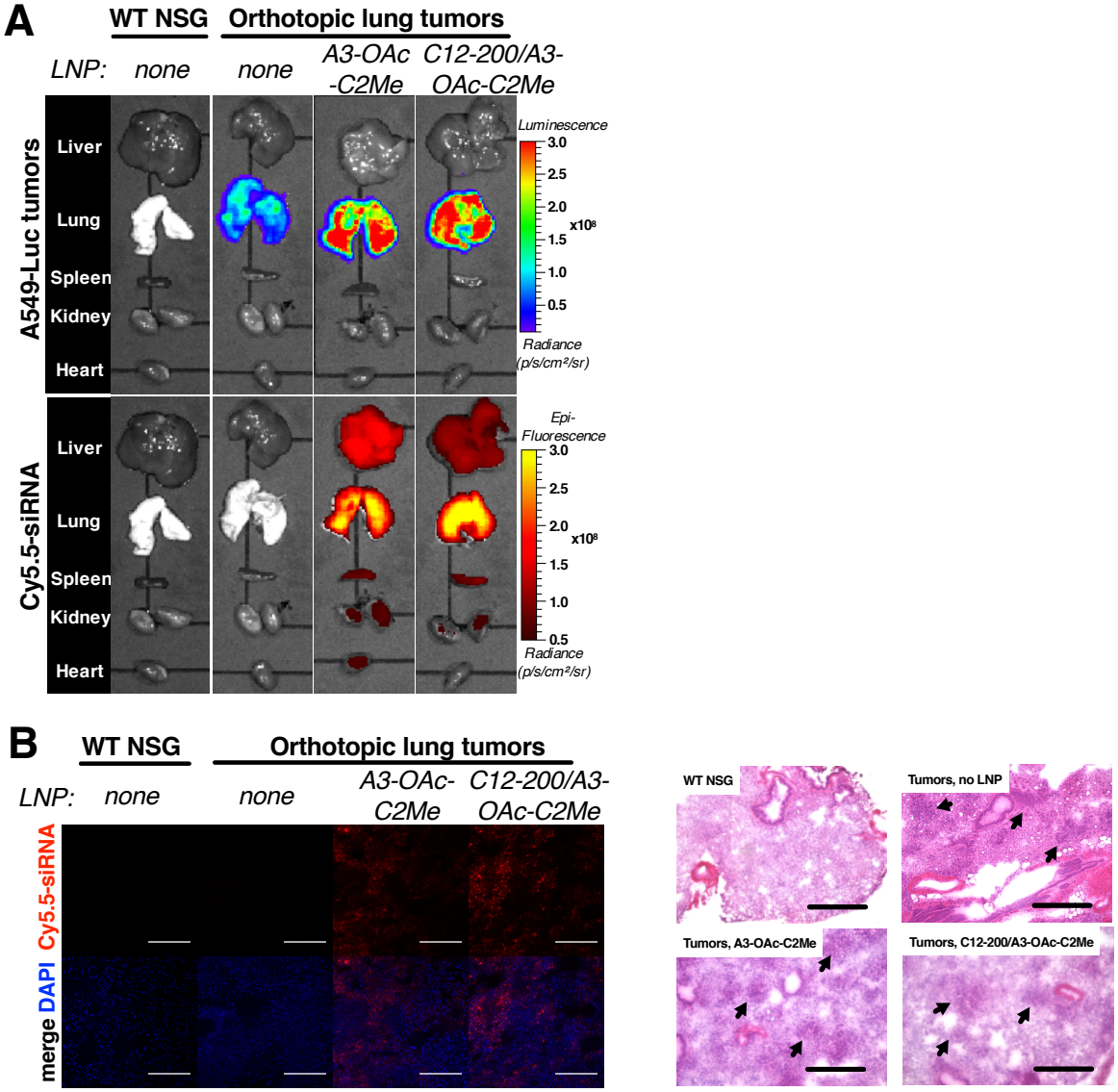

Figure 3.2.20. CSAL LNPs showed lung delivery to A549-Luc orthotopic xenograft tumors in mouse lungs. LNPs were formulated at 30:1 total lipid:siRNA ratio. C12-200 was supplemented with 30% A3-OAc-C2Me as an excipient. Formulated LNPs were administered via tail vein injection at 0.5 mg/kg Cy5.5-siRNA, 1 mg/kg siRNA total for 1.5h. **Left:** (**A**) *Ex vivo* organ imaging shows that CSAL LNPs enable delivery to cancerous lungs. The tumor was visible by bioluminescence imaging (**A**, top) while Cy5.5 fluorescence imaging showed strong lung accumulation (**A**, bottom). (**B**) Confocal microscopy of cryo-sectioned lung tissue shows strong penetration of the cancerous lung with CSAL-LNPs. Nuclei were counterstained with DAPI. (Scale bar = 200 μm). **Right:** H&E staining of NSG mouse lungs following injection of CSAL A3-OAc-C2Me or C12-200/A3-OAc-C2Me LNPs. Tumor nodules (black arrows) are visible in all samples with the exception of wild-type NSG mice. Reprinted with permission from Reference 5. Copyright 2018 American Chemical Society.

OAc-C2Me LNPs resulted in strong penetration of LNPs into the cancerous lungs as determined by Cy5.5-labeled siRNA imaging at both the whole organ (**Figure 11A**) and tissue section (**Figure B**) levels. When used as an excipient in C12-200 LNPs, A3-OAc-C2Me provided enhanced signal in the cancerous lungs, suggesting an opportunity for therapeutic siRNA delivery to the lungs. Thus, the A3-OAc-C2Me CSAL holds promise for delivering RNAs to lung tumors intravenously, either as the primary lipid in LNPs or as an excipient in cationic lipid LNPs. Because CSAL materials can shift the biodistribution of liver-targeting C12-200 LNPs from the liver to orthotopic lung tumors, they offer an opportunity to repurpose known LNPs for use in lung cancer. In future work, we plan to examine the therapeutic effects of oncogene silencing in orthotopic tumor models.

3.3 CONCLUSIONS

Systematic rational design of a library of CSALs, a new class of synthetic cationic lipids, has elucidated SAR in properties governing effective siRNA delivery: shorter dimethyl head groups, acetate side chains and higher tail numbers were favorable for delivery. This led to the discovery of lead CSAL materials that enable efficacious siRNA delivery to cancer cells, which had four tails and an acetate lipid tail side chain. Further *in vivo* evaluation showed strong lung biodistribution after IV administration, and the ability to improve lung accumulation of the potent liver-targeting siRNA carrier C12-200 with the potential to deliver therapeutic siRNAs to lung tumors. The present paper focuses on chemical development of the CSALs and their general application to siRNA delivery. Given the strong SAR, lung biodistribution, and proof of principle efficacy and orthotopic lung tumor uptake *in vivo*, we anticipate future utility in lung disease

models. Future work will focus on further examination of siRNA-mediated oncogene silencing in lung tumor models. These results demonstrate the importance of the functional cationic lipid in LNPs and provide further design guidelines for nucleic acid carriers.

3.4 MATERIALS AND METHODS

3.4.1 Materials

a) Chemicals and reagents for synthesis. All chemicals were purchased from Sigma-Aldrich unless otherwise indicated. Organic solvents were purchased from Fisher Scientific and purified with a solvent purification system (Innovative Technology). Lipid PEG2000 was chemically synthesized, as previously described.[6] $CDCl_3$ and methanol-d4 were purchased from Sigma-Aldrich or Cambridge Isotope Laboratories. C12-113 and C12-200 were synthesized as previously reported.[1]

b) Nucleic acids and other reagents for biological assays. All siRNAs were purchased from Sigma-Aldrich. The Ribogreen reagent was purchased from Life Technologies. ONE-Glo + Tox and Cell Titer Glow were purchased from Promega.

c) Cell culture. Dulbecco's Modified Eagle Medium (DMEM) was purchased from Hyclone containing high glucose, L-glutamine, and without pyruvate or phenol red. Dulbecco's modified phosphate buffered saline (PBS), Trypsin-EDTA (0.25%) and fetal bovine serum (FBS) were purchased from Sigma-Aldrich. HeLa-Luc and A549-Luc cells were cultured in DMEM supplemented with 5% FBS in a humidified incubator at 37 ^{o}C and 5% CO_2.

d) Animal studies. All experiments were approved by the Institutional Animal Care & Use Committee (IACUC) of The University of Texas Southwestern Medical Center and were consistent with local, state and federal regulations as applicable. C57BL/6 and athymic nude Foxn1^{nu} mice were purchased from Envigo.

Instrumentation

a) Nuclear magnetic resonance (NMR) spectroscopy. ^{1}H and ^{13}C NMR were performed on a Varian 400 MHz spectrometer or a Varian 500 MHz spectrometer.

b) Mass spectroscopy (MS). MS was performed on a Voyager DE-Pro MALDI-TOF. LCMS was performed on an Agilent LCMS system equipped with UV-vis and evaporative light scattering detectors (ELSD).

c) Flash chromatography. Flash chromatography was performed on a Teledyne Isco CombiFlash Rf- 200i chromatography system equipped with UV-vis and evaporative light scattering detectors (ELSD).

d) Nanoparticle size and zeta potential analysis. Particle sizes and zeta potentials were measured by Dynamic Light Scattering (DLS) using a Malvern Zetasizer Nano ZS (He-Ne laser, $\lambda = 632$ nm).

e) Nanoparticle formulation for *in vivo* studies. CSAL LNPs for *in vivo* studies were prepared using a two-channel microfluidic mixer with herringbone rapid mixing features (Precision Nanosystems NanoAssemblr). Ethanol solutions of lipid mixes (CSALs, cholesterol, DSPC and PEG-lipid) were rapidly combined with acidic aqueous solutions of nucleic acid at an aqueous: EtOH volumetric ratio of 3:1 and a flow rate of 12 mL/minute.

f) Confocal laser scanning microscopy. Tissue sections were imaged using confocal laser scanning microscopy with a Zeiss LSM-700 and images were processed using ImageJ (NIH).

g) Transmission Electron Microscopy (TEM). TEM was performed using an FEI Tecnai G2 Spirit Biotwin transmission electron microscope.

3.4.2 Nucleic Acid Sequences

Small interfering RNAs (siRNAs)

All siRNAs were purchased from Sigma-Aldrich as chemically synthesized, annealed, double-stranded sequences. dT are DNA bases. All others are unmodified RNA bases.

siLuc (siRNA against Luciferase).

sense: 5'-GAUUAUGUCCGGUUAUGUA[dT][dT]-3'

antisense: 5'-UACAUAACCGGACAUAAUC[dT][dT]-3'

siCtrl (non-targeting siRNA)

sense: 5'-GCGCGAUAGCGCGAAUAUA[dT][dT]-3'

antisense: 5'- UAUAUUCGCGCUAUCGCGC[dT][dT]-3'

Cy5.5-siLuc (fluorescently labeled siRNA against Luciferase).

sense: 5'-Cy5.5-GAUUAUGUCCGGUUAUGUA[dT][dT]-3'

antisense: 5'-UACAUAACCGGACAUAAUC[dT][dT]-3'

3.4.3 Biological assays

3.4.3.1 In vitro CSAL nanoparticle formulations: CSAL LNPs were prepared by the ethanol dilution method. The siRNA was diluted in acidic aqueous buffer (unless otherwise indicated, 10 mM citric acid/sodium citrate buffer pH 3). The lipid mixture was prepared in ethanol, with the appropriate molar ratios of CSAL, cholesterol, DSPC, and PEG-lipid from ethanol stock solutions of each component. Via pipette, the lipid dilution was added to the RNA dilution at a final volumetric ratio of 1:3, rapidly mixed by pipette, and incubated for 15-20 minutes. After this incubation period, the particles were either diluted 3-fold in, or dialyzed against 1X Dulbecco's Modified PBS without calcium and magnesium (Sigma-Aldrich). Dialyses were performed in Pur-

A-Lyzer Midi dialysis chambers (Sigma-Aldrich) for 1 hour per 200 μL sample per chamber against 4L 1X PBS.

3.4.3.2 CSAL in vitro siRNA delivery efficacy: In a white opaque 96-well plate tissue culture plate, HeLa-Luc or A549-Luc cells were seeded at a density of 10×10^3 cells per well in 100 μL growth medium (DMEM without phenol red, 5% FBS), and allowed to attach overnight. The medium was exchanged for 200 μL fresh growth medium the day of the assay. CSAL products were formulated using a lipid mixture of 50: 38.5: 10: 1.5 CSAL: cholesterol: DSPC: PEG-lipid, and screened at a mole ratio CSAL:siRNA of 666:1, 333:1 and 167:1. CSAL NP formulations were performed in a 96-well plate by rapid mixing of CSAL lipid mix (10 μL) and siLuc dilution (20 μL, 40 ng/μL in 10 mM citrate phosphate buffer, pH 3) at 2:1 aqueous:EtOH *v:v* ratio with a multichannel pipette. After a 15-20 minute incubation period, the formulations were diluted in 12 volumes (120 μL) PBS. The nanoparticles (18.75 μL) were added to the HeLa-Luc cells at a dose of 100 ng siRNA per well. The nanoparticles were incubated with the cells for 24 h after which time the cell viability and luciferase expression were evaluated with the ONE-Glo + Tox Assay cell viability and luciferase assay (Promega) and normalized to untreated cells (N = 3 or 4 +/- standard deviation).

3.4.3.3 siRNA Uptake Studies: Cellular uptake studies were performed using CSALs NPs with the same formulation as the *in vitro* delivery efficacy screen in HeLa-Luc cells and A549-Luc cells. Cells were seeded at a density of 30,000 cells per well in 8-chambered coverglass slides (Nunc) and allowed to attached for 24 hours. The nanoparticles were added to the cells at a final siRNA concentration of 34 nM. After 24 h incubation, the medium was aspirated, and washed with PBS.

Cells were fixed with 4% paraformaldehyde (15 minutes RT), washed with PBS 2 times 5 minutes, the cell nuclei were stained with DAPI (Sigma-Aldrich) and washed with PBS. Confocal microscopy imaging was performed using a Zeiss LSM 700 microscope and images were analyzed using ImageJ (NIH).

3.4.3.4 pKa modeling: CSAL microspecies pKa modeling was performed using Marvin. For simplicity, the alkyl tail was shortened from *n*-dodecyl to *n*-butyl. Calculator Plugins were used for structure property prediction and calculation, Marvin 16.7.4, 2016, ChemAxon (http://www.chemaxon.com)

3.4.3.5 Nucleic acid binding experiments: Nucleic acid binding was evaluated using the Ribogreen assay (Molecular Probes). In short, nanoparticles were prepared using the *in vitro* or *in vivo* formulation protocols. The nanoparticle formulations (5 μL) were added to a black 96-well opaque microplate (Corning). A standard curve of the appropriate nucleic acid was prepared in the same medium as the nanoparticles. Ribogreen reagent was diluted 1:1000 in 1 X PBS and 50 μL was added to each well via multichannel pipette. The mixture was stirred on an orbital mixer for 5 minutes, and the fluorescence of each well was read using a plate reader (λ_{Ex} 485 nm, λ_{Em} 535 nm). The amount of free nucleic acid was determined by fitting the signal from each nanoparticle sample to the nucleic acid standard curve, and the fraction bound determined by the following formula: Fraction nucleic acid bound = (total nucleic acid input-free nucleic acid)/ total nucleic acid input) (N = 3 or 4 +/- standard deviation).

3.4.3.6 In vivo nanoparticle formulations: In vivo nanoparticle formulations were prepared using the NanoAssemblr microfluidic mixing system (Precision Nanosystems). Lipids were dissolved in

ethanol and nucleic acids were diluted in 10 mM citric acid-sodium citrate buffer pH 3. The lipid mixture and nucleic acid dilution were combined at a volumetric ratio of 3:1 nucleic acid:lipid mix at a total flow rate of 12 mL per minute, and a waste collection of 0.1 mL at the start and end of each formulation. The nanoparticles were dialyzed against 1 X PBS in Pur-A-Lyzer midi dialysis chambers (Sigma-Aldrich) for 1 hour per 200 μL volume in each chamber, and diluted in 1 X PBS to the appropriate nucleic acid concentration.

3.4.3.7 In vivo siRNA nanoparticle biodistribution: All experiments were approved by the Institutional Animal Care & Use Committee (IACUC) of The University of Texas Southwestern Medical Center and were consistent with local, state and federal regulations as applicable. CSAL nanoparticles were prepared using the *in vivo* nanoparticle formulation method at a lipid mixture mole ratio of 50:38.5:10:1.5 CSAL: cholesterol: DSPC: PEG-lipid, and weight ratio ranging from 20:1 to 45:1 total lipid:siRNA weight ratio. For the siRNA dilution, the siRNA was spiked with 50% Cy5.5 labeled siRNA, and formulation performed as normal. After dialysis, the nanoparticles were diluted to a concentration of 1 μg per 10 μL formulation. This formulation was injected at a dose of 1 mg/kg siRNA by tail vein injection into C57BL/6J mice. After 2h or 24h time, the animals were anesthetized under isofluorane, sacrificed by cervical dislocation, and the organs resected. Fluorescence imaging of the organs was performed on an IVIS Lumina system (PerkinElmer) using the Cy5 excitation and emission filter set, and the images processed using Living Image analysis software (PerkinElmer).

3.4.3.8 Nanoparticle stability studies: A3-OAc-C2Me CSAL nanoparticles (50:38.5:10:1.5 CSAL: cholesterol: DSPC: PEG-lipid *mol:mol*, 30:1 *wt:wt* total lipid:siRNA) were formulated

using microfluidic mixing and dialyzed against 1X PBS. The nanoparticles were diluted 1:5 in 1X PBS or 12.5% fetal bovine serum in 1X PBS for 10% FBS final. The nanoparticles were incubated at ambient temperature for 1 day and nanoparticle size was measured by dynamic light scattering on a Malvern Zetasizer Nano ZS (He-Ne laser, $\lambda = 632$ nm).at 1 minute, 10 minutes, 30 minutes, 1 hour, 2 hours, 4 hours, and 20 hours. Data were plotted as mean +/- standard deviation (N = 5).

3.4.3.9 In vivo luciferase silencing in A549 subcutaneous xenografts: All experiments were approved by the Institutional Animal Care & Use Committee (IACUC) of The University of Texas Southwestern Medical Center and were consistent with local, state and federal regulations as applicable. Athymic Nude-Foxn1^{nu} mice (Envigo) were implanted with xenografts in each hind flank with firefly luciferase expressing A549 (5×10^6 cells suspended in 100 μL of 1:1 *v:v* PBS: Matrigel (Corning)). After the tumors reached adequate size, each tumor on the same animal was injected with *in vivo* formulated NPs (~50 μL per tumor) of CSAL A3OAcC2Me, with a lipid molar ratio of 50 CSAL: 38.5 cholesterol: 10 DSPC: 1.5 PEG-lipid, and total lipid:siRNA weight ratio of 30:1, and final siRNA dose of 1 mg/kg siLuc or siCtrl. After 24h and 48h the luciferase expression was evaluated by live animal bioluminescence imaging Animals were anesthetized under isofluorane, and D-luciferin monosodium hydrate (GoldBio) substrate was injected IP. After 10-12 minute incubation, the luciferase activity was imaged on an IVIS Lumina system (PerkinElmer), and the images processed using Living Image analysis software (PerkinElmer).

3.4.3.10 Ex vivo luciferase expression analysis in A549 xenografts: 48h post injection of A3OAcC2Me siLuc or siCtrl the mice were euthanized by cervical dislocation and the A549 xenografts were resected and frozen on dry ice. The tumors were weighed on a balance, cut into

strips with a straight razor and diluted at 1:3 tumor mass : volume (mg:μL) of 1× reporter lysis buffer (Promega) supplemented with protease inhibitor mini tablets (Pierce) and kept on ice. The tissue was homogenized, the insoluble fraction cleared by centrifugation, and the luciferase expression evaluated by the Luciferase assay system (Promega).

Orthotopic lung tumor xenograft model: A549-Luc cells grown on tissue culture plates were trypsinized, suspended in DMEM, and collected by centrifugation. Cells were resuspended in 1X PBS at a concentration of 30 million cells per mL. The cells (100 uL, 3 million) were injected by tail vein injection into NOD scid gamma (NSG) mice. Tumor growth was monitored by bioluminescence imaging.

3.4.3.11 Tissue sectioning for H&E staining: (Performed with Petra Kos, Ph.D. Siegwart Lab) Lung tissue was embedded in Tissue-Tek O.C.T. compound (Electron Microscopy Sciences) and frozen on dry ice. Tissues were cryosectioned into 10-micron sections using a Leica cryostat and mounted on glass slides. Slides were stored at -80 °C until use. Prior to staining, slides were warmed to room temperature. H&E staining was performed using a standard protocol. Tissue sections were fixed in 3% acetic acid in 95% ethanol for 10 minutes, followed by washing in tap water for 1 minute. Hematoxylin staining was performed for 1 minute followed by bluing in tap water for 1 minute. Eosin staining was performed for 30 seconds followed by rinsing under running tap water for at least 10 seconds. The samples were dehydrated and cleared by sequential washing (12 dips each, 1-2 seconds) in 50% EtOH, 70% EtOH, 95% EtOH, 100% EtOH, 1:1 EtOH/Xylene, and finally 100% Xylene. Cover slips were mounted with Permount mounting

medium (Fisher). Images of H&E tissue sections were captured using a Keyence BZ-X700 microscope.

3.4.3.12 Cy5.5 imaging of tissue sections: NSG mice bearing A549-Luc orthotopic lung xenograft tumors were treated with A3-OAc-C2Me LNPs or C12-200 LNPs supplemented with 30% A3-OAc-C2Me loaded with Cy5.5-loaded siRNA. After 1.5 h, animals were imaged for bioluminescence an fluorescence *in vivo* and *ex vivo*. Lung tissue was collected, embedded, and sectioned using the above protocol. Immediately before imaging, coverslips were mounted with Vectashield mounting medium with DAPI (Vector Laboratories), and imaged by a Zeiss LSM 700 confocal microscope. Images with processed with Image J (NIH).

Nanoparticle property characterization: Physical properties were measured using a Zetasizer Nano ZS (Malvern) with an He-Ne laser (λ = 632 nm). Particle sizes were measured by dynamic light scattering (DLS) (5 measurements, 3 runs x 10 seconds, automatic attenuator setting) by 173° back scattering. Zeta potential was measured in a folded capillary cell (Malvern) with samples diluted in PBS or citrate phosphate buffer pH 7.4.

3.4.3.13 Transmission electron microscopy: (Performed by Kejin Zhou, Ph.D. Siegwart Lab) A3-OAc-C2Me nanoparticles were prepared as described above at a 50:38.5:10:1.5 CSAL: Cholesterol: DSPC: PEG-lipid molar ratios, and 30:1 total lipid: siRNA weight ratio and dialyzed against 1X PBS. A 200mesh carbon coated copper grid (Electron Microscopy Science) was briefly activated by mild plasma cleaning. Afterwards, one drop of the nanoparticle solution prepared as described above was placed on the grid. Excess liquid was removed using filter paper. The copper grid was then air-dried at room temperature for 24h and analyzed using an FEI Tecnai G2 Spirit Biotwin transmission electron microscope at an accelerated voltage of 120 kW.

3.4.3.14 Statistical analysis: Statistical analyses were performed using a two-tailed Student's t-test in GraphPad Prism assuming a Gaussian distribution and unequal standard deviations.

3.4.4 Chemical synthesis

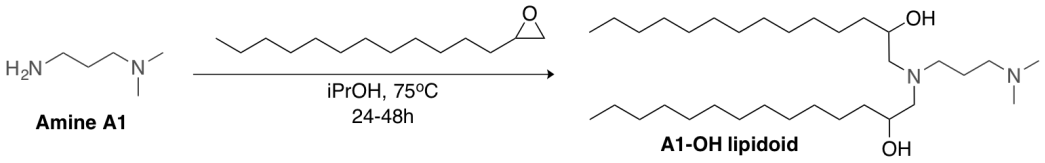

Scheme 3.4.1. Synthesis of A1-OH lipidoid precursor.

3.4.4.1 General protocol for synthesis of lipidoid precursors: In a 100 mL round bottom flask equipped with a stir bar, the amine (A1, A2, or A3) was dissolved in isopropanol at 1M concentration, followed by the addition of 1,2-epoxytetradecane (2 equivalents per expected lipid tail). A reflux condenser was installed and the reaction mixture was heated to 75 °C for 24-48h. Once the desired product was observed, the reaction mixture was concentrated under reduced pressure, dissolved in DCM and purified over silica gel using a solvent gradient of 5% MeOH in DCM to 10% MeOH in DCM supplemented with 1% aqueous ammonium hydroxide. The pure products were characterized by MALDI-TOF ms and ^{1}H NMR.

A1-OH Lipidoid: Pure product isolated as a yellow oil (13.65 g, 53.0% yield). ^{1}H NMR (400 MHz, Chloroform-*d*) δ 3.67 – 3.51 (m, 3H), 2.69 (t, *J* = 6.2 Hz, 2H), 2.55 – 2.31 (m, 5H), 2.31 – 2.22 (m, 3H), 2.19 (d, *J* = 8.5 Hz, 5H), 1.57 (p, *J* = 6.2 Hz, 2H), 1.47 – 1.02 (m, 45H), 0.89 – 0.79 (m, 6H). Mass calculated *m*/z 526.5437 observed (MALDI-TOF ms) *m/z* 527.9280

A2-OH Lipidoid: **Product** ^{1}H NMR (400 MHz, Chloroform-*d*) δ 3.68 – 3.55 (m, 2H), 2.69 (dt, *J* = 15.7, 6.2 Hz, 4H), 2.58 (q, *J* = 7.3 Hz, 3H), 2.50 – 2.40 (m, 3H), 2.36 – 2.24 (m, 2H), 1.68

– 1.58 (m, 2H), 1.26 (d, *J* = 9.1 Hz, 45H), 1.08 (dt, *J* = 23.9, 7.3 Hz, 7H), 0.88 (t, *J* = 6.7 Hz, 6H). Mass calculated *m*/z 554.5750, observed (MALDI-TOF ms) *m/z* 556.13

A3-OH Lipidoid: Product isolated as light yellow oil, 6.36 g, 63.9% yield; ^{1}H NMR (400 MHz, Chloroform-*d*) δ 3.67 (d, *J* = 24.2 Hz, 4H), 2.74 – 2.66 (m, 3H), 2.52 – 2.39 (m, 7H), 2.32 (s, 1H), 2.25 (s, 1H), 1.72 (s, 4H), 1.26 (d, *J* = 8.5 Hz, 101H), 0.88 (t, *J* = 6.7 Hz, 12H). Mass calculated *m*/z 994.0140, observed (MALDI-TOF ms) *m/z* 995.0088

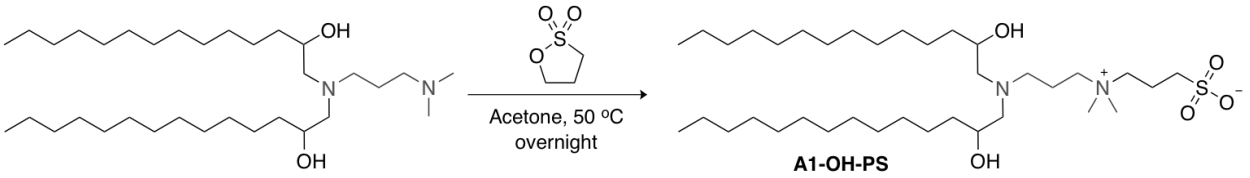

Scheme 3.4.2. Synthesis of A1-OH propanesulfonate (A1-OH-PS)

*3.4.4.2 General protocol for synthesis of An-OH propanesulfonates***:** In a 100 mL round-bottom flask equipped with a stir bar the An-OH lipidoid precursors were dissolved in acetone at 0.25 M concentration. Via pipette, 1,3 propanesultone (1.5 equiv) was added in one portion. The reaction was covered and heated to 50 °C overnight with vigorous stirring. The product formed as an in situ precipitate which could be collected by vacuum filtration. If purification was necessary, the reaction mixture was concentrated under reduced pressure, dissolved in dichloromethane and the product purified over silica gel use of solvent gradient of 10% MeOH/DCM to 10% MeOH/DCM supplemented with 1% aqueous ammonium hydroxide to yield the products as pale yellow solids.

A1-OH propanesulfonate: Product isolated by precipitation in acetone as a light yellow solid (7.46 g, 95.0% yield). ^{1}H NMR (400 MHz, Methanol-d_4) δ 3.64 (td, *J* = 8.2, 7.4, 3.6 Hz, 2H), 3.56 – 3.48 (m, 2H), 3.47 – 3.39 (m, 2H), 3.10 (s, 6H), 2.88 (t, *J* = 6.7 Hz, 2H), 2.68 (q, *J* = 6.8 Hz, 2H), 2.62 – 2.36 (m, 5H), 2.25 – 2.15 (m, 2H), 1.94 (q, *J* = 14.5, 10.9 Hz, 2H), 1.54 – 1.23 (m,

45H), 0.90 (t, *J* = 6.7 Hz, 6H). Mass calculated *m*/z 648.5475, observed (MALDI-TOF ms) *m/z* 649.5370.

A2-OH propanesulfonate: Product purified over silica gel to yield a sticky pale yellow solid (0.31 g, 50.8% yield). ^{1}H NMR (400 MHz, Methanol-d_4) δ 4.24 – 4.16 (m, 0H), 4.04 (s, 0H), 3.90 – 3.84 (m, 0H), 3.84 – 3.75 (m, 1H), 3.67 (dt, *J* = 19.1, 6.6 Hz, 2H), 3.53 (dp, *J* = 13.6, 5.1, 4.1 Hz, 3H), 3.38 (tdd, *J* = 11.0, 9.4, 7.3, 5.1 Hz, 5H), 3.27 – 2.98 (m, 3H), 2.98 – 2.84 (m, 4H), 2.20 – 1.92 (m, 4H), 1.58 – 1.21 (m, 51H), 0.90 (t, *J* = 6.8 Hz, 6H). Mass calculated *m*/z 676.5788, observed (MALDI-TOF ms) *m/z* 677.5295

A3-OH propanesulfonate: Product purified over silica gel to yield a sticky pale yellow solid (2.864 g, 85.0% yield). ^{1}H NMR (400 MHz, Chloroform-*d*) δ 3.88 – 3.56 (m, 11H), 3.18 – 2.96 (m, 6H), 2.90 (q, *J* = 6.2, 5.7 Hz, 3H), 2.84 – 2.30 (m, 14H), 2.28 – 1.79 (m, 10H), 1.25 (s, 88H), 0.87 (t, *J* = 6.8 Hz, 12H). Mass calculated *m*/z 1116.0177, observed (MALDI-TOF ms) *m/z* 1117.34.

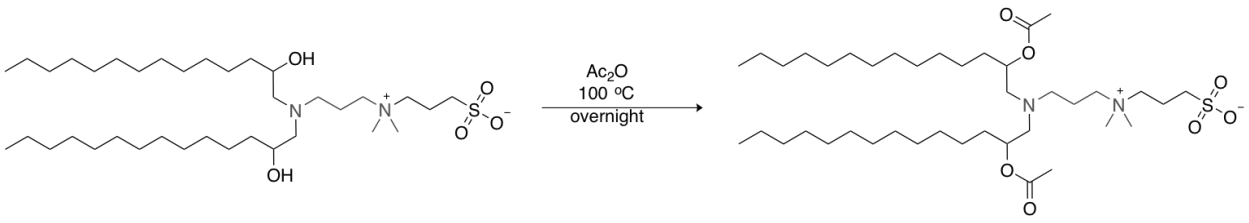

Scheme 3.4.3. Synthesis of A1-OAc-propanesulfonate (A1-OAc-PS)

*3.4.4.3 General protocol for synthesis of An-*OAc *propanefulfonate***:** In a 20 mL vial, An-OH propanesulfonate (A1, A2, or A3) (2 mmol) was dissolved in acetic anhydride (10 mL, excess equiv). The vial was sealed the reaction mixture was heated to 100 °C overnight. Following

complete conversion of the starting material, the reaction mixture was concentrated under reduced pressure, and if necessary purified over silica gel using DCM/MeOH as the elution solvent.

A1-OAc **propanesulfonate:** Product isolated by recrystallization after dilution in acetone following *in vacuo* concentration and isolated as a colorless sticky solid (0.795 g, 56.3% yield). ^{1}H NMR (400 MHz, Chloroform-*d*) δ 4.87 (tt, *J* = 8.0, 4.4 Hz, 2H), 2.85 (td, *J* = 7.9, 2.1 Hz, 2H), 2.65 (s, 4H), 2.61 – 2.36 (m, 5H), 2.08 – 2.02 (m, 1H), 2.00 (d, *J* = 3.0 Hz, 4H), 1.98 (s, 4H), 1.78 (dt, *J* = 8.5, 5.7 Hz, 2H), 1.44 (dtt, *J* = 17.7, 8.7, 4.1 Hz, 5H), 1.22 (s, 40H), 0.85 (t, *J* = 6.8 Hz, 6H). Mass calculated *m*/z 732.5686, observed (MALDI-TOF ms) *m*/*z* 733.6798

A2-OAc **propanesulfonate:** Product purified over silica gel to yield an orange sticky solid (0.2111 g, 67.0% yield) ^{1}H NMR (400 MHz, Methanol-d_4) δ 3.86 – 3.56 (m, 2H), 3.50 (dq, *J* = 18.1, 7.9, 6.3 Hz, 1H), 3.36 (q, *J* = 6.8 Hz, 2H), 3.22 (dq, *J* = 12.2, 6.9, 5.0 Hz, 4H), 3.14 – 2.92 (m, 2H), 2.92 – 2.82 (m, 2H), 2.80 – 2.41 (m, 3H), 2.30 – 2.01 (m, 4H), 1.98 (s, 6H), 1.82 (d, *J* = 5.4 Hz, 0H), 1.64 – 1.52 (m, 1H), 1.30 (d, *J* = 8.1 Hz, 52H), 0.90 (t, *J* = 6.7 Hz, 6H). Mass calculated *m*/z 760.5999, observed (MALDI-TOF ms) *m*/*z* 762.62

A3-OAc **Propanesulfonate:** Crude product isolated as an orange oil and used without further purification (0.91 g, quantitative yield). ^{1}H NMR (400 MHz, Chloroform-*d*) δ 4.98 – 4.81 (m, 4H), 3.79 – 3.61 (m, 4H), 3.27 (ddq, *J* = 16.7, 12.4, 7.6 Hz, 5H), 3.08 (d, *J* = 6.1 Hz, 3H), 2.95 (td, *J* = 14.7, 13.9, 6.9 Hz, 3H), 2.74 – 2.37 (m, 10H), 2.32 – 2.10 (m, 6H), 2.04 (d, *J* = 3.5 Hz, 11H), 1.24 (s, 87H), 0.86 (t, *J* = 6.8 Hz, 12H). Mass calculated *m*/z 1284.0600, observed (MALDI-TOF ms) *m*/*z* 1283.94.

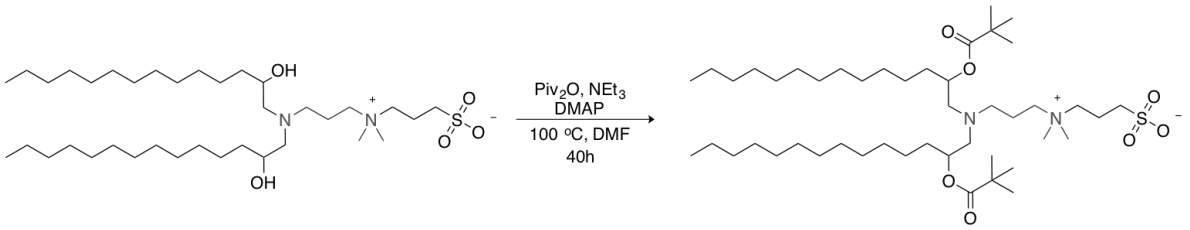

Scheme 3.4.4. Synthesis of A1-OPiv propanesulfonate.

*3.4.4.4 Synthesis of A1-OPiv Propanesulfonate***:** In a 50 mL round-bottom flask equipped with a stir bar and reflux condenser, A1-OH propanesulfonate (0.89 g, 1.37 mmol), pivalic anhydride (1.67 mL, 8.23 mmol, 6 equiv), triethylamine (0.96 mL, 6.86 mmol, 5 equiv), and 4-(dimethylamino)pyridine (1.7 mg, 0.0137 mmol, 0.1 equiv) were dissolved in 5 mL *N*,*N*-dimethylformamide. The reaction mixture was covered with a vented rubber septum and heated with stirring at 100 °C for 40h. The solvent was removed by rotary evaporation under high vacuum, and the crude product was dissolved in DCM. The product was purified over a silica gel gravity column in 10% MeOH/90% DCM to yield A1-OPiv propanesulfonate as a sticky brown solid (0.585 g, 52.2% yield). ^{1}H NMR (400 MHz, Chloroform-*d*) δ 4.82 (s, 2H), 3.72 (td, *J* = 7.9, 3.9 Hz, 2H), 3.41 – 3.13 (m, 8H), 2.92 (t, *J* = 6.5 Hz, 4H), 2.72 – 2.35 (m, 6H), 2.30 – 2.19 (m, 2H), 1.89 (s, 2H), 1.57 – 1.40 (m, 4H), 1.23 (s, 40H), 1.16 (s, 18H), 0.85 (t, *J* = 6.8 Hz, 6H). Mass calculated *m*/z 816.6625, observed (MALDI-TOF ms) *m*/*z* 817.4124.

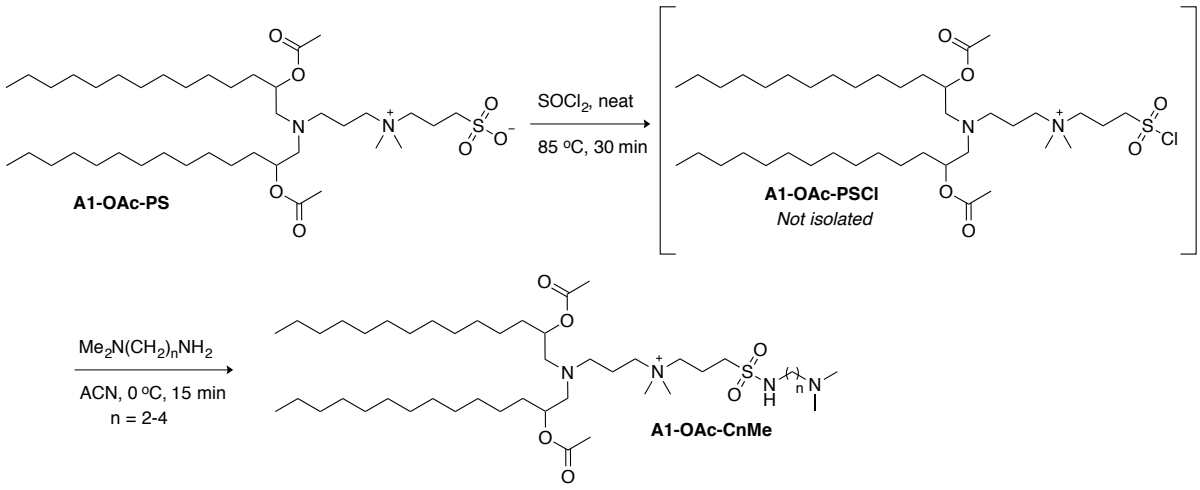

Scheme 3.4.5. Synthesis of CSAL A1-OAc-CnMe.

*3.4.4.5 General protocol for synthesis of A1-*OAc*-Cn-Me/Et and A2-*OAc*-Cn-Me/Et CSALs***:** In a 20 mL vial equipped with a stir bar was dissolved A1-OAc propanesulfonate (100 mg, 0.136 mmol) or A2-OAc propanesulfonate (50 mg, 0.066 mmol) in excess thionyl chloride (1-2 mL). The vial was sealed and the reaction mixture heated to 85 °C for 30 minutes. The reaction was cooled to room temperature, diluted in 5 mL freshly distilled toluene and concentrated under reduced pressure. The crude sulfonyl chloride intermediate was cooled on ice and to this was added the appropriate *N,N*-dimethyl diamine or *N,N*-diethyl diamine (5 equiv) dissolved in 5 mL dry acetonitrile. The reaction mixture was stirred on ice for 15 minutes, and the reaction mixture concentrated under reduced pressure. The crude product was purified on silica gel with a solvent gradient of 5% MeOH in DCM to 20% MeOH, 1% sat. NH_4OH in DCM to yield the product as a sticky yellow or brown solid.

A1-OAc**-C2Me:** ^{1}H NMR (400 MHz, Chloroform-*d*) δ 4.84 (qt, *J* = 7.7, 3.9 Hz, 2H), 3.85 – 3.76 (m, 3H), 3.40 – 3.31 (m, 6H), 3.27 (s, 6H), 2.84 (t, *J* = 6.1 Hz, 2H), 2.69 – 2.50 (m, 6H), 2.48 (s, 5H), 2.45 – 2.20 (m, 8H), 2.01 (d, *J* = 6.2 Hz, 5H), 1.86 (ddt, *J* = 15.1, 11.5, 5.8 Hz, 2H), 1.51

– 1.33 (m, 5H), 1.22 (s, 38H), 0.85 (t, *J* = 6.7 Hz, 6H). Mass calculated *m*/z 803.6654, observed (MALDI-TOF ms) *m*/*z* 803.3930

A1-OAc-**C3Me:** ^{1}H NMR (400 MHz, Chloroform-*d*) δ 4.86 (dq, *J* = 13.7, 4.8, 4.4 Hz, 2H), 3.90 – 3.80 (m, 2H), 3.47 (d, *J* = 2.1 Hz, 2H), 3.45 – 3.23 (m, 16H), 2.81 (d, *J* = 13.9 Hz, 7H), 2.65 – 2.52 (m, 5H), 2.45 (dt, *J* = 13.7, 6.3 Hz, 4H), 2.16 – 1.98 (m, 8H), 1.95 – 1.85 (m, 2H), 1.43 (dd, *J* = 15.2, 6.5 Hz, 3H), 1.24 (s, 42H), 0.87 (t, *J* = 6.7 Hz, 6H). Mass calculated *m*/z 817.6810, observed (MALDI-TOF ms) *m*/*z* 817.5598.

A1-OAc-**C4Me:** ^{1}H NMR (400 MHz, Methanol-d_4) δ 3.68 (d, *J* = 6.8 Hz, 1H), 3.57 – 3.42 (m, 3H), 3.34 (d, *J* = 1.5 Hz, 6H), 3.25 – 3.06 (m, 13H), 2.84 (d, *J* = 1.8 Hz, 7H), 2.72 – 2.48 (m, 4H), 2.27 (p, *J* = 7.7 Hz, 2H), 2.07 (d, *J* = 1.5 Hz, 2H), 2.00 – 1.87 (m, 3H), 1.81 (q, *J* = 8.6 Hz, 2H), 1.70 – 1.53 (m, 3H), 1.30 (d, *J* = 11.5 Hz, 44H), 0.93 – 0.86 (m, 6H). Mass calculated *m*/z 831.6967, observed (MALDI-TOF ms) *m*/*z* 831.5186

A1-OAc-**C2Et:** ^{1}H NMR (500 MHz, Methanol-d_4) δ 3.70 (t, *J* = 6.1 Hz, 1H), 3.61 – 3.45 (m, 5H), 3.43 – 3.26 (m, 18H), 3.26 – 3.13 (m, 6H), 2.92 (d, *J* = 6.3 Hz, 1H), 2.71 – 2.53 (m, 3H), 2.39 – 2.29 (m, 1H), 2.13 – 1.98 (m, 7H), 1.94 (q, *J* = 6.3 Hz, 1H), 1.60 (qd, *J* = 8.1, 5.8, 3.9 Hz, 1H), 1.52 (dd, *J* = 15.0, 7.0 Hz, 2H), 1.40 – 1.28 (m, 47H), 0.93 (t, *J* = 6.8 Hz, 6H). Mass calculated *m*/z 831.6967, observed (MALDI-TOF ms) *m*/*z* 831.80

A1-OAc-**C3Et:** ^{1}H NMR (500 MHz, Methanol-d_4) δ 3.67 – 3.46 (m, 3H), 3.31 – 3.20 (m, 17H), 3.17 (s, 3H), 2.76 – 2.55 (m, 2H), 2.38 – 2.28 (m, 2H), 2.18 – 2.06 (m, 4H), 2.06 – 1.91 (m, 4H), 1.62 (s, 1H), 1.57 – 1.49 (m, 3H), 1.41 – 1.29 (m, 53H), 0.93 (t, *J* = 6.8 Hz, 6H). Mass calculated *m*/z 845.7123, observed (MALDI-TOF ms) *m*/*z* 846.51

A2-OAc-**C2Me:** ^{1}H NMR (500 MHz, Methanol-d_4) δ 3.58 – 3.52 (m, 3H), 3.52 – 3.35 (m, 11H), 3.32 – 3.24 (m, 4H), 3.03 – 2.89 (m, 14H), 2.83 – 2.76 (m, 1H), 2.72 (s, 3H), 2.67 – 2.61 (m, 0H), 2.34 – 2.25 (m, 1H), 2.22 – 2.15 (m, 2H), 2.14 – 2.00 (m, 4H), 1.65 – 1.58 (m, 1H), 1.54 (s, 1H), 1.46 – 1.26 (m, 43H), 0.93 (t, J = 6.7 Hz, 6H). Mass calculated m/z 831.6967, observed M^{+1} (MALDI-TOF ms) m/z 832.62

A2-OAc-**C2Et:** ^{1}H NMR (500 MHz, Methanol-d_4) δ 3.59 – 3.53 (m, 3H), 3.53 – 3.36 (m, 11H), 3.32 – 3.19 (m, 7H), 3.07 (q, J = 7.3 Hz, 4H), 2.61 (d, J = 62.4 Hz, 2H), 2.33 – 2.11 (m, 3H), 2.08 (d, J = 6.5 Hz, 2H), 2.07 – 2.00 (m, 2H), 1.88 (d, J = 7.3 Hz, 0H), 1.62 (s, 1H), 1.54 (d, J = 9.4 Hz, 1H), 1.42 – 1.28 (m, 57H), 1.19 (s, 1H), 0.93 (q, J = 7.6, 7.0 Hz, 6H). Mass calculated m/z 859.7280, observed M^{+1} (MALDI-TOF ms) m/z 860.66

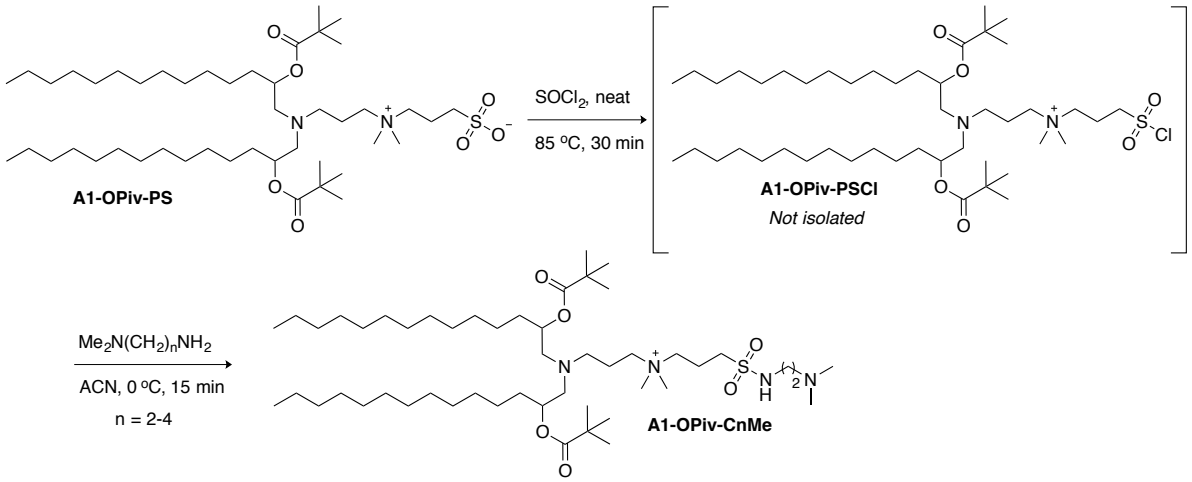

Scheme 3.4.6. Synthesis of CSAL A1-OPiv-CnMe

*3.4.4.6 Synthesis of A1-OPiv-CnMe CSALs***:** In a 20 mL vial equipped with a stir bar was dissolved A1-OPiv propanesulfonate (100 mg, 0.122 mmol) in 2 mL thionyl chloride. The vial was sealed and the reaction mixture heated to 85 °C for 30 minutes. The reaction was cooled to room temperature, diluted in 5 mL freshly distilled toluene and concentrated under reduced pressure.

The crude sulfonyl chloride intermediate was cooled on ice and to this was added the appropriate *N,N*-dimethyl diamine (5 equiv) dissolved in 5 mL dry acetonitrile. The reaction mixture was stirred on ice for 15 minutes, and then reaction mixture was concentrated under reduced pressure. The crude product was purified on silica gel with a solvent gradient of 5% methanol in DCM to 75% DCM, 20% methanol, 5% saturated ammonium hydroxide in water to yield the product as a sticky yellow or brown solid.

A1-OPiv-C2Me: ^{1}H NMR (400 MHz, Methanol-d_4) δ 3.73 (s, 1H), 3.64 – 3.47 (m, 6H), 3.39 – 3.32 (m, 4H), 3.23 – 3.12 (m, 5H), 2.99 – 2.89 (m, 9H), 2.69 (s, 1H), 2.28 (qd, *J* = 16.3, 14.8, 6.5 Hz, 5H), 1.69 (q, *J* = 7.0 Hz, 2H), 1.64 – 1.52 (m, 3H), 1.29 (q, *J* = 11.6, 9.5 Hz, 39H), 1.19 (d, *J* = 7.8 Hz, 12H), 0.90 (t, *J* = 6.8 Hz, 6H). Mass calculated *m*/z 887.7593, observed (MALDI-TOF ms) *m/z* 887.7920

A1-OPiv-C3Me: ^{1}H NMR (400 MHz, Methanol-d_4) δ 3.56 – 3.48 (m, 2H), 3.35 (ddd, *J* = 13.8, 7.3, 3.1 Hz, 3H), 3.27 – 3.08 (m, 13H), 2.74 – 2.50 (m, 9H), 2.37 (s, 3H), 2.33 – 2.21 (m, 3H), 1.99 – 1.88 (m, 3H), 1.78 (p, *J* = 6.9 Hz, 2H), 1.69 – 1.60 (m, 3H), 1.54 (d, *J* = 8.4 Hz, 2H), 1.29 (s, 37H), 1.21 (d, *J* = 2.2 Hz, 16H), 1.15 (s, 2H), 0.90 (t, *J* = 6.6 Hz, 6H). Mass calculated *m*/z 901.7749, observed (MALDI-TOF ms) *m/z* 901.4854

A1-OPiv-C4Me: ^{1}H NMR (400 MHz, Methanol-d_4) δ 3.59 – 3.48 (m, 3H), 3.34 (d, *J* = 5.0 Hz, 3H), 3.23 – 3.06 (m, 12H), 2.63 (dddd, *J* = 24.5, 22.2, 9.7, 5.8 Hz, 8H), 2.45 (t, *J* = 7.3 Hz, 3H), 2.38 – 2.21 (m, 8H), 2.00 – 1.87 (m, 3H), 1.60 (tdt, *J* = 23.9, 12.1, 7.6 Hz, 10H), 1.29 (s, 38H), 1.21 (d, *J* = 2.2 Hz, 16H), 0.90 (t, *J* = 6.6 Hz, 6H). Mass calculated *m*/z 915.7906, observed (MALDI-TOF ms) *m/z* 915.6368

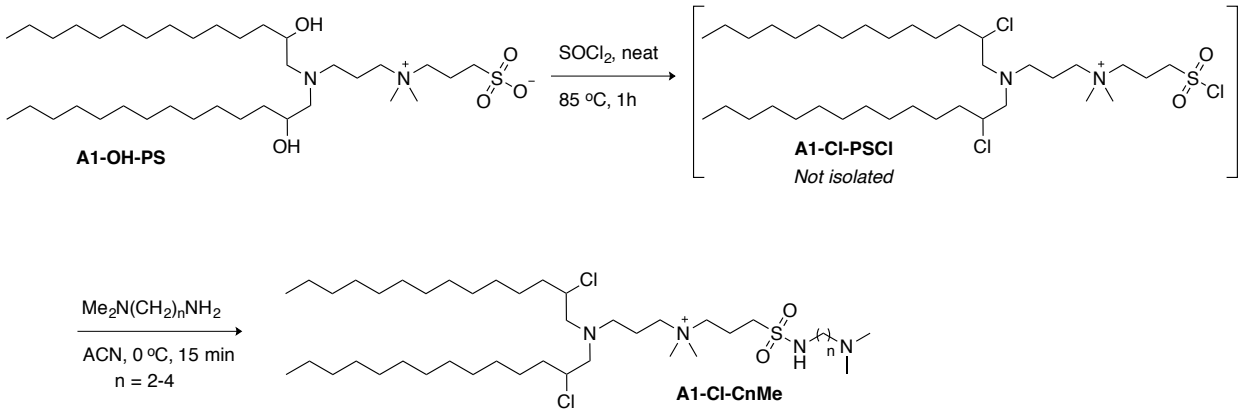

Scheme 3.4.7. Synthesis of A1-Cl-CnMe.

*3.4.4.7 Synthesis of A1-Cl-CnMe CSALs***:** In a 20 mL vial equipped with a stir bar was dissolved A1-OH propanesulfonate (100 mg, 0.154 mmol) in 2 mL thionyl chloride. The vial was sealed and the reaction mixture heated to 85 °C for 1 hour. The reaction was cooled to room temperature, diluted in 5 mL freshly distilled toluene and concentrated under reduced pressure. The crude sulfonyl chloride intermediate was dissolved in 5 mL dry acetonitrile, cooled on ice and to this was added slowly the appropriate *N,N*-dimethyl diamine (5 equiv) dissolved in 5 mL dry acetonitrile. The reaction mixture was stirred on ice for 15 minutes, and the reaction mixture concentrated under reduced pressure, and dried under vacuum. The products were purified over alumina using a solvent gradient of 0-20% methanol in dichloromethane to yield the products as sticky yellow, brown solids.

A1-Cl-C2Me: ^{1}H NMR (400 MHz, Methanol-d_4) δ 3.74 – 3.63 (m, 2H), 3.54 (ddt, J = 12.6, 8.8, 4.4 Hz, 3H), 3.43 – 3.32 (m, 4H), 3.29 – 3.08 (m, 9H), 2.91 (s, 0H), 2.88 (t, J = 6.8 Hz, 1H), 2.80 – 2.67 (m, 3H), 2.63 (t, J = 6.5 Hz, 1H), 2.57 – 2.50 (m, 1H), 2.34 (d, J = 31.7 Hz, 6H), 2.04 – 1.96 (m, 1H), 1.96 – 1.89 (m, 1H), 1.88 – 1.80 (m, 1H), 1.61 (td, J = 13.9, 13.0, 6.5 Hz, 4H), 1.47

(dt, *J* = 11.5, 4.8 Hz, 3H), 1.31 (d, *J* = 11.7 Hz, 38H), 0.90 (t, *J* = 6.7 Hz, 6H). Mass calculated *m*/z 755.5765, observed (MALDI-TOF ms) *m/z* 755.7258.

A1-Cl-C3Me: ^{1}H NMR (400 MHz, Methanol-d_4) δ 5.57 (dd, *J* = 6.4, 3.3 Hz, 1H), 5.18 – 4.92 (m, 5H), 4.84 – 4.64 (m, 11H), 4.45 (dt, *J* = 13.3, 6.1 Hz, 1H), 4.29 (dd, *J* = 28.8, 6.4 Hz, 4H), 4.15 (t, *J* = 7.6 Hz, 1H), 3.96 (d, *J* = 3.1 Hz, 2H), 3.85 (q, *J* = 8.7 Hz, 2H), 3.72 – 3.31 (m, 6H), 3.27 – 3.12 (m, 4H), 3.07 – 2.97 (m, 3H), 2.87 (d, *J* = 11.5 Hz, 40H), 2.46 (t, *J* = 6.8 Hz, 6H). Mass calculated *m*/z 769.5921, observed (MALDI-TOF ms) *m/z* 769.6628.

A1-Cl-C4Me: ^{1}H NMR (400 MHz, Methanol-d_4) δ 3.74 – 3.45 (m, 5H), 3.39 (t, *J* = 6.4 Hz, 1H), 3.30 – 3.07 (m, 12H), 2.89 (dt, *J* = 13.4, 6.6 Hz, 2H), 2.82 – 2.65 (m, 4H), 2.54 (t, *J* = 7.5 Hz, 1H), 2.40 (s, 3H), 2.36 – 2.18 (m, 3H), 2.02 – 1.81 (m, 4H), 1.74 – 1.54 (m, 7H), 1.52 – 1.41 (m, 3H), 1.31 (d, *J* = 11.7 Hz, 38H), 0.90 (t, *J* = 6.8 Hz, 6H). Mass calculated *m*/z 783.6078, observed (MALDI-TOF ms) *m/z* 783.7239.

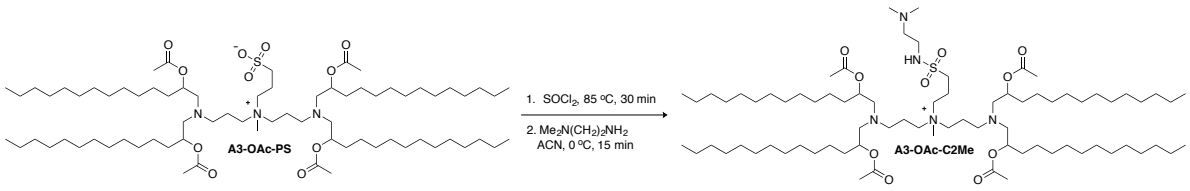

Scheme 3.4.8. Synthesis of A3-OAc-C2Me

3.4.4.8 Synthesis of A3-OAc-*C2Me***:** In a 20 mL vial equipped with a stir bar was dissolved A3-OAc propanesulfonate (200 mg, 0.155 mmol) in 2 mL thionyl chloride. The vial was sealed and the reaction mixture heated to 85 °C for 30 minutes. The reaction was cooled to room temperature, diluted in 5 mL freshly distilled toluene and concentrated under reduced pressure. The crude sulfonyl chloride intermediate was cooled on ice and to this was added the appropriate *N,N*-dimethyl ethylenediamine (0.775 mmol, 85 μL, 5 equiv) dissolved in 5 mL dry acetonitrile. The

reaction mixture was stirred on ice for 15 minutes, and then the reaction mixture concentrated under reduced pressure. The crude product was purified on silica gel with a solvent gradient of 5% MeOH in DCM to 20% MeOH, 1% sat. NH_4OH in DCM to yield the product as a sticky brown solid (79.8 mg, 38.0% yield). ^{1}H NMR (400 MHz, Chloroform-*d*) δ 4.88 (ddt, *J* = 12.7, 8.7, 4.3 Hz, 4H), 3.87 (dd, *J* = 12.8, 7.4 Hz, 2H), 3.62 (tt, *J* = 10.0, 3.1 Hz, 3H), 3.57 – 3.49 (m, 2H), 3.47 – 3.38 (m, 3H), 3.37 – 3.28 (m, 4H), 3.24 (q, *J* = 6.6 Hz, 5H), 2.93 – 2.88 (m, 1H), 2.85 – 2.74 (m, 6H), 2.68 – 2.52 (m, 11H), 2.52 – 2.38 (m, 9H), 2.32 – 2.27 (m, 1H), 2.04 (dd, *J* = 3.6, 2.0 Hz, 10H), 1.55 – 1.37 (m, 9H), 1.24 (s, 72H), 1.10 (d, *J* = 9.6 Hz, 1H), 0.87 (t, *J* = 6.8 Hz, 12H). Mass calculated *m*/z 1355.1567, observed M^{+1} (MALDI-TOF ms) *m/z* 1355.18.

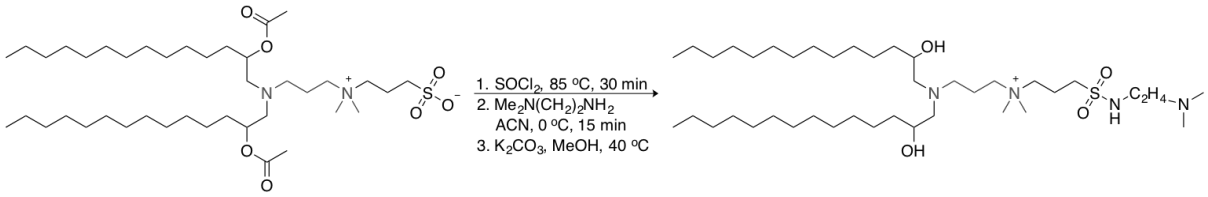

Scheme 3.4.9. Synthesis of A1-OH-C2Me

*3.4.4.9 Synthesis of A1-OH-C2Me***:** In a 20 mL vial equipped with a stir bar was dissolved A1-OAc propanesulfonate (100 mg, 0.136 mmol) in 2 mL thionyl chloride. The vial was sealed and the reaction mixture heated to 85 °C for 30 minutes. The reaction was cooled to room temperature, diluted in 5 mL freshly distilled toluene and concentrated under reduced pressure. The crude sulfonyl chloride intermediate was cooled on ice and to this was added the appropriate *N,N*-dimethyl-ethylenediamine (85.6 µL, 0.68 mmol, 5 equiv) dissolved in 5 mL dry acetonitrile. The reaction mixture was stirred on ice for 15 minutes, and the reaction mixture concentrated under reduced pressure. The reaction mixture was redissolved in 5 mL methanol and potassium

carbonate (0.93 g, 0.68 mmol, 5 equiv) was added and the reaction mixture stirred at 40 °C for 4 days. After reaction, the mixture was cooled, filtered, and concentrated under reduced pressure. The concentrate was dissolved in acetone and additional precipitate was removed by filtration to yield the crude product as a yellow sticky solid. The product was purified over silica gel (5% methanol in DCM to 20% methanol, 2% saturated ammonium hydroxide in dichloromethane to yield the product as a sticky yellow solid (17.5 mg, 17.9% yield). ^{1}H NMR (400 MHz, Methanol-d_4) δ 3.63 (tt, J = 11.2, 4.9 Hz, 3H), 3.48 (ddd, J = 19.7, 10.2, 5.8 Hz, 4H), 3.21 (dd, J = 13.4, 6.3 Hz, 5H), 3.11 (d, J = 11.1 Hz, 5H), 2.68 (t, J = 6.3 Hz, 2H), 2.61 – 2.35 (m, 6H), 2.30 (s, 6H), 1.99 – 1.87 (m, 2H), 1.54 – 1.07 (m, 44H), 0.90 (t, J = 6.6 Hz, 6H). Mass calculated m/z 719.6443, observed M^{+1} (MALDI-TOF ms) m/z 719.8963.

CHAPTER FOUR

Conclusions and Future Directions

This dissertation reports the design, synthesis, and biophysical characterization of two new classes of novel synthetic lipids with delivery capabilities to the lung. The design of effective materials for the targeting of non-liver tissues for non-viral delivery of nucleic acid therapeutics remains a major hurdle in the field in the context of developing treatments for a number of diseases including cancer. Zwitterionic amino lipids (ZALs) were synthesized with the expectation that the balance of cationic and zwitterionic moieties on the lipid structure would possess properties favorable for the delivery of messenger RNA therapeutics. The lead compound from this study was ZA3-Ep10, which demonstrated the unique ability to effectively deliver long single-stranded RNA to the lungs *in vivo*, as well as non-viral CRISPR gene editing by the co-delivery of sgRNA and mRNA encoding Cas9 in a reporter model by systemic delivery and locally via intramuscular delivery. Cationic sulfonamide amino lipids incorporated an internal quaternary ammonium molecule to effectively encapsulate siRNA, while also functioning in a membrane disrupting fashion. The CSAL A3-OAc-C2Me, was capable of not only targeting the lung tissue effectively, but also redirecting biodistribution of a previously reported potent liver-targeting nanoparticle which has shown delivery of both siRNA and mRNA to the liver. These new classes of materials represent a chemical scaffold template upon which to build effective materials for both the delivery of long RNAs and for targeting the lung *in vivo*.

However, development of a deeper understanding of the biophysical and chemical properties that confer a potent lung-targeting ability to these materials are of great interest. One ongoing study in its infancy is a histological based study being performed in conjunction with the Molecular Pathology core at UTSW in order to gain an understanding of the cell-type specificity of nanoparticle localization and functional protein expression following messenger RNA delivery. Gaining knowledge of the pharmacokinetic distribution of nanomaterials and therapeutic nucleic acids will enable improvement of design to target treatments for specific diseases with known cell-type specific pathology.

Rationally-designed chemical modifications that result in a better pharmacodynamically structure activity relationship should be undertaken to gain a full understanding of the chemical properties that enable both lung delivery and the ability to encapsulate and deliver long RNA molecules. Preliminary SAR studies of ZA3-Ep10 by masking of the secondary alcohol moieties with an acetate demonstrated significantly reduced toxicity but retained activity *in vitro*, while *in vivo* lung delivery was shifted exclusively to the spleen. Additionally, the introduction of an ester bond β to the secondary alcohol eliminated mRNA delivery, while sgRNA delivery activity was maintained. Understanding the balance of the molecular forces governing the effective delivery of the range of RNAs using a single ZNP formulation remains a major source of investigative interest. This is actively being pursued using computational modeling of the ZNP formulation in the context of siRNA and mRNA, in parallel with physical characterization of ZNP nanostructure with transmission electron microscopy. Furthermore, coupling of these studies with a comprehensive chemical SAR panel (shown in Figure 2.2.30) would elucidate the relative

contributions of various regions within the modular scaffold and enable to design of second generation ZALs and CSALs for lung delivery. These studies, if performed through the lens of both understanding SAR, while also improving the pharmacokinetic profile of the nanocarrier would greatly facilitate the clinical translation of this class of materials, in terms of improving organ specific delivery, limiting material derived toxicity, and improving the potency of delivery.

APPENDIX A: ZAL MALDI-TOF AND NMR DATA

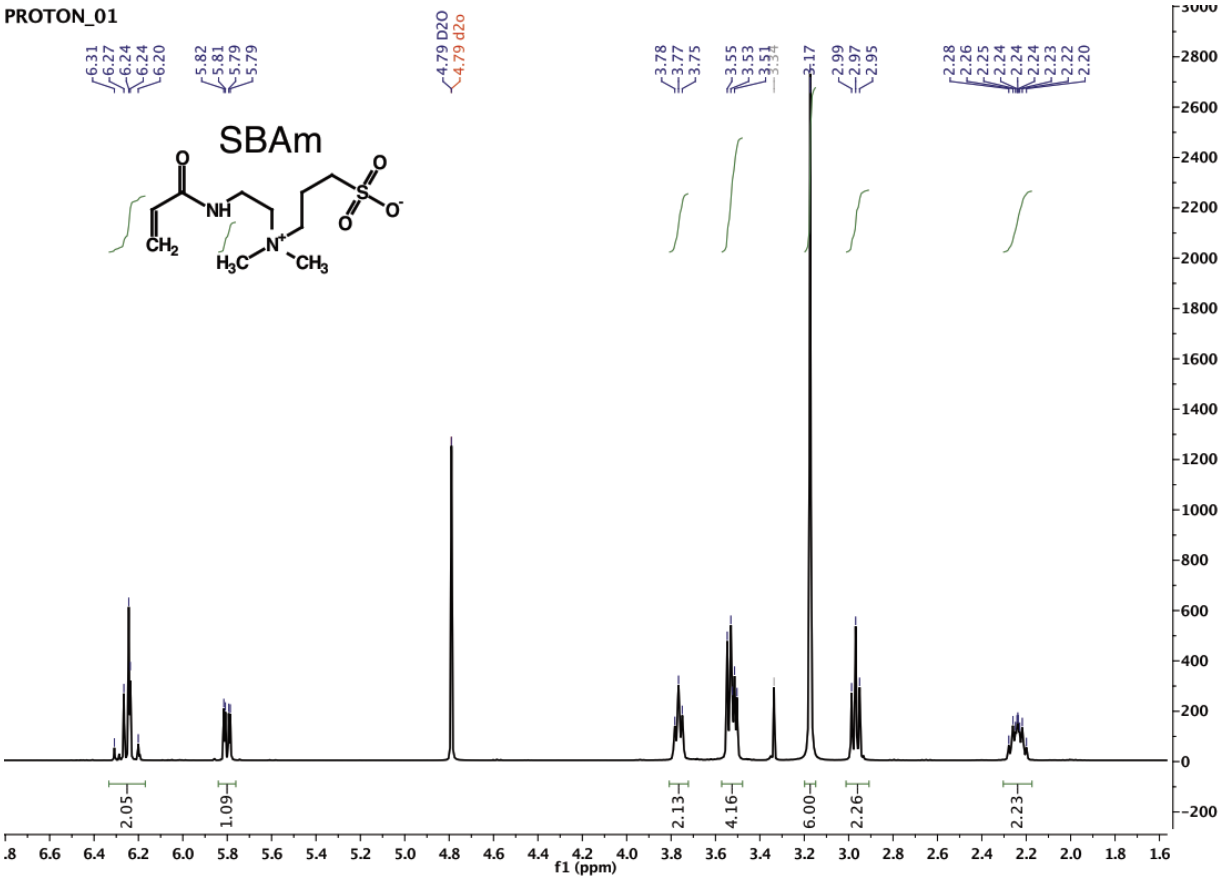

Figure A1. [1]H NMR of zwitterionic acrylamide precursor SBAm.

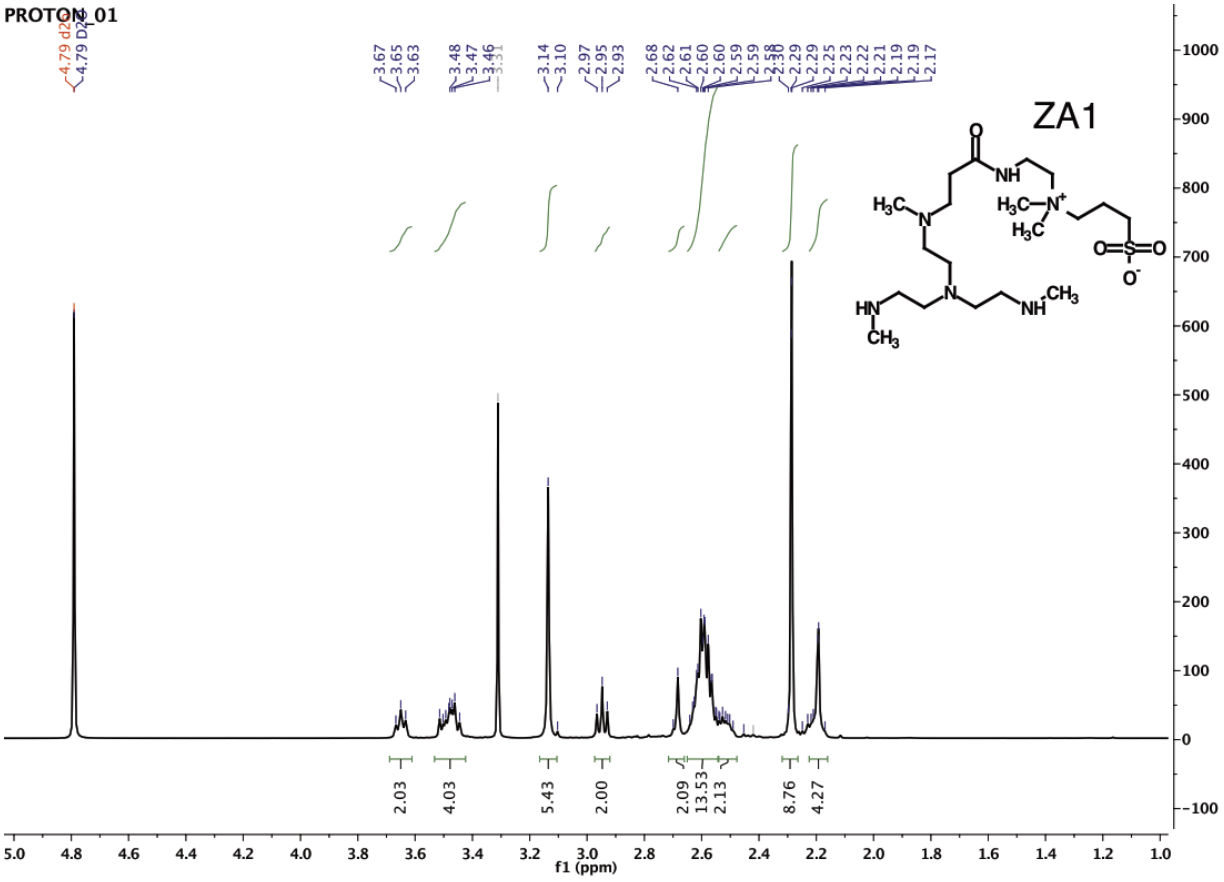

Figure A2. [1]H NMR of ZA1.

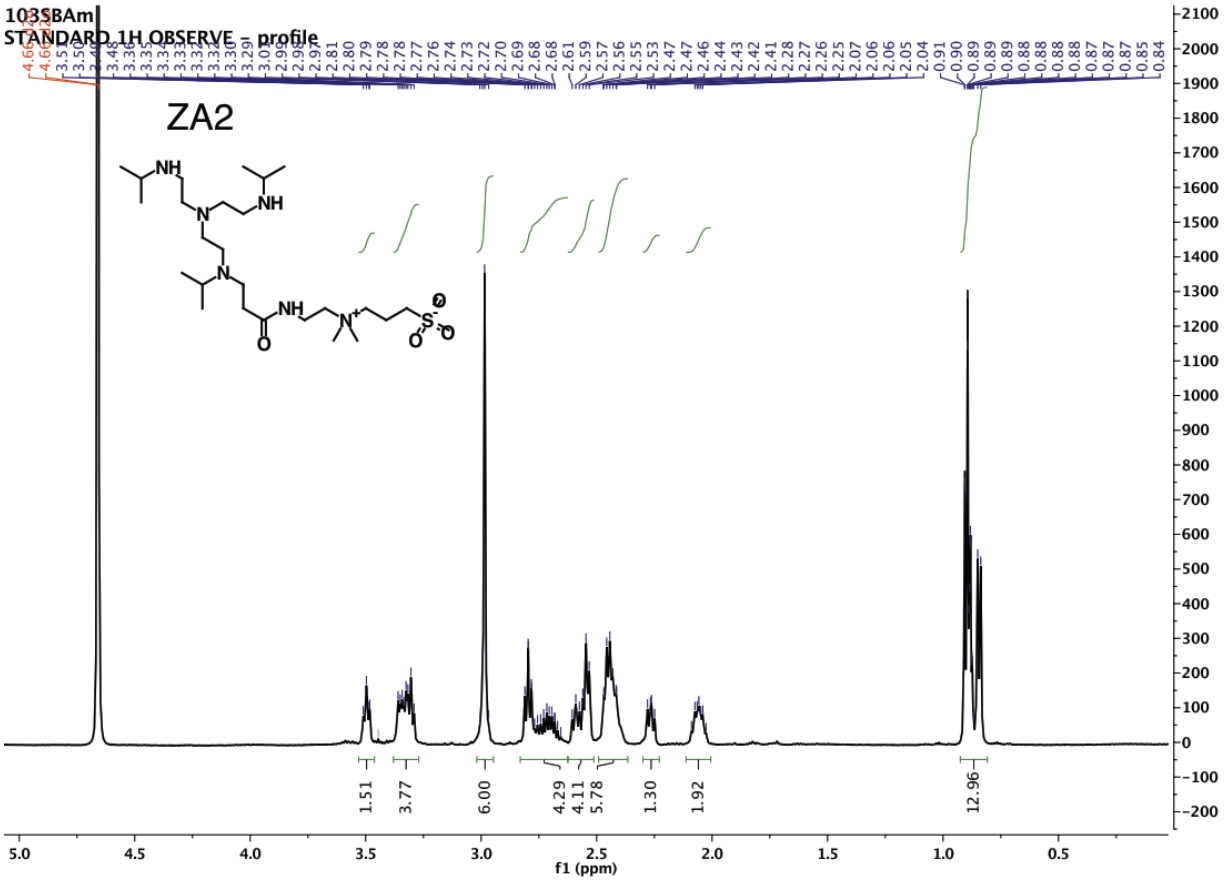

Figure A3. ^{1}H NMR of ZA2

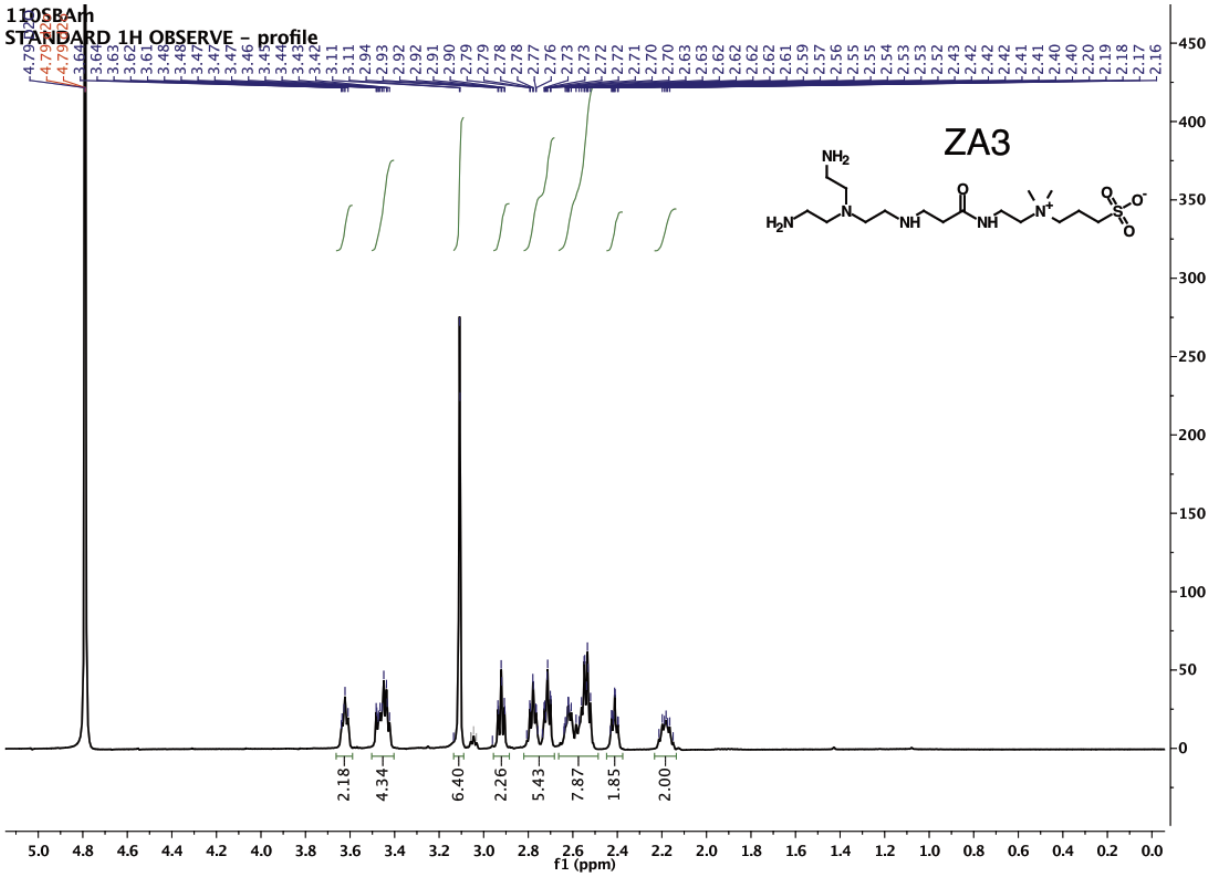

Figure A4. ^{1}H NMR of ZA3

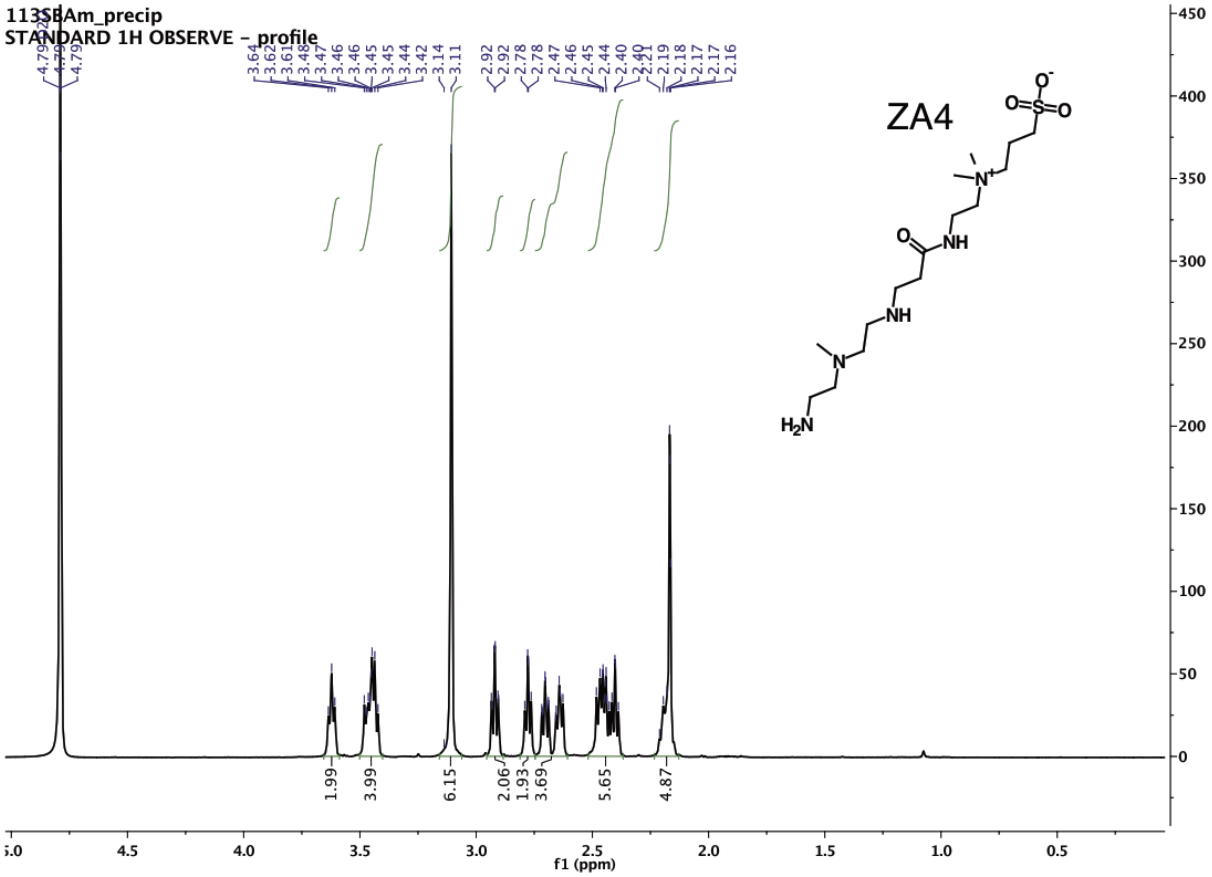

Figure A5. [1]H NMR of ZA4

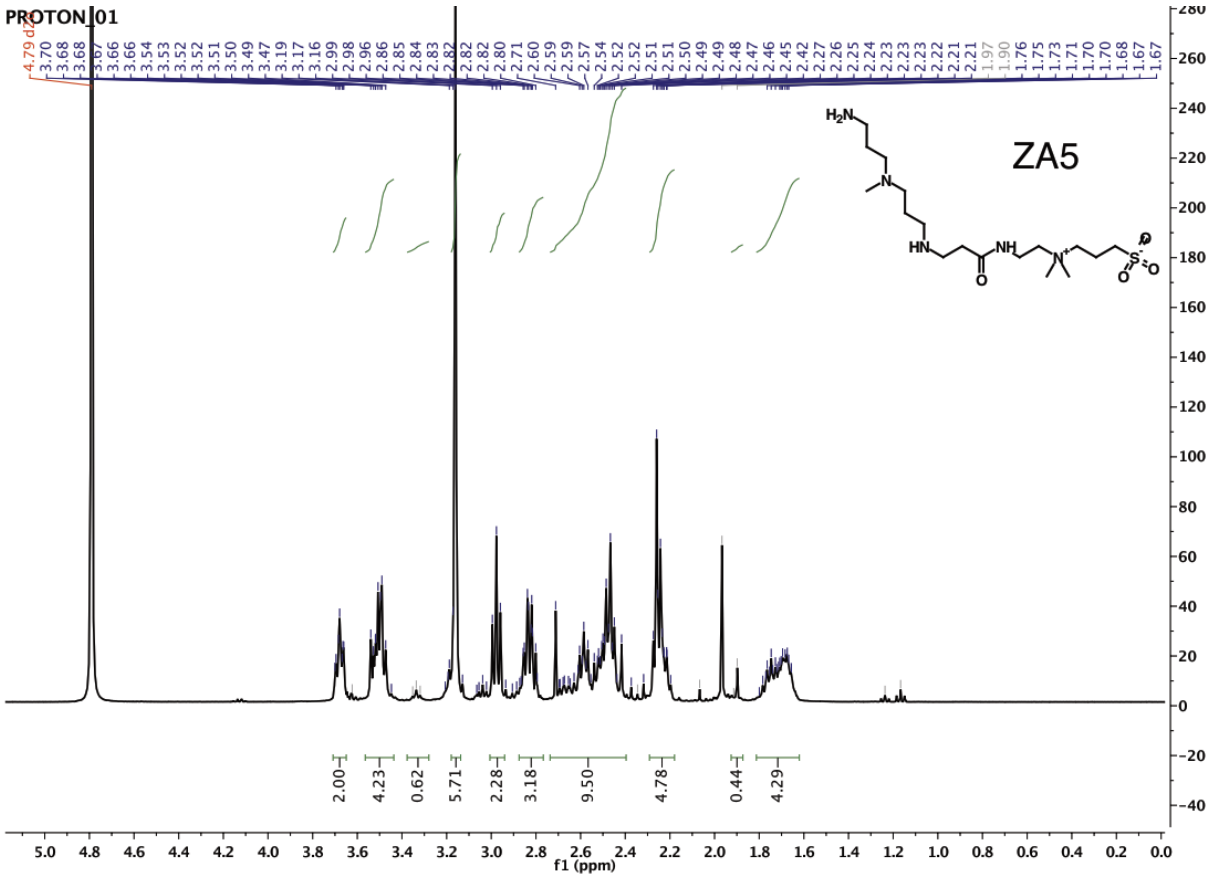

Figure A6. ^{1}H NMR of ZA5

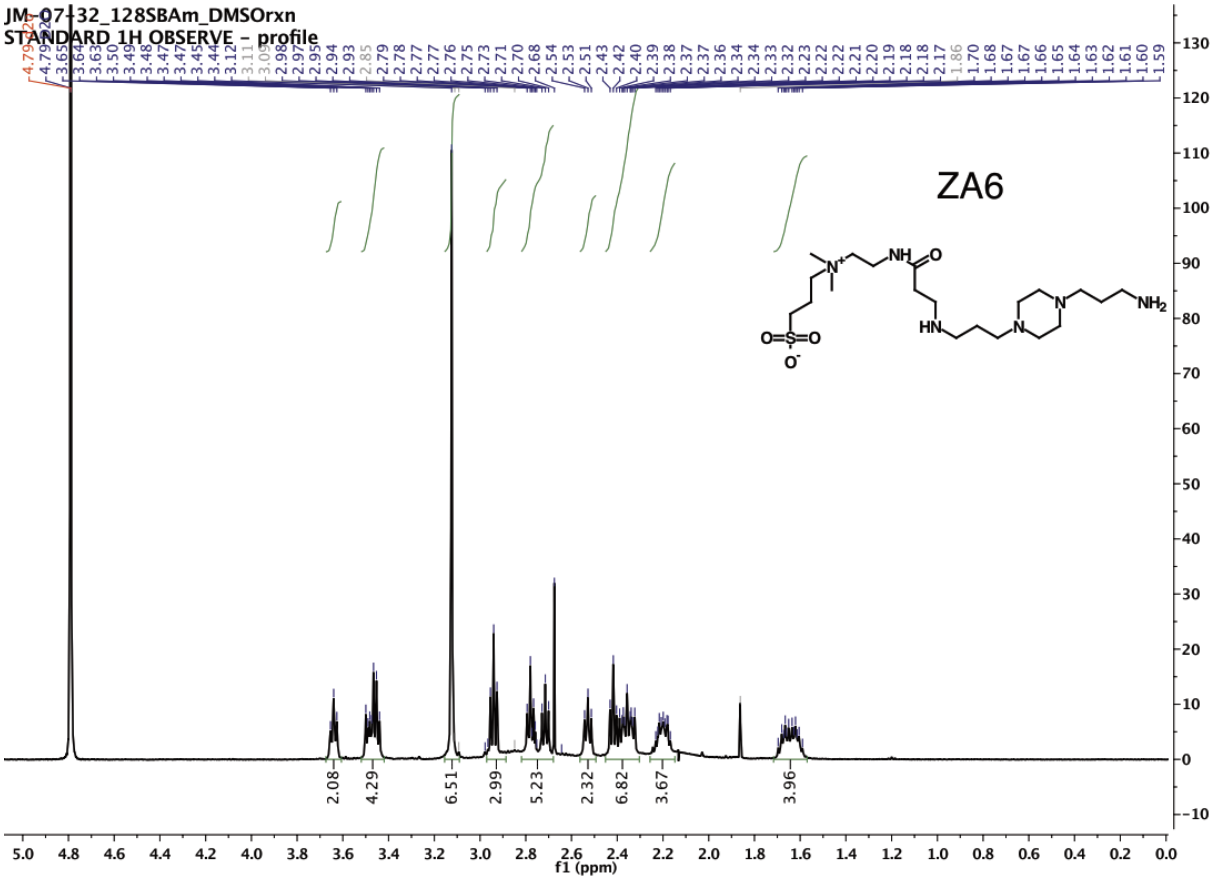

Figure A7. ^{1}H NMR of ZA6.

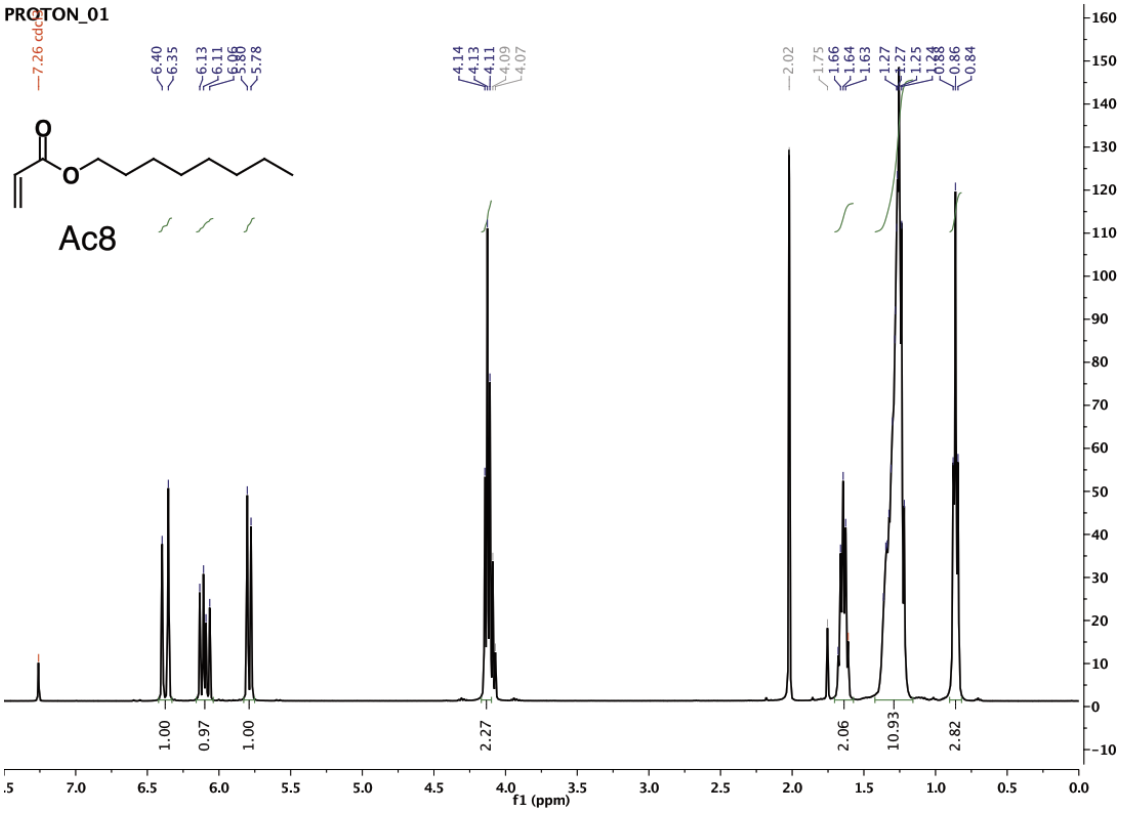

Figure A8. [1]H NMR of acrylate Ac8

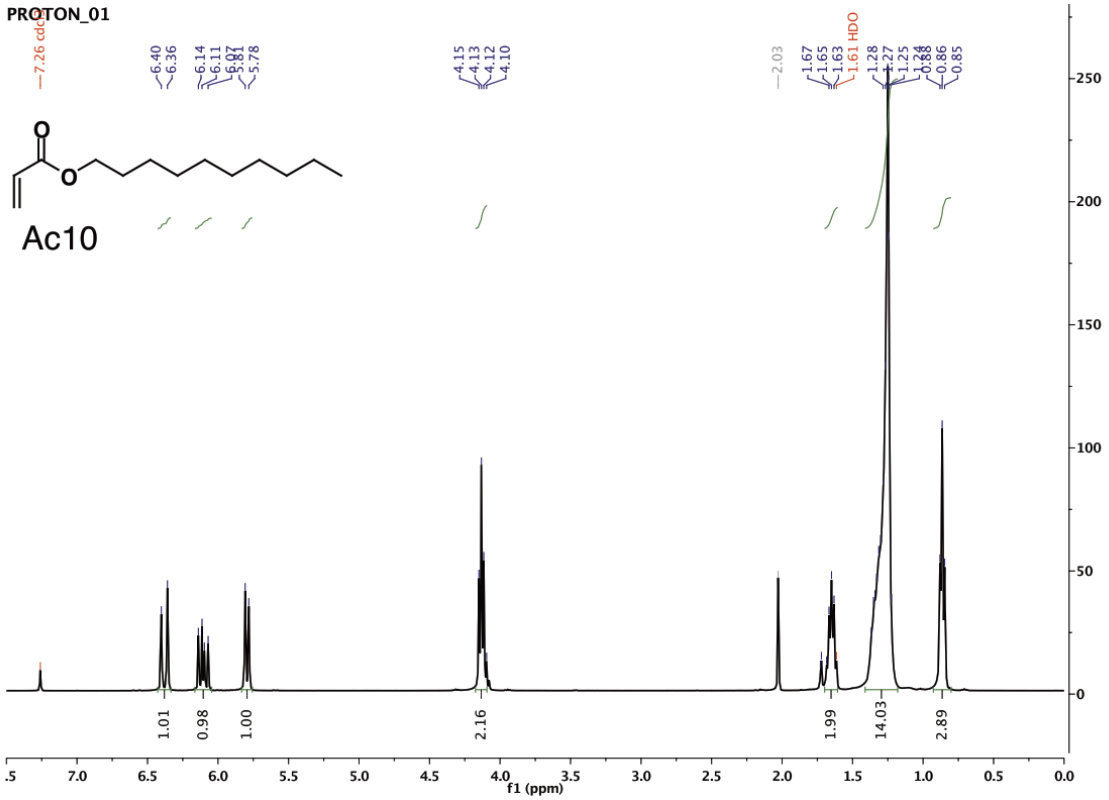

Figure A9. ^{1}H NMR of acrylate Ac10.

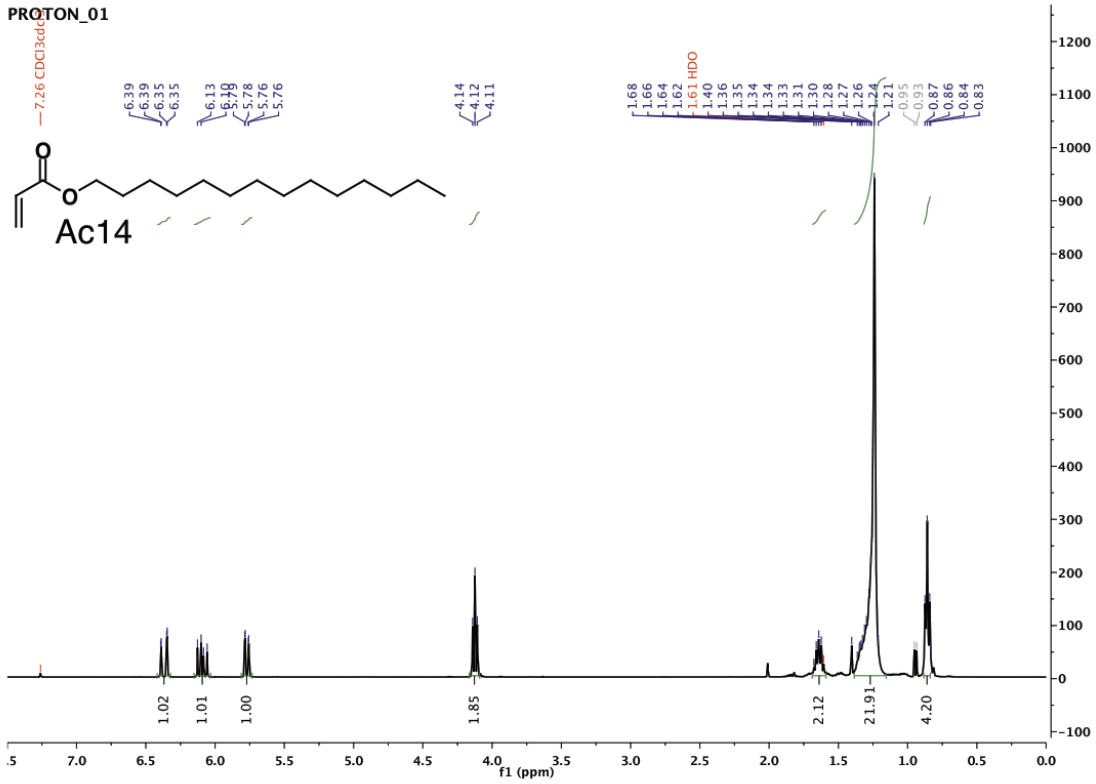

Figure A10. ^{1}H NMR of acrylate Ac14.

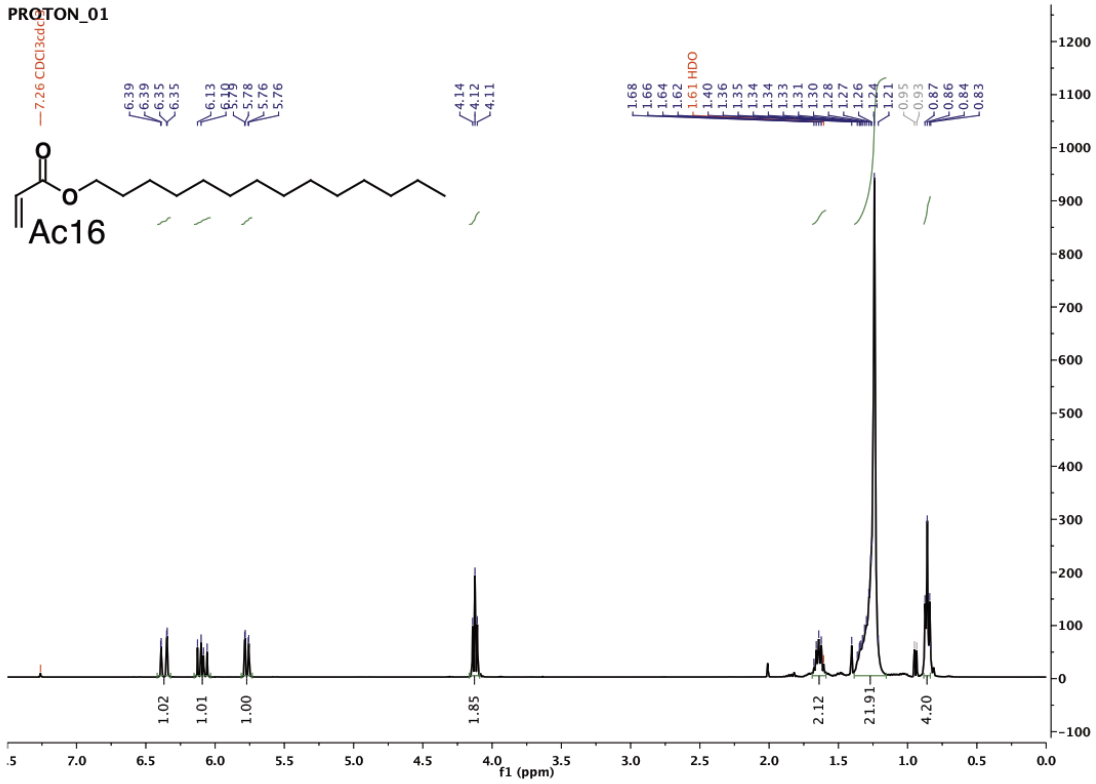

Figure A11. ^{1}H NMR of acrylate Ac16.

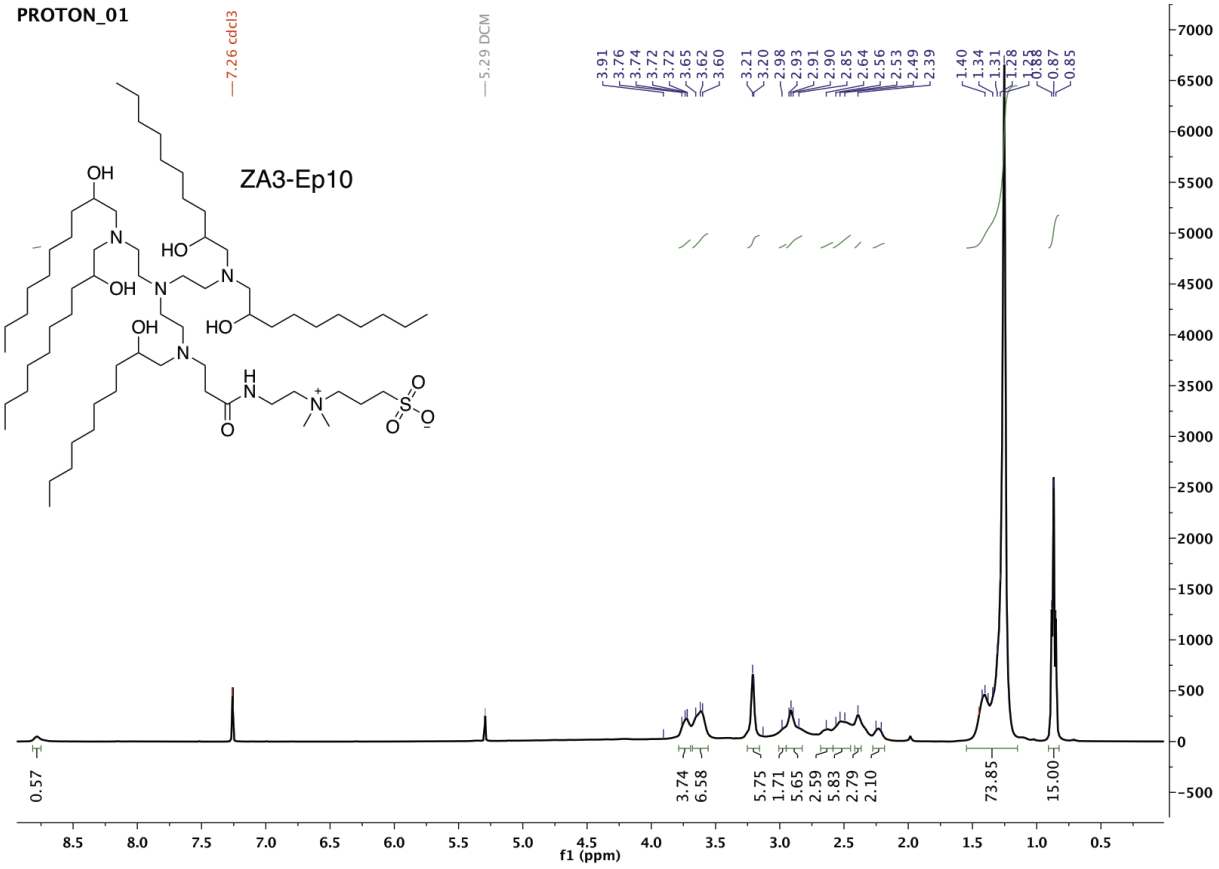

Figure A12. ^{1}H NMR of ZA3-Ep10 CD_3OD.

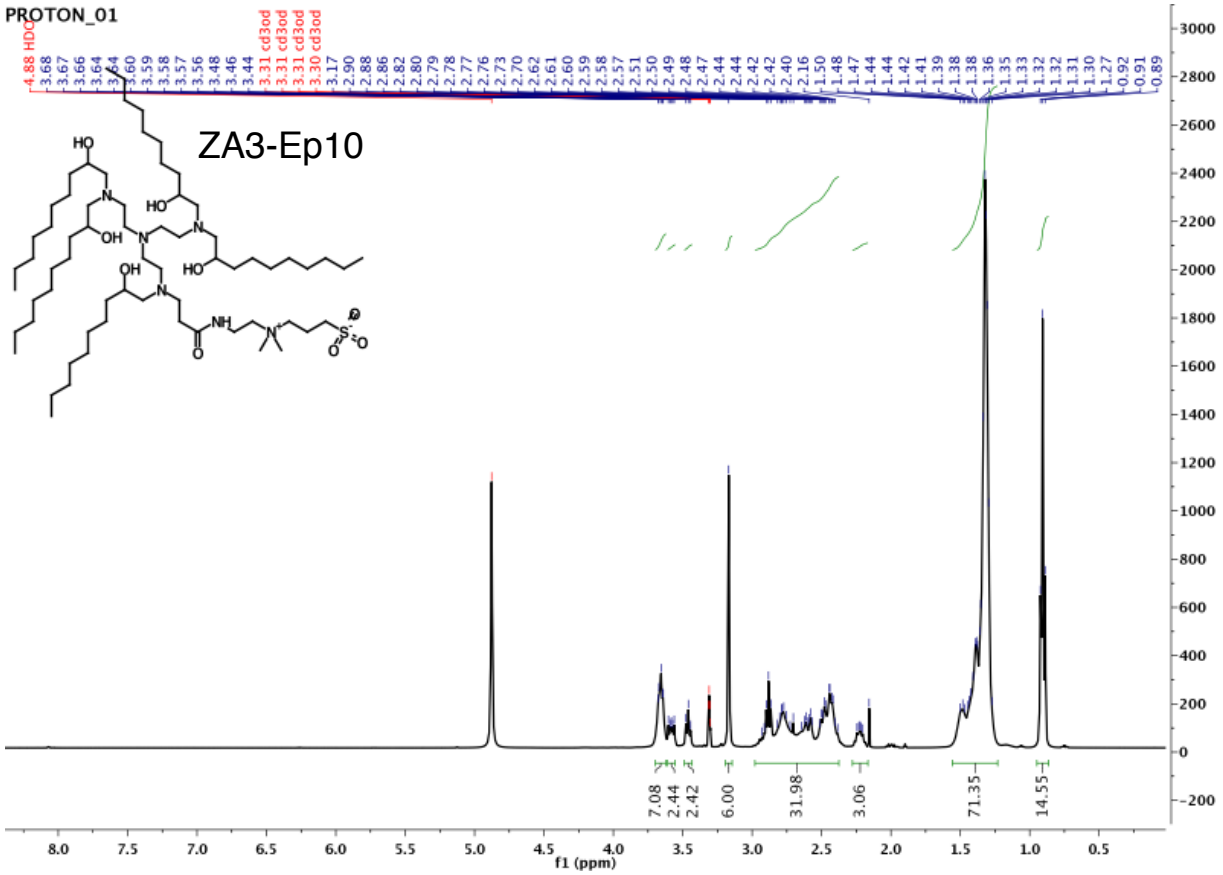

Figure A13. ^{1}H NMR of ZA3-Ep10 CD_3OD.

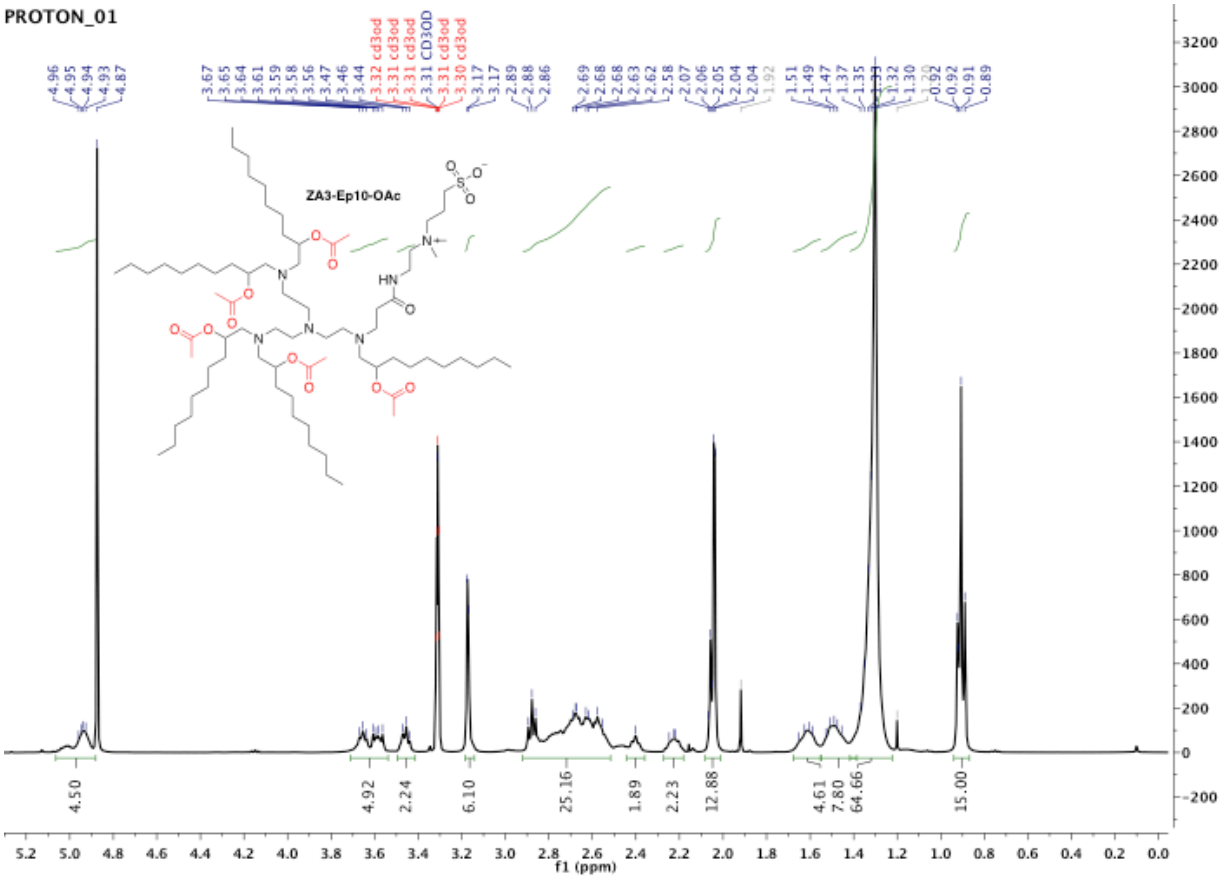

Figure A14. ^{1}H NMR of ZA3-Ep10-OAc.

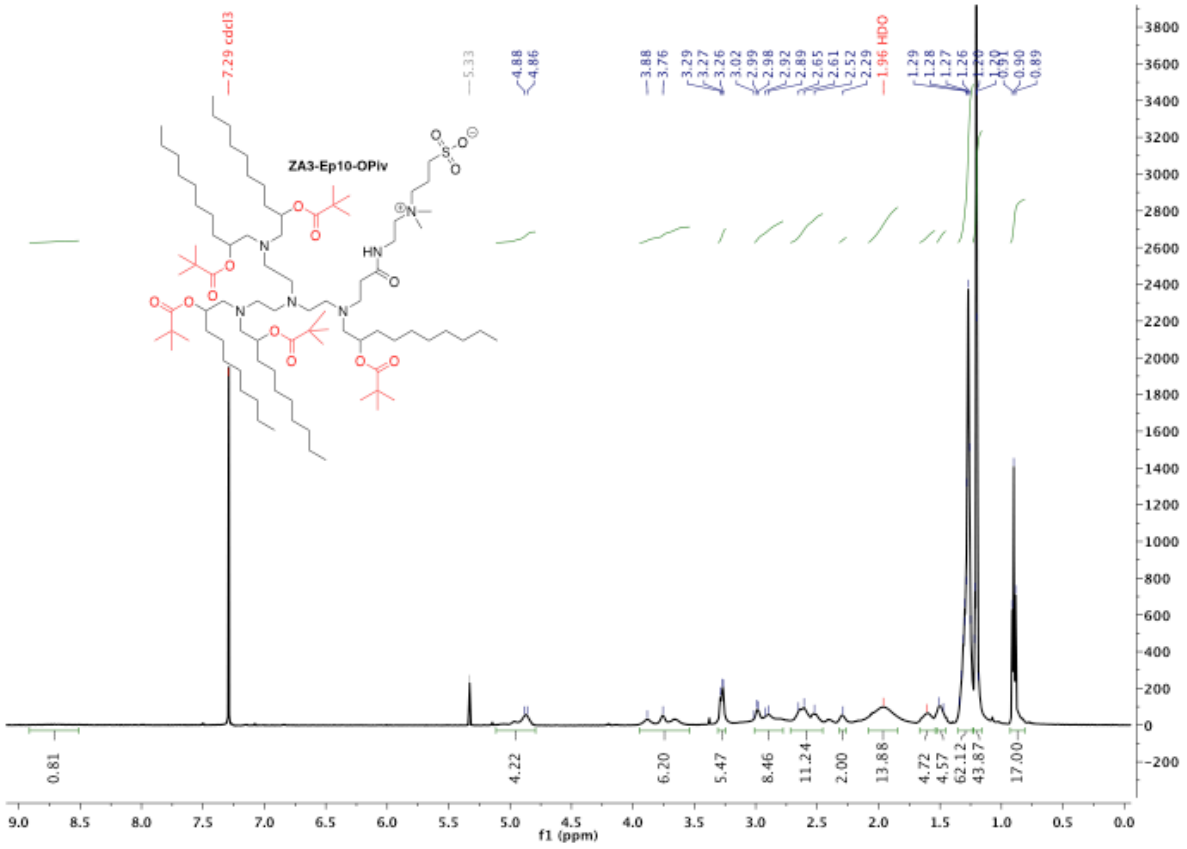

Figure A15. [1]H NMR of ZA3-Ep10-OPiv.

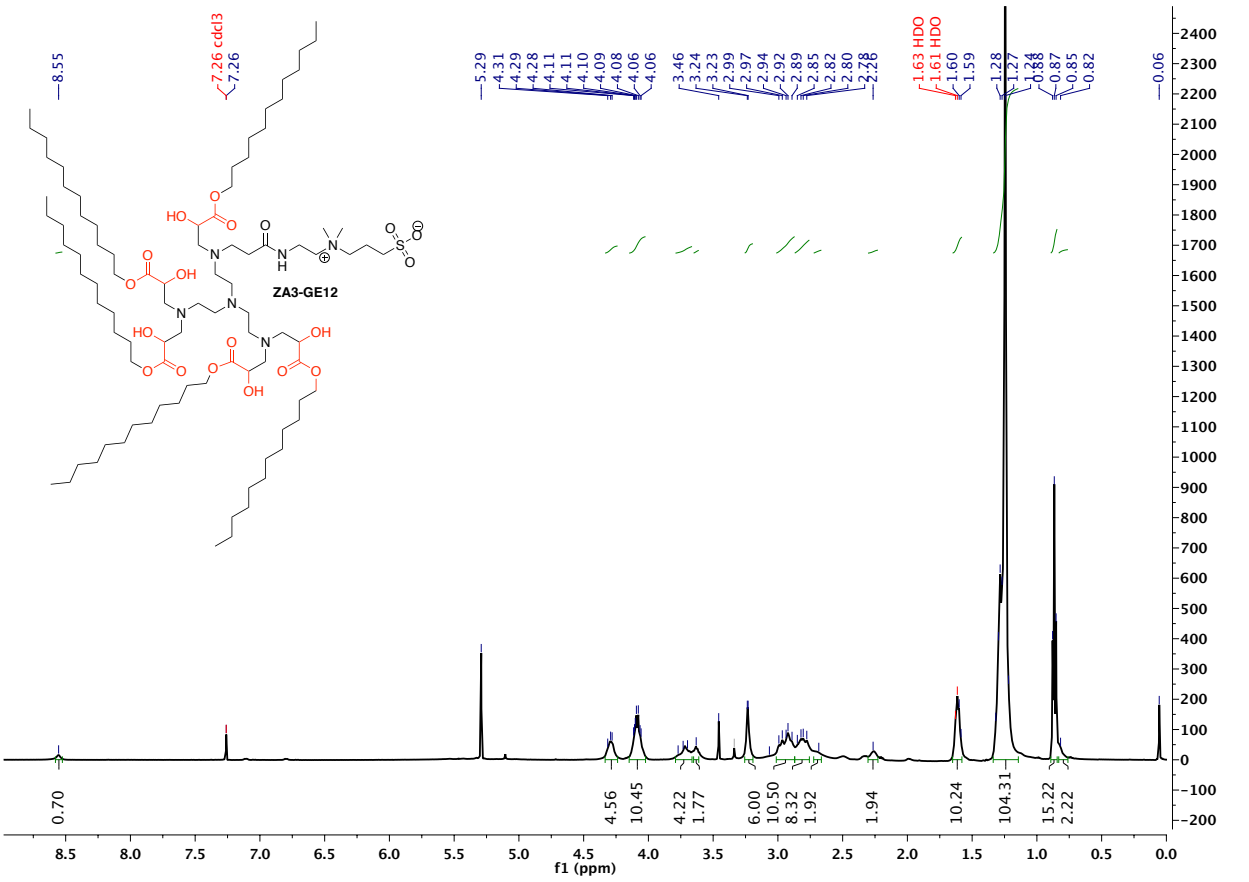

Figure A16. ^{1}H NMR of ZA3-GE12.

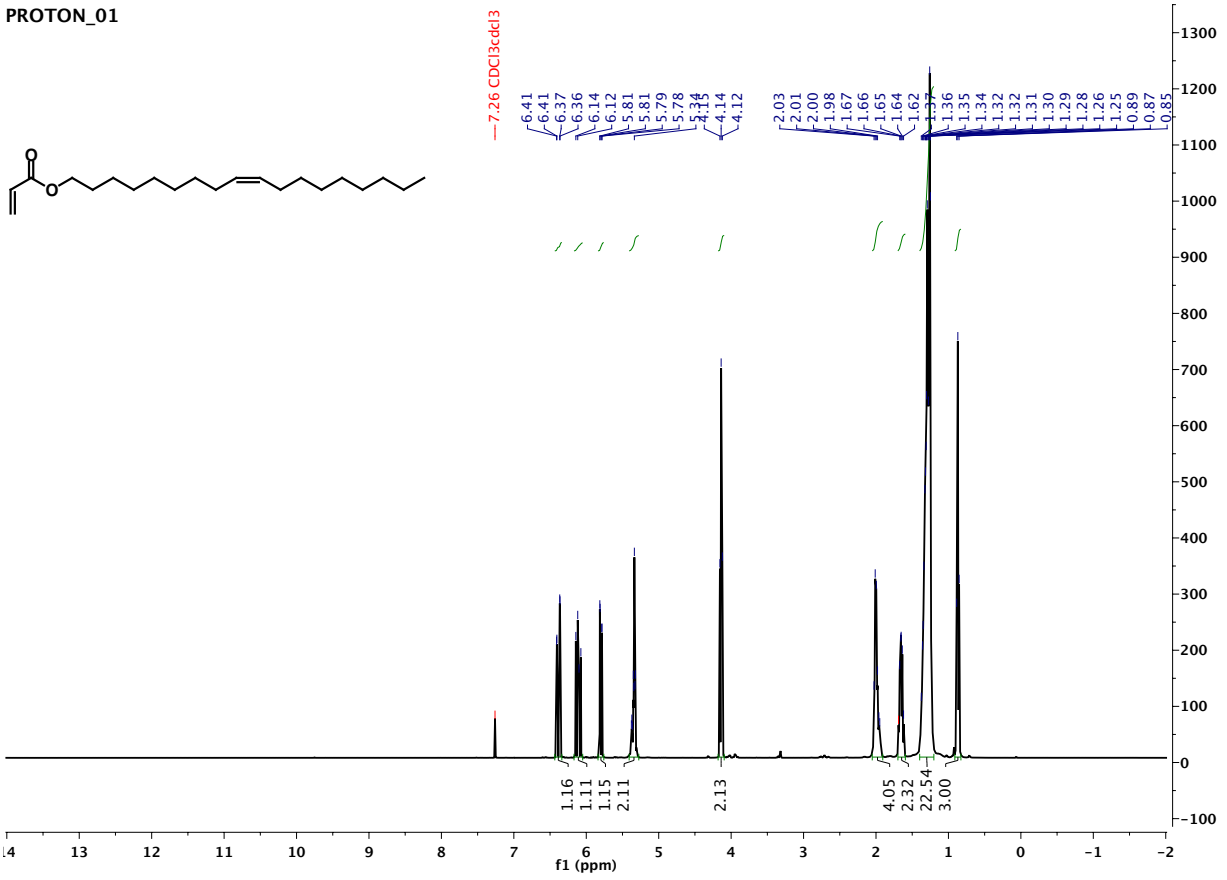

Figure A17. ^{1}H NMR of oleyl acrylate (AcOle).

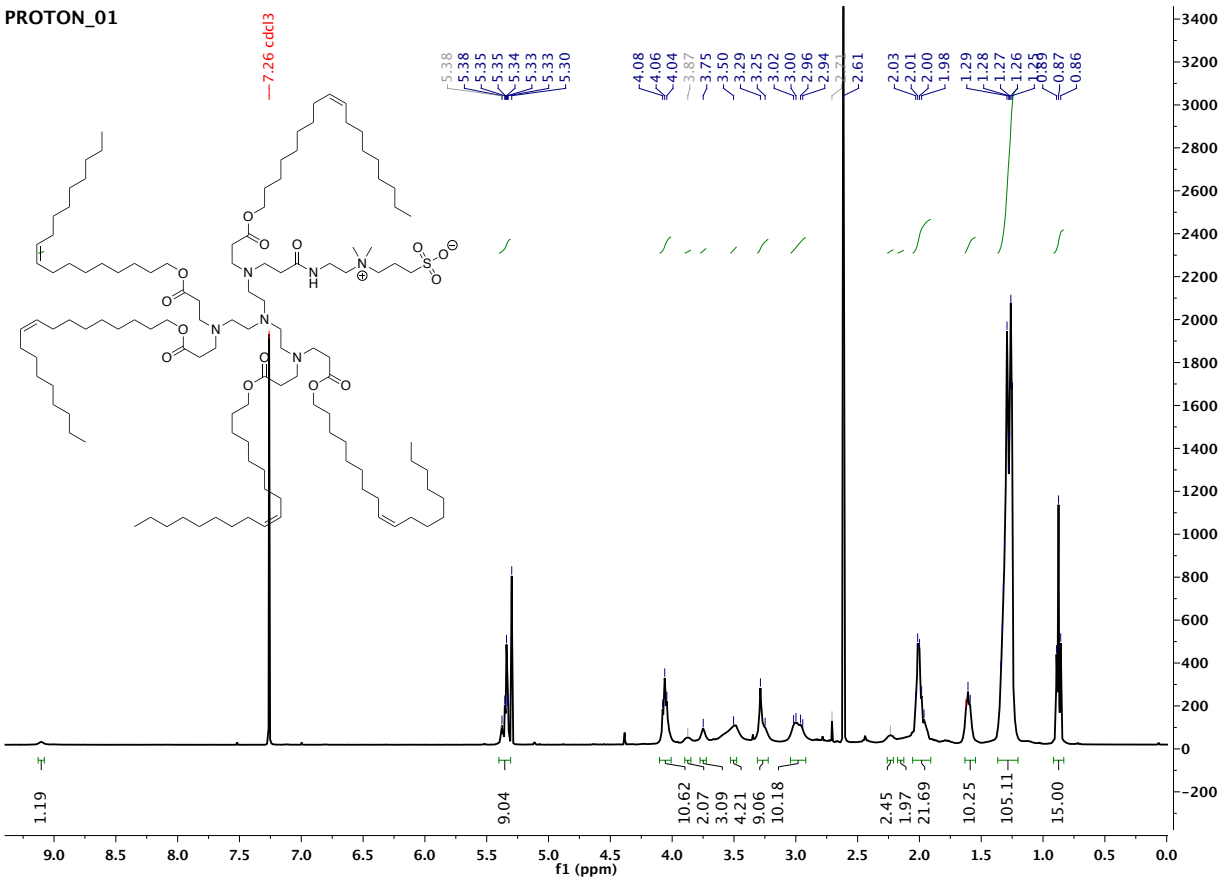

Figure A18. ^{1}H NMR of ZA3-AcOle.

APPENDIX B: CSAL MALDI-TOF, ^{1}H NMR spectra

Table B.1. Compiled mass data for new synthetic compounds reported in this manuscript as observed by MALDI-TOF MS.

Compound	Chemical Formula	Calculated m/z	Observed m/z MALDI-TOF MS
A1-OH lipidoid	$C_{33}H_{70}N_2O_2$	526.5437	527.9280
A2-OH lipidoid	$C_{35}H_{74}N_2O_2$	554.5750	556.13
A3-OH lipidoid	$C_{63}H_{131}N_3O_4$	994.0140	994.3892
A1-OH-PS	$C_{36}H_{76}N_2O_5S$	648.5475	648.2738
A2-OH-PS	$C_{38}H_{80}N_2O_5S$	676.5788	677.6521
A3-OH-PS	$C_{66}H_{137}N_3O_7S$	1116.0177	1117.34
A1-OAc-**PS**	$C_{40}H_{80}N_2O_7S$	732.5686	733.98
A2-OAc-**PS**	$C_{42}H_{84}N_2O_7S$	760.5999	762.62
A3-OAc-**PS**	$C_{74}H_{145}N_3O_{11}S$	1284.0600	1284.74
A1-OPiv-PS	$C_{46}H_{92}N_2O_7S$	816.6625	817.4124
A1-OAc-**C2Me**	$C_{44}H_{91}N_4O_6S^+$	803.6654	803.3930
A1-OAc-**C3Me**	$C_{45}H_{93}N_4O_6S^+$	817.6810	817.5598
A1-OAc-**C4Me**	$C_{46}H_{95}N_4O_6S^+$	831.6967	831.5186
A1-OPiv-C2Me	$C_{50}H_{103}N_4O_6S^+$	887.7593	887.3368
A1-OPiv-C3Me	$C_{51}H_{105}N_4O_6S^+$	901.7749	901.4854
A1-OPiv-C4Me	$C_{52}H_{107}N_4O_6S^+$	915.7906	915.6368
A1-Cl-C2Me	$C_{40}H_{85}Cl_2N_4O_2S^+$	755.5765	755.5153
A1-Cl-C3Me	$C_{41}H_{87}Cl_2N_4O_2S^+$	769.5921	769.5883
A1-Cl-C4Me	$C_{42}H_{89}Cl_2N_4O_2S^+$	783.6078	783.9320
A1-OAc-**C2Et**	$C_{46}H_{95}N_4O_6S^+$	831.6967	831.85
A1-OAc-**C3Et**	$C_{47}H_{97}N_4O_6S^+$	845.7123	846.19
A1-OH-C2Me	$C_{40}H_{87}N_4O_4S^+$	719.6443	719.8963
A2-OAc-**C2Me**	$C_{46}H_{95}N_4O_6S^+$	831.6967	832.62
A2-OAc-**C2Et**	$C_{48}H_{99}N_4O_6S^+$	859.7280	860.66
A3-OAc-**C2Me**	$C_{78}H_{156}N_5O_{10}S^+$	1355.1567	1354.8543

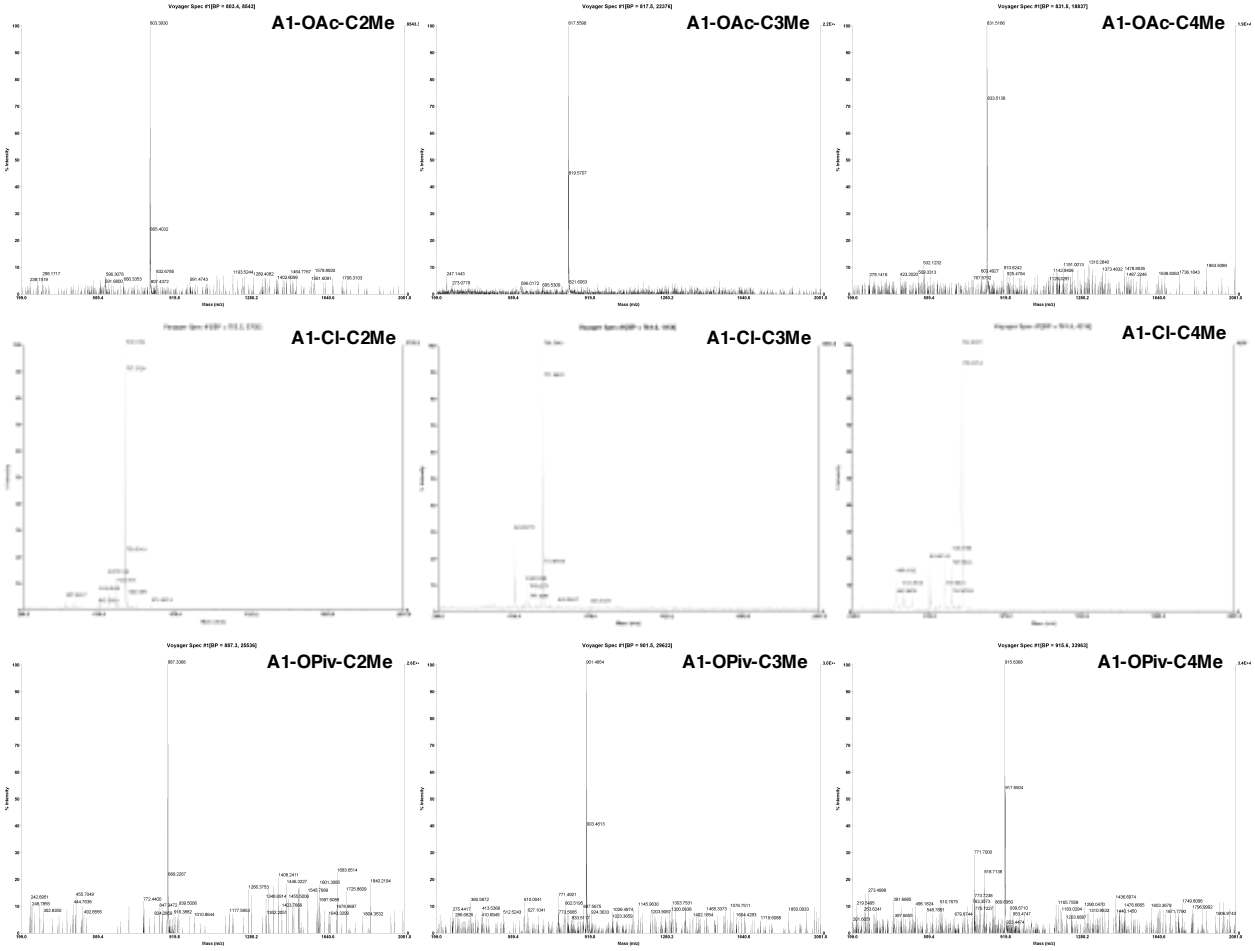

Figure B.1. MALDI-TOF mass spectrometry spectra of linker amine A1-based CSALs.

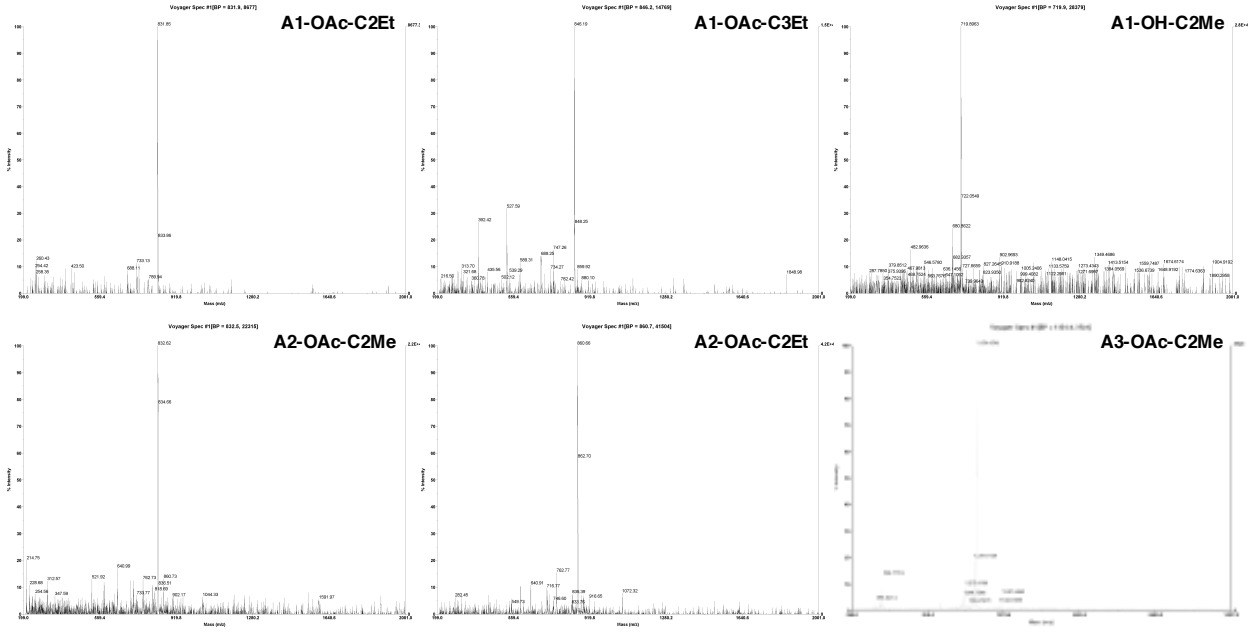

Figure B.2. MALDI-TOF MS spectra of second generation structure optimized CSALs.

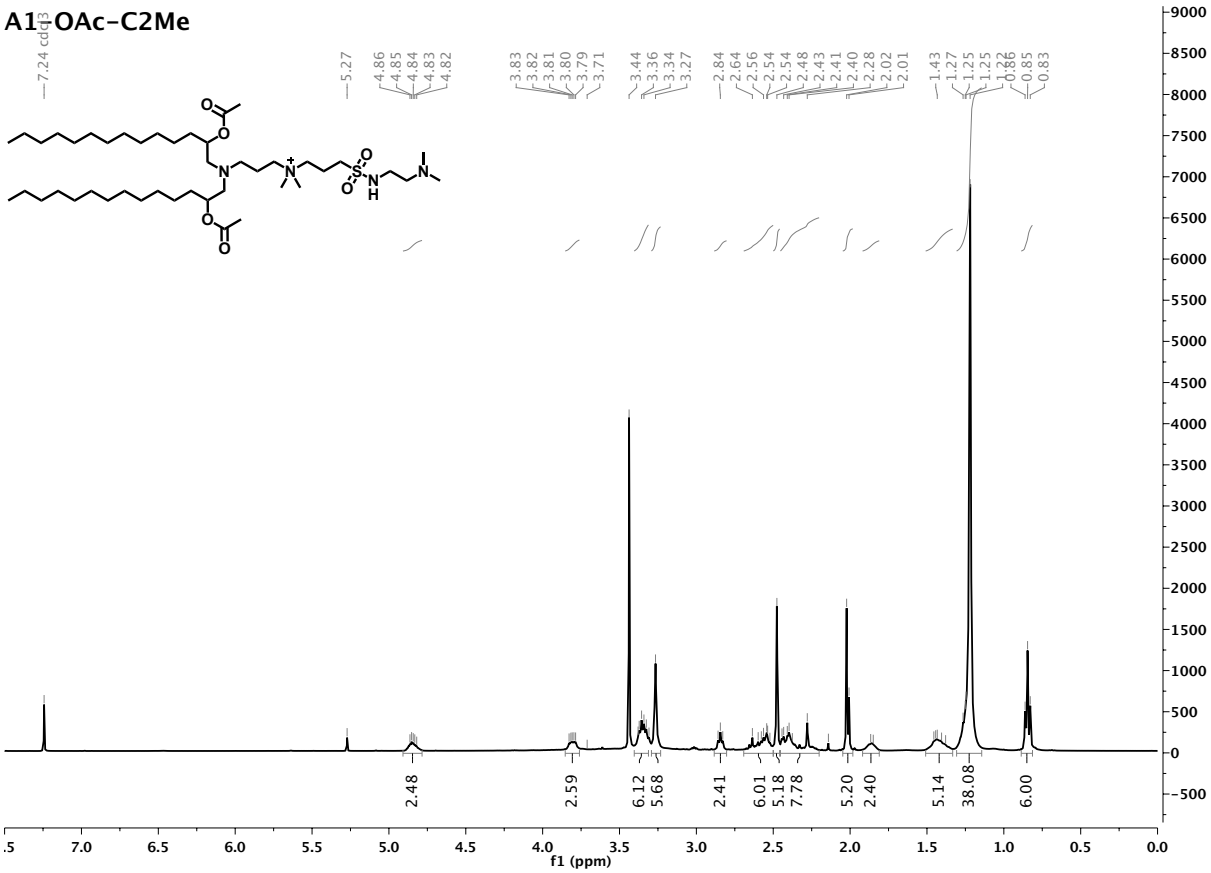

Figure B.3. [1]H NMR spectrum of CSAL A1-OAc-C2Me.

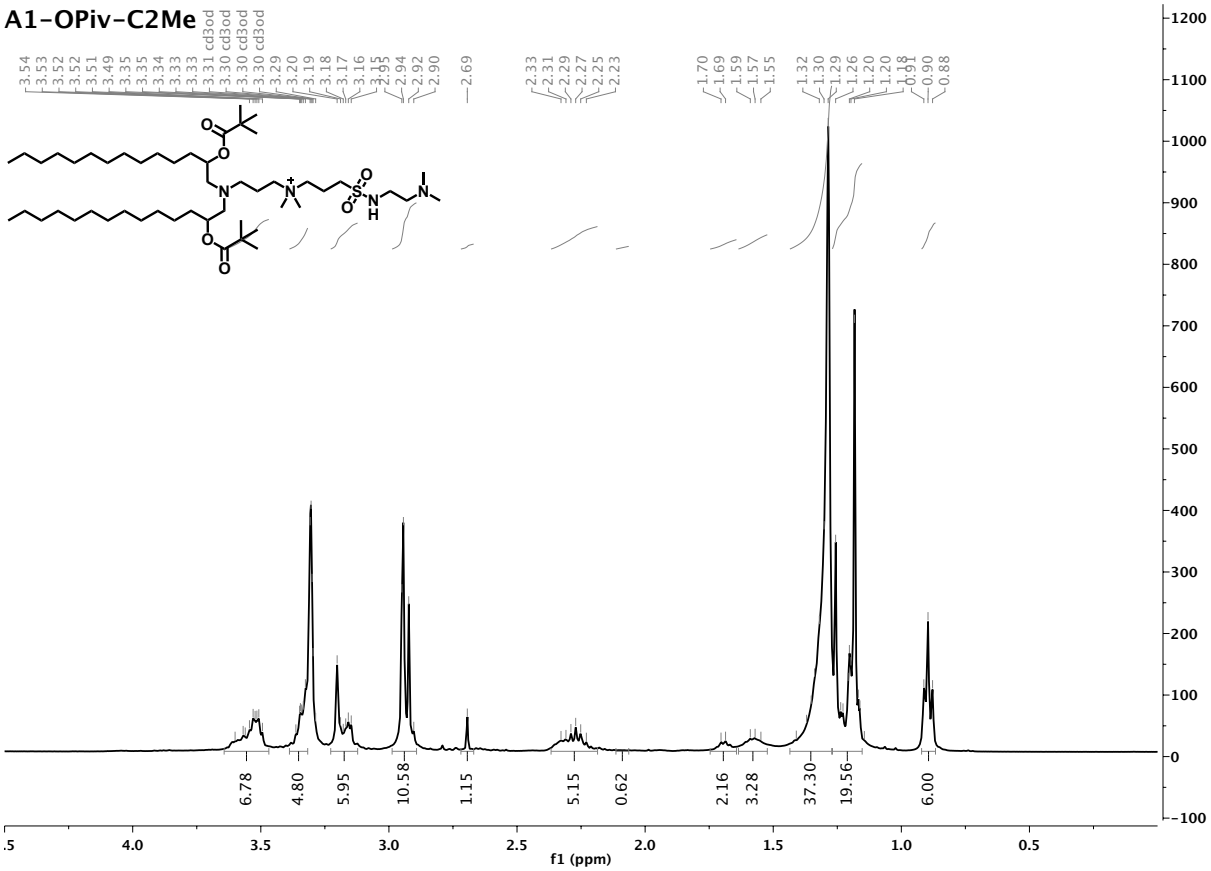

Figure B.4. ^{1}H NMR spectrum of CSAL A1-OPiv-C2Me.

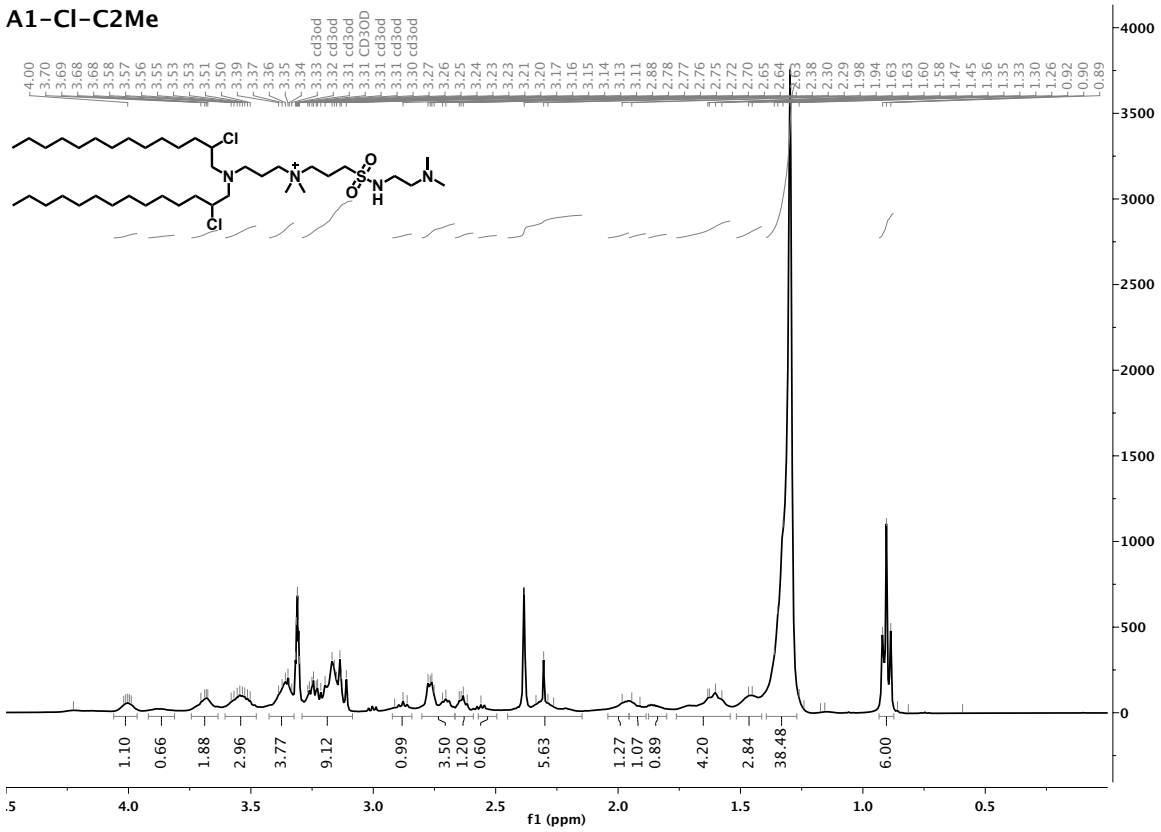

Figure B.5. ^{1}H NMR spectrum of CSAL A1-Cl-C2Me.

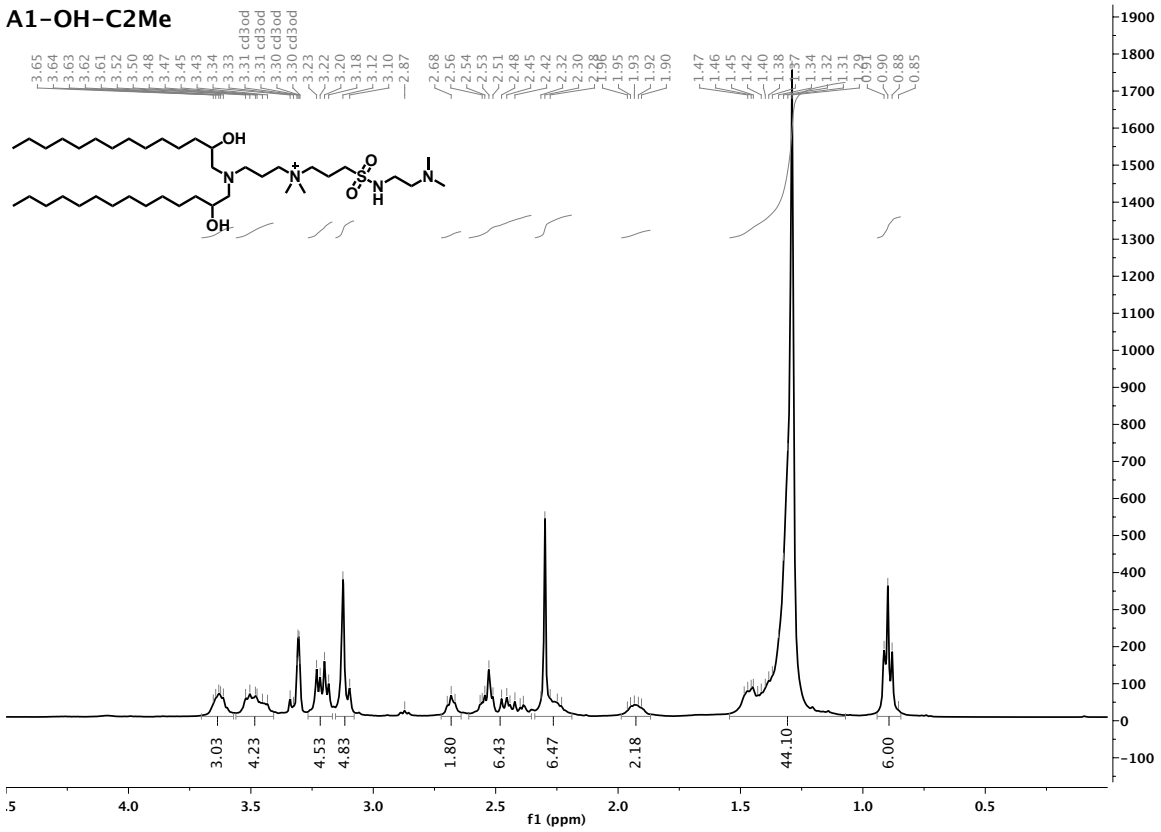

Figure B.6. ^{1}H NMR spectrum of CSAL A1-OH-C2Me.

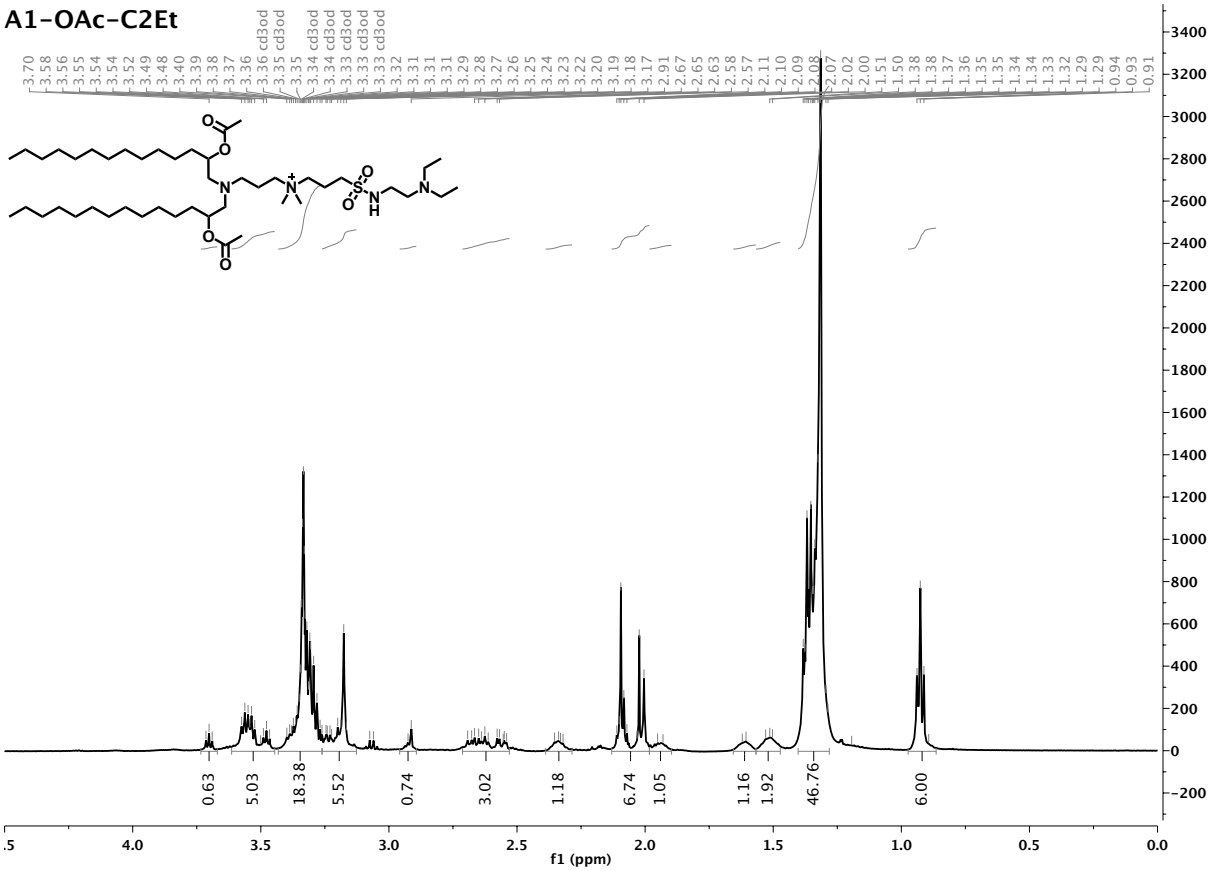

Figure B.7. ^{1}H NMR spectrum of CSAL A1-OAc-C2Et.

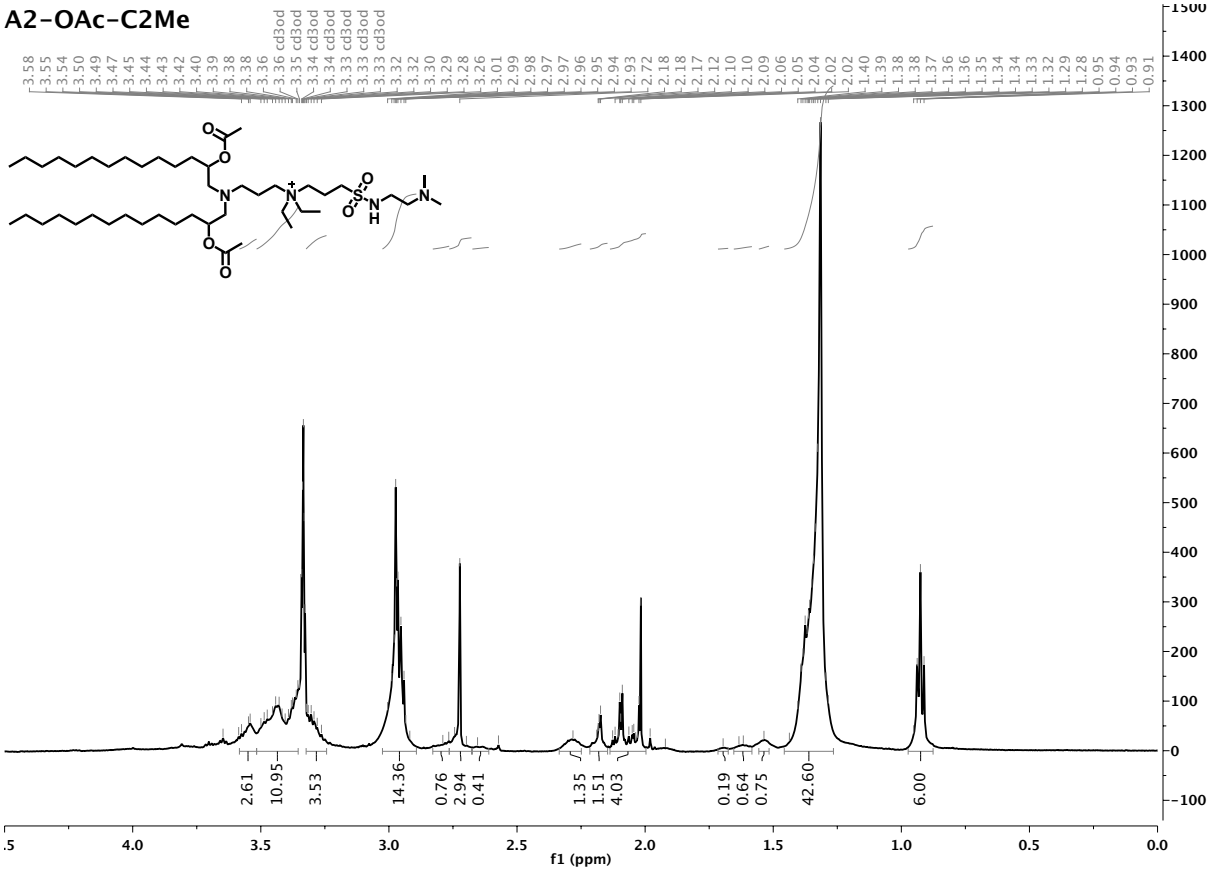

Figure B.8. [1]H NMR spectrum of CSAL A2-OAc-C2Me.

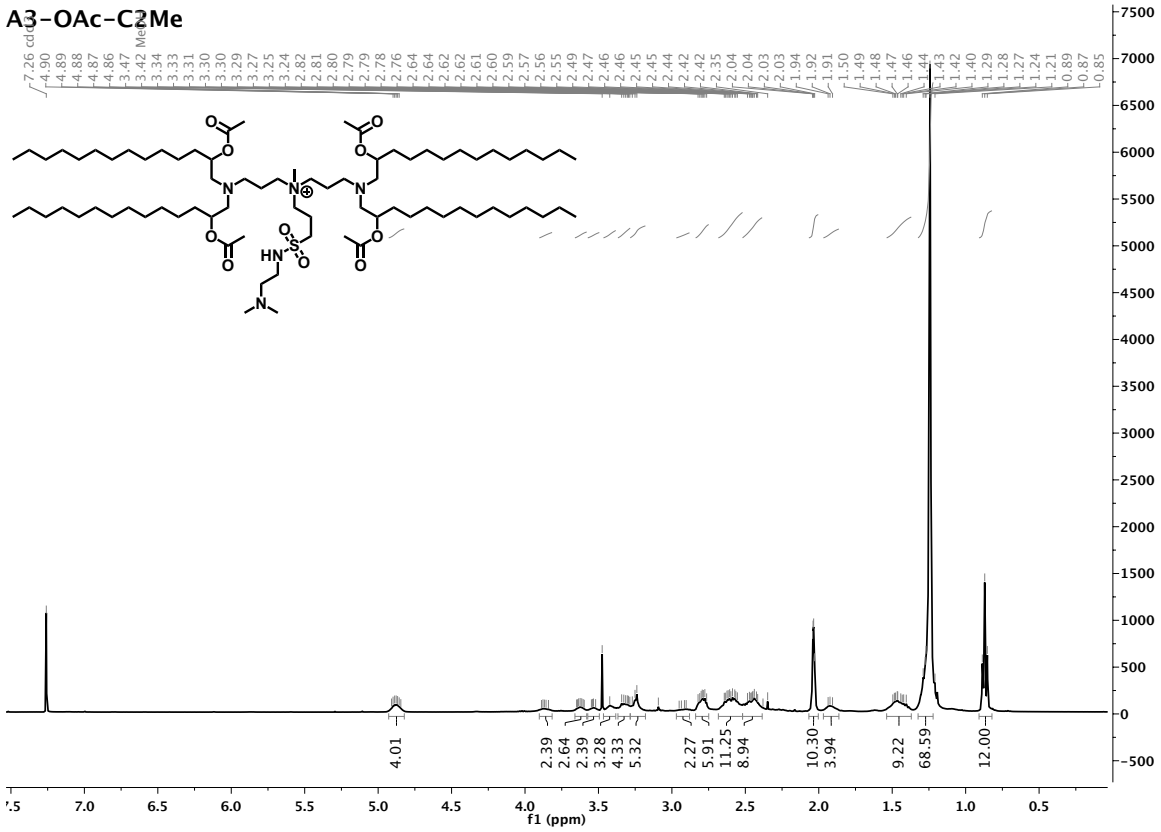

Figure B.9. [1]H NMR spectrum of CSAL A3-OAc-C2Me.

REFERENCES

1. Love, K. T.; Mahon, K. P.; Levins, C. G.; Whitehead, K. A.; Querbes, W.; Dorkin, J. R.; Qin, J.; Cantley, W.; Qin, L. L.; Racie, T.; Frank-Kamenetsky, M.; Yip, K. N.; Alvarez, R.; Sah, D. W. Y.; de Fougerolles, A.; Fitzgerald, K.; Koteliansky, V.; Akinc, A.; Langer, R.; Anderson, D. G., Lipid-like materials for low-dose, in vivo gene silencing. *Proceedings of the National Academy of Sciences* **2010,** *107* (5), 1864-1869.
2. Chen, D.; Love, K. T.; Chen, Y.; Eltoukhy, A. A.; Kastrup, C.; Sahay, G.; Jeon, A.; Dong, Y.; Whitehead, K. A.; Anderson, D. G., Rapid Discovery of Potent siRNA-Containing Lipid Nanoparticles Enabled by Controlled Microfluidic Formulation. *Journal of the American Chemical Society* **2012,** *134* (16), 6948-6951.
3. Benenato, K. E., Kumarasinghe, E.S., Cornebise, M. Compounds and compositions for intracellular delivery of therapeutic agents. 2017.
4. Yin, H.; Kanasty, R. L.; Eltoukhy, A. A.; Vegas, A. J.; Dorkin, J. R.; Anderson, D. G., Non-viral vectors for gene-based therapy. **2014,** *15*, 541.
5. Miller, J. B.; Kos, P.; Tieu, V.; Zhou, K.; Siegwart, D. J., Development of Cationic Quaternary Ammonium Sulfonamide Amino Lipids for Nucleic Acid Delivery. *ACS Applied Materials & Interfaces* **2018,** *10* (3), 2302-2311.
6. Zhou, K.; Nguyen, L. H.; Miller, J. B.; Yan, Y.; Kos, P.; Xiong, H.; Li, L.; Hao, J.; Minnig, J. T.; Zhu, H.; Siegwart, D. J., Modular degradable dendrimers enable small RNAs to extend survival in an aggressive liver cancer model. *P Natl Acad Sci USA* **2016,** *113* (3), 520-525.
7. Daige, C. L.; Wiggins, J. F.; Priddy, L.; Nelligan-Davis, T.; Zhao, J.; Brown, D., Systemic Delivery of a miR34a Mimic as a Potential Therapeutic for Liver Cancer. *Molecular Cancer Therapeutics* **2014,** *13* (10), 2352.
8. Cutting, G. R., Cystic fibrosis genetics: from molecular understanding to clinical application. *Nature reviews. Genetics* **2015,** *16* (1), 45-56.
9. Tabebordbar, M.; Zhu, K. X.; Cheng, J. K. W.; Chew, W. L.; Widrick, J. J.; Yan, W. X.; Maesner, C.; Wu, E. Y.; Xiao, R.; Ran, F. A.; Cong, L.; Zhang, F.; Vandenberghe, L. H.; Church, G. M.; Wagers, A. J., In vivo gene editing in dystrophic mouse muscle and muscle stem cells. *Science* **2016,** *351* (6271), 407-411.
10. Nelson, C. E.; Hakim, C. H.; Ousterout, D. G.; Thakore, P. I.; Moreb, E. A.; Rivera, R. M. C.; Madhavan, S.; Pan, X. F.; Ran, F. A.; Yan, W. X.; Asokan, A.; Zhang, F.; Duan, D. S.; Gersbach, C. A., In vivo genome editing improves muscle function in a mouse model of Duchenne muscular dystrophy. *Science* **2016,** *351* (6271), 403-407.
11. Long, C. Z.; Amoasii, L.; Mireault, A. A.; McAnally, J. R.; Li, H.; Sanchez-Ortiz, E.; Bhattacharyya, S.; Shelton, J. M.; Bassel-Duby, R.; Olson, E. N., Postnatal genome editing partially restores dystrophin expression in a mouse model of muscular dystrophy. *Science* **2016,** *351* (6271), 400-403.
12. Sanchez-Rivera, F. J.; Papagiannakopoulos, T.; Romero, R.; Tammela, T.; Bauer, M. R.; Bhutkar, A.; Joshi, N. S.; Subbaraj, L.; Bronson, R. T.; Xue, W.; Jacks, T., Rapid modelling of cooperating genetic events in cancer through somatic genome editing. *Nature* **2014,** *516* (7531), 428-431.

13. Akinc, A.; Zumbuehl, A.; Goldberg, M.; Leshchiner, E. S.; Busini, V.; Hossain, N.; Bacallado, S. A.; Nguyen, D. N.; Fuller, J.; Alvarez, R.; Borodovsky, A.; Borland, T.; Constien, R.; de Fougerolles, A.; Dorkin, J. R.; Jayaprakash, K. N.; Jayaraman, M.; John, M.; Koteliansky, V.; Manoharan, M.; Nechev, L.; Qin, J.; Racie, T.; Raitcheva, D.; Rajeev, K. G.; Sah, D. W. Y.; Soutschek, J.; Toudjarska, I.; Vornlocher, H. P.; Zimmermann, T. S.; Langer, R.; Anderson, D. G., A combinatorial library of lipid-like materials for delivery of RNAi therapeutics. *Nat Biotechnol* **2008,** *26* (5), 561-569.
14. Kanasty, R.; Dorkin, J. R.; Vegas, A.; Anderson, D., Delivery materials for siRNA therapeutics. *Nat Mater* **2013,** *12* (11), 967-977.
15. Whitehead, K.; Langer, R.; Anderson, D., Knocking down barriers: Advances in siRNA delivery. *Nature Reviews Drug Discovery* **2009,** *8* (2), 129-138.
16. Fire, A.; Xu, S.; Montgomery, M. K.; Kostas, S. A.; Driver, S. E.; Mello, C. C., Potent and specific genetic interference by double-stranded RNA in Caenorhabditis elegans. *Nature* **1998,** *391*.
17. Elbashir, S. M.; Harborth, J.; Lendeckel, W.; Yalcin, A.; Weber, K.; Tuschl, T., Duplexes of 21-nucleotide RNAs mediate RNA interference in cultured mammalian cells. *Nature* **2001,** *411*, 494.
18. Haussecker, D., The Business of RNAi Therapeutics. *Human Gene Therapy* **2008,** *19* (5), 451-462.
19. Haussecker, D., The Business of RNAi Therapeutics in 2012. *Molecular Therapy - Nucleic Acids* **2012,** *2* (e8).
20. Kim, H.; Kim, J.-S., A guide to genome engineering with programmable nucleases. **2014,** *15*, 321.
21. Hajj, K. A.; Whitehead, K. A., Tools for translation: non-viral materials for therapeutic mRNA delivery. *Nature Reviews Materials* **2017,** *2*, 17056.
22. Song, M., The CRISPR/Cas9 system: Their delivery, in vivo and *ex vivo* applications and clinical development by startups. *Biotechnology Progress* **2017,** *33* (4), 1035-1045.
23. Yan, Y.; Zhou, K.; Xiong, H.; Miller, J. B.; Motea, E. A.; Boothman, D. A.; Liu, L.; Siegwart, D. J., Aerosol delivery of stabilized polyester-siRNA nanoparticles to silence gene expression in orthotopic lung tumors. *Biomaterials* **2017,** *118*, 84-93.
24. Fehring, V.; Schaeper, U.; Ahrens, K.; Santel, A.; Keil, O.; Eisermann, M.; Giese, K.; Kaufmann, J., Delivery of Therapeutic siRNA to the Lung Endothelium via Novel Lipoplex Formulation DACC. *Molecular Therapy* **2014,** *22* (4), 811-820.
25. Ishiwata, H.; Suzuki, N.; Ando, S.; Kikuchi, H.; Kitagawa, T., Characteristics and biodistribution of cationic liposomes and their DNA complexes. *J Control Release* **2000,** *69* (1), 139-148.
26. Semple, S. C.; Akinc, A.; Chen, J. X.; Sandhu, A. P.; Mui, B. L.; Cho, C. K.; Sah, D. W. Y.; Stebbing, D.; Crosley, E. J.; Yaworski, E.; Hafez, I. M.; Dorkin, J. R.; Qin, J.; Lam, K.; Rajeev, K. G.; Wong, K. F.; Jeffs, L. B.; Nechev, L.; Eisenhardt, M. L.; Jayaraman, M.; Kazem, M.; Maier, M. A.; Srinivasulu, M.; Weinstein, M. J.; Chen, Q. M.; Alvarez, R.; Barros, S. A.; De, S.; Klimuk, S. K.; Borland, T.; Kosovrasti, V.; Cantley, W. L.; Tam, Y. K.; Manoharan, M.; Ciufolini, M. A.; Tracy, M. A.; de Fougerolles, A.; MacLachlan, I.; Cullis, P. R.; Madden, T. D.; Hope, M. J., Rational design of cationic lipids for siRNA delivery. *Nat Biotechnol* **2010,** *28* (2), 172-176.

27. Dong, Y.; Love, K. T.; Dorkin, J. R.; Sirirungruang, S.; Zhang, Y.; Chen, D.; Bogorad, R. L.; Yin, H.; Chen, Y.; Vegas, A. J.; Alabi, C. A.; Sahay, G.; Olejnik, K. T.; Wang, W.; Schroeder, A.; Lytton-Jean, A. K. R.; Siegwart, D. J.; Akinc, A.; Barnes, C.; Barros, S. A.; Carioto, M.; Fitzgerald, K.; Hettinger, J.; Kumar, V.; Novobrantseva, T. I.; Qin, J.; Querbes, W.; Koteliansky, V.; Langer, R.; Anderson, D. G., Lipopeptide nanoparticles for potent and selective siRNA delivery in rodents and nonhuman primates. *P Natl Acad Sci USA* **2014,** *111* (11), 3955-3960.
28. Jayaraman, M.; Ansell, S. M.; Mui, B. L.; Tam, Y. K.; Chen, J. X.; Du, X. Y.; Butler, D.; Eltepu, L.; Matsuda, S.; Narayanannair, J. K.; Rajeev, K. G.; Hafez, I. M.; Akinc, A.; Maier, M. A.; Tracy, M. A.; Cullis, P. R.; Madden, T. D.; Manoharan, M.; Hope, M. J., Maximizing the potency of siRNA lipid nanoparticles for hepatic gene silencing in vivo. *Angewandte Chemie International Edition* **2012,** *51* (34), 8529-8533.
29. Maier, M. A.; Jayaraman, M.; Matsuda, S.; Liu, J.; Barros, S.; Querbes, W.; Tam, Y. K.; Ansell, S. M.; Kumar, V.; Qin, J.; Zhang, X.; Wang, Q.; Panesar, S.; Hutabarat, R.; Carioto, M.; Hettinger, J.; Kandasamy, P.; Butler, D.; Rajeev, K. G.; Pang, B.; Charisse, K.; Fitzgerald, K.; Mui, B. L.; Du, X.; Cullis, P.; Madden, T. D.; Hope, M. J.; Manoharan, M.; Akinc, A., Biodegradable Lipids Enabling Rapidly Eliminated Lipid Nanoparticles for Systemic Delivery of RNAi Therapeutics. *Molecular Therapy* **2013,** *21* (8), 1570-1578.
30. Wittrup, A.; Ai, A.; Liu, X.; Hamar, P.; Trifonova, R.; Charisse, K.; Manoharan, M.; Kirchhausen, T.; Lieberman, J., Visualizing lipid-formulated siRNA release from endosomes and target gene knockdown. *Nat Biotechnol* **2015,** *33* (8), 870-976.
31. Sahay, G.; Querbes, W.; Alabi, C.; Eltoukhy, A.; Sarkar, S.; Zurenko, C.; Karagiannis, E.; Love, K.; Chen, D.; Zoncu, R.; Buganim, Y.; Schroeder, A.; Langer, R.; Anderson, D. G., Efficiency of siRNA delivery by lipid nanoparticles is limited by endocytic recycling. *Nat Biotechnol* **2013,** *31* (7), 653-8.
32. Gilleron, J.; Querbes, W.; Zeigerer, A.; Borodovsky, A.; Marsico, G.; Schubert, U.; Manygoats, K.; Seifert, S.; Andree, C.; Stoter, M.; Epstein-Barash, H.; Zhang, L.; Koteliansky, V.; Fitzgerald, K.; Fava, E.; Bickle, M.; Kalaidzidis, Y.; Akinc, A.; Maier, M.; Zerial, M., Image-based analysis of lipid nanoparticle-mediated siRNA delivery, intracellular trafficking and endosomal escape. *Nat Biotechnol* **2013,** *31* (7), 638-646.
33. Sahay, G.; Alakhova, D. Y.; Kabanov, A. V., Endocytosis of nanomedicines. *J Control Release* **2010,** *145* (3), 182-195.
34. Rehman, Z. u.; Zuhorn, I. S.; Hoekstra, D., How cationic lipids transfer nucleic acids into cells and across cellular membranes: Recent advances. *J Control Release* **2013,** *166* (1), 46-56.
35. Maurer, N.; Wong, K. F.; Stark, H.; Louie, L.; McIntosh, D.; Wong, T.; Scherrer, P.; Semple, S. C.; Cullis, P. R., Spontaneous Entrapment of Polynucleotides upon Electrostatic Interaction with Ethanol-Destabilized Cationic Liposomes. *Biophysical Journal* **2001,** *80* (5), 2310-2326.
36. Jeffs, L. B.; Palmer, L. R.; Ambegia, E. G.; Giesbrecht, C.; Ewanick, S.; MacLachlan, I., A Scalable, Extrusion-Free Method for Efficient Liposomal Encapsulation of Plasmid DNA. *Pharmaceutical Research* **2005,** *22* (3), 362-372.
37. Belliveau, N. M.; Huft, J.; Lin, P. J. C.; Chen, S.; Leung, A. K. K.; Leaver, T. J.; Wild, A. W.; Lee, J. B.; Taylor, R. J.; Tam, Y. K.; Hansen, C. L.; Cullis, P. R., Microfluidic Synthesis of

Highly Potent Limit-size Lipid Nanoparticles for In Vivo Delivery of siRNA. *Molecular Therapy. Nucleic Acids* **2012,** *1* (8), e37.
38. Leung, A. K. K.; Hafez, I. M.; Baoukina, S.; Belliveau, N. M.; Zhigaltsev, I. V.; Afshinmanesh, E.; Tieleman, D. P.; Hansen, C. L.; Hope, M. J.; Cullis, P. R., Lipid nanoparticles containing siRNA synthesized by microfluidic mixing exhibit an electron-dense nanostructured core. *J Phys Chem C* **2012,** *116* (41), 22104-22104.
39. Leung, A. K. K.; Tam, Y. Y. C.; Chen, S.; Hafez, I. M.; Cullis, P. R., Microfluidic Mixing: A General Method for Encapsulating Macromolecules in Lipid Nanoparticle Systems. *The Journal of Physical Chemistry B* **2015,** *119* (28), 8698-8706.
40. van Meer, G.; Voelker, D. R.; Feigenson, G. W., Membrane lipids: where they are and how they behave. *Nat Rev Mol Cell Biol* **2008,** *9* (2), 112-124.
41. Alabi, C. A.; Love, K. T.; Sahay, G.; Yin, H.; Luly, K. M.; Langer, R.; Anderson, D. G., Multiparametric approach for the evaluation of lipid nanoparticles for siRNA delivery. *P Natl Acad Sci USA* **2013,** *110* (32), 12881-12886.
42. Whitehead, K. A.; Dorkin, J. R.; Vegas, A. J.; Chang, P. H.; Veiseh, O.; Matthews, J.; Fenton, O. S.; Zhang, Y.; Olejnik, K. T.; Yesilyurt, V.; Chen, D.; Barros, S.; Klebanov, B.; Novobrantseva, T.; Langer, R.; Anderson, D. G., Degradable lipid nanoparticles with predictable in vivo siRNA delivery activity. *Nat Commun* **2014,** *5*.
43. Akinc, A.; Querbes, W.; De, S.; Qin, J.; Frank-Kamenetsky, M.; Jayaprakash, K. N.; Jayaraman, M.; Rajeev, K. G.; Cantley, W. L.; Dorkin, J. R.; Butler, J. S.; Qin, L.; Racie, T.; Sprague, A.; Fava, E.; Zeigerer, A.; Hope, M. J.; Zerial, M.; Sah, D. W. Y.; Fitzgerald, K.; Tracy, M. A.; Manoharan, M.; Koteliansky, V.; Fougerolles, A. d.; Maier, M. A., Targeted Delivery of RNAi Therapeutics With Endogenous and Exogenous Ligand-Based Mechanisms. *Molecular Therapy* **2010,** *18* (7), 1357-1364.
44. Adams, D.; Suhr, O. B.; Dyck, P. J.; Litchy, W. J.; Leahy, R. G.; Chen, J.; Gollob, J.; Coelho, T., Trial design and rationale for APOLLO, a Phase 3, placebo-controlled study of patisiran in patients with hereditary ATTR amyloidosis with polyneuropathy. *BMC Neurology* **2017,** *17*, 181.
45. Heyes, J.; Palmer, L.; Bremner, K.; MacLachlan, I., Cationic lipid saturation influences intracellular delivery of encapsulated nucleic acids. *J Control Release* **2005,** *107* (2), 276-287.
46. Santel, A.; Aleku, M.; Keil, O.; Endruschat, J.; Esche, V.; Fisch, G.; Dames, S.; Löffler, K.; Fechtner, M.; Arnold, W.; Giese, K.; Klippel, A.; Kaufmann, J., A novel siRNA-lipoplex technology for RNA interference in the mouse vascular endothelium. *Gene Therapy* **2006,** *13*, 1222.
47. Adami, R. C.; Seth, S.; Harvie, P.; Johns, R.; Fam, R.; Fosnaugh, K.; Zhu, T.; Farber, K.; McCutcheon, M.; Goodman, T. T.; Liu, Y.; Chen, Y.; Kwang, E.; Templin, M. V.; Severson, G.; Brown, T.; Vaish, N.; Chen, F.; Charmley, P.; Polisky, B.; Houston, M. E., An Amino Acid-based Amphoteric Liposomal Delivery System for Systemic Administration of siRNA. *Molecular Therapy* **2011,** *19* (6), 1141-1151.
48. Bader, A. G., miR-34 – a microRNA replacement therapy is headed to the clinic. *Frontiers in Genetics* **2012,** *3*, 120.
49. Sato, Y.; Murase, K.; Kato, J.; Kobune, M.; Sato, T.; Kawano, Y.; Takimoto, R.; Takada, K.; Miyanishi, K.; Matsunaga, T.; Takayama, T.; Niitsu, Y., Resolution of liver cirrhosis using

vitamin A–coupled liposomes to deliver siRNA against a collagen-specific chaperone. *Nat Biotechnol* **2008,** *26*, 431.
50. Liu, F.; Huang, L., Development of non-viral vectors for systemic gene delivery. *J Control Release* **2002,** *78* (1-3), 259-266.
51. Zhi, D.; Zhang, S.; Wang, B.; Zhao, Y.; Yang, B.; Yu, S., Transfection efficiency of cationic lipids with different hydrophobic domains in gene delivery. *Bioconjugate Chem* **2010,** *21* (4), 563-577.
52. Zhi, D. F.; Zhang, S. B.; Cui, S. H.; Zhao, Y. A.; Wang, Y. H.; Zhao, D. F., The Head group Evolution of Cationic Lipids for Gene Delivery. *Bioconjugate Chemistry* **2013,** *24* (4), 487-519.
53. Kohli, A. G.; Kierstead, P. H.; Venditto, V. J.; Walsh, C. L.; Szoka, F. C., Designer lipids for drug delivery: From heads to tails. *J Control Release* **2014,** *190*, 274-287.
54. Bohdanowicz, M.; Grinstein, S., Role of Phospholipids in Endocytosis, Phagocytosis, and Macropinocytosis. *Physiological Reviews* **2013,** *93* (1), 69.
55. Shao, Q.; Jiang, S. Y., Molecular Understanding and Design of Zwitterionic Materials. *Advanced Materials* **2015,** *27* (1), 15-26.
56. Kim, S. T.; Saha, K.; Kim, C.; Rotello, V. M., The Role of Surface Functionality in Determining Nanoparticle Cytotoxicity. *Accounts of Chemical Research* **2013,** *46* (3), 681-691.
57. Kim, G.; Park, S.; Jung, J.; Heo, K.; Yoon, J.; Kim, H.; Kim, I. J.; Kim, J. R.; Lee, J. I.; Ree, M., Novel Brush Polymers with Phosphorylcholine Bristle Ends: Synthesis, Structure, Properties, and Biocompatibility. *Advanced Functional Materials* **2009,** *19* (10), 1631-1644.
58. Venditto, V. J.; Dolor, A.; Kohli, A.; Salentinig, S.; Boyd, B. J.; Szoka, F. C., Sulfated quaternary amine lipids: a new class of inverse charge zwitterlipids. *Chem Commun* **2014,** *50* (65), 9109-9111.
59. Walsh, C. L.; Nguyen, J.; Szoka, F. C., Synthesis and characterization of novel zwitterionic lipids with pH-responsive biophysical properties. *Chem Commun* **2012,** *48* (45), 5575-5577.
60. Lorenzer, C.; Dirin, M.; Winkler, A. M.; Baumann, V.; Winkler, J., Going beyond the liver: Progress and challenges of targeted delivery of siRNA therapeutics. *Journal of Controlled Release* **2015,** *203*, 1-15.
61. Dahlman, J. E.; Barnes, C.; Khan, O. F.; Thiriot, A.; Jhunjunwala, S.; Shaw, T. E.; Xing, Y. P.; Sager, H. B.; Sahay, G.; Speciner, L.; Bader, A.; Bogorad, R. L.; Yin, H.; Racie, T.; Dong, Y. Z.; Jiang, S.; Seedorf, D.; Dave, A.; Sandhu, K. S.; Webber, M. J.; Novobrantseva, T.; Ruda, V. M.; Lytton-Jean, A. K. R.; Levins, C. G.; Kalish, B.; Mudge, D. K.; Perez, M.; Abezgauz, L.; Dutta, P.; Smith, L.; Charisse, K.; Kieran, M. W.; Fitzgerald, K.; Nahrendorf, M.; Danino, D.; Tuder, R. M.; von Andrian, U. H.; Akinc, A.; Panigrahy, D.; Schroeder, A.; Koteliansky, V.; Langer, R.; Anderson, D. G., In vivo endothelial siRNA delivery using polymeric nanoparticles with low molecular weight. *Nat Nanotechnol* **2014,** *9* (8), 648-655.
62. Choi, H. S.; Ashitate, Y.; Lee, J. H.; Kim, S. H.; Matsui, A.; Insin, N.; Bawendi, M. G.; Semmler-Behnke, M.; Frangioni, J. V.; Tsuda, A., Rapid translocation of nanoparticles from the lung airspaces to the body. *Nat Biotech* **2010,** *28* (12), 1300-1303.
63. Layzer, J. M.; McCaffrey, A. P.; Tanner, A. K.; Huang, Z. A. N.; Kay, M. A.; Sullenger, B. A., In vivo activity of nuclease-resistant siRNAs. *RNA* **2004,** *10* (5), 766-771.

64. Khvorova, A.; Watts, J. K., The chemical evolution of oligonucleotide therapies of clinical utility. *Nat Biotechnol* **2017,** *35* (3), 238-248.
65. Behlke, M. A., Chemical Modification of siRNAs for In Vivo Use. *Oligonucleotides* **2008,** *18* (4), 305-320.
66. Patra, A.; Paolillo, M.; Charisse, K.; Manoharan, M.; Rozners, E.; Egli, M., 2′-Fluoro RNA Shows Increased Watson-Crick H-Bonding Strength and Stacking relative to RNA: Evidence from NMR and Thermodynamic Data. *Angewandte Chemie (International ed. in English)* **2012,** *51* (47), 11863-11866.
67. Kalota, A.; Karabon, L.; Swider, C. R.; Viazovkina, E.; Elzagheid, M.; Damha, M. J.; Gewirtz, A. M., 2′-Deoxy-2′-fluoro-β- d -arabinonucleic acid (2′F-ANA) modified oligonucleotides (ON) effect highly efficient, and persistent, gene silencing. *Nucleic Acids Research* **2006,** *34* (2), 451-461.
68. Braasch, D. A.; Paroo, Z.; Constantinescu, A.; Ren, G.; Öz, O. K.; Mason, R. P.; Corey, D. R., Biodistribution of phosphodiester and phosphorothioate siRNA. *Bioorganic & Medicinal Chemistry Letters* **2004,** *14* (5), 1139-1143.
69. Corey, D. R., Nusinersen, an antisense oligonucleotide drug for spinal muscular atrophy. *Nature Neuroscience* **2017,** *20*, 497.
70. Meade, B. R.; Gogoi, K.; Hamil, A. S.; Palm-Apergi, C.; Berg, A. v. d.; Hagopian, J. C.; Springer, A. D.; Eguchi, A.; Kacsinta, A. D.; Dowdy, C. F.; Presente, A.; Lonn, P.; Kaulich, M.; Yoshioka, N.; Gros, E.; Cui, X.-S.; Dowdy, S. F., Efficient delivery of RNAi prodrugs containing reversible charge-neutralizing phosphotriester backbone modifications. *Nat Biotech* **2014,** *32* (12), 1256-1261.
71. Kole, R.; Krainer, A. R.; Altman, S., RNA therapeutics: beyond RNA interference and antisense oligonucleotides. **2012,** *11*, 125.
72. Ray, A.; Nordén, B., Peptide nucleic acid (PNA): its medical and biotechnical applications and promise for the future. *The FASEB Journal* **2000,** *14* (9), 1041-1060.
73. Almeida, M. I.; Reis, R. M.; Calin, G. A., MicroRNA history: Discovery, recent applications, and next frontiers. *Mutation Research/Fundamental and Molecular Mechanisms of Mutagenesis* **2011,** *717* (1), 1-8.
74. Ling, H.; Fabbri, M.; Calin, G. A., MicroRNAs and other non-coding RNAs as targets for anticancer drug development. *NAT REV DRUG DISCOV* **2013,** *12*, 847.
75. Matsui, M.; Corey, D. R., Non-coding RNAs as drug targets. **2016,** *16*, 167.
76. Youngblood, D. S.; Hatlevig, S. A.; Hassinger, J. N.; Iversen, P. L.; Moulton, H. M., Stability of Cell-Penetrating Peptide−Morpholino Oligomer Conjugates in Human Serum and in Cells. *Bioconjugate Chemistry* **2007,** *18* (1), 50-60.
77. Echigoya, Y.; Nakamura, A.; Nagata, T.; Urasawa, N.; Lim, K. R. Q.; Trieu, N.; Panesar, D.; Kuraoka, M.; Moulton, H. M.; Saito, T.; Aoki, Y.; Iversen, P.; Sazani, P.; Kole, R.; Maruyama, R.; Partridge, T.; Takeda, S. i.; Yokota, T., Effects of systemic multiexon skipping with peptide-conjugated morpholinos in the heart of a dog model of Duchenne muscular dystrophy. *Proceedings of the National Academy of Sciences* **2017,** *114* (16), 4213.
78. Lim, K. R. Q.; Maruyama, R.; Yokota, T., Eteplirsen in the treatment of Duchenne muscular dystrophy. *Drug Design, Development and Therapy* **2017,** *11*, 533-545.

79. Lu-Nguyen, N.; Malerba, A.; Popplewell, L.; Schnell, F.; Hanson, G.; Dickson, G., Systemic Antisense Therapeutics for Dystrophin and Myostatin Exon Splice Modulation Improve Muscle Pathology of Adult mdx Mice. *Molecular Therapy - Nucleic Acids* **2016,** *6*, 15-28.
80. Vaish, N.; Chen, F.; Seth, S.; Fosnaugh, K.; Liu, Y.; Adami, R.; Brown, T.; Chen, Y.; Harvie, P.; Johns, R.; Severson, G.; Granger, B.; Charmley, P.; Houston, M.; Templin, M. V.; Polisky, B., Improved specificity of gene silencing by siRNAs containing unlocked nucleobase analogs. *Nucleic Acids Research* **2011,** *39* (5), 1823-1832.
81. Ramaswamy, S.; Tonnu, N.; Tachikawa, K.; Limphong, P.; Vega, J. B.; Karmali, P. P.; Chivukula, P.; Verma, I. M., Systemic delivery of factor IX messenger RNA for protein replacement therapy. *Proceedings of the National Academy of Sciences* **2017,** *114* (10), E1941-E1950.
82. Yanagi, T.; Tachikawa, K.; Wilkie-Grantham, R.; Hishiki, A.; Nagai, K.; Toyonaga, E.; Chivukula, P.; Matsuzawa, S.-i., Lipid Nanoparticle-mediated siRNA Transfer Against PCTAIRE1/PCTK1/Cdk16 Inhibits In Vivo Cancer Growth. *Molecular Therapy. Nucleic Acids* **2016,** *5* (6), e327.
83. Yaghi, N. K.; Wei, J.; Hashimoto, Y.; Kong, L.-Y.; Gabrusiewicz, K.; Nduom, E. K.; Ling, X.; Huang, N.; Zhou, S.; Kerrigan, B. C. P.; Levine, J. M.; Fajt, V. R.; Levine, G.; Porter, B. F.; Marcusson, E. G.; Tachikawa, K.; Chivukula, P.; Webb, D. C.; Payne, J. E.; Heimberger, A. B., Immune modulatory nanoparticle therapeutics for intracerebral glioma. *Neuro-Oncology* **2017,** *19* (3), 372-382.
84. Aleku, M.; Schulz, P.; Keil, O.; Santel, A.; Schaeper, U.; Dieckhoff, B.; Janke, O.; Endruschat, J.; Durieux, B.; Röder, N.; Löffler, K.; Lange, C.; Fechtner, M.; Möpert, K.; Fisch, G.; Dames, S.; Arnold, W.; Jochims, K.; Giese, K.; Wiedenmann, B.; Scholz, A.; Kaufmann, J., Atu027, a Liposomal Small Interfering RNA Formulation Targeting Protein Kinase N3, Inhibits Cancer Progression. *Cancer Research* **2008,** *68* (23), 9788.
85. Santel, A.; Aleku, M.; Röder, N.; Möpert, K.; Durieux, B.; Janke, O.; Keil, O.; Endruschat, J.; Dames, S.; Lange, C.; Eisermann, M.; Löffler, K.; Fechtner, M.; Fisch, G.; Vank, C.; Schaeper, U.; Giese, K.; Kaufmann, J., Atu027 Prevents Pulmonary Metastasis in Experimental and Spontaneous Mouse Metastasis Models. *Clinical Cancer Research* **2010,** *16* (22), 5469.
86. Schultheis, B.; Strumberg, D.; Santel, A.; Vank, C.; Gebhardt, F.; Keil, O.; Lange, C.; Giese, K.; Kaufmann, J.; Khan, M.; Drevs, J., First-in-Human Phase I Study of the Liposomal RNA Interference Therapeutic Atu027 in Patients With Advanced Solid Tumors. *Journal of Clinical Oncology* **2014,** *32* (36), 4141-4148.
87. Dudek, H.; Wong, D. H.; Arvan, R.; Shah, A.; Wortham, K.; Ying, B.; Diwanji, R.; Zhou, W.; Holmes, B.; Yang, H.; Cyr, W. A.; Zhou, Y.; Shah, A.; Farkiwala, R.; Lee, M.; Li, Y.; Rettig, G. R.; Collingwood, M. A.; Basu, S. K.; Behlke, M. A.; Brown, B. D., Knockdown of β-catenin with Dicer-Substrate siRNAs Reduces Liver Tumor Burden In vivo. *Molecular Therapy* **2014,** *22* (1), 92-101.
88. Lee, S. H.; Kang, Y. Y.; Jang, H.-E.; Mok, H., Current preclinical small interfering RNA (siRNA)-based conjugate systems for RNA therapeutics. *Advanced Drug Delivery Reviews* **2016,** *104* (Supplement C), 78-92.

89. Dohmen, C.; Fröhlich, T.; Lächelt, U.; Röhl, I.; Vornlocher, H.-P.; Hadwiger, P.; Wagner, E., Defined Folate-PEG-siRNA Conjugates for Receptor-specific Gene Silencing. *Molecular therapy. Nucleic acids* **2012,** *1* (1), e7.
90. Zwicke, G. L.; Mansoori, G. A.; Jeffery, C. J., Utilizing the folate receptor for active targeting of cancer nanotherapeutics. *Nano Reviews* **2012,** *3*, 10.3402/nano.v3i0.18496.
91. Alam, M. R.; Ming, X.; Fisher, M.; Lackey, J.; Rajeev, K. G.; Manoharan, M.; Juliano, R., Multivalent Cyclic RGD Conjugates for Targeted Delivery of siRNA. *Bioconjugate chemistry* **2011,** *22* (8), 1673-1681.
92. Danhier, F.; Le Breton, A.; Préat, V., RGD-Based Strategies To Target Alpha(v) Beta(3) Integrin in Cancer Therapy and Diagnosis. *Molecular Pharmaceutics* **2012,** *9* (11), 2961-2973.
93. Alterman, J. F.; Hall, L. M.; Coles, A. H.; Hassler, M. R.; Didiot, M.-C.; Chase, K.; Abraham, J.; Sottosanti, E.; Johnson, E.; Sapp, E.; Osborn, M. F.; Difiglia, M.; Aronin, N.; Khvorova, A., Hydrophobically Modified siRNAs Silence Huntingtin mRNA in Primary Neurons and Mouse Brain. *Molecular Therapy. Nucleic Acids* **2015,** *4* (12), e266.
94. Nikan, M.; Osborn, M. F.; Coles, A. H.; Godinho, B. M. D. C.; Hall, L. M.; Haraszti, R. A.; Hassler, M. R.; Echeverria, D.; Aronin, N.; Khvorova, A., Docosahexaenoic Acid Conjugation Enhances Distribution and Safety of siRNA upon Local Administration in Mouse Brain. *Molecular Therapy. Nucleic Acids* **2016,** *5* (8), e344.
95. Nair, J. K.; Willoughby, J. L. S.; Chan, A.; Charisse, K.; Alam, M. R.; Wang, Q.; Hoekstra, M.; Kandasamy, P.; Kel'in, A. V.; Milstein, S.; Taneja, N.; O'Shea, J.; Shaikh, S.; Zhang, L.; van der Sluis, R. J.; Jung, M. E.; Akinc, A.; Hutabarat, R.; Kuchimanchi, S.; Fitzgerald, K.; Zimmermann, T.; van Berkel, T. J. C.; Maier, M. A.; Rajeev, K. G.; Manoharan, M., Multivalent N-Acetylgalactosamine-Conjugated siRNA Localizes in Hepatocytes and Elicits Robust RNAi-Mediated Gene Silencing. *Journal of the American Chemical Society* **2014,** *136* (49), 16958-16961.
96. Davis, M. E.; Zuckerman, J. E.; Choi, C. H. J.; Seligson, D.; Tolcher, A.; Alabi, C. A.; Yen, Y.; Heidel, J. D.; Ribas, A., Evidence of RNAi in humans from systemically administered siRNA via targeted nanoparticles. *Nature* **2010,** *464*, 1067.
97. Zuckerman, J. E.; Gritli, I.; Tolcher, A.; Heidel, J. D.; Lim, D.; Morgan, R.; Chmielowski, B.; Ribas, A.; Davis, M. E.; Yen, Y., Correlating animal and human phase Ia/Ib clinical data with CALAA-01, a targeted, polymer-based nanoparticle containing siRNA. *Proceedings of the National Academy of Sciences* **2014,** *111* (31), 11449-11454.
98. Rozema, D. B.; Lewis, D. L.; Wakefield, D. H.; Wong, S. C.; Klein, J. J.; Roesch, P. L.; Bertin, S. L.; Reppen, T. W.; Chu, Q.; Blokhin, A. V.; Hagstrom, J. E.; Wolff, J. A., Dynamic PolyConjugates for targeted in vivo delivery of siRNA to hepatocytes. *Proceedings of the National Academy of Sciences* **2007,** *104* (32), 12982-12987.
99. Wakefield, D. H.; Klein, J. J.; Wolff, J. A.; Rozema, D. B., Membrane Activity and Transfection Ability of Amphipathic Polycations as a Function of Alkyl Group Size. *Bioconjugate Chemistry* **2005,** *16* (5), 1204-1208.
100. Wooddell, C. I.; Yuen, M.-F.; Chan, H. L.-Y.; Gish, R. G.; Locarnini, S. A.; Chavez, D.; Ferrari, C.; Given, B. D.; Hamilton, J.; Kanner, S. B.; Lai, C.-L.; Lau, J. Y. N.; Schluep, T.; Xu, Z.; Lanford, R. E.; Lewis, D. L., RNAi-based treatment of chronically infected patients and

chimpanzees reveals that integrated hepatitis B virus DNA is a source of HBsAg. *Science Translational Medicine* **2017,** *9* (409).
101. Parmar, R. G.; Busuek, M.; Walsh, E. S.; Leander, K. R.; Howell, B. J.; Sepp-Lorenzino, L.; Kemp, E.; Crocker, L. S.; Leone, A.; Kochansky, C. J.; Carr, B. A.; Garbaccio, R. M.; Colletti, S. L.; Wang, W., Endosomolytic Bioreducible Poly(amido amine disulfide) Polymer Conjugates for the in Vivo Systemic Delivery of siRNA Therapeutics. *Bioconjugate Chemistry* **2013,** *24* (4), 640-647.
102. Zorde Khvalevsky, E.; Gabai, R.; Rachmut, I. H.; Horwitz, E.; Brunschwig, Z.; Orbach, A.; Shemi, A.; Golan, T.; Domb, A. J.; Yavin, E.; Giladi, H.; Rivkin, L.; Simerzin, A.; Eliakim, R.; Khalaileh, A.; Hubert, A.; Lahav, M.; Kopelman, Y.; Goldin, E.; Dancour, A.; Hants, Y.; Arbel-Alon, S.; Abramovitch, R.; Shemi, A.; Galun, E., Mutant KRAS is a druggable target for pancreatic cancer. *P Natl Acad Sci USA* **2013,** *110* (51), 20723-20728.
103. Pardi, N.; Hogan, M. J.; Porter, F. W.; Weissman, D., mRNA vaccines — a new era in vaccinology. *NAT REV DRUG DISCOV* **2018**.
104. Kowalska, J.; Wypijewska del Nogal, A.; Darzynkiewicz, Z. M.; Buck, J.; Nicola, C.; Kuhn, A. N.; Lukaszewicz, M.; Zuberek, J.; Strenkowska, M.; Ziemniak, M.; Maciejczyk, M.; Bojarska, E.; Rhoads, R. E.; Darzynkiewicz, E.; Sahin, U.; Jemielity, J., Synthesis, properties, and biological activity of boranophosphate analogs of the mRNA cap: versatile tools for manipulation of therapeutically relevant cap-dependent processes. *Nucleic Acids Research* **2014,** *42* (16), 10245-10264.
105. Zangi, L.; Lui, K. O.; von Gise, A.; Ma, Q.; Ebina, W.; Ptaszek, L. M.; Später, D.; Xu, H.; Tabebordbar, M.; Gorbatov, R.; Sena, B.; Nahrendorf, M.; Briscoe, D. M.; Li, R. A.; Wagers, A. J.; Rossi, D. J.; Pu, W. T.; Chien, K. R., Modified mRNA directs the fate of heart progenitor cells and induces vascular regeneration after myocardial infarction. *Nat Biotechnol* **2013,** *31*, 898.
106. Kauffman, K. J.; Dorkin, J. R.; Yang, J. H.; Heartlein, M. W.; DeRosa, F.; Mir, F. F.; Fenton, O. S.; Anderson, D. G., Optimization of Lipid Nanoparticle Formulations for mRNA Delivery in Vivo with Fractional Factorial and Definitive Screening Designs. *Nano Lett* **2015,** *15* (11), 7300-7306.
107. Yin, H.; Song, C.-Q.; Dorkin, J. R.; Zhu, L. J.; Li, Y.; Wu, Q.; Park, A.; Yang, J.; Suresh, S.; Bizhanova, A.; Gupta, A.; Bolukbasi, M. F.; Walsh, S.; Bogorad, R. L.; Gao, G.; Weng, Z.; Dong, Y.; Koteliansky, V.; Wolfe, S. A.; Langer, R.; Xue, W.; Anderson, D. G., Therapeutic genome editing by combined viral and non-viral delivery of CRISPR system components in vivo. *Nat Biotech* **2016,** *34* (3), 328-333.
108. Yin, H.; Song, C.-Q.; Suresh, S.; Wu, Q.; Walsh, S.; Rhym, L. H.; Mintzer, E.; Bolukbasi, M. F.; Zhu, L. J.; Kauffman, K.; Mou, H.; Oberholzer, A.; Ding, J.; Kwan, S.-Y.; Bogorad, R. L.; Zatsepin, T.; Koteliansky, V.; Wolfe, S. A.; Xue, W.; Langer, R.; Anderson, D. G., Structure-guided chemical modification of guide RNA enables potent non-viral in vivo genome editing. *Nat Biotechnol* **2017**.
109. Thess, A.; Grund, S.; Mui, B. L.; Hope, M. J.; Baumhof, P.; Fotin-Mleczek, M.; Schlake, T., Sequence-engineered mRNA Without Chemical Nucleoside Modifications Enables an Effective Protein Therapy in Large Animals. *Molecular Therapy* **2015,** *23* (9), 1456-1464.
110. Fenton, O. S.; Kauffman, K. J.; McClellan, R. L.; Appel, E. A.; Dorkin, J. R.; Tibbitt, M. W.; Heartlein, M. W.; DeRosa, F.; Langer, R.; Anderson, D. G., Bioinspired alkenyl amino alcohol

ionizable lipid materials for highly potent in vivo mRNA delivery. *Advanced Materials* **2016,** *28* (15), 2939-2943.
111. Fenton, O. S.; Kauffman, K. J.; Kaczmarek, J. C.; McClellan, R. L.; Jhunjhunwala, S.; Tibbitt, M. W.; Zeng, M. D.; Appel, E. A.; Dorkin, J. R.; Mir, F. F.; Yang, J. H.; Oberli, M. A.; Heartlein, M. W.; DeRosa, F.; Langer, R.; Anderson, D. G., Synthesis and Biological Evaluation of Ionizable Lipid Materials for the In Vivo Delivery of Messenger RNA to B Lymphocytes. *Advanced Materials* **2017,** *29* (33), 1606944-n/a.
112. Li, B.; Luo, X.; Deng, B.; Wang, J.; McComb, D. W.; Shi, Y.; Gaensler, K. M. L.; Tan, X.; Dunn, A. L.; Kerlin, B. A.; Dong, Y., An Orthogonal Array Optimization of Lipid-like Nanoparticles for mRNA Delivery in Vivo. *Nano Lett* **2015,** *15* (12), 8099-8107.
113. Jiang, C.; Mei, M.; Li, B.; Zhu, X.; Zu, W.; Tian, Y.; Wang, Q.; Guo, Y.; Dong, Y.; Tan, X., A non-viral CRISPR/Cas9 delivery system for therapeutically targeting HBV DNA and pcsk9 in vivo. *Cell Research* **2017,** *27*, 440.
114. Li, B.; Luo, X.; Deng, B.; Giancola, J. B.; McComb, D. W.; Schmittgen, T. D.; Dong, Y., Effects of local structural transformation of lipid-like compounds on delivery of messenger RNA. **2016,** *6*, 22137.
115. Dong, Y.; Eltoukhy, A. A.; Alabi, C. A.; Khan, O. F.; Veiseh, O.; Dorkin, J. R.; Sirirungruang, S.; Yin, H.; Tang, B. C.; Pelet, J. M.; Chen, D.; Gu, Z.; Xue, Y.; Langer, R.; Anderson, D. G., Lipid-Like Nanomaterials for Simultaneous Gene Expression and Silencing In Vivo. *Advanced Healthcare Materials* **2014,** *3* (9), 1392-1397.
116. Jarzebinska, A.; Pasewald, T.; Lambrecht, J.; Mykhaylyk, O.; Kummerling, L.; Beck, P.; Hasenpusch, G.; Rudolph, C.; Plank, C.; Dohmen, C., A Single Methylene Group in Oligoalkylamine-Based Cationic Polymers and Lipids Promotes Enhanced mRNA Delivery. *Angew Chem Int Edit* **2016,** *55* (33), 9590-9594.
117. An, D.; Schneller, J. L.; Frassetto, A.; Liang, S.; Zhu, X.; Park, J.-S.; Theisen, M.; Hong, S.-J.; Zhou, J.; Rajendran, R.; Levy, B.; Howell, R.; Besin, G.; Presnyak, V.; Sabnis, S.; Murphy-Benenato, K. E.; Kumarasinghe, E. S.; Salerno, T.; Mihai, C.; Lukacs, C. M.; Chandler, R. J.; Guey, L. T.; Venditti, C. P.; Martini, P. G. V., Systemic Messenger RNA Therapy as a Treatment for Methylmalonic Acidemia. *Cell Reports* **2017,** *21* (12), 3548-3558.
118. Ramanathan, A.; Robb, G. B.; Chan, S.-H., mRNA capping: biological functions and applications. *Nucleic Acids Research* **2016,** *44* (16), 7511-7526.
119. Grudzien-Nogalska, E.; Jemielity, J.; Kowalska, J.; Darzynkiewicz, E.; Rhoads, R. E., Phosphorothioate cap analogs stabilize mRNA and increase translational efficiency in mammalian cells. *RNA* **2007,** *13* (10), 1745-1755.
120. Kowalska, J.; Lewdorowicz, M.; Zuberek, J.; Grudzien-Nogalska, E.; Bojarska, E.; Stepinski, J.; Rhoads, R. E.; Darzynkiewicz, E.; Davis, R. E.; Jemielity, J., Synthesis and characterization of mRNA cap analogs containing phosphorothioate substitutions that bind tightly to eIF4E and are resistant to the decapping pyrophosphatase DcpS. *RNA* **2008,** *14* (6), 1119-1131.
121. Karikó, K.; Muramatsu, H.; Keller, J. M.; Weissman, D., Increased Erythropoiesis in Mice Injected With Submicrogram Quantities of Pseudouridine-containing mRNA Encoding Erythropoietin. *Molecular Therapy* **2012,** *20* (5), 948-953.
122. Karikó, K.; Muramatsu, H.; Welsh, F. A.; Ludwig, J.; Kato, H.; Akira, S.; Weissman, D., Incorporation of Pseudouridine Into mRNA Yields Superior Nonimmunogenic Vector With

Increased Translational Capacity and Biological Stability. *Molecular Therapy* **2008,** *16* (11), 1833-1840.
123. Kauffman, K. J.; Mir, F. F.; Jhunjhunwala, S.; Kaczmarek, J. C.; Hurtado, J. E.; Yang, J. H.; Webber, M. J.; Kowalski, P. S.; Heartlein, M. W.; DeRosa, F.; Anderson, D. G., Efficacy and Immunogenicity of Unmodified and Pseudouridine-Modified mRNA Delivered Systemically with Lipid Nanoparticles in Vivo. *Biomaterials* **2016,** *109*, 78-87.
124. Kormann, M. S. D.; Hasenpusch, G.; Aneja, M. K.; Nica, G.; Flemmer, A. W.; Herber-Jonat, S.; Huppmann, M.; Mays, L. E.; Illenyi, M.; Schams, A.; Griese, M.; Bittmann, I.; Handgretinger, R.; Hartl, D.; Rosenecker, J.; Rudolph, C., Expression of therapeutic proteins after delivery of chemically modified mRNA in mice. *Nat Biotechnol* **2011,** *29*, 154.
125. Li, B.; Luo, X.; Dong, Y., Effects of Chemically Modified Messenger RNA on Protein Expression. *Bioconjugate Chemistry* **2016,** *27* (3), 849-853.
126. Svitkin, Y. V.; Cheng, Y. M.; Chakraborty, T.; Presnyak, V.; John, M.; Sonenberg, N., N1-methyl-pseudouridine in mRNA enhances translation through eIF2 α -dependent and independent mechanisms by increasing ribosome density. *Nucleic Acids Research* **2017,** *45* (10), 6023-6036.
127. Mauro, V. P.; Chappell, S. A., A critical analysis of codon optimization in human therapeutics. *Trends in molecular medicine* **2014,** *20* (11), 604-613.
128. Balmayor, E. R.; Geiger, J. P.; Aneja, M. K.; Berezhanskyy, T.; Utzinger, M.; Mykhaylyk, O.; Rudolph, C.; Plank, C., Chemically modified RNA induces osteogenesis of stem cells and human tissue explants as well as accelerates bone healing in rats. *Biomaterials* **2016,** *87* (Supplement C), 131-146.
129. Doudna, J. A.; Charpentier, E., The new frontier of genome engineering with CRISPR-Cas9. *Science* **2014,** *346* (6213).
130. Jinek, M.; Chylinski, K.; Fonfara, I.; Hauer, M.; Doudna, J. A.; Charpentier, E., A Programmable Dual-RNA-Guided DNA Endonuclease in Adaptive Bacterial Immunity. *Science* **2012,** *337* (6096), 816-821.
131. Ran, F. A.; Hsu, P. D.; Wright, J.; Agarwala, V.; Scott, D. A.; Zhang, F., Genome engineering using the CRISPR-Cas9 system. *Nat Protoc* **2013,** *8* (11), 2281-2308.
132. Sternberg, S. H.; Redding, S.; Jinek, M.; Greene, E. C.; Doudna, J. A., DNA interrogation by the CRISPR RNA-guided endonuclease Cas9. *Nature* **2014,** *507* (7490), 62-67.
133. Mali, P.; Yang, L. H.; Esvelt, K. M.; Aach, J.; Guell, M.; DiCarlo, J. E.; Norville, J. E.; Church, G. M., RNA-Guided Human Genome Engineering via Cas9. *Science* **2013,** *339* (6121), 823-826.
134. Davis, A. J.; Chen, D. J., DNA double strand break repair via non-homologous end-joining. *Translational Cancer Research* **2013,** *2* (3), 130-143.
135. Richardson, C. D.; Ray, G. J.; DeWitt, M. A.; Curie, G. L.; Corn, J. E., Enhancing homology-directed genome editing by catalytically active and inactive CRISPR-Cas9 using asymmetric donor DNA. *Nat Biotechnol* **2016,** *34*, 339.
136. Wang, H.-X.; Li, M.; Lee, C. M.; Chakraborty, S.; Kim, H.-W.; Bao, G.; Leong, K. W., CRISPR/Cas9-Based Genome Editing for Disease Modeling and Therapy: Challenges and Opportunities for Nonviral Delivery. *Chemical Reviews* **2017,** *117* (15), 9874-9906.
137. Wang, M.; Glass, Z. A.; Xu, Q., Non-viral delivery of genome-editing nucleases for gene therapy. *Gene Ther* **2017,** *24* (3), 144-150.

138. Miller, J. B.; Zhang, S.; Kos, P.; Xiong, H.; Zhou, K.; Perelman, S. S.; Zhu, H.; Siegwart, D. J., Non-viral CRISPR/Cas gene editing in vitro and in vivo enabled by synthetic nanoparticle co-delivery of Cas9 mRNA and sgRNA. *Angew Chem Int Ed Engl* **2017,** *56* (4), 1059-1063.
139. MORRISSEY, D. V. P., Mihir, Chandrakant;; FINN, J. D.; SMITH, A. M. R.; SHAW, L. J.; DOMBROWSKI, C.; SHAH, R. R. LIPID NANOPARTICLE FORMULATIONS FOR CRISPR/CAS COMPONENTS. 2017.
140. Cong, L.; Ran, F. A.; Cox, D.; Lin, S. L.; Barretto, R.; Habib, N.; Hsu, P. D.; Wu, X. B.; Jiang, W. Y.; Marraffini, L. A.; Zhang, F., Multiplex Genome Engineering Using CRISPR/Cas Systems. *Science* **2013,** *339* (6121), 819-823.
141. Sanchez-Rivera, F. J.; Jacks, T., Applications of the CRISPR-Cas9 system in cancer biology. *Nat Rev Cancer* **2015,** *15* (7), 387-395.
142. Sander, J. D.; Joung, J. K., CRISPR-Cas systems for editing, regulating and targeting genomes. *Nat Biotechnol* **2014,** *32* (4), 347-355.
143. Platt, R. J.; Chen, S. D.; Zhou, Y.; Yim, M. J.; Swiech, L.; Kempton, H. R.; Dahlman, J. E.; Parnas, O.; Eisenhaure, T. M.; Jovanovic, M.; Graham, D. B.; Jhunjhunwala, S.; Heidenreich, M.; Xavier, R. J.; Langer, R.; Anderson, D. G.; Hacohen, N.; Regev, A.; Feng, G. P.; Sharp, P. A.; Zhang, F., CRISPR-Cas9 Knockin Mice for Genome Editing and Cancer Modeling. *Cell* **2014,** *159* (2), 440-455.
144. Xue, W.; Chen, S.; Yin, H.; Tammela, T.; Papagiannakopoulos, T.; Joshi, N. S.; Cai, W.; Yang, G.; Bronson, R.; Crowley, D. G.; Zhang, F.; Anderson, D. G.; Sharp, P. A.; Jacks, T., CRISPR-mediated direct mutation of cancer genes in the mouse liver. *Nature* **2014,** *514* (7522), 380-384.
145. Yin, H.; Xue, W.; Chen, S.; Bogorad, R. L.; Benedetti, E.; Grompe, M.; Koteliansky, V.; Sharp, P. A.; Jacks, T.; Anderson, D. G., Genome editing with Cas9 in adult mice corrects a disease mutation and phenotype. *Nat Biotechnol* **2014,** *32* (6), 551-553.
146. Chen, S. D.; Sanjana, N. E.; Zheng, K. J.; Shalem, O.; Lee, K.; Shi, X.; Scott, D. A.; Song, J.; Pan, J. Q.; Weissleder, R.; Lee, H.; Zhang, F.; Sharp, P. A., Genome-wide CRISPR Screen in a Mouse Model of Tumor Growth and Metastasis. *Cell* **2015,** *160* (6), 1246-1260.
147. Han, X.; Liu, Z.; Jo, M. c.; Zhang, K.; Li, Y.; Zeng, Z.; Li, N.; Zu, Y.; Qin, L., CRISPR-Cas9 delivery to hard-to-transfect cells via membrane deformation. *Science Advances* **2015,** *1*, e1500454.
148. Zuris, J. A.; Thompson, D. B.; Shu, Y.; Guilinger, J. P.; Bessen, J. L.; Hu, J. H.; Maeder, M. L.; Joung, J. K.; Chen, Z. Y.; Liu, D. R., Cationic lipid-mediated delivery of proteins enables efficient protein-based genome editing in vitro and in vivo. *Nat Biotechnol* **2015,** *33* (1), 73-80.
149. Wang, M.; Zuris, J. A.; Meng, F. T.; Rees, H.; Sun, S.; Deng, P.; Han, Y.; Gao, X.; Pouli, D.; Wu, Q.; Georgakoudi, I.; Liu, D. R.; Xu, Q. B., Efficient delivery of genome-editing proteins using bioreducible lipid nanoparticles. *P Natl Acad Sci USA* **2016,** *113* (11), 2868-2873.
150. Sun, W. J.; Ji, W. Y.; Hall, J. M.; Hu, Q. Y.; Wang, C.; Beisel, C. L.; Gu, Z., Self-Assembled DNA Nanoclews for the Efficient Delivery of CRISPR-Cas9 for Genome Editing. *Angew Chem Int Edit* **2015,** *54* (41), 12029-12033.
151. Dong, Y. Z.; Dorkin, J. R.; Wang, W. H.; Chang, P. H.; Webber, M. J.; Tang, B. C.; Yang, J.; Abutbul-Ionita, I.; Danino, D.; DeRosa, F.; Heartlein, M.; Langer, R.; Anderson, D. G.,

Poly(glycoamidoamine) Brushes Formulated Nanomaterials for Systemic siRNA and mRNA Delivery in Vivo. *Nano Lett* **2016,** *16* (2), 842-848.
152. Kaczmarek, J. C.; Patel, A. K.; Kauffman, K. J.; Fenton, O. S.; Webber, M. J.; Heartlein, M. W.; DeRosa, F.; Anderson, D. G., Polymer-Lipid Nanoparticles for Systemic Delivery of mRNA to the Lungs. *Angew Chem Int Ed Engl* **2016**.
153. Perttu, E. K.; Kohli, A. G.; Szoka, F. C., Inverse-Phosphocholine Lipids: A Remix of a Common Phospholipid. *Journal of the American Chemical Society* **2012,** *134* (10), 4485-4488.
154. Guschin, D. Y.; Waite, A. J.; Katibah, G. E.; Miller, J. C.; Holmes, M. C.; Rebar, E. J., A rapid and general assay for monitoring endogenous gene modification. *Methods Mol Biol* **2010,** *649*, 247-56.
155. Whitehead, K. A.; Matthews, J.; Chang, P. H.; Niroui, F.; Dorkin, J. R.; Severgnini, M.; Anderson, D. G., In vitro-in vivo translation of lipid nanoparticles for hepatocellular siRNA delivery. *Acs Nano* **2012,** *6* (8), 6922-6929.
156. Li, Y.; Park, A. I.; Mou, H.; Colpan, C.; Bizhanova, A.; Akama-Garren, E.; Joshi, N.; Hendrickson, E. A.; Feldser, D.; Yin, H.; Anderson, D. G.; Jacks, T.; Weng, Z.; Xue, W., A versatile reporter system for CRISPR-mediated chromosomal rearrangements. *Genome Biol* **2015,** *16*, 111.
157. Aagaard, L.; Rossi, J. J., RNAi therapeutics: Principles, prospects and challenges. *Advanced Drug Delivery Reviews* **2007,** *59*.
158. Ochiai, B.; Hirano, T., ChemInform Abstract: Facile Synthesis of Glycidates via Oxidation of Acrylates with Aqueous Solution of NaOCl in the Presence of Ammonium Salts. *ChemInform* **2014,** *45* (24), no-no.
159. Hao, J.; Kos, P.; Zhou, K.; Miller, J. B.; Xue, L.; Yan, Y.; Xiong, H.; Elkassih, S.; Siegwart, D. J., Rapid synthesis of a lipocationic polyester library via ring-opening polymerization of functional valerolactones for efficacious siRNA delivery. *Journal of the American Chemical Society* **2015,** *137* (29), 9206-9209.
160. Pack, D. W.; Hoffman, A. S.; Pun, S.; Stayton, P. S., Design and development of polymers for gene delivery. *NAT REV DRUG DISCOV* **2005,** *4* (7), 581-593.
161. Ilardi, E. A.; Vitaku, E.; Njardarson, J. T., Data-Mining for Sulfur and Fluorine: An Evaluation of Pharmaceuticals To Reveal Opportunities for Drug Design and Discovery. *Journal of Medicinal Chemistry* **2014,** *57* (7), 2832-2842.
162. Han, T.; Goralski, M.; Gaskill, N.; Capota, E.; Kim, J.; Ting, T. C.; Xie, Y.; Williams, N. S.; Nijhawan, D., Anticancer sulfonamides target splicing by inducing RBM39 degradation via recruitment to DCAF15. *Science* **2017,** *356* (6336), eaal3755.
163. Smith, B. R.; Eastman, C. M.; Njardarson, J. T., Beyond C, H, O, and N! Analysis of the Elemental Composition of U.S. FDA Approved Drug Architectures. *Journal of Medicinal Chemistry* **2014,** *57* (23), 9764-9773.
164. Chang Kang, H.; Bae, Y. H., Co-delivery of small interfering RNA and plasmid DNA using a polymeric vector incorporating endosomolytic oligomeric sulfonamide. *Biomaterials* **2011,** *32* (21), 4914-4924.
165. Sethuraman, V. A.; Na, K.; Bae, Y. H., pH-Responsive Sulfonamide/PEI System for Tumor Specific Gene Delivery: An in Vitro Study. *Biomacromolecules* **2006,** *7* (1), 64-70.

166. Mizuhara, T.; Saha, K.; Moyano, D. F.; Kim, C. S.; Yan, B.; Kim, Y.-K.; Rotello, V. M., Acylsulfonamide-Functionalized Zwitterionic Gold Nanoparticles for Enhanced Cellular Uptake at Tumor pH. *Angewandte Chemie International Edition* **2015,** *54* (22), 6567-6570.
167. Siegwart, D. J.; Whitehead, K. A.; Nuhn, L.; Sahay, G.; Cheng, H.; Jiang, S.; Ma, M.; Lytton-Jean, A.; Vegas, A.; Fenton, P.; Levins, C. G.; Love, K. T.; Lee, H.; Cortez, C.; Collins, S. P.; Li, Y. F.; Jang, J.; Querbes, W.; Zurenko, C.; Novobrantseva, T.; Langer, R.; Anderson, D. G., Combinatorial synthesis of chemically diverse core-shell nanoparticles for intracellular delivery. *Proceedings of the National Academy of Sciences of the United States of America* **2011,** *108* (32), 12996-3001.
168. Scholz, C.; Wagner, E., Therapeutic plasmid DNA versus siRNA delivery: Common and different tasks for synthetic carriers. *J Control Release* **2012,** *161* (2), 554-565.
169. Nelson, C. E.; Kintzing, J. R.; Hanna, A.; Shannon, J. M.; Gupta, M. K.; Duvall, C. L., Balancing cationic and hydrophobic content of PEGylated siRNA polyplexes enhances endosome escape, stability, blood circulation time, and bioactivity in vivo. *Acs Nano* **2013,** *7* (10), 8870-8880.
170. Zhang, L.; Cao, Z.; Bai, T.; Carr, L.; Ella-Menye, J. R.; Irvin, C.; Ratner, B. D.; Jiang, S., Zwitterionic hydrogels implanted in mice resist the foreign-body reaction. *Nature Biotechnology* **2013,** *31* (6), 553-556.
171. Forrest, M. L.; Meister, G.; Koerber, J.; Pack, D., Partial acetylation of polyethylenimine enhances in vitro gene delivery. *Pharmaceutical Research* **2004,** *21* (2), 365-371.
172. Gabrielson, N. P.; Pack, D. W., Acetylation of Polyethylenimine Enhances Gene Delivery via Weakened Polymer/DNA Interactions. *Biomacromolecules* **2006,** *7* (8), 2427-2435.
173. Coelho, T.; Adams, D.; Silva, A.; Lozeron, P.; Hawkins, P. N.; Mant, T.; Perez, J.; Chiesa, J.; Warrington, S.; Tranter, E.; Munisamy, M.; Falzone, R.; Harrop, J.; Cehelsky, J.; Bettencourt, B. R.; Geissler, M.; Butler, J. S.; Sehgal, A.; Meyers, R. E.; Chen, Q. M.; Borland, T.; Hutabarat, R. M.; Clausen, V. A.; Alvarez, R.; Fitzgerald, K.; Gamba-Vitalo, C.; Nochur, S. V.; Vaishnaw, A. K.; Sah, D. W. Y.; Gollob, J. A.; Suhr, O. B., Safety and efficacy of RNAi therapy for transthyretin amyloidosis. *New Engl J Med* **2013,** *369* (9), 819-829.
174. Bertrand, N.; Leroux, J. C., The journey of a drug-carrier in the body: an anatomo-physiological perspective. *J Control Release* **2012,** *161* (2), 152-63.
175. Xue, W.; Dahlman, J. E.; Tammela, T.; Khan, O. F.; Sood, S.; Dave, A.; Cai, W.; Chirino, L. M.; Yang, G. R.; Bronson, R.; Crowley, D. G.; Sahay, G.; Schroeder, A.; Langer, R.; Anderson, D. G.; Jacks, T., Small RNA combination therapy for lung cancer. *P Natl Acad Sci USA* **2014,** *111* (34), E3553-E3561.
176. David, S.; Pitard, B.; Benoît, J.-P.; Passirani, C., Non-viral nanosystems for systemic siRNA delivery. *Pharmacological Research* **2010,** *62* (2), 100-114.
177. DeRosa, F.; Guild, B.; Karve, S.; Smith, L.; Love, K.; Dorkin, J. R.; Kauffman, K. J.; Zhang, J.; Yahalom, B.; Anderson, D. G.; Heartlein, M. W., Therapeutic efficacy in a hemophilia B model using a biosynthetic mRNA liver depot system. *Gene Therapy* **2016,** *23* (10), 699-707.